

CHAPTER 1

General and theoretical aspects of phenols

MINH THO NGUYEN

*Department of Chemistry, University of Leuven, B-3001 Leuven, Belgium
fax: 32-16-327992; e-mail: minh.nguyen@chem.kuleuven.ac.be*

EUGENE S. KRYACHKO*

*Department of Chemistry, University of Leuven, B-3001, Belgium, and Departement SBG, Limburgs Universitaire Centrum, B-3590 Diepenbeek, Belgium
email: eugene.kryachko@luc.ac.be*

and

LUC G. VANQUICKENBORNE

*Department of Chemistry, University of Leuven, B-3001 Leuven, Belgium
email: luc.vanquickenborne@chem.kuleuven.ac.be*

I. INTRODUCTION	3
A. Summary of Key Physico-chemical Properties of Phenol	4
B. The History of the Discovery of Phenol	6
C. Usage and Production	7
II. MOLECULAR STRUCTURE AND BONDING OF PHENOL	20
A. The Equilibrium Structure of Phenol in the Ground Electronic State . .	20
B. Molecular Bonding Patterns in the Phenol S_0	21
C. Atom-in-Molecule Analysis	31
D. Vibrational Modes	34
E. Three Interesting Structures Related to Phenol	38
III. STRUCTURES AND PROPERTIES OF SUBSTITUTED PHENOLS . . .	47
A. Intramolecular Hydrogen Bond in <i>ortho</i> -Halogenophenols	47
B. <i>meta</i> - and <i>para</i> -Halogenophenols	57

* On leave of absence from Bogoliubov Institute for Theoretical Physics, Kiev, 03143 Ukraine.

C. The Bonding Trends in Monohalogenated Phenols in Terms of the Electronic Localization Function (<i>ELF</i>)	68
1. Introduction to the <i>ELF</i>	68
2. Topology of the <i>ELF</i>	68
3. Vector gradient field $\nabla_r \eta(r)$	70
4. The bonding in benzene, phenol and phenyl halides	71
5. Monohalogenated phenols: the bonding in terms of <i>ELF</i>	73
a. The <i>ortho</i> -substituted phenols	73
b. The <i>meta</i> -substituted phenols	76
c. The <i>para</i> -substituted phenols	76
D. Some Representatives of Substituted Phenols	78
IV. ENERGETICS OF SOME FUNDAMENTAL PROCESSES	83
A. Protonation	83
1. Protonation of phenol	83
2. Proton affinities of halophenols	86
3. Proton affinities of anisole and fluoroanisoles	88
4. Two views on the protonation regioselectivity	89
5. Interaction of phenol with Li^+ , Na^+ and K^+	92
B. Deprotonation	92
1. Phenolate anion	93
2. Gas-phase acidities	97
3. Acidity in solution	101
4. Correlation between intrinsic acidities and molecular properties	101
5. Alkali metal phenolates	103
C. Electronic Excitation	105
D. Ionization	110
1. Molecular and electronic structure of phenol radical cation	111
2. Relative energies of the $(\text{C}_6\text{H}_6\text{O})^{*+}$ radical cations	114
3. The $(\text{C}_6\text{H}_6\text{O})^{*+}$ potential energy surface (PES)	116
4. Mass spectrometric experiments	121
5. Keto–enol interconversion	127
E. The O–H Bond Dissociation	129
1. Phenoxy radicals	129
a. Electronic structure	129
b. Geometry and vibrational frequencies	132
c. Spin densities	135
d. Decomposition of phenoxy radical	137
2. Antioxidant activity of phenols	139
a. The O–H bond dissociation energies	139
b. Antioxidant activities	140
c. Features of hydrogen atom abstraction from phenols	141
V. HYDROGEN BONDING ABILITIES OF PHENOLS	143
A. Introductory Survey	143
B. Phenol–(Water) $_n$, $1 \leq n \leq 4$ Complexes	147
1. Introduction	147
2. Interaction of phenol with water	149
3. The most stable complexes of mono- and dihydrated phenol	149
4. Lower-energy structures of $\text{PhOH}(\text{H}_2\text{O})_3$	156
5. At the bottom of PES of $\text{PhOH}(\text{H}_2\text{O})_4$	160

C. Hydrogen Bonding between Phenol and Acetonitrile	170
1. Introductory foreground	170
2. Phenol–acetonitrile complex	171
3. Phenol bonding with two acetonitrile molecules	174
4. A rather concise discussion	177
D. Phenol–Benzonitrile Hydrogen-bonded Complex	177
E. A Very Short O–H . . . N Hydrogen Bond	178
VI. OPEN THEORETICAL PROBLEMS	178
VII. ACKNOWLEDGEMENTS	179
VIII. REFERENCES AND NOTES	179

Glossary of Acronyms

BDE	bond dissociation enthalpy	LIF	laser-induced fluorescence
BIPA	<i>trans</i> -butenylidene- isopropylamine	LUMO	lowest unoccupied MO
<i>N</i> -BMA	benzylidenemethylamine	MO	molecular orbital
CCSD(T)	coupled cluster singles doubles (triples)	MP2	second-order Møller-Plesset perturbation theory
DF	dispersed fluorescence spectroscopy	MW	microwave spectroscopy
DFT	density functional method	NBO	natural bond orbital
<i>N,N</i> -DMBA	dimethylbenzylamine	PA	proton affinity
DPE	deprotonation energy	PCA	1-pyrrolidinecarboxaldehyde
DRS	double-resonance spectroscopy	PES	potential energy surface
ED	electron diffraction	Ph	phenyl C ₆ H ₅
HF	Hartree-Fock method	PhOH	phenol
HOMO	highest occupied MO	R2PI	resonant two-photon ionization
IR-UV	infrared-ultraviolet spectroscopy		spectroscopy
		SOMO	singly occupied MO
		TMA	trimethylamine
		ZPE-ZPVE	zero-point vibrational energy

I. INTRODUCTION

The chemistry of phenols has attracted continuing interest in the last two centuries. Compounds bearing this functional group have several applications indispensable in our daily life, as discussed in the following chapters of this book. Let us mention one example: phenols constitute, among others, an important class of antioxidants that inhibit the oxidative degradation of organic materials including a large number of biological aerobic organisms and commercial products. In human blood plasma, α -tocopherol, well-known as a component of vitamin E, is proved to be the most efficient phenol derivative to date to trap the damaging peroxy radicals (ROO[•]). Phenols owe their activity to their ability to scavenge radicals by hydrogen or electron transfer in much faster processes than radical attacks on an organic substrate.

In this chapter, we attempt to give an overview on the general and theoretical aspects of phenols, including a brief history of their discovery. However, in view of the very large wealth of related literature, the coverage is by no means complete. It is also not intended to be a comprehensive review of all the theoretical work in the area, and there are certainly many important studies of which we were unaware, for which we apologize.

We refer to the compilation *Quantum Chemistry Library Data Base (QCLDB)*¹ for an extended list of available theoretical papers.

The focus of this chapter is a presentation of representative physico-chemical and spectroscopic properties of phenols revealed by quantum chemical calculations, many of them carried out by us specifically for this chapter. In the discussion, the description of methodological details will be kept to a minimum. Unless otherwise noted, all reported computations were performed using the GAUSSIAN 98² and MOPAC-7³ sets of programs. The natural bond orbital analysis⁴ was conducted using the NBO (natural bond orbital) module⁵ of the GAUSSIAN 98 software package.² For the vibrational analyses, the force constant matrices were initially obtained in terms of the cartesian coordinates and the non-redundant sets of internal coordinates were subsequently defined⁶. The calculation of potential energy distribution (PED) matrices of the vibrational frequencies⁷ was carried out using the GAR2PED program⁸.

A. Summary of Key Physico-chemical Properties of Phenol

Phenol shown in Chart 1 is the parent substance of a homologous series of compounds containing a *hydroxyl group* bound directly to the aromatic ring. Phenol, or PhOH in shorthand notation, belongs to the family of *alcohols* due to the presence of the OH group and it is in fact the simplest aromatic member of this family. The hydroxyl group of phenol determines its acidity whereas the benzene ring characterizes its basicity. Thus, it is formally the *enol* form of the *carbonyl group* (for a review, see ref. 9).

In this subsection we briefly outline the key physico-chemical properties of phenol. For its other properties consult with the NIST data located at URL <http://webbook.nist.gov>.

Phenol has a low melting point, it crystallizes in colourless prisms and has a characteristic, slightly pungent odor. In the molten state, it is a clear, colourless, mobile liquid. In the temperature range $T < 68.4^\circ\text{C}$, its miscibility with water is limited; above this temperature it is completely miscible. The melting and solidification points of phenol are quite substantially lowered by water. A mixture of phenol and *ca* 10% water is called phenolum liquefactum, because it is actually a liquid at room temperature. Phenol is readily soluble in most organic solvents (aromatic hydrocarbons, alcohols, ketones, ethers, acids, halogenated hydrocarbons etc.) and somewhat less soluble in aliphatic hydrocarbons. Phenol forms azeotropic mixtures with water and other substances.

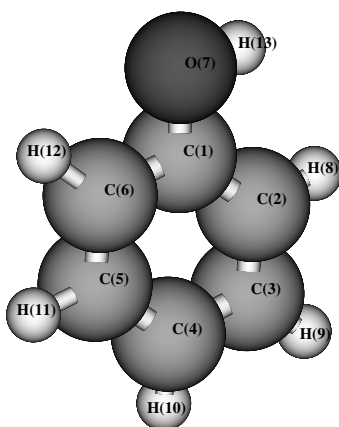


CHART 1. Chemical formulae of phenol: $\text{C}_6\text{H}_5\text{OH}$; early name: carboic acid, hydroxybenzene; CAS registry number: 108-95-2

Other physical data of phenol follow below:

Molecular weight: 94.11 (molecular mass of C_6H_5OH is equal to 94.04186).

Weakly acidic: $pK_a(H_2O) = 9.94$ (although it varies in different sources from 9.89 to 9.95).

Freezing point: 40.91 °C.

Specific heats of combustion: $C_p = 3.06 \text{ J mol}^{-1} \text{ K}^{-1}$, $C_v = 3.07 \text{ J mol}^{-1} \text{ K}^{-1}$.

First ionization energy (IE_a): 8.47 eV (experimental), $8.49 \pm 0.02 \text{ eV}$ (evaluated).

Proton affinity (PA): 820 kJ mol^{-1} ¹⁰.

Gas phase basicity: $786.3 \text{ kJ mol}^{-1}$ ¹⁰.

Gas-phase heat of formation $\Delta_f H_{298}$: $-96.2 \pm 8 \text{ kJ mol}^{-1}$ (experimental); $-93.3 \text{ kJ mol}^{-1}$ (theoretical)¹¹.

Solvation free energy:

Experimental: $-27.7 \text{ kJ mol}^{-1}$ ¹², $-27.6 \text{ kJ mol}^{-1}$ ¹³.

Theoretical: -17.3 , -20.2 , $-16.4 \text{ kJ mol}^{-1}$ (AMBER parameter¹⁴), -19.7 , -23.8 , $-12.1 \text{ kJ mol}^{-1}$,¹³⁻¹⁶.

Gas phase acidity: $\Delta_{acid} H_{298}$:

Experimental: $1465.7 \pm 10 \text{ kJ mol}^{-1}$ ^{17, 18}; $1461.1 \pm 9 \text{ kJ mol}^{-1}$ ^{18, 19};
 $1471 \pm 13 \text{ kJ mol}^{-1}$ ²⁰.

Theoretical: $1456.4 \text{ kJ mol}^{-1}$ ²⁰.

O–H bond dissociation energy $D_{298}(C_6H_5O-H)$:

Experimental: $362 \pm 8 \text{ kJ mol}^{-1}$ ²¹; $363.2 \pm 9.2 \text{ kJ mol}^{-1}$ ²²; $353 \pm 4 \text{ kJ mol}^{-1}$ ²³;
 $376 \pm 13 \text{ kJ mol}^{-1}$ ²⁴; $369.5 \text{ kJ mol}^{-1}$ ²⁵; $377 \pm 13 \text{ kJ mol}^{-1}$ ²⁶.

Theoretical: $377.7 \text{ kJ mol}^{-1}$ ²⁰.

What else is worth noting, in view of the present review on the theoretical aspects of phenol, is that its electronic subsystem consists of 50 electrons and the ground state is a singlet closed-shell state designated as S_0 .

Phenol can be considered as the enol of cyclohexadienone. While the tautomeric keto–enol equilibrium lies far to the ketone side in the case of aliphatic ketones, for phenol it is shifted almost completely to the enol side. The reason of such stabilization is the formation of the aromatic system. The resonance stabilization is very high due to the contribution of the *ortho*- and *para*-quinonoid resonance structures. In the formation of the phenolate anion, the contribution of quinonoid resonance structures can stabilize the negative charge.

In contrast to aliphatic alcohols, which are mostly less acidic than phenol, phenol forms salts with aqueous alkali hydroxide solutions. At room temperature, phenol can be liberated from the salts even with carbon dioxide. At temperatures near the boiling point of phenol, it can displace carboxylic acids, e.g. acetic acid, from their salts, and then phenolates are formed. The contribution of *ortho*- and *para*-quinonoid resonance structures allows electrophilic substitution reactions such as chlorination, sulphonation, nitration, nitrosation and mercuration. The introduction of two or three nitro groups into the benzene ring can only be achieved indirectly because of the sensitivity of phenol towards oxidation. Nitrosation in the *para* position can be carried out even at ice bath temperature. Phenol readily reacts with carbonyl compounds in the presence of acid or basic catalysts. Formaldehyde reacts with phenol to yield hydroxybenzyl alcohols, and synthetic resins on further reaction. Reaction of acetone with phenol yields bisphenol A [2,2-bis(4-hydroxyphenyl)propane].

The reaction in the presence of acid catalysts is used to remove impurities from synthetic phenol. Olefinic impurities or carbonyl compounds, e.g. mesityl oxide, can be polymerized into higher molecular weight compounds by catalytic quantities of sulphuric acid or acidic ion exchangers and can thus be separated easily from phenol, e.g. by its distillation.

Phenol readily couples with diazonium salts to yield coloured compounds. The latter can be used for the photometric detection of phenol as in the case of diazotized 4-nitroaniline. Salicylic acid (2-hydroxybenzoic acid) can be produced by the Kolbe–Schmitt reaction²⁶ (studied by the density functional method²⁷) from sodium phenolate and carbon dioxide, whereas potassium phenolate gives the *para* compound. Alkylation and acylation of phenol can be carried out with aluminium chloride as catalyst; methyl groups can also be introduced by the Mannich reaction. Diaryl ethers can only be produced under extreme conditions.

With oxidizing agents, phenol readily forms a free radical which can dimerize to form diphenols or can be oxidized to form dihydroxybenzenes and quinones. Since phenol radicals are relatively stable, phenol is a suitable radical scavenger and can also be used as an oxidation inhibitor. Such a property can also be undesirable, e.g. the autoxidation of cumene can be inhibited by small quantities of phenol.

B. The History of the Discovery of Phenol

Phenol is a constituent of coal tar and was probably first (partly) isolated from coal tar in 1834 by Runge, who called it ‘carbolic acid’ (*Karbolsäure*) or ‘coal oil acid’ (*Kohlenölsäure*)^{28–30}.

Friedlieb Ferdinand Runge (born in Billwärder, near Hamburg, 8 February 1795—Oranienburg, died on 25 March 1867) began his career as a pharmacist and, after a long residence in Paris, became an associate professor in Breslau, Germany. Later, he served in the Prussian Marine in Berlin and Oranienburg. Runge published several scientific and technological papers and books (see References 31 and 32 and references therein). He rediscovered aniline in coal-tar oil and called it *kyanol*. He also discovered quinoline (*leukol*), pyrrole (*πνρρσ*), rosolic acid and three other bases.

Pure phenol was first prepared by Laurent in 1841. Auguste Laurent (La Folie, near Langres, Haute-Marne, 14 September 1808—Paris, 15 April 1853), the son of a wine-merchant, was assistant to Dumas at the Ecole Centrale (1831) and to Brongniart at the Sevres porcelain factory (1833–1835) in France. From 1835 until 1836, he lived in a garret in the Rue St. Andre, Paris, where he had a private laboratory. In December 1837 Laurent defended his Paris doctorate and in 1838 became professor at Bordeaux. Since 1845 he worked in a laboratory at the Ecole Normale in Paris. In his studies of the distillate from coal-tar and chlorine, Laurent isolated dichlorophenol (*acide chlorophénèsique*) $C^{24}H^8Cl^4O^2$ and trichlorophenol (*acide chlorophénisique*) $C^{24}H^6Cl^6O^2$, which both suggested the existence of phenol (phenhydrate)³³. Laurent wrote: ‘I give the name *phène* (*φαινων*, I light) to the fundamental radical. . .’. He provided the table of ‘general formulae of the derived radicals of *phène*’ where phenol (*hydrate of phène*) was indicated by the incorrect formula $C^{24}H^{12} + H^4O^2$ ($=C_6H_8O$, in modern notation). In 1841, Laurent isolated and crystallized phenol for the first time. He called it ‘hydrate de phényle’ or ‘acide phénique’³⁴. His reported melting point (between 34 and 35 °C) and boiling point (between 187 and 188 °C) are rather close to the values known today. Apart from measuring these elementary physical properties, Laurent also gave some crystals to a number of persons with toothache to try it out as a possible pain killer. The effect on the pain was rather unclear, but the substance was ‘very aggressive on the lips and the gums’. In the analysis of his experiments, Laurent applied the substitution hypothesis that was originally proposed by his former supervisor, Dumas. Apparently, however, Laurent went further than Dumas and assumed that the substitution reaction did not otherwise change the structural formula of the reactant and the product, whereas Dumas limited himself to the claim that the removal of one hydrogen atom was compensated by the addition of another group, leaving open the possibility of a complete rearrangement of the molecule³⁵.

The substitution hypothesis (especially in the form proposed by Laurent) was attacked rather strongly by Berzélius, who claimed that a simple replacement of the hydrogen atom by, for instance, the chlorine atom in an organic molecule should be utterly impossible 'due to the strong electronegative character' of chlorine^{36,37}. According to Berzélius, the very idea of Laurent contradicted the first principles of chemistry and 'seems to be a bad influence (une influence nuisible) in science' (see also Reference 32, p. 388). Instead, he reinterpreted all the results of Laurent by breaking up the reaction product into smaller (more familiar) molecules, satisfying the same global stoichiometry. It looks as if Berzélius was reluctant to accept the full richness of organic chemistry. He was unwilling to accept the existence of new molecules, if the atomic count (and a few other obvious properties) could be satisfied by known molecules. Dumas replied that Berzélius 'attributes to me an opinion precisely contrary to that which I have always maintained, viz., that chlorine in this case takes the place of the hydrogen. . . . The law of substitution is an empirical fact and nothing more; it expresses a relation between the hydrogen expelled and the chlorine retained. I am not responsible for the gross exaggeration with which Laurent has invested my theory; his analyses moreover do not merit any confidence'³⁸ (see also Reference 32, p. 388).

In 1843, Charles Frederic Gerhardt (Strasbourg, 21 August 1816—19 August 1856) also prepared phenol by heating salicylic acid with lime and gave it the name 'phénol'³⁹.

Since the 1840s, phenol became a subject of numerous studies. Victor Meyer studied desoxybenzoin, benzyl cyanide and phenyl-substituted methylene groups and showed that they have similar reactivities³¹. He subsequently published a paper on 'the negative nature of the phenyl group', where he noted how phenyl together with other 'negative groups' can make the hydrogen atoms in methylene groups more reactive. In 1867, Heinrich von Brunck defended his Ph.D. thesis in Tübingen under Adolph Friedrich Ludwig Strecker and Wilhelm Staedel on the theme 'About Derivatives of Phenol', where he particularly studied the isomers of nitrophenol³¹.

The Raschig–Dow process of manufacturing phenol by cumene was discovered by Wurtz and Kekule in 1867, although the earlier synthesis was recorded by Hunt in 1849. Interestingly, Friedrich Raschig, working earlier as a chemist at BASF and known for his work on the synthesis of phenol and production of phenol formaldehyde adduct, later established his own company in Ludwigshafen.

It is also interesting to mention in this regard that in 1905, the BAAS subcommittee on 'dynamic isomerism' was established and included Armstrong (chairman), Lowry (secretary) and Lapworth. In the 1909 report, Lowry summarized that one of the types of isomerism involves the 'oscillatory transference' of the hydrogen atom from carbon to oxygen, as in ethyl acetoacetate (acetoacetic ester), or from oxygen to nitrogen, as in isatin, or from one oxygen atom to the other one, as in *para*-nitrosophenol^{40,41}.

C. Usage and Production

Phenol is one of the most versatile and important industrial organic chemicals. Until World War II, phenol was essentially a natural coal-tar product. Eventually, synthetic methods replaced extraction from natural sources because its consumption had risen significantly. For instance, as a metabolic product, phenol is normally excreted in quantities of up to 40 mg L⁻¹ in human urine. Currently, small amounts of phenol are obtained from coal tar. Higher quantities are formed in coking or low-temperature carbonization of wood, brown coal or hard coal and in oil cracking. The earlier methods of synthesis (via benzenesulphonic acid and chlorobenzene) have been replaced by modern processes, mainly by the Hock process starting from cumene, via the Raschig–Dow process and by sulphonation. Phenol is also formed during petroleum cracking. Phenol has achieved considerable importance as the starting material for numerous intermediates and final products.

Phenol occurs as a component or as an addition product in natural products and organisms. For example, it is a component of lignin, from which it can be liberated by hydrolysis. Lignin is a complex biopolymer that accounts for 20–30% of the dry weight of wood. It is formed by a free-radical polymerization of substituted phenylpropane units to give an amorphous polymer with a number of different functional groups including aryl ether linkages, phenols and benzyl alcohols⁴². Most pulp-processing methods involve oxidative degradation of lignin, since its presence is a limitation to the utilization of wood pulps for high end uses such as print and magazine grade paper. Such limitation is due to the photoinduced yellowing of lignin-rich, high-yield mechanical pulps and, as a result, the photooxidative yellowing has been extensively studied in the hope of understanding its mechanism and ultimately preventing its occurrence^{42, 43}. Phenoxyl radicals are produced during the photooxidation of lignin and their subsequent oxidation ultimately leads to quinones, which are actually responsible for the yellow colour.

Phenol was first used as a disinfectant in 1865 by the British surgeon Joseph Lister at Glasgow University, Scotland, for sterilizing wounds, surgical dressings and instruments. He showed that if phenol was used in operating theatres to sterilize equipment and dressings, there was less infection of wounds and, moreover, the patients stood a much better chance of survival. By the time of his death, 47 years later, Lister's method of antiseptic surgery (Lister spray) was accepted worldwide. Its dilute solutions are useful antiseptics and, as a result of Lister's success, phenol became a popular household antiseptic. Phenol was put as an additive in a so-called carbolic soap. Despite its benefits at that time, this soap is now banned. In Sax's book *Dangerous Properties of Industrial Materials* (quoted in Reference 44), one finds frightening phrases like 'kidney damage', 'toxic fumes' and 'co-carcinogen'. Clearly, phenol is totally unsuitable for general use, but the benefits 130 years ago plainly outweighed the disadvantages. However, because of its protein-degenerating effect, it often had a severely corrosive effect on the skin and mucous membranes.

Phenol only has limited use in pharmaceuticals today because of its toxicity. Phenol occurs in normal metabolism and is harmless in small quantities according to present knowledge, but it is definitely toxic in high concentrations. It can be absorbed through the skin, by inhalation and by swallowing. The typical main absorption route is the skin, through which phenol is resorbed relatively quickly, simultaneously causing caustic burns on the area of skin affected. Besides the corrosive effect, phenol can also cause sensitization of the skin in some cases. Resorptive poisoning by larger quantities of phenol (which is possible even over small affected areas of skin) rapidly leads to paralysis of the central nervous system with collapse and a severe drop in body temperature. If the skin is wetted with phenol or phenolic solutions, decontamination of the skin must therefore be carried out immediately. After removal of contaminated clothing, polyglycols (e.g. lutrol) are particularly suitable for washing the skin. On skin contamination, local anesthesia sets in after an initial painful irritation of the area of skin affected. Hereby the danger exists that possible resorptive poisoning is underestimated. If phenol penetrates deep into the tissue, this can lead to phenol gangrene through damage to blood vessels. The effect of phenol on the central nervous system—sudden collapse and loss of consciousness—is the same for humans and animals. In animals, a state of cramp precedes these symptoms because of the effect phenol has on the motor activity controlled by the central nervous system. Caustic burns on the cornea heal with scarred defects. Possible results of inhalation of phenol vapour or mist are dyspnea, coughing, cyanosis and lung edema. Swallowing phenol can lead to caustic burns on the mouth and esophagus and stomach pains. Severe, though not fatal, phenol poisoning can damage inner organs, namely kidneys, liver, spleen, lungs and heart. In addition, neuropsychiatric disturbances have been described after survival of acute phenol poisoning. Most of the phenol absorbed by the body is excreted in urine as phenol and/or its metabolites. Only smaller quantities are excreted with faeces or exhaled.

The reactions are:

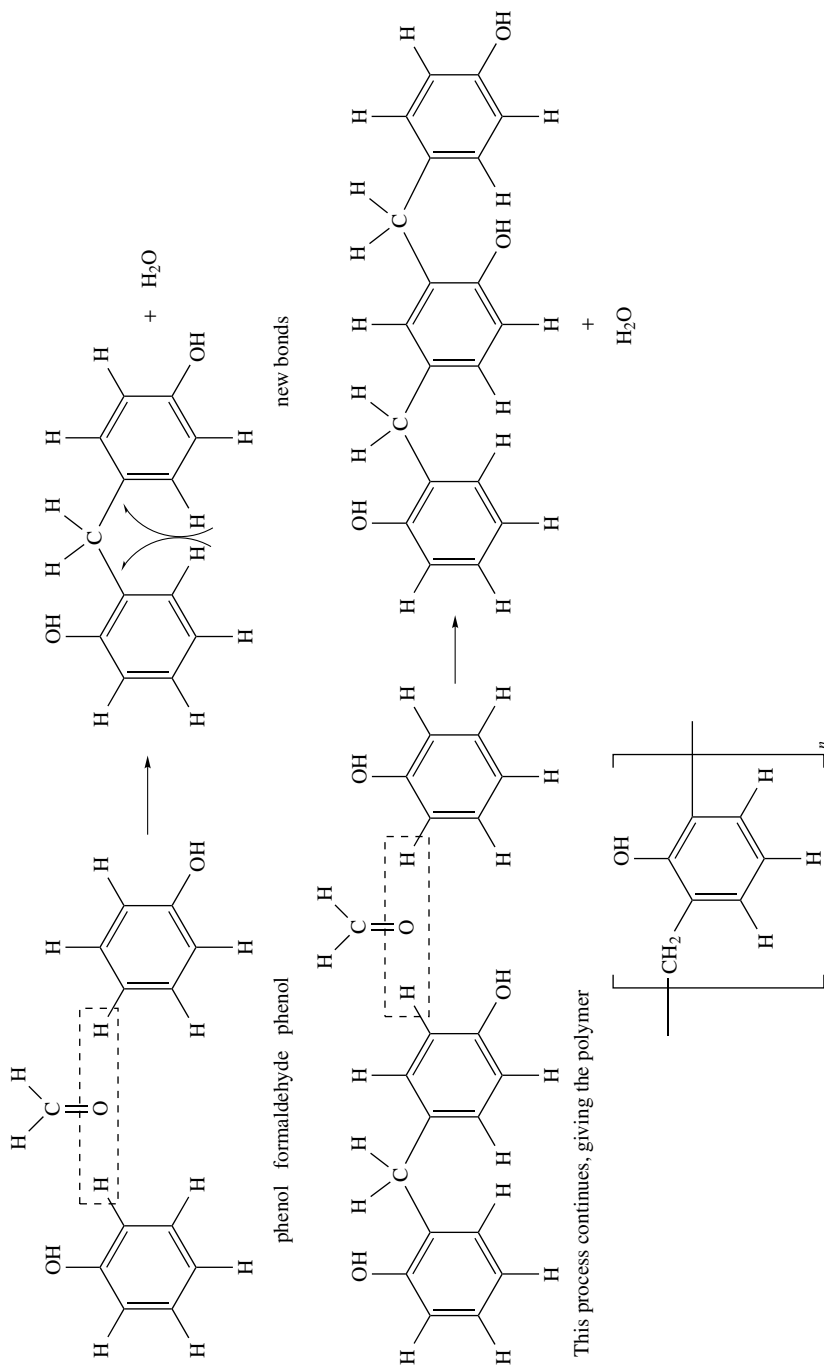


CHART 2. Production of a phenolic resin

Phenol is a violent systemic poison. Less irritating and more efficient germicides (component of some plastics) replace phenol; nevertheless, it is widely used in the manufacture of phenolic resins (e.g. with formaldehyde—see Chart 2, with furfural etc.), epoxy resins, plastics, plasticizers, polycarbonates, antioxidants, lube oil additives, nylon, caprolactam, aniline insecticides, explosives, surface active agents, dyes and synthetic detergents, polyurethanes, wood preservatives, herbicides, fungicides (for wood preparation), gasoline additives, inhibitors, pesticides and as raw material for producing medical drugs like aspirin.

Acetylsalicylic acid was first synthesized by Bayer in 1897 and named Aspirin in 1899^{45–47}. Nevertheless, its analgesic and antipyretic effects had been known long before. For example, in the 18th century, Stone discovered the medical effects of the salicin of willow bark and, since that time, salicylic acid was recognized as the active ingredient. Salicin is enzymatically hydrolysed to saligenin and glucose by β -glucosidase. Saligenin is then slowly oxidized to salicylic acid in the blood and in the liver. As is well known, the sodium salt of salicylic acid was used in the 19th century as a painkiller despite the fact that it causes stomach irritations. In his search for less-irritating derivatives of salicylic acid, the Bayer chemist Felix Hoffmann synthesized acetylsalicylic acid (Figure 1).

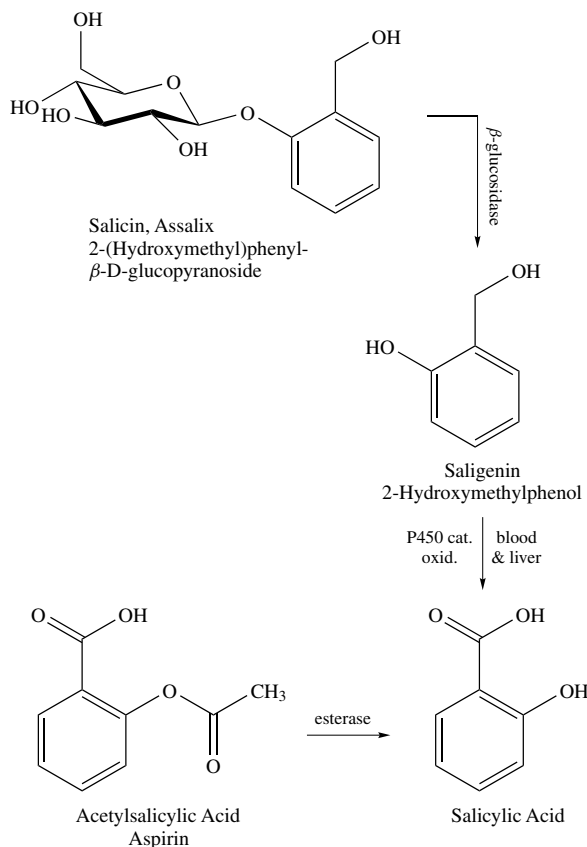


FIGURE 1. Salicin, saligenin, salicylic acid, and aspirin

The success of aspirin was terrific. In a 1994 article⁴⁸ in the *Medical Sciences Bulletin*, it was written that ‘Americans consume about 80 billion aspirin tablets a year, and more than 50 nonprescription drugs contain aspirin as the principal active ingredient’. The Aspirin Foundation of America provides systematically scientific, regulatory, legislative and general educational information about aspirin to the medical community and the public⁴⁹. In 1971, Vane⁵⁰ discovered that aspirin interferes with the biosynthesis of prostaglandins. In 1982 he was awarded the Nobel Prize in medicine in recognition of his work on the mechanism of the action of aspirin. In 1994, Garavito and coworkers^{51,52} elucidated the mechanism of aspirin interference with prostaglandin synthesis.

The crystal structure of aspirin was first determined by Wheatley⁵³ in 1964 and was refined later, in 1985, by Kim and coworkers⁵⁴. Its crystal structure data can be obtained from the Cambridge Crystallographic Database⁵⁵. The key features of the crystal structure of aspirin are shown in Figure 2. Quite recently, the potential energy surface of aspirin was studied using the B3LYP/6-31G(d) method and all its nine conformational isomers were located⁵⁶.

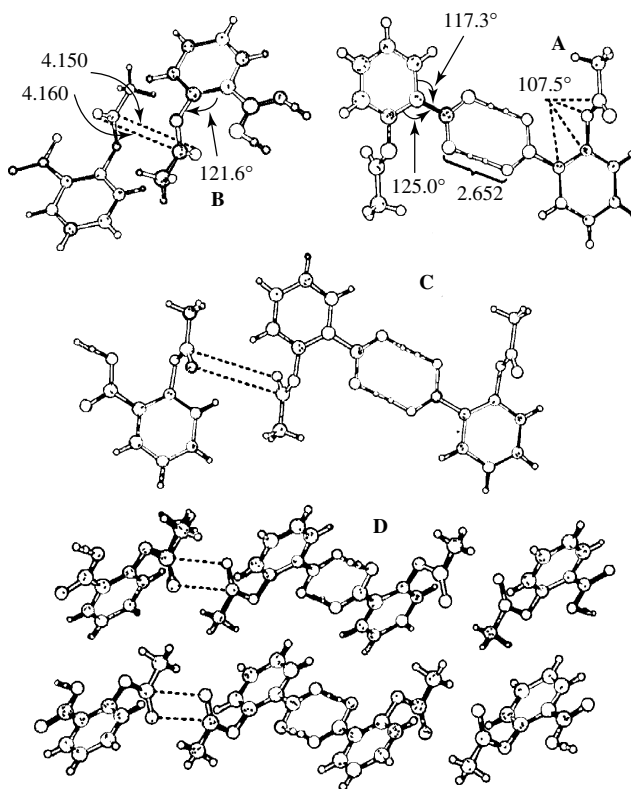


FIGURE 2. Hydrogen bonding patterns and dipole alignment in the crystal structure of aspirin. Two positions are shown for each of the hydrogen-bonded hydrogen atoms (A). Aspirin may also form another conformation of the dimer structure, a sort of inversion-symmetric dimer, with a perfect dipole–dipole alignment of the carbonyl groups of two ester functions (B). Actually, each aspirin is partly involved in a dimer of A and B. This is shown in C. D demonstrates the arrangement of the chains in the crystal. Adapted from Reference 56 with permission

Phenol is mainly used in the production of phenolic resins (plastics). These resins are important components of such items as appliance knobs, handles and housings, washing machine agitators and electrical devices. One example of its commercial usage is the phenol–formaldehyde polymer or phenol–formaldehyde resin called Bakelite (Formica, Micarta), first made in the USA in 1909. It took its name from its discoverer Leo Baekeland who developed it commercially between 1905 and 1910, and it was actually the first truly synthetic polymer. It is characterized by low cost, dimensional stability, high strength, stiffness and resistance to ageing; it is much safer than celluloid. It has insulating properties and could be moulded easily. Bakelite was the ideal plastic for electrical appliances, and in fact it was Bakelite which made possible the generation and distribution of electricity; it made electrical appliances safer for home utilization. It is also widely used in handles, table tops, cabinets and wall panels. The reaction between phenol and formaldehyde is a typical reaction of condensation polymerization, shown in Chart 2⁵⁷.

A phenol derivative, phenolphthalein is prepared by the reaction of phenol with phthalic anhydride in the presence of sulphuric acid and used as an indicator for acidity or alkalinity. Chlorinated phenol is much safer than phenol. Chlorine gas reacts with phenol to add one, two or three chlorine atoms and to form, respectively, chlorophenol, 2,4-dichlorophenol and 2,4,6-trichlorophenol⁵⁸. The chlorination of phenol proceeds by electrophilic aromatic substitution. The latter two molecules are less soluble in water than phenol and appear to be a stronger antiseptic than phenol. Interestingly, in the first half of the past century, a bottle of antiseptic chlorophenols was a common attribute as a medicine in many homes. Its solution was used for bathing cuts, cleaning grazes, rinsing the mouth and gargling to cure sore throats. Nevertheless, it was revealed that its solution likely contains dioxins.

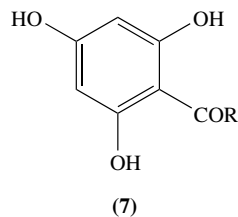
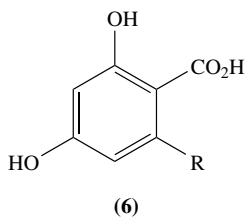
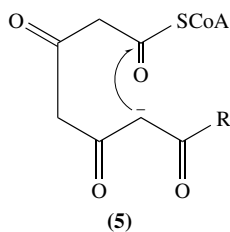
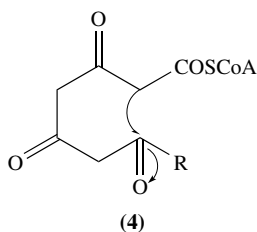
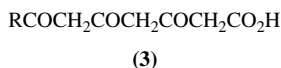
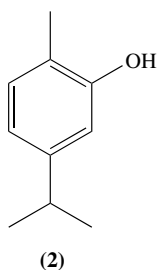
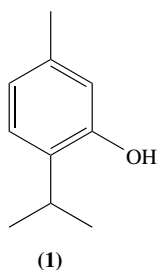
There are actually 31 different chloro- and polychlorophenols⁵⁷. One of them, 2,4-dichlorophenoxyacetic acid (2,4-D), acts as a growth hormone. This makes it particularly effective as a weedkiller against broad-leaf weeds, even in a tiny drop. Surprisingly, it is actually a superb selective weedkiller for lawns and grain crops because it does not affect grass and cereals. Sometimes, 2,4-D is used to trick plants into flowering. This is widely used in Hawaii, where visitors are greeted with pineapple flowers during the whole year! It is safe for animals in low quantity, but 35 g of it is likely a fatal dose for an average person weighing about 70 kg. 2,4-D is quite inexpensive, effective, more selective than other weedkillers and much safer than the sodium arsenate and sodium chlorate which were popular weedkillers in the 1950s. In 1948, 2,4,5-trichlorophenoxyacetic acid (2,4,5-T) came into the market⁴⁴ and contained larger quantities of dioxin than 2,4-D⁵⁹. It was used as a killer for tough weeds and was so successful in killing woody plants that it was deployed in the Vietnam War. From 1962 to 1969, at least 50,000 tonnes of a 50:50 mixture of 2,4-D and 2,4,5-T (called defoliant and widely known as Agent Orange) was sprayed from the air to destroy the dense foliage of trees covering the troops of the Vietnam National Front of Liberation. Agent Orange was contaminated with *ca* 2–4% of dioxins and for this reason it caused birth defects in new-born babies in Vietnam. It may also be linked to a form of acute myelogenous leukaemia, which represents 8% of childhood cancers among the children of Vietnam veterans, as the US Institute of Medicine (IOM) committee has recently reported⁶⁰.

Interestingly, phenols from peat smoke are included in the flavours of Scotch whisky to dry the malt⁴⁴.

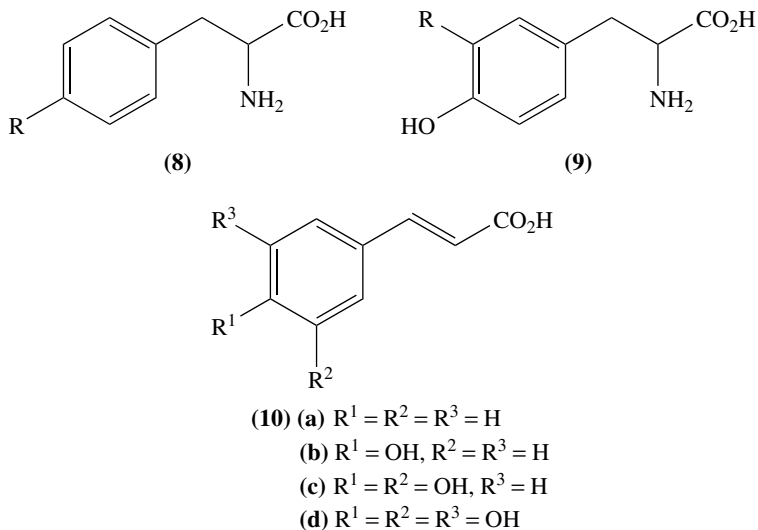
Complex phenols are widespread in nature, although the simple ones are relatively uncommon. Phenol is particularly found in mammalian urine, pine needles and oil tobacco leaves. Abundant natural substances such as thymol (1) and carvacrol (2) are derivatives of phenols.

Natural phenols^{57, 61, 62} arise in the three following manners⁵⁷:

(i) Poly- β -ketones, for example (3), derived from the acid RCO_2H and three malonate units, are intermediates (enzyme-bound) in phenol biosynthesis. Cyclization can be envisaged as being similar to the aldol reaction (cf. 4) or the Claisen condensation (cf. 5) yielding phenolic acids like orsellinic acid (6), $\text{R} = \text{Me}$, or phenolic ketones, e.g. phloracetophenone (7), $\text{R} = \text{Me}$, respectively, after enolization of the carbonyl functions. Modification processes may ensue or intervene. The reduction of a carbonyl to secondary alcohol, away from the cyclization site, may thus afford a phenol with one less hydroxyl. However, such a mode of biogenesis^{63–65} leads to phenols with *meta*-disposed hydroxyls. This character may be diagnostic of the origin.



(ii) Aromatic rings may be hydroxylated *in vivo* by mono-oxygenases. Such reactions are often encountered in aromatics derived from the shikimate–prephenate pathway⁶⁶. Phenylalanine (8) is thus *p*-hydroxylated to tyrosine (9) by phenylalanine mono-oxygenase using molecular oxygen. Cinnamic acid (10a) can be hydroxylated to *p*-hydroxycinnamic acid (10b), and on to di- and tri-hydroxy acids like, for instance, caffeic (10c) and gallic (10d) acids, with adjacent hydroxy functions. A useful list of micro-organisms and higher plant mono-oxygenases and phenolases is given elsewhere⁶⁷. Hydroxylations such as



(8 \rightarrow 9) may be accompanied by proton rearrangements as (8, R = D) \rightarrow (9, R = D), the so-called 'National Institute of Health' ('NIH') shift, whose mechanism^{68,69} is displayed in Chart 3. Related 'NIH' shifts have been observed in vitro for various synthetic arene oxides and in oxidation of aromatics by permanganate and by chromyl compounds⁷⁰ such as CrO_2Cl_2 and $CrO_2(OAc)_2$.

(iii) Alicyclic rings with oxygen functions may be dehydrogenated to phenols. Compounds **1** and **2** are likely derived from monocyclic monoterpenes carrying a 3- or 2-oxygen function. Phenolic steroids like, for instance, estrone and equilenin can be derived in a similar way. This route to phenolic products is not yet well understood.

Phenol moieties are present in salvarsan (**11**) and neosalvarsan (**12**) synthesized by the German scientist Paul Ehrlich (1854–1915), considered as the father of chemotherapy for

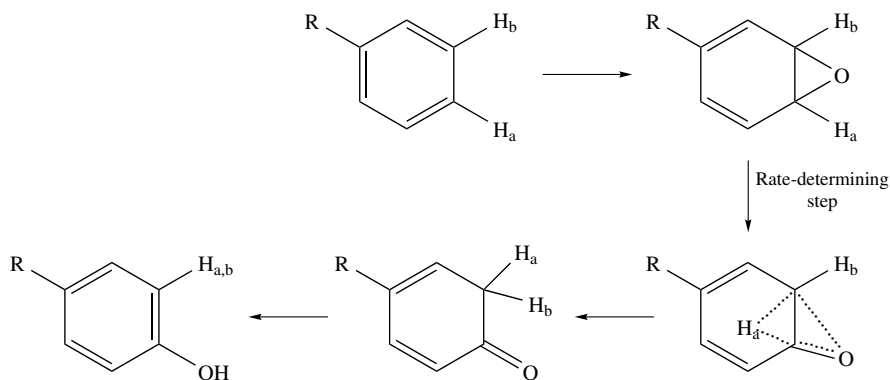
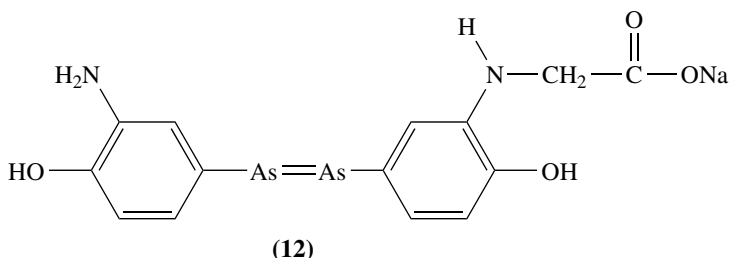
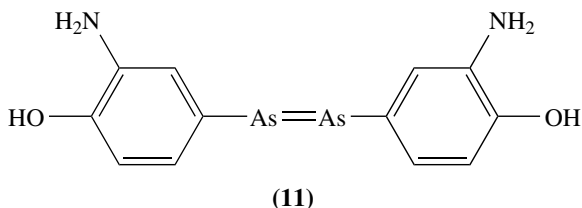


CHART 3. Mechanism of the so-called 'NIH'-shift

use in syphilis treatments prior to the discovery of penicillin. He received a Nobel Prize in 1908 for his work.

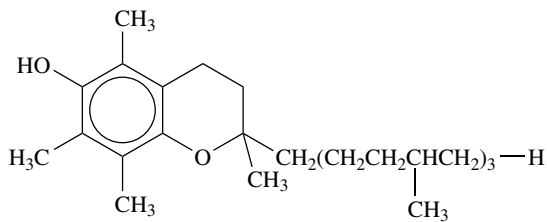


Phenol serves as a basic unit of larger molecules, e.g. tyrosine residues in proteins. The phenoxyl radical is treated as a model system for the tyrosyl radical whose formation via abstraction of the hydrogen atom from the hydroxyl group of tyrosine is a typical feature of oxidative stress in the physiological pH range^{71, 72}.

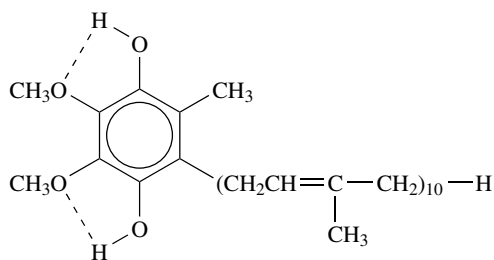
Phenols are an extremely important class of antioxidants whose utilization in living organisms and synthetic organic materials reduces the rate of the oxidative degradation which all organic materials undergo by being exposed to air^{73–77}. The antioxidant property can be related to the readily abstractable phenolic hydrogen as a consequence of the relatively low bond dissociation enthalpy of the phenolic O–H group [BDE(O–H)]. A large variety of *ortho*- and/or *para*-alkoxy-substituted phenols have been identified as natural antioxidants, such as α -tocopherol (**13**), which is known as the most effective lipid-soluble chain-breaking antioxidant in human blood plasma, and ubiquinol-10 (**14**), both present in low-density lipid proteins. The mechanism of action of many phenolic antioxidants relies on their ability to transfer the phenolic H atom to a chain-carrying peroxy radical at a rate much faster than that at which the chain-propagating step of lipid peroxidation proceeds^{73–77}. Natural phenolic antioxidants can be also isolated from plants⁷⁸ such as sesamol (**15**), from sesame seeds and coniferyl alcohol (**16**), one of the three precursors for the biosynthesis of lignin. For example, Vitamin E (**17**) is a chain-breaking antioxidant that interferes with one or more of the propagation steps in autooxidation by atmospheric oxygen⁷⁹.

Phenolic compounds are also known to suppress the lipid peroxidation in living organisms. Furthermore, they are widely used as additives in food technology.

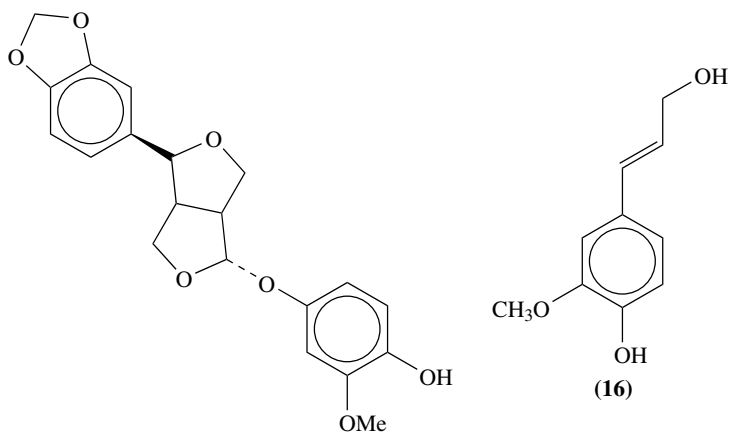
Regarding the production of phenol, small quantities of phenol are isolated from tars and coking plant water produced in the coking of hard coal and the low temperature carbonization of brown coal as well as from the wastewater from cracking plants. Most of the past and currently employed phenol syntheses are based on using benzene as a precursor which, however, is known as a volatile organic carcinogen. About 20% of the global benzene production is used for the manufacture of phenol⁸⁰. By far the greatest proportion is obtained by oxidation of benzene or toluene. Although direct oxidation of



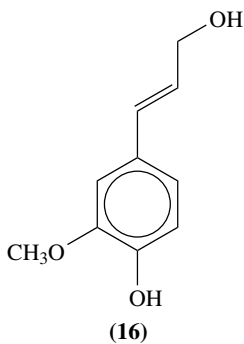
(13)



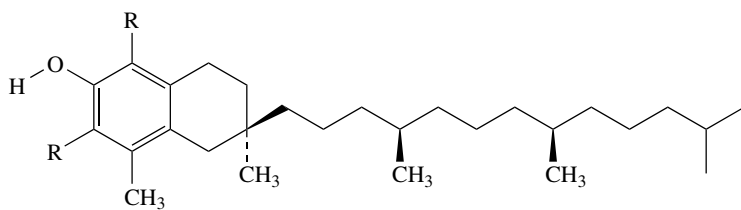
(14)



(15)



(16)



(17)

benzene is possible in principle, the phenol formed is immediately further oxidized. It is worth mentioning that a recent study⁸¹ performed a thorough computational study of the potential energy surface for the oxidation reaction of benzene in the lowest-lying triplet state (equation 1)



followed by a kinetic analysis using the Rice–Ramsperger–Kassel–Marcus (RRKM) reaction theory⁸² based on the electronic structure calculations employing the MP4/6-31G(d)//HF/6-31G(d) and B3LYP/cc-pVDZ computational levels. Below we outline the key results of this work.

Reaction 1 has a large number of energetically feasible product channels. In Figure 3, we display the theoretical triplet potential energy surface (PES) for reaction 1. The reaction initially proceeds via the addition of $\text{O}({}^3\text{P})$ to benzene, and this first step is exothermic by -37 kJ mol^{-1} and characterized by a barrier of approximately 21 kJ mol^{-1} . The chemically activated adduct reacts on the triplet PES in forming a number of products. The two lowest barriers lead to the formation of phenoxyl radical (-14 kJ mol^{-1}) and formylcyclopentadiene (-8 kJ mol^{-1} , both barriers taken relative to the reactant)⁸¹. The reaction route resulting in phenol is exothermic (-33 kJ mol^{-1}). However, it has a rather high barrier of 100 kJ mol^{-1} . The calculated enthalpy of the reaction of the formation of

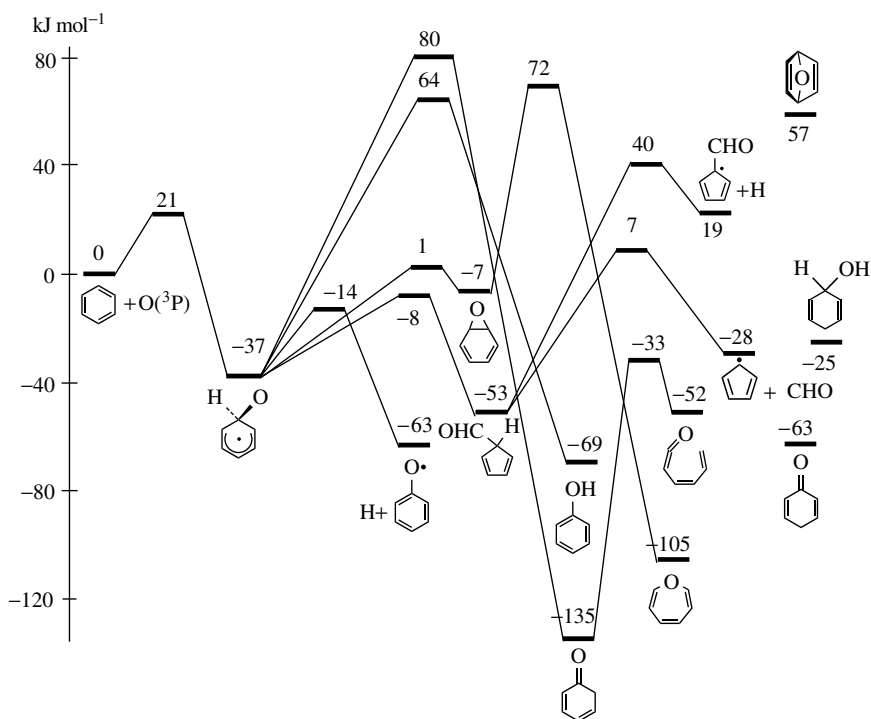


FIGURE 3. The potential energy profile of triplet products and transition structures in reaction 1. Adapted from Reference 81 with permission

phenol amounts to -433 kJ mol^{-1} , which agrees fairly well with the experimental value of -428 kJ mol^{-1} ⁸¹. The theoretical singlet–triplet splitting of phenol (352 kJ mol^{-1}) is also very close to its experimental value of 341 kJ mol^{-1} . One may conclude that such high activation is likely sufficient to overcome the barrier in order to form phenoxy radical (372 kJ mol^{-1}), and therefore one might expect that the formation of the latter dominates on the singlet PES. This concurs with the flame data of Bittner and Howard⁸³ indicating that a direct reaction route to phenol is not possible.

It has been recently revealed that ZSM-5 zeolite exhibits an extremely high catalytic selectivity for the oxidation of benzene to phenol. The high reactivity of the zeolite should be ascribed to iron impurity arising in the intermediary steps in the zeolite synthesis^{84, 85}. A surface oxygen (O) or α -oxygen, generated on Fe-ZSM-5 zeolite during N_2O decomposition^{84, 85} (equation 2)



takes part in the formation of phenol via equation 3



Reactions 2 and 3 have been thoroughly studied theoretically at the B3LYP computational level. In particular, a sound model of α -oxygen has been proposed^{85, 86}. According to Reference 87, Solutia has recently developed a one-step technology producing phenol directly from benzene and N_2O . Due to the fact that such a process provides a very high yield and can use waste N_2O from the production of adipic acid, it is now considered to be a rather promising technology in the new millennium.

Therefore, alternative routes must be chosen for the production of phenol, e.g. via halogen compounds which are subsequently hydrolysed or via cumene hydroperoxide which is then cleaved catalytically. The following processes were developed as industrial syntheses for the production of phenol⁸⁸:

1. Sulphonation of benzene and production of phenol by heating the benzenesulphonate in molten alkali hydroxide⁸⁹.
2. Chlorination of benzene and alkaline hydrolysis of the chlorobenzene.
3. Chlorination of benzene and catalytic saponification by Cu in the steam hydrolysis of the chlorobenzene^{90, 91} (Raschig process, Raschig–Hooker, Gulf oxychlorination).
4. Alkylation of benzene with propene to isopropylbenzene (cumene), oxidation of cumene to the corresponding *tert*-hydroperoxide and cleavage to phenol and acetone (Hock process).
5. Toluene oxidation to benzoic acid and subsequent oxidizing decarboxylation to phenol (Dow process).
6. Dehydrogenation of cyclohexanol–cyclohexanone mixtures.

Among these processes, only the Hock process and the toluene oxidation are important industrially. The other processes were discarded for economic reasons. In the Hock process acetone is formed as a by-product. This has not, however, hindered the expansion of this process, because there is a market for acetone. New plants predominantly use the cumene process. More than 95% of the $4,691,000 \text{ m y}^{-1}$ ($\text{m} = \text{metric tonnes}$) consumed is produced by the cumene peroxidation process. Phenol's consumption growth rate of 3% is primarily based on its use in engineering plastics such as polycarbonates, polyetherimide and poly(phenylene oxide), and epoxy resins for the electronic industry. The Mitsui Company is, for instance, the world's second largest producer of phenol. Japan's production

output (in thousands of metric tonnes) is shown below⁹².

Chemicals/Year	1996	1997	1998	1999	2000	Change 1999–2000
Phenol	768	833	851	888	916	3.2%
Phenolic resins	294	303	259	250	262	4.8%

The cumene process is based on the discovery of the oxidation of cumene with oxygen to cumene hydroperoxide and its acidic cleavage to phenol and acetone published in 1944⁹³. This reaction was developed into an industrial process shortly after World War II by the Distillers Co. in the United Kingdom and the Hercules Powder Co. in the United States. The first plant was put into operation in 1952 by Shawinigan in Canada and had an initial capacity of 8000 t y⁻¹ of phenol. Today, phenol is predominantly produced by this process in plants in the USA, Canada, France, Italy, Japan, Spain, Finland, Korea, India, Mexico, Brazil, Eastern Europe and Germany with an overall annual capacity of 5×10^6 tons^{94,95}. In addition to the economically favourable feedstock position (due to the progress in petrochemistry since the 1960s), the fact that virtually no corrosion problems occur and that all reaction stages work under moderate conditions with good yields was also decisive for the rapid development of the process. To produce cumene, benzene is alkylated with propene using phosphoric acid (UOP process) or aluminium chloride as catalyst.

The phenol-forming process via toluene oxidation developed originally by Dow (USA)^{96–98} has been carried out in the USA, Canada and the Netherlands. Snia Viscosa (Italy) uses the toluene oxidation only for the production of benzoic acid as an intermediate in the production of caprolactam^{99,100}. The process proceeds in two stages. At the first stage, toluene is oxidized with atmospheric oxygen in the presence of a catalyst to benzoic acid in the liquid phase. At the second stage the benzoic acid is decarboxylated catalytically in the presence of atmospheric oxygen to produce phenol. This is a radical-chain reaction involving peroxy radicals. The activation energy of the exothermic oxidation of toluene to benzoic acid is 136 kJ mol⁻¹⁹⁹.

Most of the phenol produced is processed further to give phenol–formaldehyde resins. The quantities of phenol used in the production of caprolactam via cyclohexanol–cyclohexanone have decreased because phenol has been replaced by cyclohexane as the starting material for caprolactam. The production route starting from phenol is less hampered by safety problems than that starting from benzene, which proceeds via cyclohexane oxidation. Bisphenol A, which is obtained from phenol and acetone, has become increasingly important as the starting material for polycarbonates and epoxy resins. Aniline can be obtained from phenol by ammonolysis in the Halcon process. Adipic acid is obtained from phenol by oxidative cleavage of the aromatic ring. Alkylphenols, such as cresols, xylenols, 4-*tert*-butylphenol, octylphenols and nonylphenols, are produced by alkylation of phenol with methanol or the corresponding olefins. Salicylic acid is synthesized by addition of CO₂ to phenol (Kolbe synthesis). Chlorophenols are also obtained directly from phenol. All these products have considerable economic importance because they are used for the production of a wide range of consumer goods and process materials. Examples are preforms, thermosets, insulating foams, binders (e.g. for mineral wool and molding sand), adhesives, laminates, impregnating resins, raw materials for varnishes, emulsifiers and detergents, plasticizers, herbicides, insecticides, dyes, flavours and rubber chemicals.

It is worth noting the recent work on the benzene-free synthesis of phenol¹⁰¹, which is actually a part of longstanding efforts¹⁰² to elaborate the alternatives to benzene. This new

alternative synthesis is based on the aromatization of shikimic acid which is now readily available by the elaboration of a microbe-catalysed synthesis from glucose in near-critical water, where phenol is the primary reaction product. An aqueous solution of shikimic acid is heated to and maintained at 350 °C for 30 min yielding 53% of phenol.

II. MOLECULAR STRUCTURE AND BONDING OF PHENOL

A. The Equilibrium Structure of Phenol in the Ground Electronic State

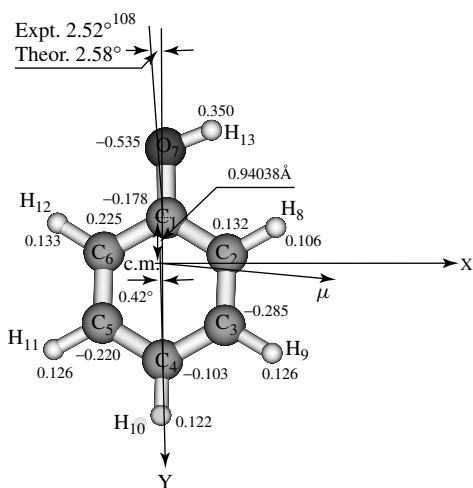
Until the mid-thirties of the 20th century electron diffraction or microwave studies of phenol had not yet been conducted and so, rather peculiarly, the equilibrium configuration of phenol remained uncertain although some indirect evidence suggested its ground electronic state S_0 to be certainly planar. The first X-ray structural data became available by 1938 for several phenolic compounds¹⁰³. At that time, it was suggested that the C–O bond is about 1.36 Å, that is by *ca* 0.07 Å shorter than the C–O bond in aliphatic alcohols. This was accounted for by the decrease in the effective radius of the carbon atom due to the change of hybridization from sp^3 to sp^2 , even though some degree of electron delocalization across the C–O bond could be assumed. Such increase in double-bond character favours a completely planar equilibrium configuration of phenol in its ground electronic state.

This character results from quinonoid resonance structures in addition to the more important Kekulé-type structures¹⁰⁴ and tends to cause the hydrogen atom to be placed in the molecular plane. This leads to two equivalent configurations with the hydrogen of the OH group being on one side of the other of the C–O bond¹⁰⁴. It implies the existence of the activation barrier V_τ of the OH torsion motion around the C–O bond estimated in the mid-thirties as equal to 14 kJ mol^{−1}.

The molecular geometry of phenol was later determined experimentally by microwave spectroscopy^{105–108} and electron diffraction¹⁰⁹ (ED). In 1960, MW experiments¹⁰⁵ of some phenol derivatives showed that their equilibrium configurations are planar (C_s symmetry). In 1966, two possible r_o -structures were determined by examining four new isotopic modifications of phenol¹⁰⁶, and three years later a partial r_s -structure was presented on the basis of the six monodeuteriated species¹⁰⁷. The full r_s -structure of phenol was reported¹⁰⁸ in 1979 and is presented in Table 1¹⁰⁹. Generally speaking, the structure of the phenyl ring in phenol deviates only slightly from the regular isolated phenyl ring. This is shown in Figure 4. All C–H distances are nearly equal, within the experimental uncertainties, although the *para*-distance seems to be shorter than the other ones. The CCC bond angles are slightly perturbed, viz. the bond angle $C_1C_3C_5$ is larger than 120° whereas the $C_2C_6C_4$ angle is smaller than 120°. The angle between the C_6O_7 bond and the C_1 – C_4 axis was reported equal to 2.52°¹⁰⁸. Our calculation performed at the B3LYP/6-31+G(d,p) computational method predicts it to be equal to 2.58°.

Since the first quantum mechanical calculation of phenol performed in 1967 using the CNDO/2 method¹¹⁰, the phenol geometry was considered at a variety of computational levels^{111–125} ranging from the HF to the MP2 method of molecular orbital theory and density functional theory (DFT) employed with several basis sets, mainly of the split valence type as, e.g. 6-31G(d,p) and 6-31+G(d,p). These computational results are summarized in Tables 1–3 and Figure 4. It seems noteworthy that the semi-empirical geometries listed in Table 1 are rather close to the experimental observations. Also, to complete the theoretical picture of the phenol molecule, its theoretical inertia moments calculated at the B3LYP/6-31+G(d,p) level are equal to 320.14639, 692.63671 and 1012.78307 a.u.

Table 3 summarizes the key properties of phenol^{107–130}. Inspecting its rotational constants collected in Table 2, we may conclude that fair agreement between experiment and



Present calculations B3LYP/6-31 + G(d, p):

Dipole moment (D):

$$\mu_x = 1.391 \quad \mu_y = 0.117$$

$$\mu_{\text{total}} = 1.396$$

Quadrupole moment ($D, \text{\AA}^2$):

$$Q_{xx} = 35.911 \quad Q_{yy} = 38.426 \quad Q_{zz} = 45.608$$

$$Q_{xy} = 4.554 \quad Q_{xz} = Q_{yz} = 0$$

Octapole moment ($D, \text{\AA}^3$):

$$Q_{xxx} = 0.595 \quad Q_{yyy} = -6.921 \quad Q_{xyy} = 13.329$$

$$Q_{xxy} = -5.677 \quad Q_{zzz} = 0.146 \quad Q_{yzz} = -5.796$$

$$Q_{zzz} = Q_{yyz} = Q_{xyz} = 0$$

Hexadecapole moment ($D, \text{\AA}^4$):

$$Q_{xxxx} = 283.505 \quad Q_{yyyy} = 500.357$$

$$Q_{zzzz} = 55.514 \quad Q_{xxxy} = 0.991$$

$$Q_{yyxx} = 36.133 \quad Q_{xxyy} = 121.589$$

$$Q_{xxzz} = 68.116 \quad Q_{yyzz} = 108.221$$

$$Q_{zzxy} = 0.269$$

$$Q_{xxxz} = Q_{yyyz} = Q_{zzzx} = Q_{zzzy} =$$

$$Q_{xxyz} = Q_{yyxz} = 0$$

Polarizability (a.u.):

$$\alpha_{xx} = 89.57$$

$$\alpha_{yy} = 43.06$$

$$\alpha_{zz} = 82.94$$

FIGURE 4. Key properties of the planar B3LYP/6-31+G(d,p) phenol molecule in the ground electronic state including the position of its centre of mass (c.m.), Mulliken charges and the direction of its total dipole moment

theory is provided by the MP2 and B3LYP methods (the mean absolute deviations are less than 0.2%) and the B3P86 method (<0.6%) whereas the HF and BLYP methods predict rather large values (*ca* 1.3% and *ca* 1.5%, respectively)¹²⁴. The latter methods have well-known shortcomings, viz. the HF bond distances are too short while the BLYP distances are too large. Regarding in particular the length of the C—O bond, note that BLYP/6-31G(d) gives 1.384 Å although the corresponding MP2/6-31G(d) value of 1.396 Å is larger by 0.012 Å.

B. Molecular Bonding Patterns in the Phenol S_0

Let us start this subsection with somewhat simple arguments about the bonding in the phenol molecule. We may consider the two σ bonds of the oxygen atom as constituted of trigonal hybrids¹³¹. The third coplanar hybrid accommodates one sp^2 lone pair while the pure p orbital is also conjugated with the other p electrons of the phenyl ring.

Speaking at a higher theoretical level, the closed-shell electronic ground-state phenol molecule is described by the 25 occupied molecular orbitals whose 3D patterns are partly pictured in Figure 5. These 25 occupied MOs are partitioned into two classes, the first comprising the seven core orbitals ($1s$ atomic orbitals on the carbon and oxygen atoms) and the second including 18 valence orbitals. The latter represent six σ C—C bonds (all

TABLE 1. Phenol geometry. Bond lengths in Å, bond angles in deg

Experiment				Theory									
MW ^[107]	MW ^[108]	ED ^[109]	MINDO ^a	MINDO/3 ^a	AM1 ^a	PM3 ^a	HF/STO-3G ^[111]	HF/4-31G ^[111]	HF/6-31G ^[111]	HF/6-31G(d) ^[111]	HF/6-31G(d,p) ^[112]	HF/DZP ^[113]	
Bond lengths													
1.398	1.3912	1.3969	1.420	1.419	1.402	1.401	1.397	1.381	1.385	1.385	1.410	1.389	
	1.3944	1.3969	1.405	1.406	1.394	1.390	1.386	1.385	1.389	1.387		1.392	
	1.3954	1.3969	1.405	1.404	1.394	1.390	1.390	1.381	1.385	1.382		1.387	
	1.3954		1.407	1.408	1.397	1.392	1.384	1.387	1.388	1.388		1.390	
	1.3922		1.403	1.403	1.391	1.388	1.382	1.389	1.383	1.381		1.386	
	1.3912		1.423	1.424	1.406	1.402	1.392	1.383	1.386	1.388		1.393	
1.364	1.3745	1.3975	1.359	1.326	1.377	1.369	1.395	1.374	1.377	1.352	1.382	1.354	
	1.0856	1.081	1.090	1.105	1.099	1.096	1.082	1.073	1.074	1.077			
1.076	1.0835		1.091	1.106	1.100	1.095	1.083	1.072	1.073	1.075	1.093		
1.082	1.0802		1.090	1.104	1.099	1.096	1.082	1.071	1.072	1.074	1.092		
	1.0836		1.091	1.107	1.100	1.096	1.083	1.072	1.072	1.075			
	1.0813		1.090	1.104	1.099	1.096	1.082	1.069	1.070	1.074			
0.956	0.9574	0.953	0.948	0.951	0.968	0.949	0.989	0.950	0.949	0.947	0.977	0.944	
Bond angles													
	119.43	118.77	119.6	119.5	119.1	119.0	119.9	119.6	119.4	119.6			
	120.48	120.57	120.6	121.0	120.4	120.4	120.5	120.5	120.4	120.5			
	119.74	119.75	119.8	119.1	120.0	120.1	119.4	119.4	119.4	119.2			
	120.79		120.7	121.4	120.6	120.6	120.8	120.7	120.6	120.7			
	119.22		119.4	119.0	118.9	118.9	119.6	119.6	119.4	119.5			
	120.01		121.2	121.3	120.4	120.9	120.4	120.2	120.3	120.0			
	119.48		119.5	119.1	119.5	119.6	120.3	119.4	119.5	119.4			
	120.25		120.1	120.5	120.1	120.0	120.4	120.3	120.3	120.4			
	119.43		119.5	118.9	119.5	119.6							
	119.23		120.8	121.7	119.5	120.4							
109.0	108.77	106.4	112.8	114.0	107.9	107.9	104.9	114.8	114.7	110.7	108.1	110.9	

TABLE 1. (continued)

Theory														
CAS(8,7) cc- pVDZ ¹¹⁴	CAS(8,9) cc- pVDZ ¹¹⁴	CAS(8,8) cc- pVDZ ¹¹⁵	B3LYP/ 6-31G(d) ¹¹⁶	B3LYP/ 6-31G (dp) ^{a,116}	BLYP/ 6-31G (dp) ¹¹²	B3LYP/ 6-311G (dp) ¹¹⁷	B3LYP/ 6-31+G (dp) ^a	B3LYP/ DZP ¹¹³	BLYP/ 6-311++G (dp) ^a	BLYP/ 6-311++G (2df,2p) ^a	B3LYP/ cc-pVDZ ¹¹⁴	MP2/ DZP ¹¹³	MP2/ 6-31G (dp) ¹¹¹	MP2/ 6-31G (dp) ¹¹²
1.395	1.394	1.394	1.410	1.401	1.389	1.397	1.399	1.404	1.396	1.393	1.394	1.404	1.395	1.396
1.400	1.400	1.400	1.403	1.401	1.401	1.390	1.398	1.402	1.394	1.391	1.400	1.404	1.395	
1.395	1.394	1.394	1.409	1.400	1.395	1.395	1.397	1.400	1.393	1.390	1.394	1.403	1.393	
1.400	1.401	1.400	1.405	1.403	1.392	1.392	1.397	1.404	1.396	1.392	1.401	1.406	1.396	
1.394	1.393	1.394	1.406	1.397	1.393	1.393	1.395	1.400	1.391	1.388	1.393	1.400	1.392	
1.399	1.399	1.399	1.410	1.401	1.396	1.396	1.399	1.405	1.396	1.392	1.399	1.404	1.396	
1.356	1.355	1.355	1.384	1.395	1.351	1.367	1.372	1.373	1.370	1.367	1.355	1.378	1.374	1.372
1.084	1.084	1.085	1.093	1.086	1.086	1.084	1.083	1.088	1.084	1.082	1.084	1.084	1.087	1.082
1.081	1.081	1.083	1.093	1.083	1.075	1.083	1.085		1.083	1.081	1.081	1.086	1.086	1.081
1.082	1.082	1.083	1.094	1.084	1.084	1.084	1.086		1.084	1.082	1.082	1.082	1.087	
1.081	1.081	1.082	1.097	1.083	1.087	1.087	1.085		1.083	1.081	1.081	1.086	1.086	
0.945	0.946	0.945	0.981	0.967	0.943	0.962	0.966	0.968	0.963	0.962	0.946	0.967	0.973	0.965
119.9	119.9	120.0					119.7		119.7	119.8	119.9		119.7	
120.4	120.4	120.4				120.5	120.5		120.5	120.4	120.4		120.5	
119.3	119.3	119.3				119.3	119.3		119.3	119.3	119.3		119.4	
120.6	120.6	120.6				120.8	120.8		120.8	120.8	120.6		120.6	
119.8	119.8	119.8				119.5	119.5		119.6	119.6	119.8		119.6	
120.1	120.1	120.0				120.1	120.1		120.0	120.0	120.0		120.1	
119.4	119.4	119.4				119.4	119.3		119.3	119.3	120.1		119.2	
120.3	120.4	120.4				120.3	120.3		120.3	120.3	119.4		120.3	
						119.3	119.3		119.3	119.3	120.4			
						119.0	119.0		119.0	119.1				
110.2	110.2	110.3			110.9	109.9	108.9	108.9	109.7	109.9	110.2	108.3	108.4	108.5

^aPresent work.

TABLE 2. Rotational constants (in MHz) of phenol in its electronic ground state. The values in parentheses are the deviation from the experimental values in percent

	HF/6- 31G(d,p) ¹²⁴	HF/6- 311++G (d,p) ¹²⁴	CAS(8,7)/ cc-pVDZ ¹²⁶	MP2/6- 31G(d,p) ¹²⁴	BLYP/6- 31G(d,p) ¹²⁴	B3LYP/6- 31G(d,p) ¹²⁴	B3LYP/6- 31++G(d,p) ^a	B3LYP/6- 311++G(d,p) ^a	B3LYP/6- 311++G (2df,2p) ^a	B3P86/6- 31G(d,p) ¹²⁴	MW Expt. ¹⁰⁸	UV Expt. ¹¹⁸	UV Expt. ¹²⁷
A	5750.0	5752.6	5659.3(0.16)	5650.6	5563.7	5650.4	5637.3	5667.2	5695.6	5679.9	5650.5154	5726.63	5650.515
B	2659.1	2660.0	2623.3(0.16)	2614.6	2573.7	2614.1	2607.3	2618.0	2629.6	2630.0	2619.2360	2660.0	2619.236
C	1818.3	1818.9	1792.4(0.14)	1787.5	1759.7	1787.3	1782.8	1790.8	1799.0	1797.3	1789.8520	1820.12	1782.855

^aPresent work.

TABLE 3. Dipole moment of phenol. Experimental data are partly reproduced from Reference 128^a

Experiment			Theory	
$\mu(\text{D})$	Phase of solvent ^b	$T(^{\circ}\text{C})$	$\mu(\text{D})$	Method
1.40 \pm 0.03	gas	20	1.73	CNDO/2 ¹¹⁰
1.41	gas	175	1.418	B3LYP/6-31+G(d,p) ¹²⁹
2.22	liq	20	1.16	HF/MiDi ¹³⁰
1.45	B	25	1.52	SM5.42R/HF/MiDi ¹³⁰
1.45	B	25		
1.45	B	30		
1.46	B	n.s.		
1.47 \pm 0.02	B	20		
1.5	B	70		
1.53 \pm 0.03	B	20		
1.53	B	26		
1.54	B	20		
1.54	B	25		
1.57	B	20		
1.59	B	(22)		
1.65	B	25		
1.72	B	25		
1.75	B	20		
1.80	D	20		
1.86	D	25		
1.92	D	20		
1.39	CCl ₄	30		
1.40	CCl ₄	20		
1.46 \pm 0.03	CCl ₄	10–60		
1.49	CCl ₄	20		
1.50	CCl ₄	20		
1.53	CCl ₄	25		
1.55	CCl ₄	27		
1.37	<i>c</i> -Hx	30		
1.32 \pm 0.03	<i>c</i> -Hx	20		
1.33 \pm 0.03	<i>c</i> -Hx	20		
1.39	<i>c</i> -Hx	30		
1.43	<i>c</i> -Hx	25		
1.37	Hp	20		
1.44	Hp	20		
1.86	Hp	20		
1.44 – 1.53	Tol	0–75		
1.46	Tol	30		
1.38	CS ₂	20		
1.39	CS ₂	30		
1.64	CS ₂	25		
2.14	Ether	25		
2.14	Ether	20		
2.29	Ether	20		
1.45	ClB	20		
1.53 ¹²⁸	B			

^aSee also Figure 4.^bB = benzene, D = dioxan, *c*-Hx = cyclohexane, Hp = *n*-heptane, Tol = toluene, ClB = chlorobenzene; n.s. = not specified.

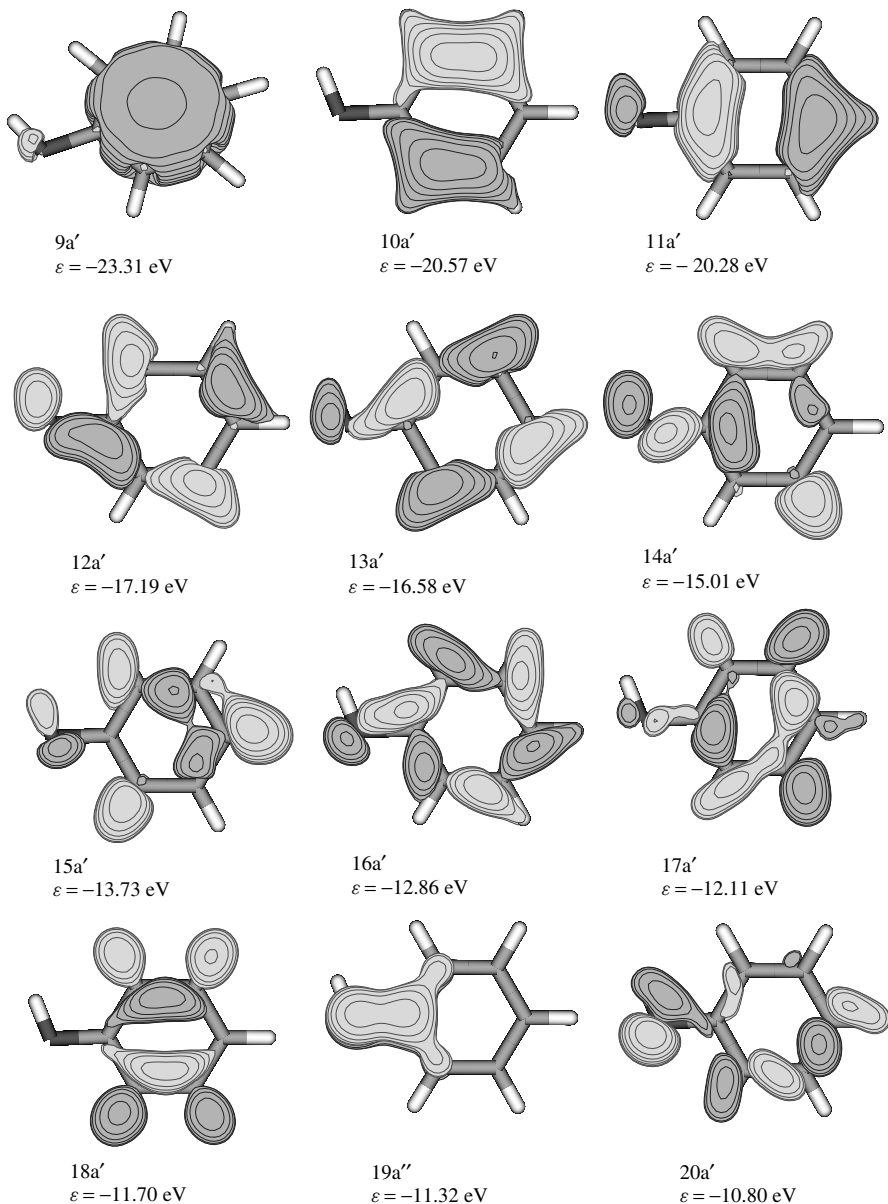


FIGURE 5. Some molecular orbital patterns of the electronic ground state of the phenol molecule. Due to the C_s symmetry of phenol, its MOs are characterized by the a' or a'' irreducible representations of this group; ε denotes the corresponding orbital energy in eV

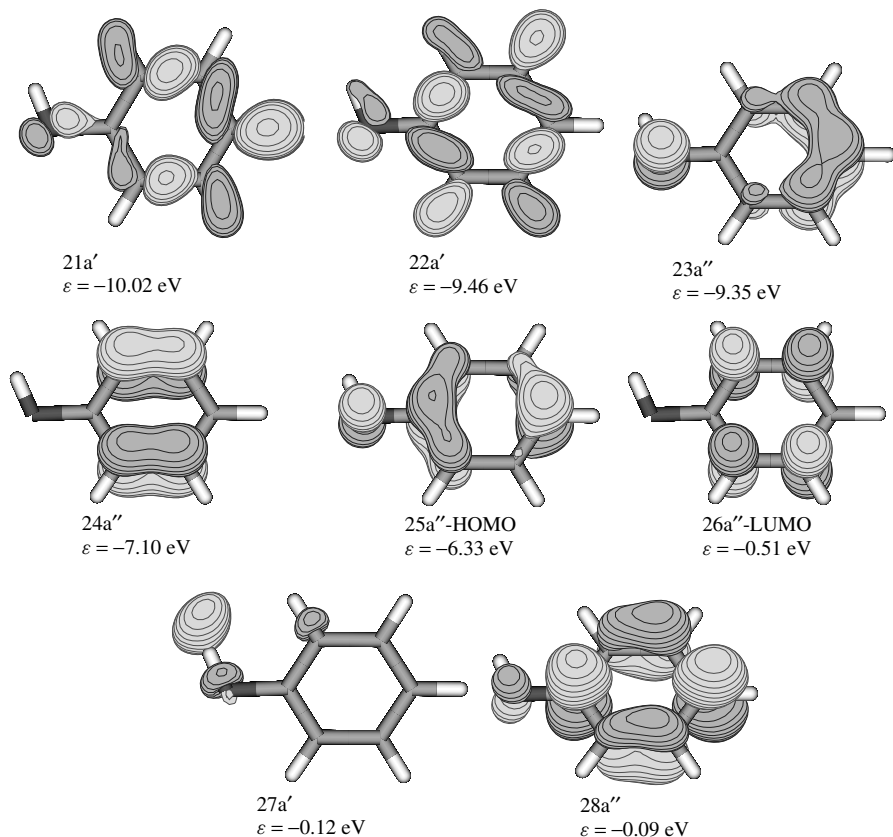


FIGURE 5. (continued)

of a' symmetry), five σ C—H bonds (also all of a' symmetry), the C—O σ bond (one a' orbital), the oxygen σ -type lone pair (one a' orbital), the oxygen p -type lone pair (19 a'' orbital) and, finally, the C—C π -bonds (three a'' orbitals, namely 23a'', 24a'' and the HOMO 25a''). In addition, three unoccupied π molecular orbitals, the LUMO 26a'', 27a' and 28a'', are also shown in Figure 5.

In Table 4, we collect the natural atomic charges (nuclear charge minus the summed natural populations of the natural atomic occupancies, NAOs, on the atom) and the total core, valence and Rydberg populations on each atom. Table 4 presents a slightly larger positive charge on the hydroxyl hydrogen atom H₁₃ relative to other atoms, arising due to the proximity of the electronegative oxygen atom. The other hydrogen atom H₈ next to the hydroxyl group is characterized by the lowest positive charge. This feature originates from electron donation from the ring to the corresponding C—H antibonding orbital taking place in order to decrease the electrostatic repulsion between the neighboring C—H and O—H bonds.

The HOMO and LUMO are of particular interest. As seen in Figure 5, the shape of the HOMO is generated by the out-of-phase overlap of the p_z AOs localized, on the one

TABLE 4. Natural atomic orbital (NAO) occupancies, natural population of the MOs, summary of natural population analysis and Mulliken atomic charges of the electronic ground state of phenol

<i>NAOs</i>					
N	Atom	N lm	Type(AO)	Occupancy	Energy (eV)
1	C	1 s	Cor(1s)	1.998	-9.95
2	C	1 s	Val(2s)	0.947	-0.16
3	C	1 s	Ryd(3s)	0.000	1.63
4	C	1 px	Val(2p)	1.170	-0.05
5	C	1 px	Ryd(3p)	0.004	1.11
6	C	1 py	Val(2p)	1.114	-0.04
7	C	1 py	Ryd(3p)	0.005	0.97
8	C	1 pz	Val(2p)	1.049	-0.10
9	C	1 pz	Ryd(3p)	0.000	0.80
10	C	2 s	Cor(1s)	1.998	-10.04
11	C	2 s	Val(2s)	0.832	-0.15
12	C	2 s	Ryd(3s)	0.000	1.58
13	C	2 px	Val(2p)	1.105	-0.06
14	C	2 px	Ryd(3p)	0.006	1.03
15	C	2 py	Val(2p)	0.762	-0.04
16	C	2 py	Ryd(3p)	0.008	1.01
17	C	2 pz	Val(2p)	0.991	-0.12
18	C	2 pz	Ryd(3p)	0.001	0.80
19	C	3 s	Cor(1s)	1.998	-9.96
20	C	3 s	Val(2s)	0.944	-0.17
21	C	3 s	Ryd(3s)	0.000	1.63
22	C	3 px	Val(2p)	1.165	-0.06
23	C	3 px	Ryd(3p)	0.004	1.12
24	C	3 py	Val(2p)	1.121	-0.06
25	C	3 py	Ryd(3p)	0.006	0.94
26	C	3 pz	Val(2p)	1.087	-0.11
27	C	3 pz	Ryd(3p)	0.000	0.79
28	C	4 s	Cor(1s)	1.998	-9.96
29	C	4 s	Val(2s)	0.944	-0.17
30	C	4 s	Ryd(3s)	0.000	1.62
31	C	4 px	Val(2p)	1.179	-0.05
32	C	4 px	Ryd(3p)	0.005	1.14
33	C	4 py	Val(2p)	1.100	-0.04
34	C	4 py	Ryd(3p)	0.004	0.94
35	C	4 pz	Val(2p)	0.989	-0.10
36	C	4 pz	Ryd(3p)	0.000	0.79
37	C	5 s	Cor(1s)	1.998	-9.95
38	C	5 s	Val(2s)	0.943	-0.16
39	C	5 s	Ryd(3s)	0.000	1.63
40	C	5 px	Val(2p)	1.070	-0.04
41	C	5 px	Ryd(3p)	0.005	0.84
42	C	5 py	Val(2p)	1.208	-0.05
43	C	5 py	Ryd(3p)	0.004	1.24
44	C	5 pz	Val(2p)	1.041	-0.10
45	C	5 pz	Ryd(3p)	0.000	0.80
46	C	6 s	Cor(1s)	1.998	-9.96
47	C	6 s	Val(2s)	0.946	-0.16
48	C	6 s	Ryd(3s)	0.000	1.63
49	C	6 px	Val(2p)	1.178	-0.05

TABLE 4. (continued)

NAOs N	Atom	N lm	Type(AO)	Occupancy	Energy (eV)
50	C	6 px	Ryd(3p)	0.005	1.15
51	C	6 py	Val(2p)	1.104	-0.04
52	C	6 py	Ryd(3p)	0.004	0.93
53	C	6 pz	Val(2p)	0.986	-0.10
54	C	6 pz	Ryd(3p)	0.000	0.79
55	O	7 s	Cor(1s)	1.999	-18.81
56	O	7 s	Val(2s)	1.664	-0.93
57	O	7 s	Ryd(3s)	0.000	3.22
58	O	7 px	Val(2p)	1.628	-0.30
59	O	7 px	Ryd(3p)	0.000	1.79
60	O	7 py	Val(2p)	1.467	-0.29
61	O	7 py	Ryd(3p)	0.001	1.62
62	O	7 pz	Val(2p)	1.850	-0.29
63	O	7 pz	Ryd(3p)	0.000	1.48
64	H	8 s	Val(1s)	0.765	0.06
65	H	8 s	Ryd(2s)	0.001	0.71
66	H	9 s	Val(1s)	0.757	0.09
67	H	9 s	Ryd(2s)	0.000	0.70
68	H	10 s	Val(1s)	0.757	0.09
69	H	10 s	Ryd(2s)	0.000	0.70
70	H	11 s	Val(1s)	0.756	0.09
71	H	11 s	Ryd(2s)	0.000	0.70
72	H	12 s	Val(1s)	0.745	0.09
73	H	12 s	Ryd(2s)	0.001	0.71
74	H	13 s	Val(1s)	0.546	0.05
75	H	13 s	Ryd(2s)	0.001	0.82

Natural population of the MOs

Core	13.990 (99.9319% of 14)
Valence	35.927 (99.7975% of 36)
Natural Minimal Basis	49.917 (99.8352% of 50)
Natural Rydberg Basis	0.082 (0.1648% of 50)

Summary of natural population analysis

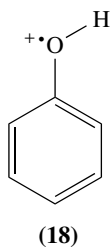
Atom N	Charge	Core	Valence	Rydberg	Total
C 1	-0.252	1.999	4.234	0.018	6.252
C 2	0.315	1.998	3.662	0.022	5.684
C 3	-0.284	1.999	4.267	0.018	6.284
C 4	-0.183	1.999	4.165	0.018	6.183
C 5	-0.236	1.999	4.218	0.018	6.236
C 6	-0.182	1.999	4.165	0.017	6.182
O 7	-0.678	1.999	6.665	0.013	8.678
H 8	0.200	0.000	0.797	0.002	0.799
H 9	0.204	0.000	0.793	0.002	0.795
H 10	0.206	0.000	0.791	0.002	0.793
H 11	0.204	0.000	0.793	0.002	0.795
H 12	0.217	0.000	0.780	0.002	0.782
H 13	0.467	0.000	0.528	0.004	0.532
<Total>	0.000	13.994	35.863	0.142	50.000

(continued overleaf)

TABLE 4. (continued)

<i>Mulliken charges on atoms</i>	
1 C	−0.186
2 C	0.295
3 C	−0.223
4 C	−0.184
5 C	−0.195
6 C	−0.185
7 O	−0.607
8 H	0.173
9 H	0.187
10 H	0.182
11 H	0.187
12 H	0.199
13 H	0.357

hand, on the carbon atoms C_1 , C_2 and C_6 , and, on the other hand, on C_4 and the oxygen atom. The LUMO shape is quite different and composed of the out-of-phase overlap of the p_z AOs on the C_2 , C_3 , C_5 and C_6 . Both HOMO and LUMO possess two nodal surfaces perpendicular to the phenolic ring. Both frontier orbitals have negative orbital energies: $\varepsilon_{\text{HOMO}} = -6.33$ eV and $\varepsilon_{\text{LUMO}} = -0.51$ eV. According to Koopmans' theorem^{132, 133}, the Koopmans ionization potential, which is simply the HOMO energy taken with the opposite sign, might be in general considered as a good approximation to the first vertical ionization energy. Therefore, in the case of phenol, $\varepsilon_{\text{HOMO}}$ must be interpreted as the energy required to remove a π electron from phenol to form phenol radical cation $\text{PhOH}^{\bullet+}$ (cf. **18** for one of its many possible resonance structures). As seen in Section 1, the experimental value of the adiabatic first ionization energy IE_a of phenol is equal to 8.49 ± 0.2 eV and settled to 8.51 eV or 68639.4 cm^{-1} ^{134, 135} or 68628 cm^{-1} ¹³⁶. Interestingly, it is lower by nearly 71 kJ mol^{-1} than $\text{IE}_a(\text{benzene}) = 74556.58 \pm 0.05 \text{ cm}^{-1}$ ¹³⁷. Summarizing, we may conclude that Koopmans' theorem is rather inadequate for phenol, even in predicting its vertical ionization energy (for a further discussion see Reference 131, p. 128).



In order to theoretically determine the ionization energy of phenol, the same method/basis should be employed for both parent and cation. Table 5 summarizes the optimized geometries and the energies (including ZPVE) of phenol and phenol radical cation calculated using the B3LYP method in conjunction with 6-31G(d,p) and 6-311++G(d,p) basis sets. It is interesting to notice a rather drastic change in the geometry of phenol radical cation compared to the parent phenol molecule (Table 5), especially in the vicinity of the carbonyl group, whereas the difference between IE_{vert} and IE_{ad} is

TABLE 5. The B3LYP data of phenol and phenol radical cation^{a,b}

Geometry	Phenol		Phenol radical cation	
	6-31G(d,p)	6-311++G(d,p)	6-31G(d,p)	6-311++G(d,p)
C ₁ –C ₂	1.399	1.396	1.433	1.431(+0.035)
C ₂ –C ₃	1.396	1.394	1.371	1.368(–0.026)
C ₃ –C ₄	1.395	1.393	1.425	1.423(–0.030)
C ₄ –C ₅	1.398	1.396	1.418	1.416(+0.020)
C ₅ –C ₆	1.393	1.391	1.372	1.369(–0.021)
C ₁ –C ₆	1.399	1.396	1.438	1.435(+0.039)
C ₁ –O ₇	1.368	1.370	1.312	1.310(–0.060)
O ₇ –H ₁₃	0.966	0.963	0.975	0.972(+0.009)
C ₁ O ₇ H ₁₃	108.9	109.7	113.6	113.8(+4.1)
–Energy +307				
	0.478469	0.558732	0.183858	0.252608
–Energy _{vert} ^c + 307			0.176780	0.245650
ZPVE + 65				
	0.765	0.229	0.745	0.295
IE _{ad}			8.016	8.333
			7.03 HF/DZP ¹¹³	
			8.70 MP2/DZP ¹¹³	
			8.15 B3LYP/DZP ¹¹³	
IE _{vert}			8.209	8.519

^aThe phenol radical cation have recently been studied theoretically^{113, 138, 140}. See different properties in Reference 139.

^bBond lengths are given in Å, bond angle in degrees, energies in hartree, ZPVE in kJ mol^{–1} and ionization energy in eV. The atomic numbering is indicated in Chart 1. Deviations in the bond lengths of phenol radical cation from those of phenol are shown in parentheses.

^cThe energy_{vert} of phenol radical cation is determined at the corresponding geometry of the parent phenol.

rather small. The potential energy surface of the ionized phenol will be discussed in a subsequent section.

C. Atom-in-Molecule Analysis

In this subsection, we briefly review the use of the function $L(\mathbf{r})$ of the electronic ground-state phenol which is defined as minus the Laplacian of its electron density, $\nabla_r^2 \rho(\mathbf{r})$, fully in the context of Bader’s ‘*Atoms in Molecule*’ (AIM) approach^{141, 142} (the electronic localization function is discussed below). The topology of $L(\mathbf{r})$ can be almost faithfully mapped onto the electron pairs of the VSEPR model^{143, 144}. The topology of the one-electron density $\rho(\mathbf{r})$ (see, e.g., Reference 145 and references therein for the definition) is fully understood within the AIM theory resulting in its partition which defines ‘*atoms*’ inside a molecule or a molecular aggregate via the *gradient vector field* $\nabla_r \rho(\mathbf{r})$. Such a vector field is a collection of gradient paths simply viewed as curves in the three-dimensional (3D) space following the direction of steepest ascent in $\rho(\mathbf{r})$. Therefore, the meaning of a gradient path is absolutely clear: it starts and ends at those points where $\nabla_r \rho(\mathbf{r})$ vanishes. These points are called *critical points* (CPs). The CPs of $\rho(\mathbf{r})$ are special and useful points of the corresponding molecule.

The classification of the critical points is the following¹⁴². There are three types of CPs: maximum, minimum or saddle point. In 3D, one has two different types of saddle points.

CPs of the 3D function $\rho(\mathbf{r})$ can be classified in terms of the eigenvalues λ_i ($i = 1, 2$ and 3) of the Hessian of $\rho(\mathbf{r})$, which is defined as $\nabla^2\rho(\mathbf{r})$ and is actually a 3×3 matrix evaluated at a given CP. Therefore, a given CP is classified by an (r,s) pattern, where r is the rank of this CP equal to the number of non-zero eigenvalues of the Hessian matrix and s is the signature equal to the sum of the signs of the eigenvalues. One example is worth discussing. One type of saddle point has two non-zero negative eigenvalues and one which is strictly positive, so its rank $r = 3$ and its signature $s = (-1) + (-1) + 1 = -1$, and therefore this CP is denoted as $(3, -1)$ CP. Such a CP is called a *bond critical point* because it indicates the existence of a bond between two nuclei of a given molecule. The bond critical points are linked to the adjacent nuclei via an *atomic interaction line*. This line in fact consists of a pair of gradient paths, each of which originates at the bond CP and terminates at a nucleus. The set of all atomic interaction lines occurring in a given molecule constitutes the *molecular graph*.

The AIM analysis of the electron density and the Laplacian of the electron density have been performed at the B3LYP/cc-pVDZ level using the MORPHY suite of codes¹⁴⁶. The resulting AIM charges are given in Table 6. In Figures 6 and 7, we display the molecular graph $L(\mathbf{r})$ from different views of the one-electron density of the electronic ground-state phenol. Thus, the regions of local charge concentration correspond to the maxima in $L(\mathbf{r})$ and the regions of local charge depletion to minima in $L(\mathbf{r})$. Figure 6 shows the geometric positions of all the critical points in the valence shell charge concentration (VSCC) graph of phenol. The graph contains 87 CPs in total, 27 $(3, -3)$ CPs, 41 $(3, -1)$ CPs and 19 $(3, +1)$ CPs. The $(3, -3)$ CPs in $L(\mathbf{r})$ can be separated into three subsets: the two non-bonding maxima of oxygen; the bonding maxima between two carbons, oxygen and carbon, carbon and hydrogen and oxygen and hydrogen; the nuclear maxima, each virtually coincident with the hydrogen nucleus. The $(3, -1)$ CPs in general have a function which is analogous to a bond critical point, i.e. to link maxima. We trace the gradient paths in $L(\mathbf{r})$ starting from the $(3, -1)$ CPs. Usually, these would be expected to connect maxima and this is the case for the overwhelming majority of $(3, -1)$ CPs for phenol but, as may be seen occasionally in $\rho(\mathbf{r})$ ¹⁴², we observe two $(3, -1)$ CPs connected in the vicinity of the oxygen atom. The presence of this unusual connectivity, generally only observed for ‘conflict’ structures, means that a planar graph cannot be drawn for the VSCC.

Figure 7 displays the geometric positions of all the CPs in the valence shell charge depletion (VSCD) graph of phenol. The graph contains 55 $(3, -1)$ CPs, 80 $(3, +1)$ CPs and 22 $(3, +3)$ CPs. The VSCD graph is considerably more complex than the VSCC one

TABLE 6. AIM charges of the ground-state phenol

	Charge	Dipole _x	Dipole _y	Dipole _z
C1	0.506	0.025	0.661	-0.000
C2	-0.014	0.086	0.014	0.000
C3	0.016	0.037	0.037	0.000
C4	0.000	-0.004	0.078	0.000
C5	0.014	-0.042	0.050	0.000
C6	0.004	-0.122	0.021	0.000
H8	-0.020	0.111	-0.074	0.000
H9	-0.002	0.114	0.065	0.000
H10	-0.005	-0.000	0.133	0.000
H11	-0.001	-0.115	0.064	0.000
H12	0.015	-0.117	-0.063	0.000
O7	-1.111	0.254	0.100	0.000
H13	0.600	0.158	-0.057	0.000

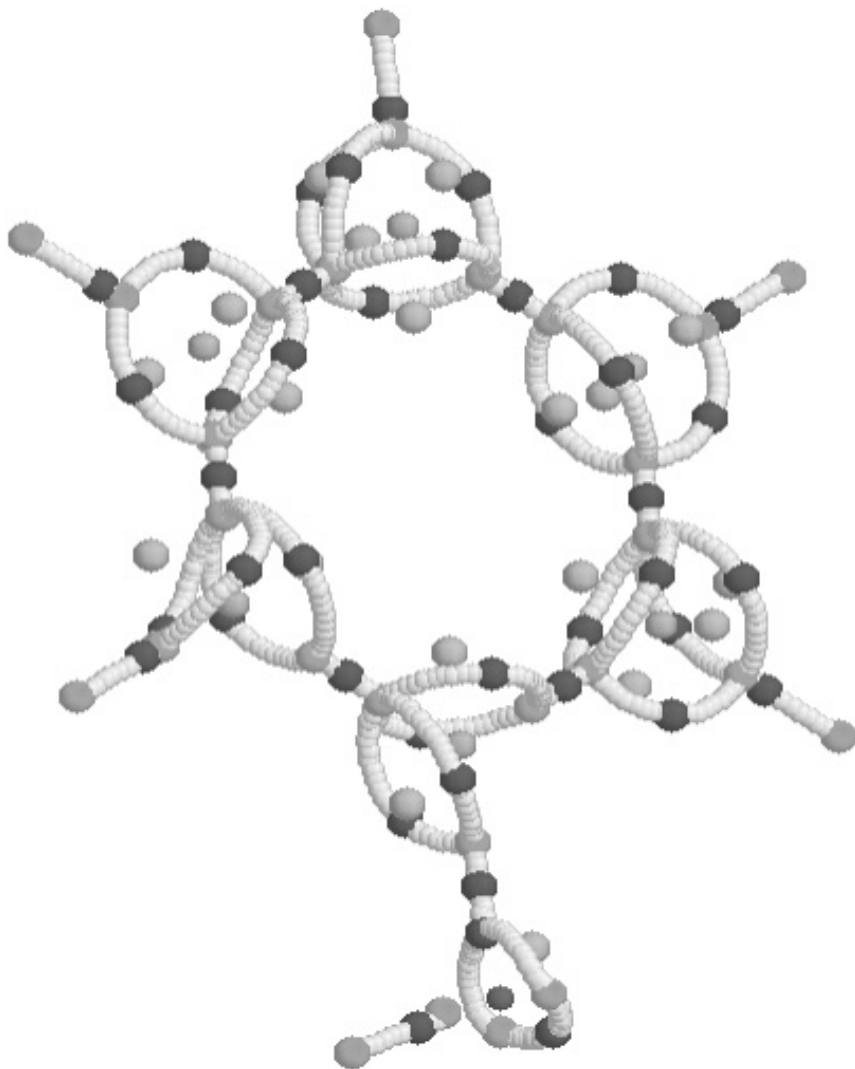


FIGURE 6 (PLATE 1). The VSCC graph for phenol. The oxygen atom is marked in red. The green spheres therein are the CPs $(3, -3)$ (maxima) in the phenolic $L(r)$ while the violet ones determine the $(3, -1)$ CPs. The yellow spheres correspond to the $(3, +1)$ CPs. The domain interaction lines (in light gray) link two $(3, -3)$ CPs via a $(3, -1)$ CP

and encompasses the whole molecule. In reality, of course, the separation of the VSCC and VSCD graphs is artificial; however, it allows for a much easier visual understanding of the significance of the two. The gradient paths belonging to the VSCC graph define the connectivities of the charge concentration maxima (*attractors*); the gradient paths belonging to the VSCD graph indicate the extensions of the *basins* of these attractors. Finally, the principal AIM properties of the atoms of phenol are collected in Table 7.

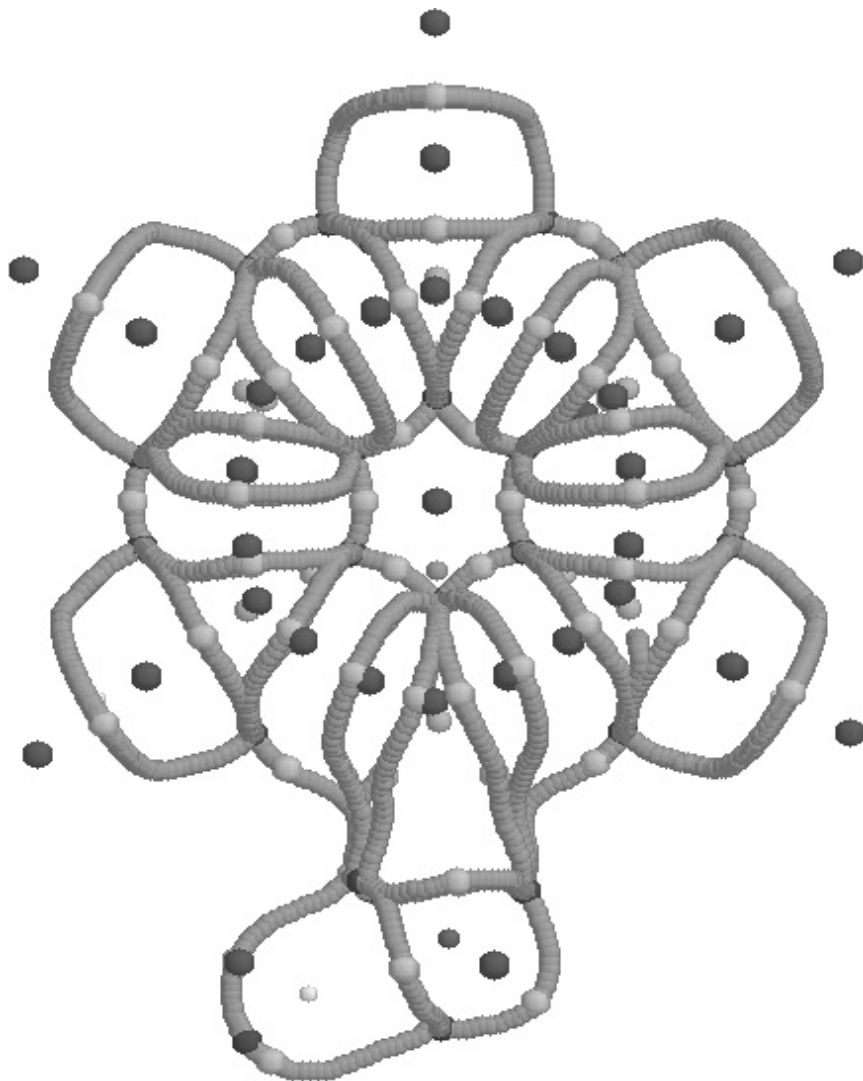


FIGURE 7 (PLATE 2). The VSCD graph for phenol. The oxygen atom is marked in red and the hydrogen in white. The brown spheres therein are the CPs $(3, +3)$ (minima) in the phenolic $L(r)$ while the purple ones determine the $(3, -1)$ CPs. The yellow spheres correspond to the $(3, +1)$ CPs. The $(3, +1)$ CPs link the $(3, +3)$ CPs via a pair of gradient paths shown in white, each of which is repelled by a $(3, +3)$ CP

D. Vibrational Modes

The phenol molecule has 13 atoms, and is therefore characterized by the 33 normal vibrational modes. Their overtone and combination bands are infrared active. The proper assignment of the fundamental vibrational modes of phenol in its electronic ground state

TABLE 7. The AIM properties of the ground-state phenol

Total volume	3727.90
Total molecular dipole moment	0.5124
Average $L(\Omega)^{141,142}$	-0.34E-03
Total $K(\Omega)^{141,142}$	304.76268
Total $E(\Omega)^{141,142}$	-307.49493
E(wave function)	-307.49478
Total charge	-49.999416285
Z + Q(total) ^{141,142}	0.000583715
Total dipole (in components)	-0.0001 0.3853 1.0577

has a long history that started in 1941 by assigning the observed Raman bands¹⁴⁷ of phenol confined to the region above 600 cm^{-1} followed by a study on the changes of its vibrational spectra under association¹⁴⁸. The first examination of the phenol-OD infrared spectra was performed in 1954–1955^{149, 150}. In the electronic ground state S_0 , the assignment of all fundamental vibrations of phenol was based on the earlier studies^{151–153}. The lowest vibrational mode, a so-called mode 10b, had been assigned to 242 cm^{-1} in 1960¹⁵¹ and to 241 cm^{-1} one year later¹⁵² from the Raman spectra of molten phenol. In 1981, a slightly lower mode at 235 cm^{-1} was observed¹⁵⁴ by Raman spectroscopy in the gas phase. The frequency of the mode 10b in phenol and phenol-*d*1 were determined¹⁵⁵ at 225.2 and 211.5 cm^{-1} , respectively, and this led to the conclusion that the assignment of Reference 153 might be incorrect. Interestingly, during the last two decades, this mode and its correct value have not received much attention because the values predicted by a variety of *ab initio* methods appear to be lower than the experimental ones^{151–155}.

The vibrational modes of the ground-state phenol were examined by a number of spectroscopic techniques including UV-VIS^{154, 156–158}, IR for the vapour^{151, 152, 159, 160}, and the IR and Raman spectra in the solid and liquid phases^{151, 152, 159, 161, 162}, and microwave spectroscopy^{105, 107, 163}, see also References 164–166. They are collected in Table 8, where both nomenclatures by Wilson and coworkers¹⁵⁴ and Varsanyi¹⁶⁷ are used. Recently, the vibrational modes of phenol have become a benchmark for testing *ab initio* and density functional methods^{111, 124, 168–170}. The Hartree-Fock calculations of the vibrational spectrum of phenol were first performed using the 6-31G(d,p) basis set¹²². An MP2 study with the same basis set was later carried out¹²¹. A combination¹¹² of three methods, viz. HF, MP2 and density functional BLYP, in conjunction with the 6-31G(d,p) basis was used to study the phenol spectrum and to make the complete and clear assignment of its vibrational modes (see Table 9).

In Figure 8 we display the normal displacements and in Table 10 we provide the corresponding vibrational assignments. Let us start from the end of Table 10 and Figure 8 where the stretching ν_{OH} mode is placed and its normal displacement is shown. It is a pure localized mode^{111, 112}. Furthermore, it is a well-known mode subject to numerous studies related to the hydrogen-bonding abilities of phenol¹⁷³. Its second overtone in phenol and the phenol halogen derivatives has been studied experimentally¹⁷⁴.

The OH group of phenol participates in two additional modes, in-plane and out-of-plane bending vibrations. The latter is also called the torsional mode τ_{OH} observed near 300 cm^{-1} (see Table 8) in the IR spectra of phenol vapour and of dilute solutions of phenol in *n*-hexane¹⁵². In the associated molecules, it appears as a rather broad featureless band in the region of $600\text{--}740\text{ cm}^{-1}$ ¹⁴⁹. It results from the hydrogen-bonded association. The spectra of liquid and solid phenol-OD also exhibit a variety of broad bands near 500 cm^{-1} . The first overtone of the τ_{OH} was found at 583 cm^{-1} in the IR spectrum of phenol vapour¹⁵². This assignment of the torsional mode allows one to model the torsional motion of the OH group of phenol by assuming that it is described by the

TABLE 8. Experimental (infrared and Raman) and theoretical vibrational spectra of phenol

Nomenclature		Sym	Expt.							
Wilson and coworkers ¹⁵⁴	Vars ányi ¹⁶⁷		IR ¹⁵³ Raman ¹⁵⁴	IR ^{171,172} Raman ¹⁶⁷	IR ¹¹¹ Raman ¹¹¹	IR ¹⁶⁹	HF/6-31G(d,p) ¹¹²		MP2/6-31G(d,p) ¹¹²	
			ν A	ν	ν	ν	ν A		ν A	
11	10b	a''	244	241	242	225 ^a	256.2	5	226.8	0.8
$\tau(\text{OH})$		a''	309	300	310		314.2	141	327.5	126
16a		a''	409	410	410	404 ^b	461.2	0.3	403.3	0.9
16b	15	a''	403	408	420		440.6	11	404.9	10
16b		a'	503	500	503	504 ^b	568.2	7	522.0	3
6a		a''	527	526	526	526	574.3	2	535.1	1
6b		a'	619	617	618	618	678.6	0.3	632.6	0.3
4		a'	686	688	687	686 ^b	767.8	13	464.8	4
10b	11	a''	751	749	752		846.7	83	736.0	78
10a		a''	817	825	823		924.2	0.0	814.3	0.2
12	1	a''	823	810	810	820	892.0	20	837.1	18
17b		a''	881	881	881		996.0	13	849.7	0.7
17a		a''	973	958	956		1090.1	0.0	904.8	0.5
5		a''	995	978	973		1111.4	0.6	913.4	0.1
1	12	a'	1000	999	999	999	1085.2	3	1024.8	0.3
18a		a'	1025	1026	1026	1026	1122.8	4	1064.5	5
15	18b	a'	1072	1071	1070		1176.9	10	1117.0	12
9b		a'	1151	1145	1150		1197.0	33	1205.6	10
9a		a'	1169	1167	1176		1282.1	0.4	1218.1	0.5
$\beta(\text{COH})$		a'	1177	1207	1197	1174	1291.0	85	1221.0	157
7a	13	a'	1261	1259	1261	1261	1404.4	114	1320.3	66
3		a'	1277	1313	1361		1488.6	36	1388.2	22
14		a'	1343	1354	1344	1349	1370.5	53	1478.5	12
19b		a'	1472	1465	1472		1635.2	29	1531.9	22
19a		a'	1501	1497	1501	1505	1671.2	76	1567.2	54
8b		a'	1610	1596	1604		1797.8	45	1681.2	27
8a		a'	1603	1604	1609		1810.6	66	1695.6	39
13		a'	3027	3030	3021		3326.4	16	3241.9	12
7b		a'	3049	3044	3046		3343.7	0.2	3261.4	0.1
2		a'	3063	3048	3052		3354.1	29	3269.6	16
20b		a'	3070	3076	3061		3370.9	28	3284.3	15
20a		a'	3087	3091	3074		3379.6	7	3290.6	5
$\nu(\text{OH})$		a'	3656	3623	3655		4197.2	84	3881.8	53

^aDetermined from the first and third overtone and the combination band with the mode 1a.^bCalculated from the first overtone of these normal modes.^cPresent work (see page 37).

potential $V_{\tau}(1 - \cos 2\theta)/2^{152}$. Here, θ is the torsional angle and V_{τ} is the corresponding barrier height. Within this model, the reduced moment of inertia can be chosen equal to $1.19 \times 10^{-40} \text{ g cm}^2$.

The β_{COH} is the in-plane bending of the OH group placed at around $1175\text{--}1207 \text{ cm}^{-1}$. It is observed at 1176.5 cm^{-1} in the IR spectrum of phenol vapour^{152–154}. This band is shifted to *ca* 910 cm^{-1} in dilute solution under deuteration¹⁵³ and gives rise to a broad absorption ranging from 930 to 980 cm^{-1} in the spectrum of crystal. The first HF/6-31G(d,p) calculations¹²² predicted it at 1197.3 cm^{-1} (the scaled value is 1081 cm^{-1} ¹⁷⁵).

Twenty-four vibrational modes of phenol are well assigned to the phenyl ring modes because they are not so sensitive to the nature of the substituent¹⁷⁶. On the other hand, the six modes which involve a substantial motion of the phenyl and CO groups are rather sensitive to the isotopic substitution of OH by OD. These are the following modes¹⁵²: 1260 (1253), 814 (808), 527 (523), 503 (503), 398 (380) and 242 (241) cm^{-1} for phenol and phenol–OD (in parentheses), respectively.

TABLE 8. (continued)

Theor.						Expt.			
BLYP/6-31G(d,p) ¹¹²		B3LYP/6-31G(d,p) ¹²⁴	B3LYP/6-311++G(d,p) ¹²⁴	B3LYP/6-311++G(2df,2p) ^c		Expt-Phenol-d ₁ IR ¹⁵³		Phenol-d ₅ IR ¹⁵³	
ν	A			ν	A	ν	A	ν	A
225.4	0.2	234	227	229.5	1	232	2		
384.6	108	365	338	338.4	100	246	5	307	30
406.6	0.9	405	403	406.4	10				
394.0	9	421	414	421.7	1	382	6	386	3
499.2	6	518	508	514.9	14	503	15	431	20
520.7	1	536	537	537.5	2	522	3	513	2
616.1	0.3	633	633	634.3	0	617			
674.8	8	699	667	690.7	18	687	35	550	25
732.2	44	761	745	761.6	69	751	50	625	10
788.9	0.0	834	828	827.3	0				
805.0	17	822	816	830.5	21	805	8	754	2
846.2	3	884	834	894.0	6	881			
911.1	0.0	955	948	970.1	0				
939.5	0.1	981	969	986.5	0	997	4	960	
982.7	2	1013	1012	1017.6	3				
1017.4	3	1051	1043	1045.0	5	1025	2		
1069.8	10	1102	1094	1095.0	14				
1156.6	8	1183	1177	1177.8	36	1150	5		
1165.7	5	1197	1191	1191.9	90	1168	20		
1173.3	146	1200	1192	1193.4	32	917	44	1179	802
1254.0	64	1305	1275	1280.4	89	1257	90	1187	75
1329.7	7	1365	1349	1347.5	7			1021	15
1349.3	29	1378	1369	1375.2	23	1309	4	1300	12
1468.8	28	1514	1500	1505.3	23	1465		1372	40
1495.5	34	1547	1528	1533.2	53	1500	65	1405	40
1589.5	37	1654	1636	1636.0	48	1609		1578	
1602	32	1668	1646	1646.7	38	1603	60	1572	40
3079	19	3163	3152	3152.0	13	3024		2262	
3100.2	0.2	3183	3069	3170.1	0	3051		2283	
3107.9	27	3191	3178	3178.5	16	3060		2295	
3123.9	27	3207	3192	3192.1	15	3073		2302	
3131.4	7	3214	9198	3198.5	3	3087		2313	
3664.2	25	3827	3839	3835.2	62	2699		2700	35

Early work on the near-IR spectra of phenol has been focused on the study of the influence of the solvent or hydrogen-bond formation on the frequency of the first overtone of the ν_{OH} stretching vibration^{177–179}. The frequency of the ν_{OH} vibration for the vibrational quantum numbers $\nu = 0$ to $\nu = 5$ has been reported, based on the photoacoustic spectroscopic measurements¹⁸⁰. Recently, the near-IR spectrum between 4000 and 7000 cm^{-1} of phenol in solution has been investigated by conventional FT-IR spectroscopy¹⁸¹. Vibrational transitions in this range have also been detected by non-resonant two-photon ionization spectroscopy¹⁸² and some of the transitions have been assigned to combinations involving mainly the ν_{OH} vibration and other fundamental modes of phenol. The interesting problem in this area is to resolve the origin of the cluster of peaks around 6000 cm^{-1} which were observed in solution and assigned to the first overtone of the ν_{CH} vibrations of phenol–OH because their fundamental vibrations are placed at 3000 cm^{-1} ^{181, 182} (Figure 9). The ν_{CH} absorptions of phenol–OH and phenol–OD and their first and second overtones are studied by a deconvolution procedure and the near-IR spectra are

TABLE 9. Theoretical assignments of the vibrational modes of phenol¹¹². Potential energy distribution (PED) elements are given in parentheses, frequencies in cm⁻¹, IR intensities in km mol⁻¹^a

Q1	11	<i>a''</i>	τ_3 ring(52) + τ_2 ring(18) + γ CO(17) + τ_l ring(10)
Q2	OH torsion	<i>a''</i>	τ (O–H)(100)
Q3	18b	<i>a'</i>	δ CO(81)
Q4	16a	<i>a''</i>	τ_2 ring (76) + τ_3 ring (24)
Q5	16b	<i>a''</i>	γ CO(46) + τ_3 ring (30) + τ_l ring (13)
Q6	6a	<i>a'</i>	δ_2 ring def.(77) + ν (C–O) (12)
Q7	6b	<i>a'</i>	δ_3 ring def.(83)
Q8	4	<i>a''</i>	τ_l ring (90)
Q9	10b	<i>a''</i>	γ C ₆ H(31) + γ CO(23) + γ C ₃ H(15) + γ C ₂ H(12) + γ C ₅ H(11)
Q10	10a	<i>a''</i>	γ C ₂ H(53) + γ C ₆ H(22) + γ C ₅ H(17)
Q11	12	<i>a'</i>	ν (C–O)(25) + δ_1 ring def.(19) + ν (C ₁ –C ₂)(17) + ν (C ₁ –C ₆)(17) + δ_2 ring def.(14)
Q12	17b	<i>a''</i>	γ C ₆ H(42) + γ C ₄ H(26) + γ C ₂ H(21) + γ C ₃ H(17)
Q13	17a	<i>a''</i>	γ C ₃ H(52) + γ C ₅ H(22) + γ C ₆ H(17) + γ C ₂ H(12)
Q14	5	<i>a''</i>	γ C ₅ H(44) + γ C ₄ H(22) + τ_l ring(13) + γ C ₆ H(12) + γ C ₃ H(10)
Q15	1	<i>a'</i>	δ_1 ring def.(65) + ν (C ₁ –C ₆)(10)
Q16	18a	<i>a'</i>	ν (C ₅ –C ₄)(32) + ν (C ₄ –C ₃)(26) + δ CH(25)
Q17	15	<i>a'</i>	ν (C ₃ –C ₂)(22) + ν (C ₆ –C ₅)(19) + δ C ₆ H(13) + ν (C ₄ –C ₃)(11) + δ C ₄ H(11) + δ C ₂ H(10)
Q18	9b	<i>a'</i>	δ C ₄ H(36) + δ C ₅ H(23) + δ C ₆ H(12) + δ C ₃ H(11)
Q19	9a	<i>a'</i>	δ C ₃ H(27) + δ C ₂ H(26) + δ C ₆ H(14) + δ C ₅ H(10)
Q20	OH bend	<i>a'</i>	δ OH(55) + ν (C ₁ –C ₆)(13) + δ C ₆ H(10)
Q21	7a	<i>a'</i>	ν (C–O)(52) + ν (C–C)(20)
Q22	3	<i>a'</i>	δ C ₂ H(18) + δ C ₆ H(18) + δ C ₅ H(18) + δ C ₃ H(14) + δ C ₄ H(12)
Q23	14	<i>a'</i>	ν (C–C)(56) + δ OH(21) + δ C ₅ H(22)
Q24	19b	<i>a'</i>	δ C ₄ H(25) + δ C ₃ H(13) + ν (C ₆ –C ₅)(13) + ν (C ₃ –C ₂)(13) + δ C ₆ H(10)
Q25	19a	<i>a'</i>	δ C ₃ H(19) + δ C ₂ H(16) + ν (C ₄ –C ₃)(13) + δ C ₃ H(12)
Q26	8b	<i>a'</i>	ν (C ₂ –C ₁)(25) + ν (C ₅ –C ₄)(22)
Q27	8a	<i>a'</i>	ν (C ₁ –C ₆)(21) + ν (C ₆ –C ₅)(17) + ν (C ₃ –C ₂)(16) + ν (C ₄ –C ₃)(14)
Q28	13	<i>a'</i>	ν (C ₂ –H)(90) + ν (C ₃ –H)(10)
Q29	7b	<i>a'</i>	ν (C ₅ –H)(52) + ν (C ₄ –H)(26) + ν (C ₃ –H)(13)
Q30	2	<i>a'</i>	ν (C ₃ –H)(58) + ν (C ₅ –H)(28)
Q31	20b	<i>a'</i>	ν (C ₄ –H)(50) + ν (C ₆ –H)(33) + ν (C ₃ –H)(17)
Q32	20a	<i>a'</i>	ν (C ₆ –H)(61) + ν (C ₄ –H)(19) + ν (C ₅ –H)(18)
Q33	OH stretch	<i>a'</i>	ν (O–H)(100)

^aSee footnote of Table 10.

reassigned¹⁸³. At a concentration of 0.1 M, dimers of phenol and its higher associates might be present in solution. In the fundamental region, there appears a weak band at 3485 cm⁻¹ in phenol–OH and at 2584 cm⁻¹ in phenol–OD which originates from the dimer¹¹¹. Weaker and broader bands around 3300 and 2500 cm⁻¹ are assigned to higher associates of phenol. In the near-IR spectrum, a very weak absorption band at 6714 cm⁻¹ refers to the dimer.

E. Three Interesting Structures Related to Phenol

Before ending the present section, we would like to briefly discuss the following three structures closely linked to the *S*₀-state phenol molecule.

It is well known that aliphatic carbonyl compounds with the hydrogens on C _{α} to the carbonyl group may undergo tautomeric transitions from the keto to the enol forms. The most stable tautomeric form of the *S*₀-state phenol molecule is in fact the enol form^{184–186}. The reason why the enol form of phenol is favoured over the keto form is quite simple¹³¹.

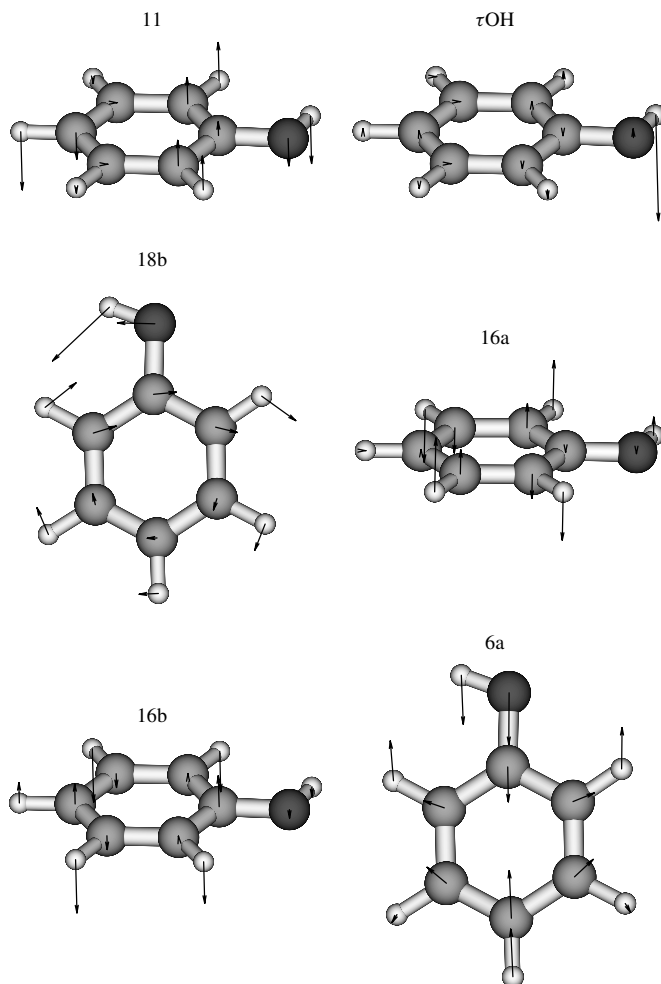
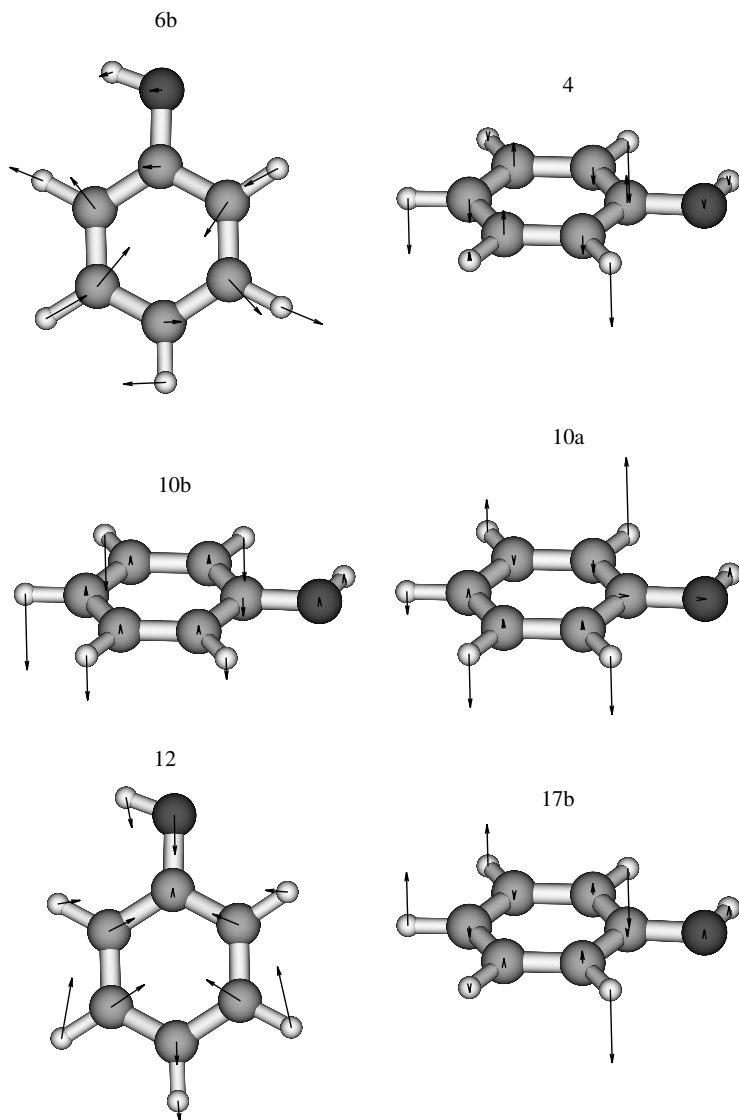
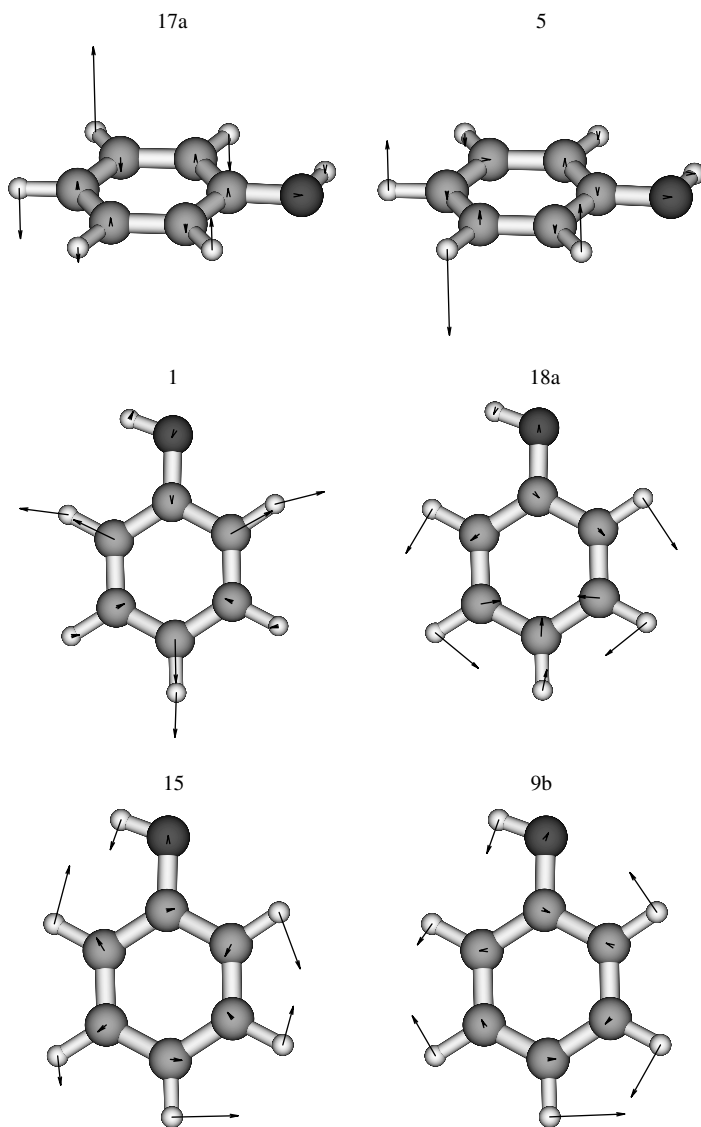


FIGURE 8. The normal displacements of the vibrational modes of phenol according to the Wilson's nomenclature. The B3LYP/6-31+G(d,p) method is employed. The assignments of the vibrational modes of phenol are presented in Table 10

On the one hand, due to the virtual absence of the electronic delocalization in the keto form, it has a larger intrinsic stability which can easily be accounted for in terms of the sum of the bond energies (*ca* 59 kJ mol⁻¹). On the other hand, the enol form is characterized by a larger resonance energy, by *ca* 126 kJ mol⁻¹, compared to that of the keto form. Therefore, the enol form is more stable by *ca* 67 kJ mol⁻¹. Such simple arguments are pretty well confirmed by the B3LYP/6-31+G(d,p) calculations performed in the present work (cf. also Reference 186) resulting in that the enol–keto tautomeric energy difference amounts to 69 kJ mol⁻¹ after ZPVE. In Figure 10 we display the most stable keto form of phenol (cyclohexa-2,5-dienone) together with its most characteristic

FIGURE 8. (*continued*)

vibrational modes. Interestingly, the keto form possesses a total dipole moment of 5.0 D and thus it is more polar than the favourable enol form. The standard heats of formation of both cyclohexa-2,4- and -2,5-dienones have recently been re-evaluated as -31 and -34 kJ mol^{-1} , respectively, in better agreement with theoretical estimates¹⁸⁷.

FIGURE 8. (*continued*)

In Figure 11 we display two other theoretical structures. The TS_τ structure is the transition state governing the torsional motion of the OH group of phenol between its equi-energetical structures shown in Chart 4. The energy difference between this structure and the S_0 -state phenol molecule determines the torsional barrier V_τ as equal to 13 kJ mol^{-1}

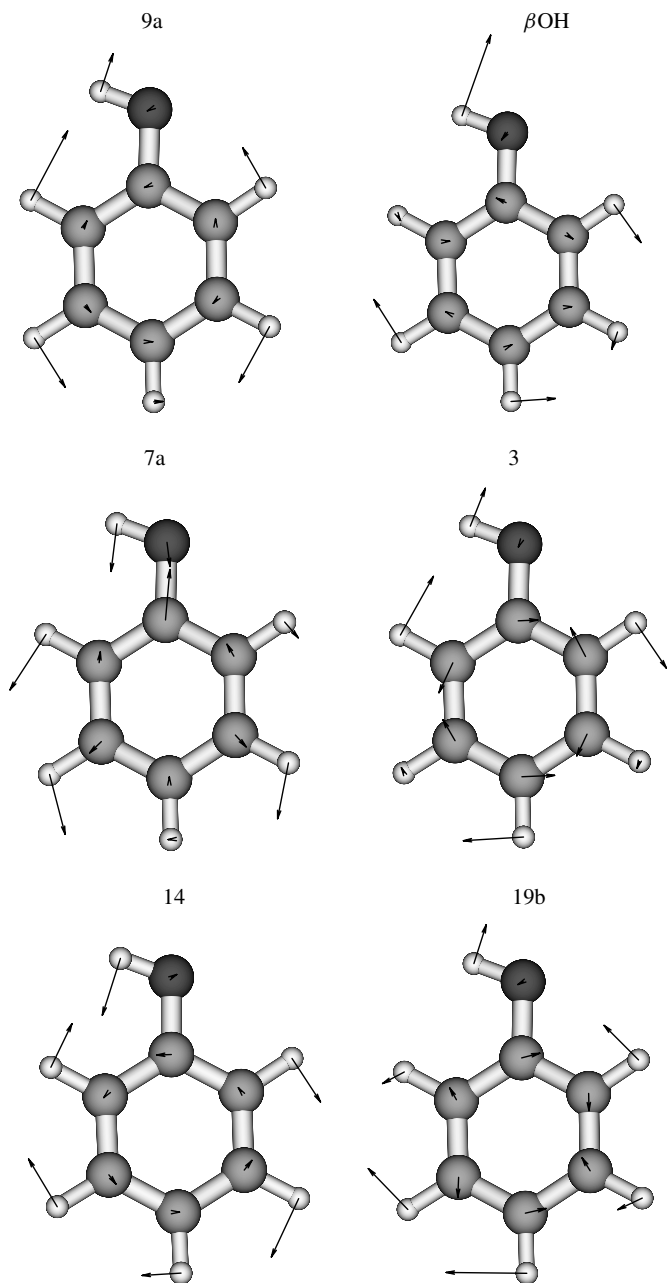


FIGURE 8. (continued)

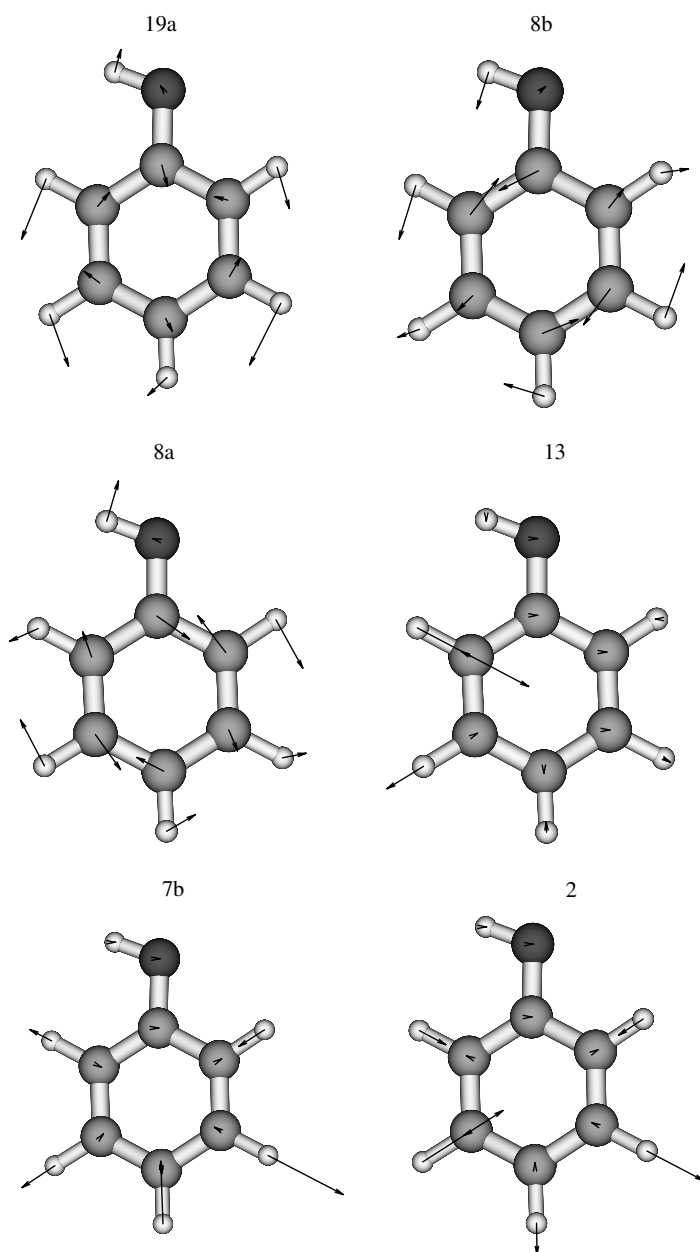
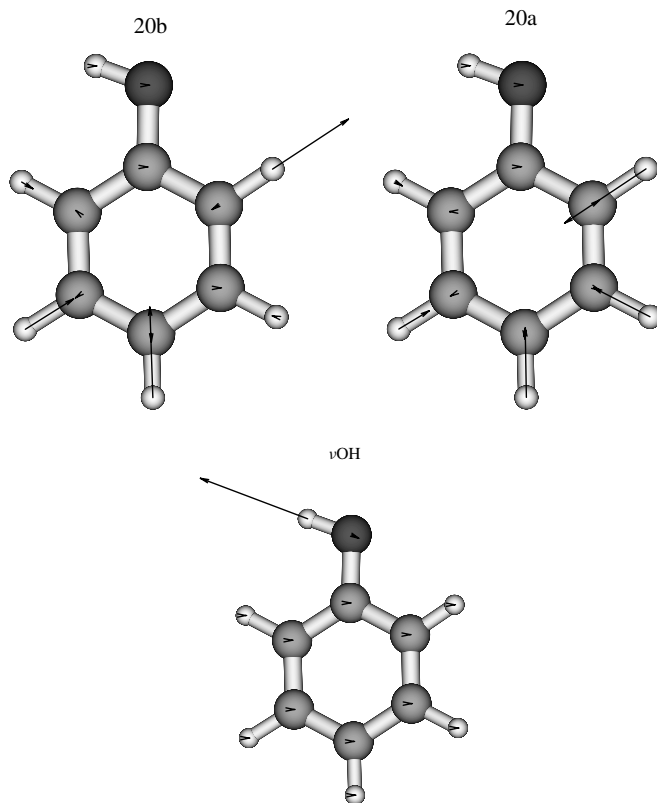
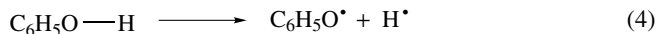


FIGURE 8. (continued)

FIGURE 8. (*continued*)

after ZPVE at the B3LYP/6-311++G(d,p) computational level. The MP2/cc-pVTZ calculation recently performed yields 15 kJ mol^{-1} ¹²⁰. Note that the imaginary frequency characterizing this saddle point is predicted at $343 i \text{ cm}^{-1}$.

The second structure shown in Figure 11 is the saddle point of second order lying 113 kJ mol^{-1} above the phenol molecule at the B3LYP/6-31+G(d,p) level taking ZPVE into account. As a second-order saddle structure, it has two imaginary frequencies, $1222 i$ and $1150 i \text{ cm}^{-1}$. The former describes the in-plane hindered rotation of the OH group whereas in the latter its rotation is perpendicular to the phenyl ring. We suppose that both these structures are directly linked to the gas-phase bond dissociation enthalpy (BDE) of phenol defined (see, e.g., Reference 188 and references therein) as the enthalpy change for the reaction



where the bond indicated by the horizontal line breaks, yielding the radicals as the products. The experimental and theoretical determination of the BDE of phenol and phenol

TABLE 10. Harmonic vibrational frequencies, IR intensities and assignments for phenol^a

No.	Freq.	IR	Sym.	Assignment, PED(%)
1	227.8	1	A''	$\tau_2\text{rg}(65)$, $\tau_1\text{rg}(12)$
2	311.4	111	A''	$\tau\text{OH}(93)$ Expt: 310^b , 310^c
3	405.1	11	A'	$\beta\text{CO}(77)$, $\beta_3\text{rg}(11)$
4	416.8	1	A''	$\tau_3\text{rg}(83)$
5	508.8	14	A''	$\tau_2\text{rg}(38)$, $\gamma\text{CO}(37)$, $\gamma\text{C}_4\text{H}(11)$
6	536.0	2	A'	$\beta_2\text{rg}(77)$
7	632.6	0	A'	$\beta_3\text{tg}(85)$
8	668.5	10	A''	$\tau_1\text{rg}(69)$, $\gamma\text{CO}(12)$
9	749.5	85	A''	$\gamma\text{C}_4\text{H}(27)$, $\gamma\text{C}_2\text{H}(16)$, $\gamma\text{CO}(15)$, $\tau_1\text{rg}(12)$, $\gamma\text{C}_3\text{H}(11)$
10	819.5	0	A''	$\gamma\text{C}_2\text{H}(44)$, $\gamma\text{C}_6\text{H}(25)$, $\gamma\text{C}_5\text{H}(20)$
11	827.4	23	A'	$\nu\text{CO}(26)$, $\beta_2\text{rg}(20)$, $\beta_1\text{rg}(16)$
12	878.1	5	A''	$\gamma\text{C}_6\text{H}(33)$, $\gamma\text{C}_2\text{H}(24)$, $\gamma\text{C}_4\text{H}(17)$
13	951.9	0	A''	$\gamma\text{C}_3\text{H}(53)$, $\gamma\text{C}_4\text{H}(18)$, $\gamma\text{C}_6\text{H}(10)$
14	971.8	0	A''	$\gamma\text{C}_5\text{H}(54)$, $\gamma\text{C}_4\text{H}(18)$, $\gamma\text{C}_6\text{H}(16)$
15	1012.6	2	A'	$\beta_1\text{rg}(65)$
16	1043.1	6	A'	$\nu\text{C}_4\text{C}_5(31)$, $\nu\text{C}_3\text{C}_4(24)$
17	1093.0	15	A'	$\nu\text{C}_2\text{C}_3(18)$, $\nu\text{C}_5\text{C}_6(15)$, $\beta\text{C}_6\text{H}(12)$, $\beta\text{C}_4\text{H}(11)$, $\nu\text{C}_3\text{C}_4(11)$, $\beta\text{C}_2\text{H}(10)$
18	1176.5	26	A'	$\beta\text{C}_4\text{H}(26)$, $\beta\text{C}_5\text{H}(16)$, $\beta\text{C}_6\text{H}(11)$, $\beta\text{C}_3\text{H}(10)$
19	1190.5	2	A'	$\beta\text{C}_2\text{H}(26)$, $\beta\text{C}_5\text{H}(17)$, $\beta\text{C}_3\text{H}(15)$, $\beta\text{C}_6\text{H}(11)$
20	1192.0	128	A'	$\beta\text{OH}(41)$, $\nu\text{C}_1\text{C}_6(13)$, $\beta\text{C}_3\text{H}(12)$, $\beta\text{C}_4\text{H}(10)$
21	1274.9	91	A'	$\nu\text{CO}(52)$, $\beta_1\text{rg}(12)$
22	1348.4	6	A'	$\nu\text{C}_2\text{C}_3(14)$, $\nu\text{C}_5\text{C}_6(14)$, $\nu\text{C}_3\text{C}_4(14)$, $\nu\text{C}_4\text{C}_5(13)$, $\nu\text{C}_1\text{C}_2(11)$, $\nu\text{C}_1\text{C}_6(10)$
23	1368.3	28	A'	$\beta\text{C}_5\text{H}(22)$, $\beta\text{OH}(18)$, $\beta\text{C}_3\text{H}(16)$, $\beta\text{C}_6\text{H}(13)$, $\beta\text{C}_2\text{H}(10)$
24	1499.4	23	A'	$\beta\text{C}_4\text{H}(26)$, $\beta\text{C}_3\text{H}(13)$, $\nu\text{C}_2\text{C}_3(13)$, $\nu\text{C}_5\text{C}_6(12)$, $\beta\text{C}_6\text{H}(10)$
25	1526.8	59	A'	$\beta\text{C}_5\text{H}(19)$, $\beta\text{C}_2\text{H}(16)$, $\nu\text{C}_3\text{C}_4(12)$, $\beta\text{C}_3\text{H}(12)$
26	1635.4	49	A'	$\nu\text{C}_1\text{C}_2(24)$, $\nu\text{C}_4\text{C}_5(21)$, $\nu\text{C}_5\text{C}_6(10)$
27	1645.9	39	A'	$\nu\text{C}_1\text{C}_6(23)$, $\nu\text{C}_3\text{C}_4(17)$, $\nu\text{C}_2\text{C}_3(13)$, $\nu\text{C}_5\text{C}_6(13)$
28	3149.0	14	A'	$\nu\text{C}_2\text{H}(88)$, $\nu\text{C}_3\text{H}(10)$
29	3167.4	0	A'	$\nu\text{C}_5\text{H}(51)$, $\nu\text{C}_4\text{H}(27)$, $\nu\text{C}_3\text{H}(11)$
30	3176.0	17	A'	$\nu\text{C}_3\text{H}(56)$, $\nu\text{C}_5\text{H}(26)$
31	3190.0	16	A'	$\nu\text{C}_4\text{H}(41)$, $\nu\text{C}_6\text{H}(41)$, $\nu\text{C}_3\text{H}(16)$
32	3196.6	4	A'	$\nu\text{C}_6\text{H}(47)$, $\nu\text{C}_4\text{H}(24)$, $\nu\text{C}_5\text{H}(21)$
33	3836.0	62	A'	$\nu\text{OH}(100)$

^aPresent calculations performed at B3LYP/6-311++G(d,p) computational level. Values taken from Reference 244 with permission. Frequencies in cm^{-1} , IR intensities in km mol^{-1} . Glossary of vibrational mode acronyms: ν , stretch; β , in-plane bend; γ , out-of-plane bend; τ , torsion; rg, ring; β_1 , β_2 and β_3 , ring deformations and τ_1 , τ_2 and τ_3 , ring torsions. PED elements $\geq 10\%$ only are included.

^bThe gas-phase IR experiment¹⁷¹.

^cThe IR experiment in solution¹⁷².

derivatives has been a matter of enormous interest^{125, 140, 189–196}. The BDE of phenol is rather low and is estimated experimentally at $356.9 \text{ kJ mol}^{-1}$ (NIST Standard Reference Database), $365.3 \pm 6.3 \text{ kJ mol}^{-1}$ ¹⁹¹, and $371.3 \pm 2.3 \text{ kJ mol}^{-1}$ ¹⁹⁴ while the accurate theoretical estimations fell within $363.2 \text{ kJ mol}^{-1}$ (DFT) and $364.4 \text{ kJ mol}^{-1}$ ¹⁴⁰. Note finally that the BDE of phenol gives the reference value for all phenolic antioxidants^{140, 197–201}. This property and the relevant reaction will be discussed in a subsequent section.

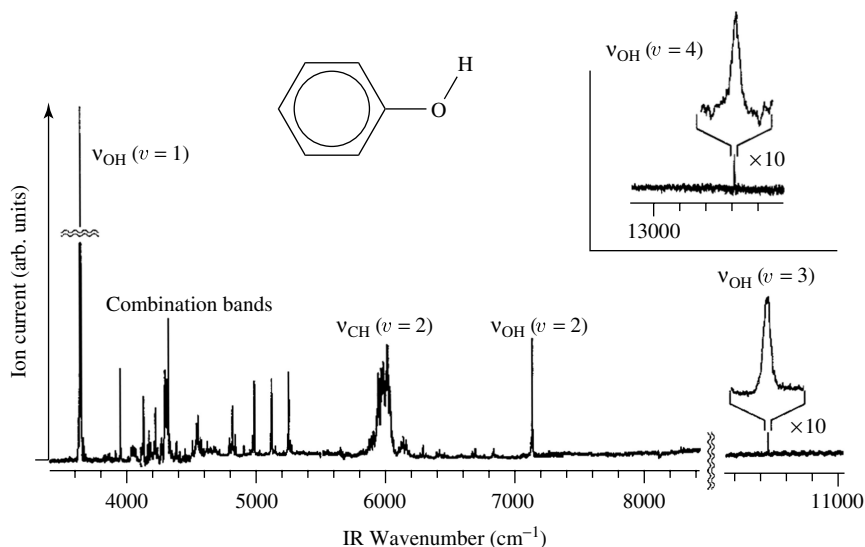


FIGURE 9. Vibrational spectrum of jet-cooled phenol measured by the non-resonant ionization-detected IR spectroscopy¹⁸² fixing ν_{UV} to 34483 cm^{-1} . All peaks are attributed to the vibrational transitions of the phenol molecule in its ground electronic state S_0 . The strongest peak at 3656 cm^{-1} is assigned to the fundamental of the ν_{OH} stretch. The cluster of peaks around 6000 cm^{-1} is assigned to the first overtone of the ν_{CH} modes. The sharp peaks at 7143 , 10461 and 13612 cm^{-1} are assigned to the first ($2\nu_{OH}$), second ($3\nu_{OH}$) and third ($4\nu_{OH}$) overtones of the ν_{OH} stretch, respectively. Reproduced with permission from Reference 182

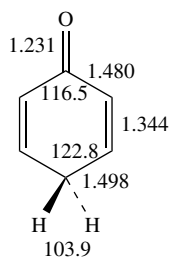


FIGURE 10. The keto tautomeric form of phenol viewed at the B3LYP/6-31+G(d,p) computational level. Bond lengths in Å, bond angles in degrees

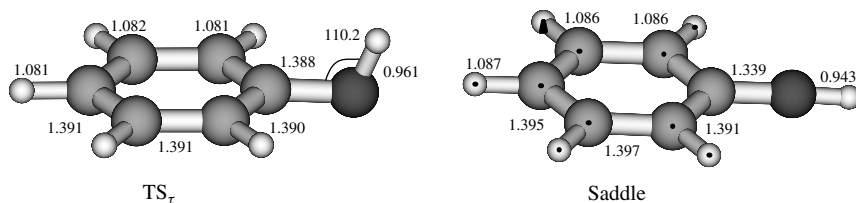


FIGURE 11. Calculated transition structure TS_r (B3LYP/6-311++G(d,p)) and the second-order saddle structure (B3LYP/6-31+G(d,p)). Bond lengths are given in Å, bond angles in degrees

III. STRUCTURES AND PROPERTIES OF SUBSTITUTED PHENOLS

During the 160 years since the discovery of phenol, thousands of studies were conducted on halophenols, partly due to their significance in the theory of hydrogen bonding; indeed their hydrogen bonding abilities can be varied nearly continuously over a wide pK_a range from 10.2 to 0.4^{202–211}.

A. Intramolecular Hydrogen Bond in *ortho*-Halogenophenols

One of the most remarkable moments in the history of mono-halogen-substituted phenols occurred in 1936 when Pauling^{104, 212} suggested the co-existence of two inequivalent rotational isomers (rotamers or conformers) of the *ortho*-Cl-substituted phenol in order to explain the experimental splitting of the first overtone of its ν_{OH} vibrational mode observed in the CCl_4 solution^{213–217}. Instead of phenol whose first overtone $\nu_{OH}^{(1)}$ is sharply peaked at 7050 cm^{-1} , *o*-ClC₆H₄OH reveals a doublet at 7050 and 6910 cm^{-1} resulting in a band splitting $\Delta\nu_{OH}^{(1)} = 140\text{ cm}^{-1}$ and having the former band placed at the same wavenumbers as in phenol. Almost two decades later, a splitting of the fundamental ν_{OH} mode by 83 cm^{-1} was observed in CCl_4 solvent²¹⁸. What then lies behind Pauling's suggestion?

Let us consider Figure 12, which displays two conformers *cis* and *trans* of *o*-ClC₆H₄OH (computational details are given elsewhere^{219, 220}). The former possesses the intramolecular hydrogen bond O–H...Cl whereas the latter does not. This makes (as long believed) the *cis* conformer energetically favoured, with a gain of energy $\Delta_{cis-trans}E_{ortho}^{Cl} = 12.5\text{ kJ mol}^{-1}$. Pauling's estimation of the corresponding free energy difference derived from the ratio of the areas of the peaks was 5.8 kJ mol^{-1} ¹⁰⁴ in CCl_4 solution (a more precise value is 6.1 kJ mol^{-1} ¹⁷⁰; another value is 7.5 kJ mol^{-1} ²²¹). Our calculated energy difference agrees fairly well with the free energy difference of $14.2\text{--}16.3\text{ kJ mol}^{-1}$ in the vapour²²² bounded by $16.3 \pm 3.0\text{ kJ mol}^{-1}$ ²²³ and $14.3 \pm 0.6\text{ kJ mol}^{-1}$ ²²⁴. However, there is yet another feature that distinguishes *cis* and *trans* conformers from each other: the *trans* form is more polar (3.0 vs 1.04 D). The directions of the total dipole moments of the *cis* and *trans* conformers are shown in Figure 12. Nevertheless, the gross difference between the *cis* and *trans* conformers consists, as mentioned, in the presence of the intramolecular hydrogen bond. Hence, $\Delta_{cis-trans}E_{ortho}^{Cl}$ can be interpreted as the energy of its formation. Indeed, it looks rather weak for *cis* *o*-ClC₆H₄OH.

Inspection of Table 11, which gathers the harmonic vibrational modes of both conformers with the corresponding potential energy distribution patterns, reveals that the *trans* ν_{OH} is calculated at 3835.4 cm^{-1} , which is almost identical to ν_{OH} of phenol in Table 10, while its *cis* partner is red-shifted (as expected according to the theory of hydrogen bonding^{225, 226}) by $\Delta_{cis-trans}\nu_{OH}^{Cl} = 69\text{ cm}^{-1}$. This calculated value lies rather close to the experimental red shifts ranging from 58 ²²⁷ to 60 ²²⁸ and 63 cm^{-1} ^{222, 229}, depending on the solvent. On the other hand, we note that our red shift is smaller, by 91 cm^{-1} , compared to that observed by Wulf and coworkers²¹⁷ for $\nu_{OH}^{(1)}$ that might be attributed to anharmonic effects²³⁰. After all, it is worth mentioning another indication of the rather weak intramolecular hydrogen bond in *cis* *o*-ClC₆H₄OH, namely the value of the corresponding hydrogen bridge stretching vibration ν_{σ} (mode 2 in Table 11) compared to mode 2 in its *trans* partner.

In this regard, the more than two decades following the appearance of Pauling's work¹⁰⁴ deserve to be recalled. Indeed, on the one hand, they were full of criticism²²⁷ of the earlier experimental results^{213–217} because it was believed that the higher frequency band appears 'more likely due to a trace of phenol impurity than to the presence of *trans* isomer'²¹⁸ and the new experiment demonstrated the ratio of the absorptions being much smaller and equal to $1/56 \approx 17.9 \times 10^{-3}$, which anyway is about three times larger than

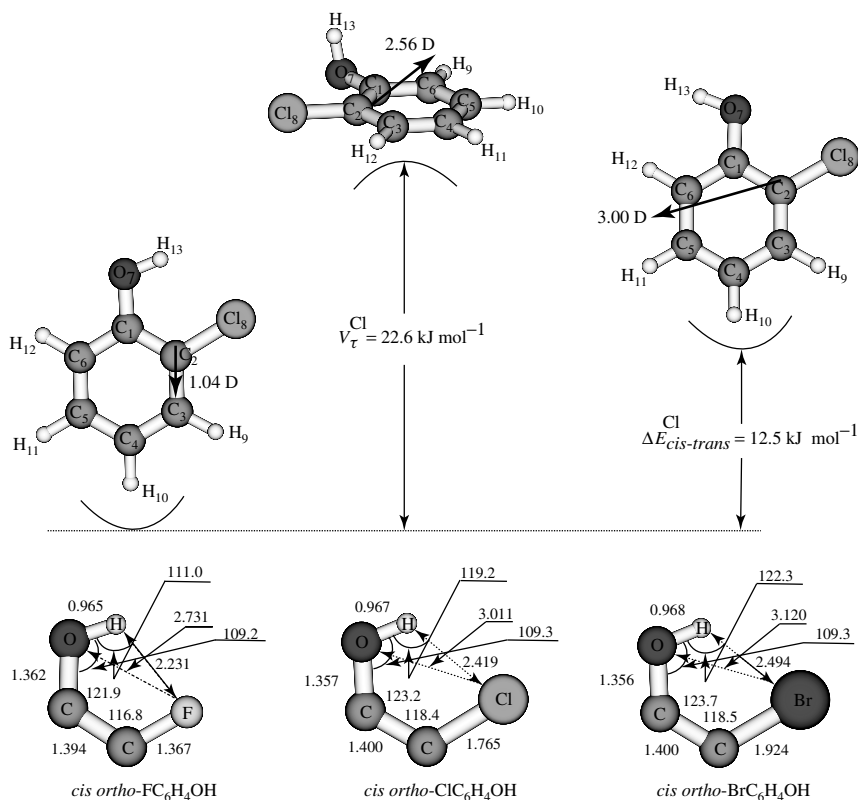


FIGURE 12. The portion of the potential energy surface of *o*-C₆H₄OH governing the *cis*-*trans* conversion is displayed at the top. Numbering of atoms follows Chart 1. Five-member sub-ring sections of the *cis* *ortho*-halogenophenols with the intramolecular hydrogen bond are shown at the bottom. Bond lengths are in Å, bond angles in degrees. Adapted from Reference 220 with permission

our theoretical magnitude. On the other hand, these years were also characterized by a further development of the Pauling model^{231, 232} and its further experimental support²¹⁷ although, alas, the ‘unsatisfactory state of affairs’ in the area of the *cis*-*trans* doublet paradigm²¹⁷ remained at that time. Paradoxically, it still remains nowadays, even widening the gap between the experiments originating at the end of the 1950s and modern high-level theoretical studies²²⁰. This particularly concerns *o*-fluorophenol.

In 1958, it was verified experimentally²²⁷ that the *cis*-*trans* doublet could not be detected for *o*-FC₆H₄OH: the *trans* ν_{OH} band was suggested to be too weak to show up in IR experiments and $\Delta_{cis-trans} \nu_{OH}^F$ to be too small ($< 20 \text{ cm}^{-1}$; it is estimated at 18 cm^{-1} ²²²). Our prediction is $\Delta_{cis-trans} E_{ortho}^F = 11.4 \text{ kJ mol}^{-1}$, which demonstrates that indeed the intramolecular O-H...F hydrogen bond in *o*-FC₆H₄OH is weaker (by 1.09 kJ mol^{-1}) than its analogue in *o*-ClC₆H₄OH. Furthermore, as follows from Table 12, the theoretical splitting $\Delta_{cis-trans} \nu_{OH}^F = 30 \text{ cm}^{-1}$ is larger than 20 cm^{-1} , as predicted by IR experiments. We also note that the dipole moment of *trans* *o*-FC₆H₄OH (2.95 D) exceeds that of the *cis* form (1.0 D) by almost a factor of three.

TABLE 11. Harmonic vibrational frequencies, IR intensities and assignments for *cis* and *trans ortho*-chlorophenols^a

No.	Freq.	IR	Sym.	Assignment, PED(%)	No.	Freq.	IR	Sym.	Assignment, PED(%)
1	155.6	0	A''	$\tau_2\text{rg}(49)$, $\tau_3\text{rg}(19)$, $\gamma\text{CCI}(13)$, $\tau_1\text{rg}(11)$	1	152.6	1	A''	$\tau_2\text{rg}(50)$, $\tau_3\text{rg}(19)$, $\tau_1\text{rg}(13)$, $\gamma\text{CCI}(10)$
2	249.3	3	A'	$\beta\text{CCI}(75)$, $\beta\text{CO}(15)$	2	239.7	2	A'	$\beta\text{CCI}(72)$, $\beta\text{CO}(17)$
3	262.8	1	A''	$\gamma\text{CCI}(31)$, $\tau_2\text{rg}(29)$, $\gamma\text{C}_6\text{H}(11)$, $\gamma\text{CO}(10)$	3	260.3	11	A''	$\tau_2\text{rg}(27)$, $\gamma\text{CCI}(27)$, $\tau_3\text{rg}(13)$, $\gamma\text{CO}(10)$
4	375.8	3	A'	$\nu\text{CCI}(27)$, $\beta_3\text{rg}(19)$, $\beta\text{CO}(17)$, $\beta_2\text{rg}(16)$	4	317.7	96	A''	$\tau\text{OH}(88)$
5	407.2	108	A''	$\tau\text{OH}(90)$		Expt: 373 ^b , 361 ^c			
					5	380.8	3	A'	$\nu\text{CCI}(26)$, $\beta_3\text{rg}(20)$, $\beta\text{CO}(17)$, $\beta_2\text{rg}(15)$, $\beta\text{CCI}(10)$
6	447.2	0	A''	$\tau_3\text{rg}(60)$, $\gamma\text{CCI}(24)$	6	445.4	7	A''	$\tau_3\text{rg}(58)$, $\gamma\text{CCI}(22)$
7	493.6	12	A'	$\beta\text{CO}(57)$, $\nu\text{CCI}(16)$, $\beta\text{CCI}(11)$	7	492.5	8	A'	$\beta\text{CO}(55)$, $\nu\text{CCI}(12)$, $\beta\text{CCI}(11)$
8	542.5	1	A''	$\tau_2\text{rg}(39)$, $\gamma\text{CO}(29)$	8	548.5	1	A''	$\tau_2\text{rg}(35)$, $\tau_1\text{rg}(20)$, $\gamma\text{CO}(18)$
9	563.9	5	A'	$\beta_2\text{rg}(61)$, $\beta_3\text{rg}(10)$	9	566.0	4	A'	$\beta_2\text{rg}(57)$, $\beta_3\text{rg}(12)$
10	672.6	0	A''	$\tau_1\text{rg}(63)$, $\gamma\text{CO}(17)$, $\gamma\text{CCI}(10)$	10	690.8	19	A'	$\beta_3\text{rg}(54)$, $\nu\text{CCI}(25)$, $\nu\text{C1C2}(11)$
11	685.1	25	A'	$\beta_3\text{rg}(56)$, $\nu\text{CCI}(24)$, $\nu\text{C1C2}(10)$	11	702.6	0	A''	$\tau_1\text{rg}(58)$, $\gamma\text{CO}(19)$, $\gamma\text{CCI}(13)$
12	758.6	74	A''	$\gamma\text{C}_6\text{H}(39)$, $\gamma\text{C}_3\text{H}(24)$, $\gamma\text{C}_3\text{H}(20)$, $\gamma\text{C}_6\text{H}(12)$	12	751.6	82	A''	$\gamma\text{C}_4\text{H}(32)$, $\gamma\text{C}_5\text{H}(23)$, $\gamma\text{C}_6\text{H}(22)$, $\gamma\text{C}_3\text{H}(11)$
13	842.7	13	A'	$\beta_1\text{rg}(27)$, $\nu\text{CO}(24)$, $\beta_2\text{rg}(19)$, $\nu\text{C}_1\text{C}_6(10)$	13	835.1	0	A''	$\gamma\text{C}_6\text{H}(47)$, $\gamma\text{CCL}(22)$, $\gamma\text{C}_4\text{H}(12)$, $\tau_1\text{rg}(10)$
14	850.2	1	A''	$\gamma\text{C}_6\text{H}(45)$, $\gamma\text{C}_3\text{H}(28)$	14	841.4	21	A'	$\beta_1\text{rg}(28)$, $\nu\text{CO}(24)$, $\beta_2\text{rg}(19)$
15	942.2	3	A''	$\gamma\text{C}_3\text{H}(41)$, $\gamma\text{C}_4\text{H}(22)$, $\gamma\text{C}_6\text{H}(20)$	15	929.4	2	A''	$\gamma\text{C}_3\text{H}(38)$, $\gamma\text{C}_3\text{H}(35)$, $\gamma\text{C}_6\text{H}(17)$
16	974.2	0	A''	$\gamma\text{C}_5\text{H}(49)$, $\gamma\text{C}_4\text{H}(24)$, $\gamma\text{C}_6\text{H}(13)$	16	962.6	0	A''	$\gamma\text{C}_3\text{H}(42)$, $\gamma\text{C}_5\text{H}(24)$, $\gamma\text{C}_3\text{H}(22)$
17	1042.9	45	A'	$\beta_1\text{rg}(34)$, $\nu\text{C}_4\text{C}_5(21)$, $\nu\text{C}_5\text{C}_6(13)$, $\nu\text{CCI}(11)$	17	1055.2	26	A'	$\nu\text{C}_4\text{C}_5(29)$, $\beta_1\text{rg}(19)$, $\nu\text{C}_5\text{C}_6(15)$, $\nu\text{C}_3\text{C}_4(11)$
18	1060.9	13	A'	$\beta_1\text{rg}(29)$, $\nu\text{C}_4\text{C}_5(16)$, $\beta\text{C}_3\text{H}(10)$, $\nu\text{CCI}(10)$	18	1071.1	25	A'	$\beta_1\text{rg}(40)$, $\nu\text{CCI}(13)$

(continued overleaf)

TABLE 11. (*continued*)

No.	Freq.	IR	Sym.	Assignment, PED(%)	No.	Freq.	IR	Sym.	Assignment, PED(%)
19	1140.7	5	A'	ν C ₃ C ₄ (23), β C ₃ H(14), ν C ₆ H(14), β C ₄ H(12)	19	1139.9	75	A'	ν C ₃ C ₄ (20), β C ₄ H(13), β COH(12)
20	1179.5	3	A'	β C ₄ H(34), β C ₃ H(28), ν C ₆ H(10), β C ₃ H(10), ν C ₄ C ₅ (10)	20	1182.1	3	A'	β C ₃ H(33), β C ₄ H(31), β C ₃ H(10)
21	1211.0	115	A'	β COH(38), ν C ₁ C ₆ (17), ν C ₆ H(12), β C ₃ H(10)	21	1189.6	85	A'	β COH(40), β C ₆ H(15), β C ₃ H(11), ν C ₁ C ₆ (10)
22	1274.7	75	A'	ν CO(31), ν C ₂ C ₃ (25), β C ₃ H(21)	22	1285.4	23	A'	ν CO(33), ν C ₂ C ₃ (24), β C ₃ H(15)
23	1323.3	28	A'	ν C ₅ C ₆ (17), ν C ₁ C ₂ (17), ν C ₆ H(15), ν CO(14)	23	1316.5	77	A'	β C ₆ H(24), ν CO(15), ν C ₁ C ₂ (12), ν C ₅ C ₆ (11)
24	1366.3	23	A'	β COH(26), β C ₃ H(12), ν C ₄ C ₅ (10), ν C ₂ C ₃ (10), ν C ₃ C ₄ (10)	24	1353.0	45	A'	β COH(17), ν C ₃ C ₄ (14), ν C ₁ C ₆ (13), β C ₃ H(11), ν C ₄ C ₅ (10), ν C ₅ C ₆ (11),
25	1489.1	4	A'	β C ₄ H(30), β C ₃ H(15), ν C ₂ C ₃ (12)	25	1477.9	48	A'	β C ₄ H(26), β C ₃ H(23), ν C ₁ C ₆ (11), ν C ₂ C ₃ (10)
26	1510.0	136	A'	β C ₃ H(19), ν C ₆ H(16), ν C ₁ C ₂ (15),	26	1524.7	61	A'	β C ₃ H(18), β C ₆ H(18), ν C ₁ C ₂ (11), ν C ₄ C ₅ (11)
27	1624.0	15	A'	ν C ₄ C ₅ (22), ν C ₁ C ₂ (18), ν C ₁ C ₆ (15), ν C ₃ C ₄ (12)	27	1622.7	14	A'	ν C ₃ C ₄ (23), ν C ₁ C ₆ (23)
28	1634.5	38	A'	ν C ₅ C ₆ (25), ν C ₂ C ₃ (17), ν C ₁ C ₆ (11), β_2 Tg(10)	28	1635.7	27	A'	ν C ₅ C ₆ (20), ν C ₁ C ₂ (20), ν C ₄ C ₅ (16), ν C ₂ C ₃ (13)
29	3174.5	2	A'	ν C ₃ H(61), ν C ₄ H(24), ν C ₆ H(10)	29	3151.3	11	A'	ν C ₆ H(92)
30	3188.2	6	A'	ν C ₄ H(43), ν C ₃ H(26), ν C ₆ H(17), ν C ₅ H(13)	30	3178.0	4	A'	ν C ₅ H(44), ν C ₄ H(43)
31	3196.5	5	A'	ν C ₆ H(63), ν C ₃ H(21), ν C ₅ H(15)	31	3190.5	8	A'	ν C ₅ H(40), ν C ₃ H(38), ν C ₄ H(19)
32	3203.5	4	A'	ν C ₃ H(49), ν C ₄ H(31), ν C ₅ H(10)	32	3202.2	5	A'	ν C ₃ H(54), ν C ₄ H(36)
33	3766.7	93	A'	ν OH(100)	33	3835.4	73	A'	ν OH(100)

^aSee footnote *a* in Table 10.^bThe gas-phase IR experiments¹⁷¹.^cIR experiments in solution¹⁷².^dIR experiments in solution¹⁶⁵.

TABLE 12. Harmonic vibrational frequencies, IR intensities and assignments for *cis* and *trans* *ortho*-fluorophenols^a

No.	ω	A	Sym.	Assignment, PED(%)	No.	ω	A	Sym.	Assignment, PED(%)
1	190.4	0	A''	$\tau_2\text{rg}(59)$, $\tau_1\text{rg}(17)$, $\tau_3\text{rg}(16)$	1	183.1	0	A''	$\tau_2\text{rg}(59)$, $\tau_1\text{rg}(20)$, $\tau_3\text{rg}(15)$
2	290.9	1	A''	$\gamma\text{CF}(28)$, $\tau_3\text{rg}(24)$, $\gamma\text{CO}(18)$, $\gamma\text{C}_6\text{H}(11)$	2	274.2	60	A''	$\tau\text{OH}(43)$, $\tau_3\text{rg}(20)$, $\gamma\text{CF}(15)$
3	296.9	8	A'	$\beta\text{CO}(42)$, $\beta\text{CF}(40)$, $\beta_3\text{rg}(10)$	3	297.7	2	A'	$\beta\text{CO}(42)$, $\beta\text{CF}(41)$
4	396.3	126	A''	$\tau\text{OH}(90)$	4	308.2	51	A''	$\tau\text{OH}(41)$, $\tau_3\text{rg}(16)$, $\gamma\text{CO}(14)$, $\gamma\text{CF}(11)$
5	443.3	1	A'	$\beta_2\text{rg}(29)$, $\beta\text{CF}(22)$, $\beta\text{CO}(19)$, $\beta_3\text{rg}(10)$	5	447.1	6	A'	$\beta_2\text{rg}(29)$, $\beta\text{CF}(23)$, $\beta\text{CO}(20)$, $\beta_3\text{rg}(10)$
6	454.7	0	A''	$\tau_3\text{rg}(45)$, $\gamma\text{CF}(24)$, $\gamma\text{CO}(15)$	6	456.6	4	A''	$\tau_3\text{rg}(44)$, $\gamma\text{CF}(22)$, $\gamma\text{CO}(18)$
7	555.8	4	A'	$\beta_2\text{rg}(25)$, $\beta\text{CO}(23)$, $\beta\text{CF}(21)$	7	547.4	8	A'	$\beta_2\text{rg}(28)$, $\beta\text{CO}(22)$, $\beta\text{CF}(20)$
8	557.8	1	A''	$\tau_2\text{rg}(30)$, $\tau_1\text{rg}(26)$, $\gamma\text{CO}(10)$	8	556.8	0	A''	$\tau_1\text{rg}(36)$, $\tau_2\text{rg}(25)$
9	584.4	5	A'	$\beta_3\text{rg}(50)$, $\beta_2\text{rg}(25)$	9	587.8	3	A'	$\beta_3\text{rg}(53)$, $\beta_2\text{rg}(22)$
10	683.6	0	A''	$\tau_1\text{rg}(55)$, $\gamma\text{CO}(19)$, $\gamma\text{CF}(17)$	10	692.9	0	A''	$\tau_1\text{rg}(50)$, $\gamma\text{CO}(20)$, $\gamma\text{CF}(19)$
11	757.8	84	A''	$\gamma\text{C}_4\text{H}(36)$, $\gamma\text{C}_3\text{H}(29)$, $\gamma\text{C}_3\text{H}(18)$, $\gamma\text{C}_6\text{H}(12)$	11	750.5	91	A''	$\gamma\text{C}_5\text{H}(32)$, $\gamma\text{C}_4\text{H}(28)$, $\gamma\text{C}_6\text{H}(23)$, $\gamma\text{C}_3\text{H}(10)$
12	772.7	42	A'	$\nu\text{C}_1\text{C}_2(25)$, $\nu\text{CF}(21)$, $\beta_3\text{rg}(17)$, $\nu\text{C}_2\text{C}_3(10)$	12	773.4	21	A'	$\nu\text{C}_1\text{C}_2(27)$, $\nu\text{CF}(17)$, $\beta_3\text{rg}(15)$, $\nu\text{CO}(11)$, $\nu\text{C}_2\text{C}_3(11)$
13	847.3	0	A''	$\gamma\text{C}_6\text{H}(39)$, $\gamma\text{C}_3\text{H}(31)$, $\tau_1\text{rg}(10)$	13	829.5	0	A''	$\gamma\text{C}_6\text{H}(45)$, $\gamma\text{C}_3\text{H}(24)$, $\tau_1\text{rg}(10)$, $\gamma\text{C}_4\text{H}(10)$
14	857.1	17	A'	$\beta_1\text{rg}(44)$, $\nu\text{CO}(17)$, $\beta_2\text{rg}(16)$, $\nu\text{CF}(11)$	14	860.0	27	A'	$\beta_1\text{rg}(48)$, $\nu\text{CO}(15)$, $\beta_2\text{rg}(15)$, $\nu\text{CF}(10)$
15	931.6	5	A''	$\gamma\text{C}_3\text{H}(38)$, $\gamma\text{C}_4\text{H}(26)$, $\gamma\text{C}_6\text{H}(21)$	15	920.3	4	A''	$\gamma\text{C}_3\text{H}(37)$, $\gamma\text{C}_5\text{H}(31)$, $\gamma\text{C}_6\text{H}(18)$
16	959.2	0	A''	$\gamma\text{C}_5\text{H}(52)$, $\gamma\text{C}_4\text{H}(22)$, $\gamma\text{C}_6\text{H}(14)$	16	945.3	1	A''	$\gamma\text{C}_4\text{H}(46)$, $\gamma\text{C}_5\text{H}(27)$, $\gamma\text{C}_3\text{H}(17)$
17	1043.6	16	A'	$\nu\text{C}_4\text{C}_5(37)$, $\nu\text{C}_5\text{C}_6(15)$, $\beta\text{C}_3\text{H}(15)$, $\nu\text{C}_3\text{C}_4(14)$, $\beta\text{C}_6\text{H}(12)$	17	1052.9	5	A'	$\nu\text{C}_4\text{C}_5(36)$, $\nu\text{C}_3\text{C}_4(17)$, $\beta\text{C}_3\text{H}(16)$, $\nu\text{C}_5\text{C}_6(15)$, $\beta\text{C}_6\text{H}(10)$

(continued overleaf)

TABLE 12. (continued)

No.	ω	A	Sym.	Assignment, PED(%)	No.	ω	A	Sym.	Assignment, PED(%)
18	1106.2	28	A'	$\beta_1\text{rg}(27)$, $\nu\text{C}_3\text{C}_4(10)$, $\nu\text{CF}(10)$	18	1111.2	64	A'	$\beta_1\text{rg}(22)$, $\beta\text{COH}(12)$, $\nu\text{C}_3\text{C}_4(11)$
19	1175.4	2	A'	$\beta\text{C}_5\text{H}(34)$, $\beta\text{C}_4\text{H}(26)$, $\beta\text{C}_6\text{H}(12)$, $\nu\text{C}_4\text{C}_5(12)$	19	1175.8	33	A'	$\beta\text{C}_4\text{H}(31)$, $\beta\text{C}_3\text{H}(21)$, $\beta\text{C}_3\text{H}(17)$, $\beta\text{COH}(12)$
20	1182.0	58	A'	$\beta\text{C}_6\text{H}(21)$, $\nu\text{CF}(17)$, $\beta\text{COH}(13)$, $\nu\text{C}_1\text{C}_6(10)$	20	1183.4	33	A'	$\beta\text{C}_6\text{H}(28)$, $\beta\text{COH}(20)$, $\beta\text{C}_5\text{H}(20)$, $\nu\text{C}_5\text{C}_6(10)$
21	1234.9	104	A'	$\beta\text{COH}(25)$, $\nu\text{CF}(16)$, $\nu\text{CO}(14)$, $\beta_1\text{rg}(12)$	21	1240.1	124	A'	$\nu\text{CF}(40)$, $\beta_1\text{rg}(19)$, $\beta\text{COH}(12)$
22	1284.3	130	A'	$\beta\text{C}_3\text{H}(27)$, $\nu\text{CO}(26)$, $\nu\text{C}_2\text{C}_3(12)$	22	1298.9	61	A'	$\nu\text{CO}(29)$, $\beta\text{C}_3\text{H}(20)$, $\nu\text{C}_2\text{C}_3(13)$
23	1324.0	21	A'	$\beta\text{C}_6\text{H}(17)$, $\nu\text{C}_5\text{C}_6(17)$, $\nu\text{C}_1\text{C}_2(15)$	23	1317.4	78	A'	$\beta\text{C}_6\text{H}(26)$, $\nu\text{C}_1\text{C}_2(11)$, $\nu\text{CO}(10)$, $\nu\text{C}_5\text{C}_6(10)$
24	1380.8	12	A'	$\beta\text{COH}(24)$, $\nu\text{C}_4\text{C}_5(15)$, $\beta\text{C}_5\text{H}(13)$, $\nu\text{C}_2\text{C}_3(12)$	24	1362.0	49	A'	$\beta\text{COH}(15)$, $\nu\text{C}_1\text{C}_6(15)$, $\nu\text{C}_4\text{C}_5(14)$, $\nu\text{C}_3\text{C}_4(11)$, $\nu\text{C}_2\text{C}_3(11)$, $\nu\text{C}_5\text{C}_6(10)$
25	1499.3	4	A'	$\beta\text{C}_4\text{H}(26)$, $\beta\text{C}_5\text{H}(20)$, $\nu\text{C}_5\text{C}_6(13)$, $\nu\text{C}_3\text{C}_4(11)$	25	1488.2	29	A'	$\beta\text{C}_5\text{H}(27)$, $\beta\text{C}_4\text{H}(21)$, $\nu\text{C}_3\text{C}_4(11)$, $\nu\text{C}_1\text{C}_6(10)$
26	1530.1	189	A'	$\beta\text{C}_3\text{H}(16)$, $\beta\text{C}_6\text{H}(15)$, $\nu\text{C}_1\text{C}_2(13)$, $\nu\text{CO}(11)$	26	1545.1	131	A'	$\beta\text{C}_6\text{H}(17)$, $\nu\text{C}_4\text{C}_5(13)$, $\beta\text{C}_3\text{H}(13)$, $\nu\text{C}_2\text{C}_3(10)$
27	1640.1	6	A'	$\nu\text{C}_1\text{C}_6(25)$, $\nu\text{C}_3\text{C}_4(18)$, $\nu\text{C}_1\text{C}_2(10)$	27	1636.0	19	A'	$\nu\text{C}_1\text{C}_6(21)$, $\nu\text{C}_3\text{C}_4(20)$, $\nu\text{C}_2\text{C}_3(12)$
28	1653.7	47	A'	$\nu\text{C}_2\text{C}_3(21)$, $\nu\text{C}_5\text{C}_6(18)$, $\nu\text{C}_1\text{C}_2(17)$, $\nu\text{C}_4\text{C}_5(11)$	28	1655.9	28	A'	$\nu\text{C}_1\text{C}_2(26)$, $\nu\text{C}_4\text{C}_5(16)$, $\nu\text{C}_5\text{C}_6(14)$, $\nu\text{C}_2\text{C}_3(13)$
29	3176.7	2	A'	$\nu\text{C}_5\text{H}(59)$, $\nu\text{C}_4\text{H}(25)$, $\nu\text{C}_6\text{H}(12)$	29	3152.6	10	A'	$\nu\text{C}_6\text{H}(92)$
30	3189.4	8	A'	$\nu\text{C}_4\text{H}(40)$, $\nu\text{C}_3\text{H}(25)$, $\nu\text{C}_6\text{H}(25)$	30	3179.6	4	A'	$\nu\text{C}_4\text{H}(45)$, $\nu\text{C}_5\text{H}(41)$
31	3197.1	5	A'	$\nu\text{C}_6\text{H}(53)$, $\nu\text{C}_3\text{H}(28)$, $\nu\text{C}_5\text{H}(18)$	31	3191.4	9	A'	$\nu\text{C}_3\text{H}(47)$, $\nu\text{C}_5\text{H}(39)$, $\nu\text{C}_4\text{H}(11)$
32	3204.4	3	A'	$\nu\text{C}_3\text{H}(43)$, $\nu\text{C}_4\text{H}(34)$, $\nu\text{C}_5\text{H}(13)$	32	3202.4	4	A'	$\nu\text{C}_3\text{H}(43)$, $\nu\text{C}_4\text{H}(43)$, $\nu\text{C}_5\text{H}(13)$
33	3807.0	105	A'	$\nu\text{OH}(100)$	33	3837.1	75	A'	$\nu\text{OH}(100)$

^aSee footnote *a* in Table 10.

Regarding the transition state between the *cis* and *trans* isomers of *o*-FC₆H₄OH, we obtain that it has nearly the same slope as in the case of Cl, viz. 347 i cm⁻¹, although its barrier $V_{\tau}^F = 20.3 \text{ kJ mol}^{-1}$ is by 2.2 kJ mol⁻¹ smaller than V_{τ}^{Cl} . Since $\Delta_{cis-trans} E_{ortho}^F < \Delta_{cis-trans} E_{ortho}^{Cl}$, we might expect that the equilibrium constant $k_{cis \rightleftharpoons trans}^F$ is larger than $k_{cis \rightleftharpoons trans}^{Cl}$, which is indeed found to be true: $k_{cis \rightleftharpoons trans}^F = 10.1 \times 10^{-3}$. On the contrary, no known IR experiment has ever revealed a *cis-trans* transition in *o*-FC₆H₄OH^{223-229, 233-235}. The question is: Why?

The disparity between the older IR experiments and modern high-level theory becomes even sharper if we turn to the *o*-Br-substituted phenols whose harmonic vibrational modes are presented in Table 13. It is then easy to obtain $\Delta_{cis-trans} \nu_{OH}^{Br} = 94 \text{ cm}^{-1}$, which agrees with the experimental values ranging from 74 to 93 cm⁻¹^{218, 224, 229} (Tables 1 and 5 of Reference 222). On the other hand, the calculated $\Delta_{cis-trans} E_{ortho}^{Br} = 12.9 \text{ kJ mol}^{-1}$ (the experimental free energy difference in the vapour is $13.1 \pm 14.6 \text{ kJ mol}^{-1}$ ²²⁴) implies that, first, the intramolecular hydrogen bond is slightly stronger with Br than with Cl, which surely contradicts the common order of the hydrogen bond acceptors^{155, 171, 236, 237}, and, second, the equilibrium constant $k_{cis \rightleftharpoons trans}^{Br} = 5.2 \times 10^{-3} < k_{cis \rightleftharpoons trans}^{Cl}$, although the experiments show the reverse trend^{233, 234}. Altogether, this was dubbed as an ‘anomalous’ order in the strength of the intramolecular hydrogen bond^{223, 224, 229, 231, 238-240}; the ‘state of affairs’ was summarized by Sandorfy and coauthors²²⁹ in their 1963 work: ‘Nothing emerges from our work, however, to explain this order. . . . For a more thorough treatment we shall likely have to wait until the next stage in the development of quantum chemistry’. What modern calculations might tell us in this context is briefly outlined below:

(i) Under the assumption that $\Delta_{cis-trans} E_{ortho}^X$ (X = F, Cl, Br) defines the energy of formation of the intramolecular hydrogen bond in *cis ortho*-X-substituted phenols, the order of its strength in the gas phase (in kJ mol)⁻¹ appears to be that given in equation 5.

$$\text{Br} \overset{0.46}{\approx} \text{Cl} \overset{1.09}{>} \text{F}. \quad (5)$$

The numbers in equation 5 indicate the corresponding difference (in kJ mol⁻¹) in the energies of formation of the intramolecular hydrogen bond between the left-hand complex and its right-hand one. This order is confirmed to a certain extent by the order of red shifts $\Delta_{cis-trans} \nu_{OH}^X$ (in cm⁻¹) given in equation 6.

$$\text{Br} \overset{25}{>} \text{Cl} \overset{39}{>} \text{F}. \quad (6)$$

By comparing equations 5 and 6 it is seen that $\Delta_{cis-trans} \nu_{OH}^X$ is not proportional to $\Delta_{cis-trans} E_{ortho}^X$. The order in equation 6 more likely resembles the van der Waals radii of the halogen atoms: Br(1.85Å) > Cl(1.75Å) > F(1.47Å) rather than their electronegativity trend (in Pauling units): F(3.98) > Cl(3.16) > Br(2.96), which is usually chosen to differentiate the strength of the conventional intermolecular hydrogen bonds^{225, 226}.

Both equations 5 and 6 unambiguously imply that in *cis ortho*-XC₆H₄OH, the strength of the O—H . . . X intramolecular hydrogen bond decreases as Br ≈ Cl > F (cf. Table 2 in Reference 236), which is completely opposite to that widely accepted for usual intermolecular hydrogen bonds^{225, 226}. Such variance was in fact a matter of numerous investigations in the past^{155, 236, 237}. Here, we could offer an explanation²³⁹ relying on the geometrical criteria of the hydrogen bond^{225, 226} that are simply expressed in terms of the elongation of the O—H bond length and the value of the ∠O—H . . . X bond angle: the larger they are the stronger the hydrogen bond^{222, 240}. The fact that the strength of the intramolecular hydrogen bond in *cis ortho*-X-substituted phenols exactly follows the order of equations 5 and 6

TABLE 13. Harmonic vibrational frequencies, IR intensities and assignments for *cis* and *trans ortho*-bromophenols^a

No.	Freq.	IR	Sym.	Assignment, PED(%)	No.	Freq.	IR	Sym.	Assignment, PED(%)
1	140.8	0	A''	$\tau_2\text{rg}(42), \gamma\text{CBr}(20), \tau_3\text{rg}(18), \tau_1\text{rg}(10)$	1	137.7	2	A''	$\tau_2\text{rg}(44), \tau_3\text{rg}(19), \gamma\text{CBr}(17), \tau_1\text{rg}(12)$
2	208.7	1	A'	$\beta\text{CBr}(83)$	2	197.8	2	A'	$\beta\text{CBr}(78), \beta\text{CO}(11)$
3	253.7	1	A''	$\tau_2\text{rg}(34), \gamma\text{CBr}(32), \gamma\text{C}_6\text{H}(11)$	3	250.7	13	A''	$\tau_2\text{rg}(33), \gamma\text{CBr}(27)$
4	292.8	1	A'	$\nu\text{CBr}(56), \beta_3\text{rg}(13), \beta_2\text{rg}(10)$	4	299.2	0	A'	$\nu\text{CBr}(53), \beta_3\text{rg}(14), \beta_2\text{rg}(10)$
5	417.6	84	A''	$\tau\text{OH}(54), \tau_3\text{rg}(29), \gamma\text{CBr}(11)$	5	318.5	94	A''	$\tau\text{OH}(87)$ Expt: 372 ^b 361 ^c
Expt: 404 ^b , 395 ^c , 395 ^d									
6	443.4	13	A''	$\tau_3\text{rg}(55), \gamma\text{CBr}(21), \tau\text{OH}(12)$	6	441.7	6	A''	$\tau_3\text{rg}(61), \gamma\text{CBr}(21)$
7	472.5	14	A'	$\beta\text{CO}(68), \nu\text{CBr}(10)$	7	469.3	9	A'	$\beta\text{CO}(68), \beta\text{CBr}(10)$
8	539.1	1	A''	$\tau_2\text{rg}(39), \gamma\text{CO}(30)$	8	545.1	1	A''	$\tau_2\text{rg}(35), \gamma\text{CO}(20), \tau_1\text{rg}(18)$
9	556.5	4	A'	$\beta_2\text{rg}(69)$	9	558.0	4	A'	$\beta_2\text{rg}(67)$
10	660.0	0	A''	$\tau_1\text{rg}(63), \gamma\text{CO}(18)$	10	668.7	15	A'	$\beta_3\text{rg}(67), \nu\text{CBr}(17)$
11	664.7	19	A'	$\beta_3\text{rg}(68), \nu\text{CBr}(17)$	11	685.1	1	A''	$\tau_1\text{rg}(59), \gamma\text{CO}(19), \gamma\text{CBr}(11)$
12	757.5	72	A''	$\gamma\text{C}_4\text{H}(40), \gamma\text{C}_5\text{H}(22), \gamma\text{C}_3\text{H}(21), \gamma\text{C}_6\text{H}(12)$	12	751.8	80	A''	$\gamma\text{C}_4\text{H}(32), \gamma\text{C}_5\text{H}(23), \gamma\text{C}_6\text{H}(22), \gamma\text{C}_3\text{H}(11)$
13	840.4	13	A'	$\nu\text{CO}(25), \beta_1\text{rg}(24), \beta_2\text{rg}(19), \nu\text{C}_1\text{C}_6(11), \nu\text{C}_1\text{C}_2(10)$	13	834.6	0	A''	$\gamma\text{C}_6\text{H}(49), \gamma\text{C}_3\text{H}(21), \gamma\text{C}_4\text{H}(14)$
14	848.7	1	A''	$\gamma\text{C}_6\text{H}(46), \gamma\text{C}_3\text{H}(28)$	14	838.7	20	A'	$\nu\text{CO}(25), \beta_1\text{rg}(25), \beta_2\text{rg}(19), \nu\text{C}_1\text{C}_6(11)$
15	941.3	2	A''	$\gamma\text{C}_3\text{H}(42), \gamma\text{C}_4\text{H}(24), \gamma\text{C}_6\text{H}(19)$	15	932.8	1	A''	$\gamma\text{C}_5\text{H}(38), \gamma\text{C}_3\text{H}(36), \gamma\text{C}_5\text{H}(16)$
16	974.6	0	A''	$\gamma\text{C}_5\text{H}(51), \gamma\text{C}_4\text{H}(22), \gamma\text{C}_6\text{H}(13)$	16	964.3	0	A''	$\gamma\text{C}_4\text{H}(41), \gamma\text{C}_5\text{H}(24), \gamma\text{C}_3\text{H}(23)$
17	1028.2	48	A'	$\beta_1\text{rg}(54), \nu\text{CBr}(13)$	17	1041.7	43	A'	$\beta_1\text{rg}(50), \nu\text{CBr}(14)$

18	1056.6	5	A'	$\nu_{\text{C}_4\text{C}_5(33)}, \beta_{\text{C}_6\text{H}(13)}, \beta_{\text{C}_3\text{H}(11)}, \nu_{\text{C}_3\text{C}_4(11)}$	18	1064.8	5	A	$\nu_{\text{C}_4\text{C}_5(29)}, \nu_{\text{C}_3\text{C}_4(14)}, \beta_{1\text{rg}(13)}, \beta_{\text{C}_3\text{H}(12)}$
19	1135.5	2	A'	$\nu_{\text{C}_3\text{C}_4(24)}, \beta_{\text{C}_5\text{H}(14)}, \beta_{\text{C}_4\text{H}(13)}, \beta_{\text{C}_6\text{H}(12)}, \nu_{\text{C}_5\text{C}_6(10)}$	19	1132.1	69	A'	$\nu_{\text{C}_3\text{C}_4(19)}, \beta_{\text{COH}(15)}, \beta_{\text{C}_4\text{H}(14)}$
20	1179.9	4	A'	$\beta_{\text{C}_4\text{H}(33)}, \beta_{\text{C}_5\text{H}(28)}, \beta_{\text{C}_6\text{H}(12)}$	20	1183.3	2	A'	$\beta_{\text{C}_5\text{H}(35)}, \beta_{\text{C}_4\text{H}(28)}, \beta_{\text{C}_6\text{H}(13)}$
21	1213.7	117	A'	$\beta_{\text{COH}(35)}, \nu_{\text{C}_1\text{C}_6(19)}, \beta_{\text{C}_6\text{H}(12)}, \beta_{\text{C}_3\text{H}(11)}$	21	1189.2	74	A'	$\beta_{\text{COH}(40)}, \beta_{\text{C}_3\text{H}(13)}, \beta_{\text{C}_3\text{H}(12)}, \nu_{\text{C}_1\text{C}_6(10)}$
22	1273.9	63	A'	$\nu_{\text{CO}(31)}, \nu_{\text{C}_2\text{C}_3(27)}, \beta_{\text{C}_3\text{H}(20)}$	22	1283.7	21	A'	$\nu_{\text{CO}(34)}, \nu_{\text{C}_2\text{C}_3(24)}, \beta_{\text{C}_3\text{H}(14)}$
23	1323.7	27	A'	$\nu_{\text{C}_1\text{C}_2(17)}, \nu_{\text{C}_5\text{C}_6(17)}, \beta_{\text{C}_6\text{H}(14)}, \nu_{\text{CO}(14)}$	23	1316.8	73	A'	$\beta_{\text{C}_6\text{H}(24)}, \nu_{\text{CO}(15)}, \nu_{\text{C}_1\text{C}_2(12)}, \nu_{\text{C}_5\text{C}_6(10)}$
24	1366.4	26	A'	$\beta_{\text{COH}(29)}, \beta_{\text{C}_5\text{H}(12)}, \beta_{\text{C}_3\text{H}(11)}, \nu_{\text{C}_3\text{C}_4(10)}$	24	1350.5	49	A'	$\beta_{\text{COH}(18)}, \nu_{\text{C}_3\text{C}_4(14)}, \nu_{\text{C}_1\text{C}_6(13)}, \beta_{\text{C}_3\text{H}(13)}, \nu_{\text{C}_5\text{C}_6(11)}, \nu_{\text{C}_4\text{C}_5(10)}$
25	1486.4	3	A'	$\beta_{\text{C}_4\text{H}(30)}, \beta_{\text{C}_5\text{H}(14)}, \nu_{\text{C}_2\text{C}_3(12)}$	25	1474.5	51	A'	$\beta_{\text{C}_4\text{H}(26)}, \beta_{\text{C}_5\text{H}(23)}, \nu_{\text{C}_1\text{C}_6(11)}, \nu_{\text{C}_2\text{C}_3(10)}$
26	1504.9	129	A'	$\beta_{\text{C}_3\text{H}(20)}, \beta_{\text{C}_6\text{H}(16)}, \nu_{\text{C}_1\text{C}_2(15)}, \nu_{\text{CO}(11)}$	26	1520.3	49	A'	$\beta_{\text{C}_3\text{H}(20)}, \beta_{\text{C}_5\text{H}(18)}, \nu_{\text{C}_1\text{C}_2(12)}, \nu_{\text{C}_4\text{C}_5(11)}$
27	1618.5	10	A'	$\nu_{\text{C}_4\text{C}_5(20)}, \nu_{\text{C}_1\text{C}_6(19)}, \nu_{\text{C}_3\text{C}_4(15)}, \nu_{\text{C}_1\text{C}_2(14)}$	27	1617.2	13	A'	$\nu_{\text{C}_1\text{C}_6(23)}, \nu_{\text{C}_3\text{C}_4(23)}$
28	1630.4	43	A'	$\nu_{\text{C}_5\text{C}_6(27)}, \nu_{\text{C}_2\text{C}_3(17)}, \beta_{2\text{rg}(10)}$	28	1632.9	27	A'	$\nu_{\text{C}_5\text{C}_6(21)}, \nu_{\text{C}_1\text{C}_2(19)}, \nu_{\text{C}_4\text{C}_5(17)}, \nu_{\text{C}_2\text{C}_3(12)}$
29	3174.5	2	A'	$\nu_{\text{C}_5\text{H}(57)}, \nu_{\text{C}_4\text{H}(27)}, \nu_{\text{C}_6\text{H}(12)}$	29	3150.6	10	A'	$\nu_{\text{C}_6\text{H}(93)}$
30	3187.6	7	A'	$\nu_{\text{C}_4\text{H}(41)}, \nu_{\text{C}_6\text{H}(26)}, \nu_{\text{C}_3\text{H}(22)}, \nu_{\text{C}_5\text{H}(11)}$	30	3177.9	4	A	$\nu_{\text{C}_4\text{H}(46)}, \nu_{\text{C}_5\text{H}(41)}$
31	3195.9	5	A'	$\nu_{\text{C}_6\text{H}(55)}, \nu_{\text{C}_3\text{H}(23)}, \nu_{\text{C}_5\text{H}(21)}$	31	3190.8	8	A'	$\nu_{\text{C}_5\text{H}(43)}, \nu_{\text{C}_3\text{H}(35)}, \nu_{\text{C}_4\text{H}(19)}$
32	3203.3	5	A'	$\nu_{\text{C}_3\text{H}(51)}, \nu_{\text{C}_4\text{H}(31)}, \nu_{\text{C}_5\text{H}(11)}$	32	3202.3	5	A'	$\nu_{\text{C}_3\text{H}(57)}, \nu_{\text{C}_4\text{H}(34)}$
33	3739.7	97	A'	$\nu_{\text{OH}(100)}$	33	3833.8	71	A'	$\nu_{\text{OH}(100)}$

^aFootnotes *a*–*d* are identical to those in Table 11.

is clearly seen in Figure 12: due to a larger van der Waals radius, the Br atom slightly better accommodates the intramolecular bond, even ‘overcoming the innate lower H-bonding tendency to Br’²⁴⁰ than Cl which, in turn, does better than F. Such a conclusion is also supported by the inequalities in equation 7.

$$\text{OH bond length (\AA): } \text{Br}^{0.001} > \text{Cl}^{0.002} > \text{F} \quad (7)$$

$$\angle \text{O-H} \cdots \text{X}(\text{deg}): \text{Br}^{3.1} > \text{Cl}^{9.2} > \text{F}$$

(ii) The gas-phase theoretical equilibrium constants $k_{cis \rightleftharpoons trans}^X$ follow the order in equation 8,

$$\text{F}^{1.56} > \text{Cl}^{1.27} > \text{Br} \quad (8)$$

where the quantity above the inequality indicates the ratio of the equilibrium constants between the left-hand complex and the right-hand complex. Such order in the equilibrium constants is mirrored in the order of the calculated *cis-trans* barriers V_τ^X (equation 9):

$$\text{F}^{0.43} < \text{Cl}^{0.15} < \text{Br} \quad (9)$$

It would be expected that the *trans/cis* ratio follows the order of equation 5 for the hydrogen bond energies, but surprisingly the opposite is known. It has even been argued²²⁷ that ‘the fact that both the *trans/cis* ratio and the $\Delta\nu$ shift increase in the same order appears to argue against the applicability of Badger’s rule²⁴¹ which stated that the progressive shift to lower frequencies is an indication of increasing strength of the hydrogen bond. If the rule is valid here ...’.

In order to resolve the longstanding controversy between experiment and theory, let us first suggest that the dipole moments of the *cis* and *trans* forms and their polarizability might play a key role, bearing in mind that all aforementioned experiments were conducted in a solvent although its role in theory was underestimated. This is clearly seen from the inequalities between the *trans/cis* ratio of the total dipole moments: $2.95_{\text{F}} > 2.87_{\text{Cl}} > 2.77_{\text{Br}}$. A similar ratio was also determined elsewhere^{223, 238} (for a discussion see Reference 229). By analogy, we have the corresponding *trans/cis* ratio for the mean polarizability $\alpha = (\alpha_{xx} + \alpha_{yy} + \alpha_{zz})/3$ (in a.u.) in equation 10.

$$\frac{92.19}{91.77}_{\text{Br}} > \frac{84.63}{84.00}_{\text{Cl}} > \frac{71.60}{71.13}_{\text{F}} \quad (10)$$

The experimental data for the equilibrium constants in CCl_4 solution (equation 11)^{233, 234},

$$\text{Br}^{1.47} > \text{Cl} \quad (11)$$

are in complete disagreement with the theoretical expectations based on equations 8 and 9. In order to explain this discrepancy, one must take into account a stabilizing effect of the solvent on the *trans* form²³¹, and we propose the following model²²⁰.

The presence of the *ortho*-halogen atom in a phenol generates two distinct *cis* and *trans* conformers and changes the shape of the torsional transition barrier V_τ , making it partly asymmetric. Within the *cis* form, the halogen atom is capable of forming an intramolecular hydrogen bond, rather bent and quite weak. Its formation has a stabilizing effect on the *cis* (particularly in the gas phase) over the *trans* form. On the other hand, due to the larger polarity and larger polarizability of the *trans* *o*X- $\text{C}_6\text{H}_4\text{OH}$, the latter conformer might, in some rather polar solvents, be favoured over the *cis* form. We suggest that solvent

TABLE 14. AM1 and SM5.4/AM1 data on *ortho*-XC₆H₄OH (X = F, Cl and Br) and their *cis*–*trans* transition state (TS) including the heat of formation ΔH (kJ mol^{−1}), free solvation energy ΔG^{solv} (kJ mol^{−1}) and ν_{OH} stretching frequency (in cm^{−1})

		<i>cis ortho</i> -XC ₆ H ₄ OH		
		r_{OH} (Å)	$\angle \text{O} \cdots \text{X}$ (deg)	$r_{\text{H} \cdots \text{X}}$ (Å)
F	gas phase	0.970	111.2	2.325
	solvent	0.979	110.5	2.335
Cl	gas phase	0.970	117.1	2.506
	solvent	0.975	116.3	2.524
Br	gas phase	0.971	119.8	2.617
	solvent	0.975	119.0	2.634

	Gas phase		CCl ₄		
	$-\Delta H$	ν_{OH}	$-\Delta H$	$-\Delta G^{\text{solv}}$	ν_{OH}
<i>cis o</i> -FC ₆ H ₄ OH	280	3431	300	22	3316
<i>trans o</i> -FC ₆ H ₄ OH	273	3452	297	27	3309
<i>cis-trans</i> TS	266		289		
<i>cis o</i> -ClC ₆ H ₄ OH	120	3420	144	25	3350
<i>trans o</i> -ClC ₆ H ₄ OH	112	3451	142	32	3313
<i>cis-trans</i> TS	105		133		
<i>cis o</i> -BrC ₆ H ₄ OH	61	3407	96	28	3346
<i>trans o</i> -BrC ₆ H ₄ OH	61	3448	94	35	3311
<i>cis-trans</i> TS	54		85		

^aCompare with the free energy of hydration: AM1-SM2: −20 kJ mol^{−1}; PM3-SM3: −20 kJ mol^{−1} (Reference 243). Values are taken from Reference 220 with permission.

stabilizes the *trans* more strongly than the *cis* and hence decreases $\Delta_{\text{cis-trans}} E_{\text{ortho}}^{\text{X}}$, thus making it more accessible than in the gas phase.

In order to describe theoretically the *cis* and *trans ortho*-XC₆H₄OH in a solvent mimicking CCl₄, we invoke a rather simple but accurate computational model²⁴². Its results are summarized in Table 14, which displays the following three key effects of the solvent. First, the solvent reduces the gas-phase $\Delta_{\text{cis-trans}} \nu_{\text{OH}}^{\text{X}}$ to 7, 37 and 35 cm^{−1} for F, Cl and Br, respectively. We think that this is a satisfactory explanation of why the *cis*–*trans* ν_{OH} doublet in *o*-FC₆H₄OH was not observed in CCl₄. Second, the solvent strongly stabilizes the *trans* form so that the *cis*–*trans* gap $\Delta_{\text{cis-trans}} E_{\text{ortho}}^{\text{X}}$ appears to be equal to 3.4, 2.8 and 2.0 kJ mol^{−1} for F, Cl and Br, respectively. This straightforwardly implies an increase in the equilibrium constants $k_{\text{cis} \rightleftharpoons \text{trans}}^{\text{X}}$ in the series of F, Cl and Br equal to 0.25, 0.33 and 0.45, respectively with respect to that in the parent phenol. Third, the solvent reduces the *cis*–*trans* barrier V_{r} to 11.8, 11.4 and 11.7 kJ mol^{−1} for F, Cl and Br, respectively. Altogether, we may conclude that even a rather simple modelling of solvent is able to resolve the aforementioned controversial ‘state of affairs’ in the *ortho*-X-substituted phenols.

B. *meta*- and *para*-Halogenophenols

The corresponding substituted phenols are displayed symbolically in Figure 13 and their characteristic vibrational modes, showing a rather strong dependence on the X substitution,

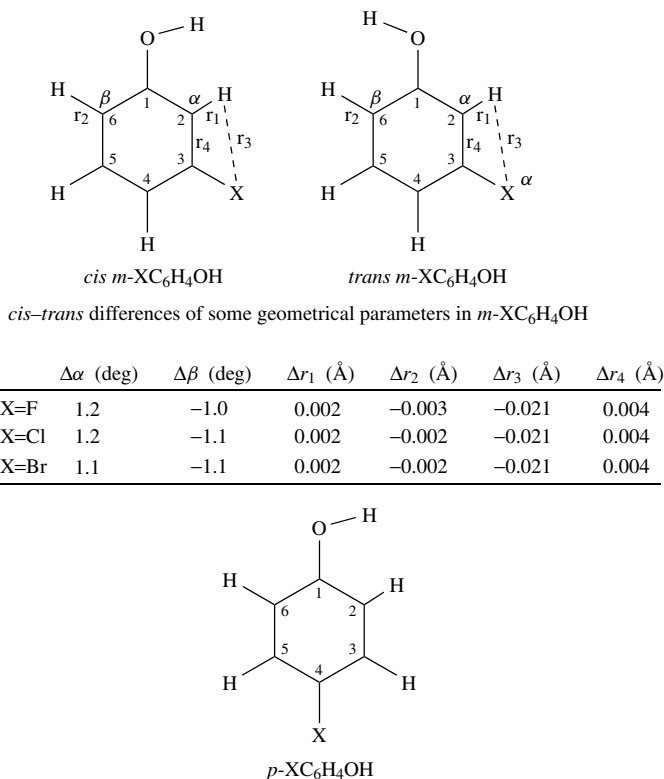


FIGURE 13. The minimum energy structures of *cis* and *trans meta*- and *para-XC₆H₄OH* (X = F, Cl and Br). Bond lengths are in Å, bond angles in degrees. Adapted from Reference 220 with permission

are presented in Tables 11–13 and 15–20²⁴⁴. Note that the spectra of *p*-ClC₆H₄OH and *p*-BrC₆H₄OH have been analyzed critically on the basis of DFT computations^{170, 245}. It follows from these Tables that, first, a *para* substitution by fluorine downshifts the torsional vibrational mode τ_{OH} by 29 cm⁻¹ in perfect agreement with the experimental red shift¹⁷² of 30 cm⁻¹. In *m-XC₆H₄OH*, the mode τ_{OH} is placed higher than in the corresponding *para*-halophenols. This observation is partly supported by the NBO analysis, demonstrating a strong conjugative interaction of the *p*-type oxygen lone pair with the π -antibond of the ring, viz. $n_p \rightarrow \pi^*(\text{C}_1\text{-C}_2)$, a little increased in all *meta* structures, resulting in upshifting of the τ_{OH} in *m-XC₆H₄OH* with respect to *p-XC₆H₄OH*. This concurs with the earlier experimental findings¹⁷².

Furthermore, one obtains certain subtle features in the spectra of *m-XC₆H₄OH* whose origin can only be explained by the co-existence of two very slightly inequivalent conformers of the *cis* and *trans* types. This is seen, for example, from the magnitude of $\Delta_{\text{cis-trans}} E_{\text{meta}}^{\text{X}}$ ranging from -0.8 kJ mol⁻¹ for F to +0.08 kJ mol⁻¹ for Cl, and finally to +0.04 kJ mol⁻¹ for Br. If the difference is extremely small for Cl and Br, F is then an exception. Contrary to Cl and Br, we obtain that the *trans* conformer of *m*-FC₆H₄OH is a little more stable than its *cis* conformer. The *cis-trans* differences in the geometrical

TABLE 15. Harmonic vibrational frequencies, IR intensities and assignments for *cis* and *trans meta*-fluorophenols^a

No.	Freq.	IR	Sym.	Assignment, PED(%)	No.	Freq.	IR	Sym.	Assignment, PED(%)
1	224.0	0	A''	$\tau_2\text{rg}(23)$, $\tau_1\text{rg}(22)$, $\gamma\text{C}_2\text{H}(18)$, $\tau_3\text{rg}(14)$	1	223.2	3	A''	$\tau_1\text{rg}(24)$, $\tau_2\text{rg}(23)$, $\gamma\text{C}_2\text{H}(22)$, $\tau_3\text{rg}(10)$
2	239.9	2	A''	$\tau_2\text{rg}(50)$, $\tau_3\text{rg}(30)$	2	238.0	0	A''	$\tau_2\text{rg}(49)$, $\tau_3\text{rg}(33)$
3	314.0	111	A'	$\tau\text{OH}(90)$	3	320.7	109	A'	$\tau\text{OH}(90)$
Expt: 318.5 ^b , 318 ^c , 317 ^d									
4	328.7	9	A'	$\beta\text{CF}(40)$, $\beta\text{CO}(38)$	4	330.1	2	A'	$\beta\text{CF}(39)$, $\beta\text{CO}(39)$
5	460.1	12	A'	$\tau_3\text{rg}(47)$, $\tau_2\text{rg}(13)$, $\gamma\text{CF}(11)$, $\gamma\text{CO}(10)$	5	459.7	2	A''	$\tau_3\text{rg}(47)$, $\tau_2\text{rg}(12)$, $\gamma\text{CF}(10)$
6	480.3	5	A'	$\beta\text{CO}(43)$, $\beta\text{CF}(40)$	6	476.4	11	A'	$\beta\text{CO}(41)$, $\beta\text{CF}(39)$
7	520.5	8	A'	$\beta_3\text{rg}(40)$, $\beta_2\text{rg}(36)$, $\nu\text{CF}(8)$	7	520.7	6	A'	$\beta_3\text{rg}(38)$, $\beta_2\text{rg}(36)$
8	536.9	4	A'	$\beta_1\text{rg}(44)$, $\beta_3\text{rg}(25)$	8	538.2	4	A'	$\beta_2\text{rg}(41)$, $\beta_3\text{rg}(28)$
9	612.2	0	A''	$\gamma\text{CF}(35)$, $\gamma\text{CO}(33)$, $\tau_2\text{rg}(23)$	9	614.5	1	A''	$\gamma\text{CO}(40)$, $\gamma\text{CF}(27)$, $\tau_2\text{rg}(23)$
10	666.5	14	A''	$\tau_1\text{rg}(67)$, $\gamma\text{CO}(12)$, $\gamma\text{CF}(11)$	10	657.6	11	A''	$\tau_1\text{rg}(65)$, $\gamma\text{CF}(16)$
11	750.8	6	A'	$\beta_3\text{rg}(25)$, $\beta_1\text{rg}(18)$, $\nu\text{CO}(10)$	11	748.2	5	A'	$\beta_3\text{rg}(25)$, $\beta_1\text{rg}(17)$, $\nu\text{CO}(10)$
12	775.9	38	A''	$\gamma\text{C}_4\text{H}(36)$, $\gamma\text{C}_6\text{H}(25)$, $\gamma\text{C}_5\text{H}(21)$	12	758.4	67	A''	$\gamma\text{C}_6\text{H}(39)$, $\gamma\text{C}_4\text{H}(22)$, $\gamma\text{C}_5\text{H}(16)$, $\tau_1\text{rg}(12)$
13	827.5	50	A''	$\gamma\text{C}_5\text{H}(58)$, $\tau_1\text{rg}(19)$	13	844.4	10	A''	$\gamma\text{C}_2\text{H}(36)$, $\gamma\text{C}_6\text{H}(25)$, $\gamma\text{C}_4\text{H}(15)$
14	876.6	0	A''	$\gamma\text{C}_4\text{H}(41)$, $\gamma\text{C}_6\text{H}(40)$	14	862.7	22	A''	$\gamma\text{C}_2\text{H}(38)$, $\gamma\text{C}_4\text{H}(26)$, $\gamma\text{CF}(10)$, $\tau_1\text{rg}(10)$
15	967.1	0	A''	$\gamma\text{C}_5\text{H}(61)$, $\gamma\text{C}_6\text{H}(18)$, $\gamma\text{C}_4\text{H}(10)$	15	945.2	0	A''	$\gamma\text{C}_5\text{H}(63)$, $\gamma\text{C}_4\text{H}(17)$
16	970.3	54	A'	$\nu\text{CF}(17)$, $\nu\text{CO}(16)$, $\nu\text{C}_1\text{C}_6(14)$, $\nu\text{C}_1\text{C}_2(10)$	16	968.6	88	A'	$\nu\text{CF}(16)$, $\nu\text{C}_1\text{C}_6(15)$, $\nu\text{CO}(15)$
17	1014.4	7	A'	$\beta_1\text{rg}(60)$	17	1013.9	5	A'	$\beta_1\text{rg}(61)$
18	1088.0	13	A'	$\beta\text{C}_4\text{H}(27)$, $\nu\text{C}_4\text{C}_5(24)$, $\beta\text{C}_6\text{H}(18)$, $\nu\text{C}_5\text{C}_6(16)$	18	1095.1	3	A'	$\beta\text{C}_4\text{H}(32)$, $\nu\text{C}_4\text{C}_5(24)$, $\nu\text{C}_5\text{C}_6(18)$, $\beta\text{C}_6\text{H}(13)$
19	1152.2	94	A'	$\beta\text{C}_2\text{H}(29)$, $\nu\text{CF}(21)$, $\beta\text{C}_4\text{H}(12)$, $\beta\text{C}_6\text{H}(10)$, $\nu\text{CO}(10)$	19	1141.4	168	A'	$\beta\text{C}_2\text{H}(38)$, $\nu\text{CF}(20)$, $\nu\text{CO}(15)$
20	1181.4	17	A'	$\beta\text{C}_6\text{H}(22)$, $\beta\text{COH}(17)$, $\beta\text{C}_5\text{H}(13)$, $\beta\text{C}_2\text{H}(12)$	20	1179.2	14	A'	$\beta\text{C}_6\text{H}(27)$, $\beta\text{C}_5\text{H}(23)$, $\beta\text{C}_4\text{H}(12)$, $\nu\text{C}_5\text{C}_6(11)$, $\beta\text{COH}(11)$

(continued overleaf)

TABLE 15. (continued)

No.	Freq.	IR	Sym.	Assignment, PED(%)	No.	Freq.	IR	Sym.	Assignment, PED(%)
21	1192.6	175	A'	β COH(38), β C ₅ H(19), ν CO(12)	21	1209.2	33	A'	β COH(42), β C ₅ H(16), ν CF(14), ν C ₁ C ₂ (11)
22	1299.3	75	A'	ν CO(22), ν CF(18), β rg(13), β C ₄ H(13), β C ₂ H(10)	22	1299.2	45	A'	ν CO(19), ν CF(18), β C ₄ H(14), β rg(13)
23	1334.5	7	A'	β C ₅ H(18), β C ₆ H(15), β COH(14), ν CO(12), β C ₂ H(11), β C ₄ H(10)	23	1322.7	82	A'	ν CO(21), β C ₆ H(15), β C ₅ H(13), β C ₂ H(13), β COH(11)
24	1354.7	11	A'	ν C ₂ C ₃ (16), ν C ₃ C ₄ (16), ν C ₅ C ₆ (14), ν C ₄ C ₅ (14), ν C ₁ C ₆ (12), ν C ₁ C ₂ (11)	24	1354.3	16	A'	ν C ₅ C ₆ (15), ν C ₃ C ₄ (15), ν C ₄ C ₅ (15), ν C ₂ C ₃ (15), ν C ₁ C ₆ (13), ν C ₁ C ₂ (10)
25	1488.5	44	A'	β C ₆ H(22), ν C ₁ C ₂ (14), ν C ₂ C ₃ (13), ν C ₄ C ₅ (10), β C ₄ H(10)	25	1507.4	18	A'	β C ₆ H(19), ν C ₂ C ₃ (16), β C ₄ H(13), ν C ₁ C ₂ (11)
26	1529.0	81	A'	β C ₅ H(22), ν C ₃ C ₄ (14), β C ₂ H(14), ν C ₁ C ₆ (10)	26	1515.9	125	A'	β C ₅ H(26), β C ₂ H(12), ν C ₃ C ₄ (12), ν C ₁ C ₆ (10)
27	1637.3	147	A'	ν C ₁ C ₂ (23), ν C ₄ C ₅ (20)	27	1642.1	72	A'	ν C ₃ C ₄ (23), ν C ₁ C ₆ (21), ν C ₁ C ₂ (13), ν C ₄ C ₅ (10)
28	1657.9	98	A'	ν C ₁ C ₆ (19), ν C ₂ C ₃ (19), ν C ₃ C ₄ (18), ν C ₅ C ₆ (15)	28	1652.2	164	A'	ν C ₂ C ₃ (23), ν C ₃ C ₄ (19), ν C ₁ C ₂ (13), β rg(10)
29	3179.8	8	A'	ν C ₅ H(77)	29	3160.4	10	A'	ν C ₆ H(89), ν C ₅ H(10)
30	3181.5	1	A'	ν C ₂ H(91)	30	3184.9	8	A'	ν C ₅ H(82), ν C ₆ H(10)
31	3202.7	4	A'	ν C ₆ H(83), ν C ₄ H(10)	31	3210.9	1	A'	ν C ₄ H(91)
32	3211.1	1	A'	ν C ₄ H(84)	32	3213.9	0	A'	ν C ₅ H(99)
33	3836.4	70	A'	ν OH(100)	33	3835.7	71	A'	ν OH(100)

^aFootnotes *a*–*d* are identical to those in Table 11.

TABLE 16. Harmonic vibrational frequencies, IR intensities and assignments for *cis* and *trans meta*-chlorophenols^a

No.	Freq.	IR	Sym.	Assignment, PED(%)	No.	Freq.	IR	Sym.	Assignment, PED(%)
1	180.4	0	A''	$\tau_3\text{rg}(34)$, $\gamma\text{CCI}(30)$, $\gamma\text{C}_2\text{H}(13)$	1	180.6	3	A''	$\tau_3\text{rg}(33)$, $\gamma\text{CCI}(29)$, $\gamma\text{C}_2\text{H}(15)$
2	228.8	3	A''	$\tau_2\text{rg}(69)$	2	229.2	1	A''	$\tau_2\text{rg}(68)$, $\tau_1\text{rg}(10)$
3	247.6	2	A'	$\beta\text{CCI}(69)$, $\beta\text{CO}(16)$	3	248.7	1	A'	$\beta\text{CCI}(69)$, $\beta\text{CO}(16)$
4	311.9	110	A''	$\tau\text{OH}(90)$ Expt: 312.5^b , 312^c , 313^d	4	307.8	111	A''	$\tau\text{OH}(93)$
5	406.2	6	A'	$\nu\text{CCI}(49)$, $\beta_3\text{rg}(22)$	5	407.3	5	A'	$\nu\text{CCI}(50)$, $\beta_3\text{rg}(23)$
6	447.1	10	A'	$\beta\text{CO}(59)$, $\beta\text{CCI}(16)$, $\beta_3\text{rg}(13)$	6	443.8	9	A'	$\beta\text{CO}(59)$, $\beta\text{CCI}(16)$, $\beta_3\text{rg}(12)$
7	448.7	11	A''	$\tau_3\text{rg}(57)$, $\gamma\text{CCI}(13)$	7	449.7	2	A''	$\tau_3\text{rg}(57)$, $\gamma\text{CCI}(12)$
8	535.7	3	A'	$\beta_2\text{rg}(75)$	8	536.3	3	A'	$\beta_2\text{rg}(73)$
9	579.9	0	A''	$\gamma\text{CO}(34)$, $\tau_2\text{rg}(27)$, $\gamma\text{CCI}(27)$	9	580.1	1	A''	$\gamma\text{CO}(39)$, $\tau_2\text{rg}(28)$, $\gamma\text{CCI}(24)$
10	677.3	13	A''	$\tau_1\text{rg}(69)$, $\gamma\text{CO}(13)$	10	670.7	11	A''	$\tau_1\text{rg}(68)$, $\gamma\text{CO}(11)$, $\gamma\text{CCI}(10)$, $\gamma\text{C}_5\text{H}(10)$
11	697.1	7	A'	$\beta_3\text{rg}(56)$, $\nu\text{CCI}(20)$	11	695.0	8	A'	$\beta_3\text{rg}(56)$, $\nu\text{CCI}(20)$
12	780.9	45	A''	$\gamma\text{C}_4\text{H}(36)$, $\gamma\text{CO}(23)$, $\gamma\text{C}_5\text{H}(21)$, $\tau_1\text{rg}(12)$	12	764.3	61	A''	$\gamma\text{C}_6\text{H}(33)$, $\gamma\text{C}_4\text{H}(25)$, $\gamma\text{C}_5\text{H}(16)$, $\tau_1\text{rg}(15)$
13	835.3	28	A''	$\gamma\text{C}_2\text{H}(68)$, $\tau_1\text{rg}(16)$	13	859.3	4	A''	$\gamma\text{C}_6\text{H}(37)$, $\gamma\text{C}_4\text{H}(27)$, $\gamma\text{C}_2\text{H}(15)$
14	886.1	0	A''	$\gamma\text{C}_6\text{H}(46)$, $\gamma\text{C}_4\text{H}(40)$	14	866.9	17	A''	$\gamma\text{C}_2\text{H}(62)$, $\gamma\text{C}_4\text{H}(12)$, $\tau_1\text{rg}(11)$
15	893.7	82	A'	$\nu\text{CO}(22)$, $\nu\text{CCI}(22)$, $\beta_2\text{rg}(15)$, $\beta_1\text{rg}(11)$, $\nu\text{C}_1\text{C}_6(10)$	15	894.8	108	A'	$\nu\text{CO}(23)$, $\nu\text{CCI}(21)$, $\beta_2\text{rg}(14)$, $\beta_1\text{rg}(11)$, $\nu\text{C}_1\text{C}_6(11)$
16	975.6	0	A''	$\gamma\text{C}_5\text{H}(58)$, $\gamma\text{C}_6\text{H}(18)$, $\gamma\text{C}_4\text{H}(13)$	16	954.1	0	A''	$\gamma\text{C}_5\text{H}(59)$, $\gamma\text{C}_4\text{H}(21)$
17	1009.1	9	A'	$\beta_1\text{rg}(64)$, $\nu\text{C}_1\text{C}_6(11)$	17	1009.5	6	A'	$\beta_1\text{rg}(64)$, $\nu\text{C}_1\text{C}_2(10)$
18	1087.3	15	A'	$\nu\text{C}_4\text{C}_5(29)$, $\beta\text{C}_6\text{H}(16)$, $\nu\text{C}_5\text{C}_6(10)$	18	1087.8	30	A'	$\beta\text{C}_2\text{H}(20)$, $\nu\text{C}_5\text{C}_4(18)$, $\nu\text{C}_4\text{C}_5(17)$, $\nu\text{CCI}(13)$
19	1107.6	38	A'	$\nu\text{C}_4\text{C}_3(19)$, $\nu\text{C}_2\text{C}_3(15)$, $\beta\text{C}_4\text{H}(15)$, $\beta\text{C}_2\text{H}(12)$	19	1107.6	0	A'	$\beta\text{C}_4\text{H}(23)$, $\nu\text{C}_5\text{C}_6(18)$, $\beta\text{C}_6\text{H}(12)$, $\nu\text{C}_4\text{C}_5(12)$
20	1180.4	43	A'	$\beta\text{C}_6\text{H}(28)$, $\beta\text{C}_5\text{H}(23)$, $\beta\text{C}_4\text{H}(14)$	20	1183.8	27	A'	$\beta\text{C}_6\text{H}(23)$, $\beta\text{COH}(20)$, $\beta\text{C}_5\text{H}(19)$, $\beta\text{C}_4\text{H}(10)$

(continued overleaf)

TABLE 16. (continued)

No.	Freq.	IR	Sym.	Assignment, PED(%)	No.	Freq.	IR	Sym.	Assignment, PED(%)
21	1191.1	89	A'	β COH(46), β C ₅ H(11), ν C ₁ C ₂ (10)	21	1192.3	111	A'	β COH(38), β C ₅ H(17), ν C ₁ C ₂ (13), β C ₂ H(11)
22	1271.3	87	A'	ν CO(42), β C ₂ H(20), β rg(12)	22	1271.5	29	A'	ν CO(40), β rg(12), β C ₂ H(12)
23	1333.6	3	A'	β C ₅ H(21), β C ₄ H(17), β COH(16), β C ₂ H(14)	23	1322.3	81	A'	β C ₂ H(17), β COH(15), β C ₅ H(15), ν CO(13), β C ₄ H(13), β C ₆ H(10)
24	1342.4	15	A'	ν C ₃ C ₄ (16), ν C ₂ C ₃ (16), ν C ₅ C ₆ (14), ν C ₄ C ₅ (14), ν C ₁ C ₂ (11), ν C ₁ C ₆ (10)	24	1342.9	9	A'	ν C ₂ C ₃ (15), ν C ₃ C ₄ (15), ν C ₄ C ₅ (15), ν C ₅ C ₆ (14), ν C ₁ C ₆ (11), ν C ₁ C ₂ (10)
25	1470.8	52	A'	β C ₆ H(21), ν C ₂ C ₃ (15), β C ₄ H(13), ν C ₄ C ₅ (12), ν C ₁ C ₂ (11)	25	1487.1	24	A'	ν C ₂ C ₃ (21), β C ₄ H(21), β C ₆ H(14)
26	1515.0	73	A'	β C ₅ H(21), β C ₂ H(17), ν C ₃ C ₄ (15), β C ₄ H(11)	26	1504.6	93	A'	β C ₅ H(27), ν C ₃ C ₄ (12), β C ₂ H(12)
27	1623.7	117	A'	ν C ₁ C ₂ (24), ν C ₄ C ₅ (21)	27	1625.5	62	A'	ν C ₁ C ₆ (27), ν C ₃ C ₄ (19)
28	1640.5	81	A'	ν C ₁ C ₆ (22), ν C ₅ C ₆ (17), ν C ₂ C ₃ (15), ν C ₃ C ₄ (14)	28	1637.6	133	A'	ν C ₁ C ₂ (20), ν C ₅ C ₆ (19), ν C ₂ C ₃ (15), ν C ₄ C ₅ (13)
29	3177.4	9	A'	ν C ₅ H(49), ν C ₂ H(42)	29	3159.2	10	A'	ν C ₆ H(87), ν C ₅ H(12)
30	3178.5	1	A'	ν C ₂ H(57), ν C ₅ H(35)	30	3182.9	9	A'	ν C ₅ H(81), ν C ₆ H(11)
31	3201.6	3	A'	ν C ₆ H(84)	31	3210.6	1	A'	ν C ₄ H(85)
32	3210.6	2	A'	ν C ₄ H(86)	32	3212.2	1	A'	ν C ₅ H(91)
33	3833.7	68	A'	ν OH(100)	33	3835.6	74	A'	ν OH(97)

^aFootnotes *a*–*d* are identical to those in Table 11.

TABLE 17. Harmonic vibrational frequencies, IR intensities and assignments for *cis* and *trans meta*-bromophenols^a

No.	Freq.	IR	Sym.	Assignment, PED(%)	No.	Freq.	IR	Sym.	Assignment, PED(%)
1	161.0	0	A''	γ CBr(39), τ_3 rg(30), γ C ₂ H(11)	1	160.9	4	A''	γ CBr(38), τ_3 rg(29), γ C ₂ H(13)
2	204.0	1	A'	β CBr(75), β CO(11)	2	204.7	1	A'	β CBr(76), β CO(11)
3	228.0	2	A''	τ_2 rg(68), τ_1 rg(10)	3	227.8	1	A''	τ_2 rg(68), τ_1 rg(10)
4	307.4	2	A'	ν CBr(65), β_3 rg(16)	4	308.1	2	A'	ν CBr(65), β_3 rg(16)
5	314.7	109	A''	τ OH(89) Expt: 314 ^b , 312 ^c , 309 ^d	5	310.4	110	A''	τ OH(92)
6	438.3	13	A'	β CO(67), β CBr(13), β_3 rg(10)	6	435.3	8	A'	β CO(66), β CBr(13)
7	443.3	12	A''	τ_3 rg(60), γ CBr(15)	7	445.0	2	A''	τ_3 rg(61), γ CBr(14)
8	535.6	2	A'	β_2 rg(76)	8	535.9	3	A'	β_2 rg(76)
9	564.5	0	A''	γ CO(28), τ_2 rg(28), γ CBr(26)	9	567.4	0	A''	γ CO(31), τ_2 rg(28), γ CBr(25)
10	668.4	11	A''	τ_1 rg(69), γ CO(16)	10	664.7	11	A''	τ_1 rg(68), γ CO(14)
11	679.5	7	A'	β_3 rg(65), ν CBr(17)	11	678.0	8	A'	β_3 rg(66), ν CBr(16)
12	779.0	48	A''	γ C ₄ H(35), γ C ₆ H(23), γ C ₅ H(23), τ_1 rg(11)	12	762.5	61	A''	γ C ₆ H(32), γ C ₄ H(26), γ C ₅ H(18), τ_1 rg(13)
13	832.5	22	A''	γ C ₃ H(73), τ_1 rg(14)	13	863.1	0	A''	γ C ₆ H(45), γ C ₄ H(38)
14	874.1	76	A'	ν CO(23), ν CBr(17), β_2 rg(17), β_1 rg(15), ν C ₁ C ₆ (10)	14	866.2	16	A''	γ C ₂ H(74), τ_1 rg(12)
15	888.3	1	A''	γ C ₆ H(46), γ C ₄ H(40)	15	875.0	97	A'	ν CO(23), ν CBr(17), β_2 rg(16), β_1 rg(16), ν C ₁ C ₆ (11)
16	974.5	0	A''	γ C ₃ H(57), γ C ₆ H(18), γ C ₄ H(14)	16	953.9	0	A''	γ C ₅ H(58), γ C ₄ H(22)
17	1007.4	13	A'	β_1 rg(64), ν C ₁ C ₆ (11)	17	1007.9	9	A'	β_1 rg(64), ν C ₁ C ₂ (11), ν C ₁ C ₆ (10)
18	1080.6	12	A'	ν C ₄ C ₅ (27), ν C ₃ C ₄ (13), β C ₂ H(11), β C ₆ H(11)	18	1079.4	18	A'	ν C ₃ C ₄ (23), β C ₂ H(18), ν C ₄ C ₅ (17)
19	1106.0	23	A'	ν C ₃ C ₄ (16), β C ₄ H(15), ν C ₂ C ₃ (14), ν C ₅ C ₆ (12), β C ₆ H(12)	19	1108.0	1	A'	β C ₄ H(21), ν C ₅ C ₆ (19), β C ₆ H(14), ν C ₄ C ₅ (13)
20	1181.4	45	A'	β C ₆ H(27), β C ₅ H(23), β C ₄ H(15)	20	1184.5	32	A'	β C ₆ H(22), β COH(20), β C ₅ H(18), β C ₄ H(10)

(continued overleaf)

TABLE 17. (*continued*)

No.	Freq.	IR	Sym.	Assignment, PED(%)	No.	Freq.	IR	Sym.	Assignment, PED(%)
21	1194.0	91	A'	β COH(46), β C ₅ H(10), ν C ₁ C ₂ (10), ν C ₁ C ₆ (10), β C ₂ H(10)	21	1192.4	116	A'	β COH(34), β C ₃ H(18), β C ₂ H(13), ν C ₁ C ₂ (13)
22	1269.1	86	A'	ν CO(43), β C ₂ H(21), β_1 rg(12)	22	1269.2	26	A'	ν CO(38), β C ₂ H(12), β_1 rg(12)
23	1334.0	2	A'	β C ₃ H(20), β C ₄ H(19), β C ₂ H(16), β COH(14), β C ₆ H(10)	23	1322.3	83	A'	β C ₂ H(19), β C ₅ H(15), β C ₄ H(15), ν CO(12), β COH(12), β C ₆ H(10)
24	1339.6	18	A'	ν C ₂ C ₃ (17), ν C ₃ C ₄ (17), ν C ₄ C ₅ (14), C ₅ C ₆ (14), ν C ₁ C ₂ (11), ν C ₁ C ₆ (10)	24	1339.9	10	A'	ν C ₂ C ₃ (16), ν C ₃ C ₄ (15), ν C ₄ C ₅ (15), ν C ₂ C ₃ (21), β C ₄ H(21), β C ₆ H(14), β COH(10), ν C ₄ C ₅ (10)
25	1467.3	58	A'	β C ₆ H(21), ν C ₂ C ₃ (15), β C ₄ H(13), ν C ₄ C ₅ (12), ν C ₁ C ₂ (11)	25	1483.1	21	A'	β C ₃ C ₄ (14), ν C ₁ C ₆ (11), ν C ₁ C ₂ (10)
26	1511.9	73	A'	β C ₅ H(20), β C ₂ H(18), ν C ₃ C ₄ (15), β C ₄ H(12)	26	1501.6	95	A'	β C ₃ H(27), ν C ₃ C ₄ (13), β C ₂ H(13)
27	1618.5	123	A'	ν C ₁ C ₂ (24), ν C ₄ C ₅ (21)	27	1621.9	54	A'	ν C ₁ C ₆ (28), ν C ₃ C ₄ (18), ν C ₄ C ₅ (10)
28	1637.7	76	A'	ν C ₁ C ₆ (23), ν C ₅ C ₆ (17), ν C ₂ C ₃ (15), ν C ₃ C ₄ (13)	28	1633.0	142	A'	ν C ₅ C ₆ (21), ν C ₁ C ₂ (17), ν C ₂ C ₃ (16), ν C ₄ C ₅ (11)
29	3176.4	9	A'	ν C ₅ H(70), ν C ₂ H(18)	29	3157.8	10	A'	ν C ₆ H(88), ν C ₅ H(11)
30	3177.8	2	A'	ν C ₂ H(81), ν C ₅ H(15)	30	3181.9	9	A'	ν C ₅ H(82), ν C ₆ H(11)
31	3200.4	3	A'	ν C ₆ H(86)	31	3210.5	1	A'	ν C ₄ H(85)
32	3211.0	1	A'	ν C ₄ H(89)	32	3212.4	1	A'	ν C ₃ H(91)
33	3834.3	69	A'	ν OH(100)	33	3835.3	75	A'	ν OH(100)

^aFootnotes *a*–*d* are identical to those in Table 11.

TABLE 18. Harmonic vibrational frequencies, IR intensities and assignments for *para*-fluorophenol^a

No.	Freq.	IR	Sym.	Assignment, PED(%)
1	155.6	0	A''	$\tau_2\text{rg}(75)$
2	282.3	113	A''	$\tau\text{OH}(92)$ Expt: 280 ^b , 280 ^c , 283 ^d
3	343.0	6	A'	$\beta\text{CF}(44)$, $\beta\text{CO}(40)$
4	366.0	0	A''	$\tau_1\text{rg}(36)$, $\gamma\text{CF}(29)$, $\gamma\text{CO}(14)$
5	427.3	1	A''	$\tau_3\text{rg}(83)$
6	447.3	7	A'	$\beta\text{CO}(35)$, $\beta\text{CF}(32)$, $\beta_3\text{rg}(27)$
7	463.0	1	A'	$\beta_2\text{rg}(76)$
8	512.7	23	A''	$\tau_2\text{rg}(33)$, $\gamma\text{CF}(29)$, $\gamma\text{CO}(29)$
9	652.5	1	A'	$\beta_3\text{rg}(74)$
10	680.6	0	A''	$\tau_1\text{rg}(64)$, $\gamma\text{CO}(16)$, $\gamma\text{CF}(14)$
11	751.5	68	A'	$\beta_1\text{rg}(36)$, $\nu\text{CF}(24)$, $\nu\text{CO}(21)$
12	797.6	11	A''	$\gamma\text{C}_2\text{H}(49)$, $\gamma\text{C}_3\text{H}(27)$, $\gamma\text{C}_5\text{H}(10)$
13	836.1	63	A''	$\gamma\text{C}_6\text{H}(33)$, $\gamma\text{C}_5\text{H}(24)$, $\gamma\text{C}_2\text{H}(12)$, $\tau_2\text{rg}(12)$, $\gamma\text{CO}(10)$
14	861.1	0	A'	$\beta_2\text{rg}(22)$, $\nu\text{C}_1\text{C}_6(13)$, $\nu\text{C}_1\text{C}_2(12)$, $\nu\text{CF}(12)$, $\nu\text{CO}(12)$
15	907.1	3	A''	$\gamma\text{C}_3\text{H}(48)$, $\gamma\text{C}_2\text{H}(21)$, $\tau_1\text{rg}(14)$
16	949.4	0	A''	$\gamma\text{C}_5\text{H}(40)$, $\gamma\text{C}_6\text{H}(38)$
17	1024.7	1	A'	$\beta_1\text{rg}(46)$, $\nu\text{C}_4\text{C}_5(10)$
18	1110.4	19	A'	$\beta\text{C}_5\text{H}(21)$, $\beta\text{C}_3\text{H}(17)$, $\beta\text{C}_6\text{H}(15)$, $\nu\text{C}_5\text{C}_6(13)$, $\nu\text{C}_2\text{C}_3(12)$, $\beta\text{C}_2\text{H}(10)$
19	1169.3	3	A'	$\beta\text{C}_3\text{H}(27)$, $\beta\text{C}_5\text{H}(20)$, $\beta\text{C}_2\text{H}(15)$, $\beta\text{C}_6\text{H}(14)$
20	1186.2	144	A'	$\beta\text{OH}(52)$, $\nu\text{C}_1\text{C}_6(15)$
21	1229.0	174	A'	$\nu\text{CF}(43)$, $\beta_1\text{rg}(20)$
22	1280.1	26	A'	$\nu\text{CO}(49)$, $\nu\text{C}_5\text{C}_6(10)$, $\nu\text{C}_2\text{C}_3(10)$, $\nu\text{CF}(7)$
23	1317.3	3	A'	$\beta\text{C}_2\text{H}(18)$, $\beta\text{C}_6\text{H}(15)$, $\nu\text{C}_3\text{C}_4(14)$, $\beta\text{C}_5\text{H}(13)$, $\nu\text{C}_4\text{C}_5(12)$, $\beta\text{C}_3\text{H}(11)$
24	1355.6	26	A'	$\nu\text{C}_2\text{C}_3(14)$, $\beta\text{COH}(13)$, $\nu\text{C}_5\text{C}_6(12)$, $\nu\text{C}_1\text{C}_2(11)$, $\nu\text{C}_4\text{C}_5(11)$, $\nu\text{C}_3\text{C}_4(11)$
			A'	$\nu\text{C}_1\text{C}_6(10)$
25	1466.9	29	A'	$\nu\text{C}_5\text{C}_6(19)$, $\nu\text{C}_2\text{C}_3(16)$, $\beta\text{C}_6\text{H}(14)$, $\beta\text{OH}(11)$
26	1538.4	232	A'	$\beta\text{C}_2\text{H}(15)$, $\nu\text{C}_3\text{C}_4(12)$, $\beta\text{C}_5\text{H}(12)$, $\beta\text{C}_3\text{H}(11)$
27	1645.3	4	A'	$\nu\text{C}_4\text{C}_5(25)$, $\nu\text{C}_1\text{C}_2(23)$
28	1655.6	0	A'	$\nu\text{C}_1\text{C}_6(21)$, $\nu\text{C}_3\text{C}_4(20)$, $\nu\text{C}_5\text{C}_6(13)$, $\nu\text{C}_2\text{C}_3(13)$
29	3159.5	12	A'	$\nu\text{C}_2\text{H}(96)$
30	3191.6	3	A'	$\nu\text{C}_6\text{H}(57)$, $\nu\text{C}_5\text{H}(42)$
31	3201.3	2	A'	$\nu\text{C}_3\text{H}(95)$
32	3205.3	1	A'	$\nu\text{C}_5\text{H}(56)$, $\nu\text{C}_6\text{H}(42)$
33	3840.2	66	A'	$\nu\text{OH}(100)$

^aFootnotes *a*–*d* are identical to those in Table 11.TABLE 19. Some harmonic vibrational frequencies, IR intensities and assignments for *para*-chlorophenols^a

Freq.	IR	Sym.	Assignment, PED(%)
300.1	104	A''	τOH (89)
836.0	2	A'	$\beta_2\text{rg}(23)$, $\nu\text{CO}(21)$, $\nu\text{C}_1\text{C}_2(13)$, $\nu\text{C}_1\text{C}_6(13)$, $\beta_1\text{rg}(11)$
1279.1	107	A'	$\nu\text{CO}(53)$, $\beta_1\text{rg}(10)$
3836.0	73	A'	$\nu\text{OH}(100)$

^aSee Footnote *a* in Table 10.

TABLE 20. Some harmonic vibrational frequencies, IR intensities and assignments for *para*-bromophenols^a

Freq.	IR	Sym.	Assignment, PED(%)
303.1	51	A''	$\tau\text{OH}(50)$, $\gamma\text{CBr}(22)$, $\tau_2\text{rg}(11)$, $\tau_1\text{rg}(10)$
312.0	63	A''	$\tau\text{OH}(43)$, $\gamma\text{CBr}(21)$, $\tau_2\text{rg}(11)$, $\gamma\text{CO}(10)$
831.7	1	A'	$\beta_2\text{rg}(22)$, $\nu\text{CO}(22)$, $\beta_1\text{rg}(15)$, $\nu\text{C}_1\text{C}_2(13)$, $\nu\text{C}_1\text{C}_6(13)$
1279.1	125	A'	$\nu\text{CO}(53)$, $\beta_1\text{rg}(10)$
3835.3	76	A'	$\nu\text{OH}(100)$

^aSee Footnote a in Table 10.

parameters of these conformers are demonstrated in Figure 13. This is also manifested in the vibrational spectra.

Let us deal first with the torsional mode τ_{OH} . In both *cis m*-ClC₆H₄OH and *cis m*-BrC₆H₄OH, it is predicted to be at higher wavenumbers compared to their *trans* partners while in *m*-fluorophenols it is placed higher, at 320.7 cm⁻¹ ($\tau_{\text{OH}}^{\text{expt}} = 319 \text{ cm}^{-1246}$), in the *trans* conformer than in the *cis* one, viz. 314.0 ($\tau_{\text{OH}}^{\text{expt}} = 311 \text{ cm}^{-1246}$). Due to a small difference of about 7 cm⁻¹, it would be premature to offer a theoretical explanation of such 'misbehaviour' of τ_{OH} in *m*-XC₆H₄OH until it is fully proved or disproved experimentally, particularly in the related overtones where such a difference could be more pronounced. However, we suggest that such features are presumably related to the changes in the electrostatic repulsion between the O–H bond and its *cis ortho* C–H bond due to a different electron-withdrawing vs. electron-donating ability of the X atoms and a possible weak interaction between this *ortho* C–H bond and the halogen atom. The former repulsion might make the potential well more shallow for the planar orientation of the OH bond and thus cause a red shift of the τ_{OH} . Noteworthy is a rather strong dependence of τ_{OH} on the C₁C₂₍₆₎H angle of this C–H bond which partly determines the strength of this repulsive interaction. Thus, a positive departure of this angle from the phenolic one by 3° produces a blue shift of the τ_{OH} by about 5 cm⁻¹, while a negative deviation moves it downward by nearly the same value. Interestingly, the analogous Hartree–Fock calculations lead to approximately the same frequency alterations, thus indicating the dominant electrostatic origin of the *cis*–*trans* non-similarity.

The CO stretch internal coordinate in XC₆H₄OH is involved in several vibrational modes. Similarly to the parent phenol, ν_{CO} contributes dominantly to the two modes whose atomic displacements are inherent to modes 13 and 1 of benzene, according to Varsanyi nomenclature¹⁶⁷. While the latter characterized by a lower frequency retains its radial skeleton character and describes a ring breathing, the former can be likely interpreted as the CO stretch due to a larger contribution of ν_{CO} . In the theoretical spectrum of the parent phenol (Table 10), it is centred at 1274.8 cm⁻¹ (expt: 1259–1262 cm⁻¹¹⁵³) and characterized by IR intensity of 91 km mol⁻¹. The X-substitution of phenol affects both its position and the IR intensity. Analysis of Tables 11–13 and 15–20 leads to the following conclusions: (a) all *cis ortho*-substituted phenols have this mode at lower frequencies and larger IR intensities compared to their *trans* partners; (b) in all *cis meta*-substituted structures, it is more IR active than in the corresponding *trans*-substituted ones, while its frequency in each pair of conformers is nearly the same. In *ortho*-substituted forms, it develops into a rather intense band placed at 1284.3 cm⁻¹ (130 km mol⁻¹) and 1298.8 cm⁻¹ (61 km mol⁻¹) in *cis* and *trans o*-FC₆H₄OH, respectively, 1274.8 cm⁻¹ (75 km mol⁻¹) (expt: 1255 cm⁻¹¹⁶⁷) and 1285.6 cm⁻¹ (23 km mol⁻¹) in *cis* and *trans o*-ClC₆H₄OH, respectively, and 1273.9 cm⁻¹ (63 km mol⁻¹) (expt: 1247 cm⁻¹¹⁶⁷) and 1282.9 cm⁻¹ (21 km mol⁻¹) in *cis* and *trans o*-BrC₆H₄OH, respectively.

The ring breathing vibrational mode predicted at 1010.5 cm^{-1} (expt: 993.1 cm^{-1} ^{247–250}) in the prototype benzene downshifts to 827.3 cm^{-1} (23 km mol^{-1}) (expt: 823 cm^{-1} (20 km mol^{-1} ¹⁵³)) upon substitution of one hydrogen atom by the OH group. In phenol and its halo-derivatives, this mode is mixed with the stretching vibrations of the light substituents, namely ν_{CO} and ν_{CF} . In halophenols, it is placed at higher wavenumbers compared to phenol, in particular at 861.1 cm^{-1} (expt: 854 cm^{-1}), 836.0 cm^{-1} (expt: 836 cm^{-1}) and 831.7 cm^{-1} (expt: 825 cm^{-1})²⁵¹ in the spectra of *para*-fluoro-, chloro- and bromophenols, respectively. This supports the earlier assignment of this vibrational mode in a series of *para*-substituted phenols²⁵¹ (cf. also Reference 245).

Further, if in all *para*-substituted phenols the CO stretching vibration is mainly localized on these two fundamental modes, in some *ortho*- and *meta*-phenols it appears coupled with the mode corresponding to the fundamental three of benzene whose displacements resemble a distortion towards a ‘Catherine wheel’ type of structure. Such vibration appears to be rather sensitive to the position (i.e. either *cis* or *trans*) of the X atom, being almost independent of its nature. In all *trans ortho*- and *meta*-substituted phenols, it is placed at slightly lower wavenumbers and characterized by a consistently larger IR intensity compared to the *cis* conformers. Consider the following example. For all *trans m*-XC₆H₄OH, it is centred at *ca* 1322 cm^{-1} ($81\text{--}83\text{ km mol}^{-1}$) and blue shifts to *ca* 1334 cm^{-1} ($2\text{--}7\text{ km mol}^{-1}$) for the *cis* conformer. In *trans ortho*-substituted forms, it is found at $1316\text{--}1317\text{ cm}^{-1}$ ($73\text{--}78\text{ km mol}^{-1}$), while in the *cis* forms it is at $1323\text{--}1324\text{ cm}^{-1}$ ($21\text{--}28\text{ km mol}^{-1}$).

We end this subsection with a surprise which is quite obsolete, since it is about twenty years old^{252–254}. However, wise people always say that a forgotten surprise is often better than a new one. Anyway, we think that wrapping it within the present theoretical method is worth mentioning to complete our understanding of the stability of XC₆H₄OH. In equation 12 we present the relative energies (in kJ mol^{-1}) of all forms of the monohalogeno-substituted phenols.

$$\begin{aligned}
 \text{F: } & \textit{trans m}^{0.79} > \textit{cis m}^{3.64} > \textit{cis o}^{1.63} > \textit{para}^{9.75} > \textit{trans o} \\
 \text{Cl: } & \textit{cis o}^{3.31} > \textit{cis m}^{0.08} \approx \textit{trans m}^{1.84} > \textit{para}^{7.24} > \textit{trans o} \\
 \text{Br: } & \textit{cis o}^{1.16} > \textit{cis m}^{0.04} \approx \textit{trans m}^{1.05} > \textit{para}^{6.99} > \textit{trans o}
 \end{aligned} \tag{12}$$

Its analysis leads to the following conclusions. First, the intramolecular hydrogen bond in the *cis o*-Cl- and *cis o*-Br-phenols is rather strong and leads all *meta*- and *para*-chloro- and bromophenols to fall energetically between their *cis ortho*- and *trans ortho*-conformers. Such order of stability breaks down for FC₆H₄OH where the *trans meta*-conformer appears to be the most stable one and reluctant to be engaged in the intramolecular hydrogen bonding and is followed by the *cis meta*-conformer. Surprisingly, the *cis ortho*-conformer occupies only the third place in the rank of the most energetically stable ones being by 4.4 kJ mol^{-1} lower than the most stable conformer. The *para*-conformer falls between the *cis* and *trans ortho*-conformers. Interestingly, the earlier orders of stability of FC₆H₄OH obtained at rather lower (from the present point of view) computational levels are given in kJ mol^{-1} in equation 13:

$$\begin{aligned}
 & \textit{cis o}^{0.17} \approx \textit{cis m}^{0.17} \approx \textit{trans m}^{0.75} > \textit{para}^{15.3} > \textit{trans o}^{252} \\
 & \textit{cis m}^{0.55} > \textit{trans m}^{4.98} > \textit{para}^{2.09} > \textit{cis o}^{7.07} > \textit{trans o}^{145} \\
 & \textit{cis m}^{1.30} > \textit{trans m} = \textit{cis o}^{4.73} > \textit{para}^{13.9} > \textit{trans o}^{146}
 \end{aligned} \tag{13}$$

In summary, although we have succeeded in explaining the order of the strength of the intramolecular hydrogen bond in *ortho*-XC₆H₄OH in the gas phase and in the model solvent mimicking CCl₄ and reconcile the longstanding conflict between experiment and theory on the basis of a generalized solvent-including Pauling model, we still feel that our explanation looks rather incomplete. Therefore, we attempt to build such a bridge in the next subsection using the concept of the electronic localization function.

C. The Bonding Trends in Monohalogenated Phenols in Terms of the Electronic Localization Function (ELF)

1. Introduction to the ELF

Nearly a decade ago, Becke and Edgecombe in their seminal paper²⁵⁵ introduced the electron localization function (ELF) $\eta(\mathbf{r})$ of an arbitrary N -electron system (equation 14) as

$$\eta(\mathbf{r}) = (1 + [(t - t_W)/t_{TF}]^2)^{-1} \quad (14)$$

where $t = \frac{1}{2} \sum_{i=1}^N |\nabla \psi_i|^2$ is the kinetic energy density of the studied system within the Hartree–Fock or Kohn–Sham approach and ψ_i ($i = 1, \dots, N$) are the corresponding molecular orbitals. Here, $t_W[\rho(\mathbf{r})] = (\nabla \rho)^2/8\rho$ is the Weizsäcker kinetic energy density determined by the one-electron density $\rho(\mathbf{r}) = \sum_{i=1}^N |\psi_i(\mathbf{r})|^2$, and finally $t_{TF}[\rho(\mathbf{r})] = \alpha_{TF}[\rho(\mathbf{r})]^{5/3}$ is the Thomas–Fermi kinetic energy density with numerical coefficient $\alpha_{TF} = 3(6\pi^2)^{2/3}/5$ derived within the uniform electron gas approximation¹⁴⁵.

The ELF $\eta(\mathbf{r})$ has a rather simple normalized Lorentzian-type form and thus its domain lies in the interval $0 \leq \eta(\mathbf{r}) \leq 1$. The upper limit of $\eta(\mathbf{r}) = 1$ corresponds to the electron system whose kinetic energy density becomes identical to the Weizsäcker one. Bearing in mind that the latter was derived on the basis of the Pauli principle, $\eta(\mathbf{r}) = 1$ implies that all electrons are paired if $2/N$, and there is only one unpaired electron in the opposite case. Its value $\eta(\mathbf{r}) = \frac{1}{2}$ determining the FWHM (\equiv full width at half maximum) describes a case when $t = t_W[\rho(\mathbf{r})] \pm t_{TF}[\rho(\mathbf{r})]$, where the lower sign is valid if $t_W[\rho(\mathbf{r})] \geq t_{TF}[\rho(\mathbf{r})]$.

2. Topology of the ELF

The purpose of the topological analysis of the electron localization function is to provide a sound mathematical model of the Lewis^{256, 257}, and VSEPR^{143, 144, 258, 259} theories which removes the contradictions that the latter present with quantum mechanics. The ELF analysis therefore attempts to provide a mathematical bridge between chemical intuition and quantum mechanics. Since both Lewis and VSEPR phenomenological models describe the bonding within a molecule in the usual 3D space, the mathematical model should make a partition of this space into regions related to chemical properties. The theory of dynamical systems^{260–262} then provides a very convenient mathematical framework to achieve the partition of the molecular space into such regions. The simplest dynamical systems are the gradient dynamical systems in which the vector field is the gradient field of a scalar function, say $V(\mathbf{r})$, called the potential function. The theory of atoms in molecules (AIM)¹⁴¹ discussed above uses the gradient dynamical field of the charge density $\rho(\mathbf{r})$ to determine atomic basins. In order to provide evidence of electronic domains one has to choose another local function related to the pair-electron density. Unfortunately, the pair-electron functions depend on two space variables and therefore cannot be used directly as potential function.

The ELF defined in equation 14 is a local function which describes to what extent the Pauli repulsion is efficient at a given point of the molecular space. Originally, the ELF was derived from the Laplacian of the conditional probability $[\nabla_{\mathbf{r}_1}^2 P_{cond}(\mathbf{r}_1, \mathbf{r}_2)]_{\mathbf{r}_1=\mathbf{r}_2}$. An

alternative interpretation was later proposed²⁶³ in terms of the local excess kinetic energy density due to the Pauli exclusion principle. This interpretation not only gives a deeper physical meaning to the *ELF* function but also allows one to generalize the *ELF* to any wave function, in particular to the exact one. Therefore, the *ELF* provides a rigorous basis for the analysis of the wave function and of the bonding in molecules and crystals. In 1994, it was proposed to use the gradient field of *ELF* in order to perform a topological analysis of the molecular space²⁶⁴ in the spirit of AIM theory. The attractors of *ELF* determine basins which are either core basin encompassing nuclei or valence basin when no nucleus except a proton lies within it. The valence basins are characterized by the number of core basins with which they share a common boundary; this number is called the valence basin synaptic order²⁶⁵. There are therefore asynaptic, monosynaptic, disynaptic and polysynaptic valence basins. Monosynaptic basins usually correspond to the lone pair regions whereas di- and polysynaptic basins characterize chemical bonds. An advantage of such representation is that it provides a clear criterion to identify multicentric bonds. In a way, this is a complementary view to the traditional valence representation: instead of counting bonds from a given centre which only accounts for two-body links, the count is performed from the ‘piece of glue’ which sticks the atoms one to another.

From a quantitative point of view a localization basin (core or valence) is characterized by its population, i.e. the integrated one-electron density $\rho(\mathbf{r})$ over the basin (equation 15)

$$\bar{N}(\Omega_i) = \int_{\Omega_i} d^3\mathbf{r} \rho(\mathbf{r}) \quad (15)$$

where Ω_i is the volume of the basin. It is worthwhile to calculate the variance of the basin population by equation 16,

$$\sigma^2(\bar{N}; \Omega_i) = \int_{\Omega_i} d^3\mathbf{r}_1 \int_{\Omega_i} d^3\mathbf{r}_2 P(\mathbf{r}_1, \mathbf{r}_2) - [\bar{N}(\Omega_i)]^2 + N(\Omega_i) \quad (16)$$

where $P(\mathbf{r}_1, \mathbf{r}_2)$ is the spinless pair-electron density¹⁴⁵. It has been shown that the variance can readily be written as a sum of contributions arising from the other basins (covariance)²⁶⁶ (equation 17)

$$\sigma^2(\bar{N}; \Omega_i) = \sum_{j \neq i} \bar{N}(\Omega_i) \bar{N}(\Omega_j) - \int_{\Omega_i} d^3\mathbf{r}_1 \int_{\Omega_j} d^3\mathbf{r}_2 P(\mathbf{r}_1, \mathbf{r}_2) \quad (17)$$

In equation 17, $\bar{N}(\Omega_i) \bar{N}(\Omega_j)$ is the number of the electron pairs classically expected from the basin population whereas $\bar{N}(\Omega_i, \Omega_j)$ is the actual number of pairs obtained by integration of the pair-electron function over the basins Ω_i and Ω_j . The variance is then a measure of the quantum mechanical uncertainty of the basin population which can be interpreted as a consequence of the electron delocalization, whereas the pair covariance indicates how much the population fluctuations of two given basins are correlated. Within the AIM framework, the atomic localization and delocalization indices $\lambda(A)$ and $\delta(A, B)$ have been introduced²⁶⁷ and defined by equations 18 and 19:

$$\lambda(A) = \bar{N}(\Omega_A) - \sigma^2(\bar{N}; \Omega_A) \quad (18)$$

$$\delta(A, B) = 2\bar{N}(\Omega_A) \bar{N}(\Omega_B) - 2 \int_{\Omega_A} d^3\mathbf{r}_1 \int_{\Omega_B} d^3\mathbf{r}_2 P(\mathbf{r}_1, \mathbf{r}_2) \quad (19)$$

The AIM delocalization indices are sometimes referred to as bond orders^{268, 269}. The above notation²⁶⁵ can be generalized to any partition in the direct space and therefore is adopted in the present work. Within the *ELF* approach, the core population variance and

the core valence delocalization indices can be used to decide if a given core contributes to the synaptic order of an adjacent valence basin. For example, in the LiF molecule, the variances of the C(Li) and C(F) basins are 0.09 and 0.38, respectively, whereas $\delta(C(Li), V(F)) = 0.16$ and $\delta(C(F), V(F)) = 0.74$, where C stands for core and V for valence.

The concept of localization domain has been introduced²⁶⁵ for graphical purposes and also in order to define a hierarchy of the localization basins which can be related to chemical properties. A localization domain is a volume limited by one or more closed isosurfaces $\eta(\mathbf{r}) = f$. A localization domain surrounds at least one attractor—in this case it is called *irreducible*. If it contains more than one attractor, it is *reducible*. Except for atoms and linear molecules, the irreducible domains are always filled volumes whereas the reducible ones can be either filled volumes, hollow volumes or donuts. Upon the increase in the value of $\eta(\mathbf{r})$ defining the boundary isosurface, a reducible domain splits into several domains, each containing less attractors than the parent one. The reduction of localization occurs at the turning points, which are critical points of index 1 located on the separatrix of two basins involved in the parent domain. Ordering these turning points (localization nodes) by increasing $\eta(\mathbf{r})$ enables one to build tree diagrams reflecting the hierarchy of the basins. A core basin is counted in the synaptic order of valence basins if there exists a value of the localization function which gives rise to a hollow volume localization domain (containing the considered valence basin attractors) with the core domain in its hole.

Before proceeding further with bridging the *ELF* with the key properties of monohalophenols, we pause briefly to analyse analytically the vector gradient field of *ELF*.

3. Vector gradient field $\nabla_{\mathbf{r}}\eta(\mathbf{r})$

Applying the gradient to $\eta(\mathbf{r})$ defined by equation 14, we derive equation 20,

$$\nabla\eta(\mathbf{r}) = \frac{2(t - t_W)t_{TF}}{[(t - t_W)^2 + t_{TF}^2]^2} [(t - t_W)\nabla t_{TF} - t_{TF}\nabla(t - t_W)] \quad (20)$$

where $\nabla_{\mathbf{r}} \equiv \nabla$ for short. Assuming molecular orbitals to be real valued, equation 20 is then easily transformed to equation 21,

$$\begin{aligned} & \frac{\rho^{1/3}[(t - t_W)^2 + t_{TF}^2]^2}{2\alpha_{TF}(t - t_W)t_{TF}} \nabla\eta(\mathbf{r}) \\ &= \sum_{i,j,k=1}^N \left[\frac{8}{3} \nabla\psi_i\psi_j\psi_k \nabla\psi_k (\psi_i\nabla\psi_j - \psi_j\nabla\psi_i) + \psi_i\psi_j^2 \nabla\psi_k (\psi_k\nabla^2\psi_i - \psi_i\nabla^2\psi_k) \right] \\ &= \frac{8}{3} \nabla\rho \sum_{i<j}^N (\psi_i\nabla\psi_j - \psi_j\nabla\psi_i)^2 - \rho \sum_{i<j}^N (\psi_i\nabla\psi_j - \psi_j\nabla\psi_i)(\psi_i\nabla^2\psi_j - \psi_j\nabla^2\psi_i). \end{aligned} \quad (21)$$

Therefore, we finally obtain equation 22^{260, 261},

$$\nabla\eta(\mathbf{r}) = -\frac{\alpha_{TF}(t - t_W)t_{TF}}{[(t - t_W)^2 + t_{TF}^2]^2} \rho^{10/3} \nabla(J^2/\rho^8/3) \quad (22)$$

where J^2 is given by equation 23^{270, 271},

$$J^2 = \frac{1}{4} \sum_{i<j}^N (\psi_i\nabla\psi_j - \psi_j\nabla\psi_i)^2 \quad (23)$$

Summarizing, the vector field $\nabla\eta(\mathbf{r})$ of the *ELF* vanishes at those $\mathbf{r} \in \mathbf{R}^3$ which obey the condition $t(\mathbf{r}) = t_W[\rho(\mathbf{r})]$ or equation 24,

$$J^2(\mathbf{r}) = C\rho^{8/3}(\mathbf{r}) \quad (24)$$

where C is a constant in \mathbf{R}^3 .

For one purpose let us rewrite equation 23 as equation 25,

$$J^2 = \sum_{i < j}^N |\mathbf{j}_{ij}|^2 \quad (25)$$

where $\mathbf{j}_{ij} = (\psi_i \nabla \psi_j - \psi_j \nabla \psi_i)/2$ is the real time-independent electron transition current density between the i th and j th molecular orbitals. Hence, J^2 determines the square of the net charge transferred between all occupied molecular orbitals. Thus, the zero-flux surfaces of the *ELF* are defined by the condition that net charge or, in other words, the electron transition current density $\mathbf{Q}_{tr}(\mathbf{r}) \equiv \sqrt{J^2(\mathbf{r})}$ associated with the transitions between all occupied molecular orbitals, is proportional to the electron density to the four-thirds power. This is the key difference in the vector gradient fields of $\rho(\mathbf{r})$ underlying the AIM theory and the *ELF*^{272, 273}.

4. The bonding in benzene, phenol and phenyl halides

In order to get some insight on how *ELF* works, we will analyse a number of parent molecules $\text{C}_6\text{H}_5\text{X}$ ($\text{X} = \text{H}, \text{OH}, \text{F}, \text{Cl}, \text{Br}$ and I). Their localization domains are displayed in Figure 14. Except for the substituent itself, all these molecules have 6 $\text{V}(\text{C}, \text{C})$, 5 $\text{V}(\text{C}, \text{H})$ and one $\text{V}(\text{C}, \text{X})$ basins. The differences are to be found in the hierarchy of the $\text{V}(\text{C}, \text{C})$ basins which is ruled by the nature of the substituent. In benzene, all the $\text{V}(\text{C}, \text{C})$ basins are equivalent and therefore the six critical points of index 1 between these basins have the same value, i.e. $\eta(\mathbf{r}_c) = 0.659$. In the phenyl halides where the molecular symmetry is lowered from D_{6h} to C_{2v} , the former critical points are then distributed in four sets according to the common carbon position: *ipso*, *ortho*, *meta* and *para*. In phenol with a C_s symmetry, the two *ortho* and the two *meta* positions are not totally equivalent. In all studied molecules, the $\eta(\mathbf{r}_c)$ values are enhanced in the *ipso*, *ortho* and *para* positions and decreased in the *meta* position. It has been remarked that the electrophilic substitution sites correspond to the carbon for which $\eta(\mathbf{r}_c)$ is enhanced²⁷⁴. Moreover, it is worthwhile to introduce *electrophilic substitution positional indices* defined by equation 26,

$$RI_c(S) = \eta(C_i; S) - \eta(C_i; H) \quad (26)$$

where the subscript c denotes the position of the carbon labeled by i , i.e. *ortho*, *meta* or *para*. Interestingly, there exists a rather good correlation between the $RI_c(S)$ indices and the Hammett constants. Moreover, the positional indices are additive, enabling one to predict their values in a di-substituted molecule from the mono-substituted data.

The $\text{V}(\text{C}_i, \text{C}_j)$ basin populations, their variance and the electrophilic substitution positional indices of the studied $\text{C}_6\text{H}_5\text{X}$ molecules are listed in Table 21. The $\text{V}(\text{C}, \text{X})$ populations and their variance are close to their values in the CH_3X series. As expected the $\text{V}(\text{C}, \text{C})$ basin populations are intermediate between those inherent to a single and a double C–C bond and subject to a large fluctuation of the charge density. The classical meaning of the variance is the square of the standard deviation; though the standard deviation cannot be defined for a quantum system, the classical limit provides at least qualitative information about the delocalization. In the present case $\sigma \sim 1.16$, which is consistent with the resonance picture involving the Kekulé structures.

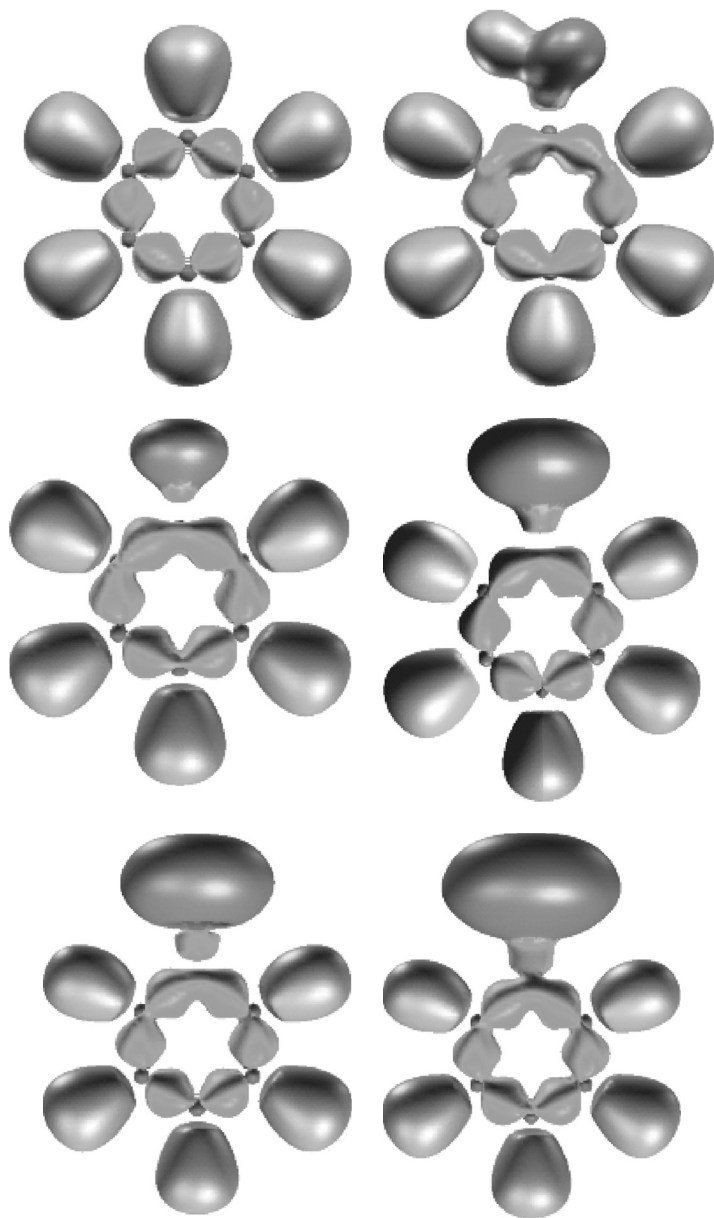


FIGURE 14 (PLATE 3). Localization domains of mono-X-substituted benzenes C_6H_5X (from left to right top $X = H, OH, F$, bottom $X = Cl, Br, I$). The ELF value defining the boundary isosurface, $\eta(\mathbf{r}) = 0.659$ corresponds to the critical point of index 1 on the separatrix between adjacent $V(C, C)$ basins of benzene. Colour code: magenta = core, orange = monosynaptic, blue = protonated disynaptic, green = disynaptic. Adapted from Reference 220 with permission

TABLE 21. Basin populations $\bar{N}(V)$, variance of the basin populations $\sigma^2(V)$ and electrophilic substitution positional indices RI_c of the C_6H_5X molecules

	H	OH	F	Cl	Br	I
$\bar{N}(V(C_1, X))$	2.09	1.50	0.99	1.50	1.47	1.32
$\sigma^2(V(C_1, X))$	0.65	0.61	0.71	0.93	0.94	0.84
$\bar{N}(V(C_1, C_2))$	2.81	2.86	2.85	2.85	2.86	2.85
$\sigma^2(V(C_1, C_2))$	1.36	1.36	1.31	1.33	1.34	1.34
$\bar{N}(V(C_1, C_6))$	2.81	2.82	2.85	2.85	2.85	2.85
$\sigma^2(V(C_1, C_6))$	1.32	1.32	1.31	1.33	1.34	1.34
$\bar{N}(V(C_2, C_3))$	2.81	2.93	2.90	2.92	2.91	2.91
$\sigma^2(V(C_2, C_3))$	1.32	1.41	1.37	1.37	1.38	1.37
$\bar{N}(V(C_3, C_4))$	2.81	2.82	2.88	2.85	2.85	2.85
$\sigma^2(V(C_3, C_4))$	1.32	1.32	1.35	1.33	1.34	1.34
$\bar{N}(V(C_4, C_5))$	2.81	2.82	2.88	2.85	2.85	2.85
$\sigma^2(V(C_4, C_5))$	1.31	1.32	1.35	1.33	1.34	1.34
$\bar{N}(V(C_5, C_6))$	2.96	2.96	2.90	2.92	2.91	2.91
$\sigma^2(V(C_5, C_6))$	1.38	1.32	1.35	1.33	1.34	1.34
RI_1	0.0	0.032	0.077	0.059	0.053	0.049
RI_2	0.0	0.039	0.017	0.008	0.007	0.010
RI_3	0.0	-0.007	-0.005	-0.003	-0.003	0.003
RI_4	0.0	0.015	0.008	0.002	0.001	0.005
RI_5	0.0	-0.008	-0.005	-0.003	-0.003	0.003
RI_6	0.0	0.025	0.017	0.008	0.007	0.010

Values taken from Reference 220 with permission.

In phenol we reveal a noticeable increase in the $V(C_o, C_m)$ population with respect to benzene (0.11 e) whereas the populations of the other basins remain almost unchanged. Indeed, the net charge transfer towards the aromatic ring amounts to 0.20 e . The halogen atoms induce a larger net charge transfer: 0.34, 0.32, 0.32 and 0.30 for F, Cl, Br and I, respectively. However, this transfer is charged by all basins although the $V(C_o, C_m)$ populations are more enhanced than the $V(C_i, C_o)$ and $V(C_m, C_p)$ ones. The RI_s 's are positive in the *ipso*, *ortho* and *para* positions and negative (except for I) in the *meta* ones. In the halogen series F–Br, the RI_c absolute values decrease with the electronegativity.

5. Monohalogenated phenols: the bonding in terms of ELF

The substitution of the CH group by the CX one ($X = F, Cl, Br, I$) in phenol is expected to be felt by the aromatic ring as a rather weak perturbation which would enhance the electron donation and modify the electrophilic substitutional indices according to the additive law²⁷⁴. As we have shown in Subsections III.A and III.B, in the *ortho* and *meta* substituted phenols the orientation of the OH bond in the molecular plane permits the existence of two conformers (Figures 12 and 13).

a. The ortho-substituted phenols. The localization domains of the *ortho*-substituted species are displayed in Figure 15: the *cis* conformers with the intramolecular hydrogen bond $O-H \cdots X$ are represented in the bottom row, the *trans* ones in the top row. Their basin populations and electrophilic substitution positional indices are given in Table 22.

Let us consider first the *trans* conformers in which the halogen substituent is not perturbed by an extra intramolecular interaction. In all molecules the $V(C_1, O)$ basin population is slightly increased with respect to phenol: the largest effect occurs for $X = Cl$, whereas for $X = Br$ and I this effect is weaker than for the fluorinated species. The

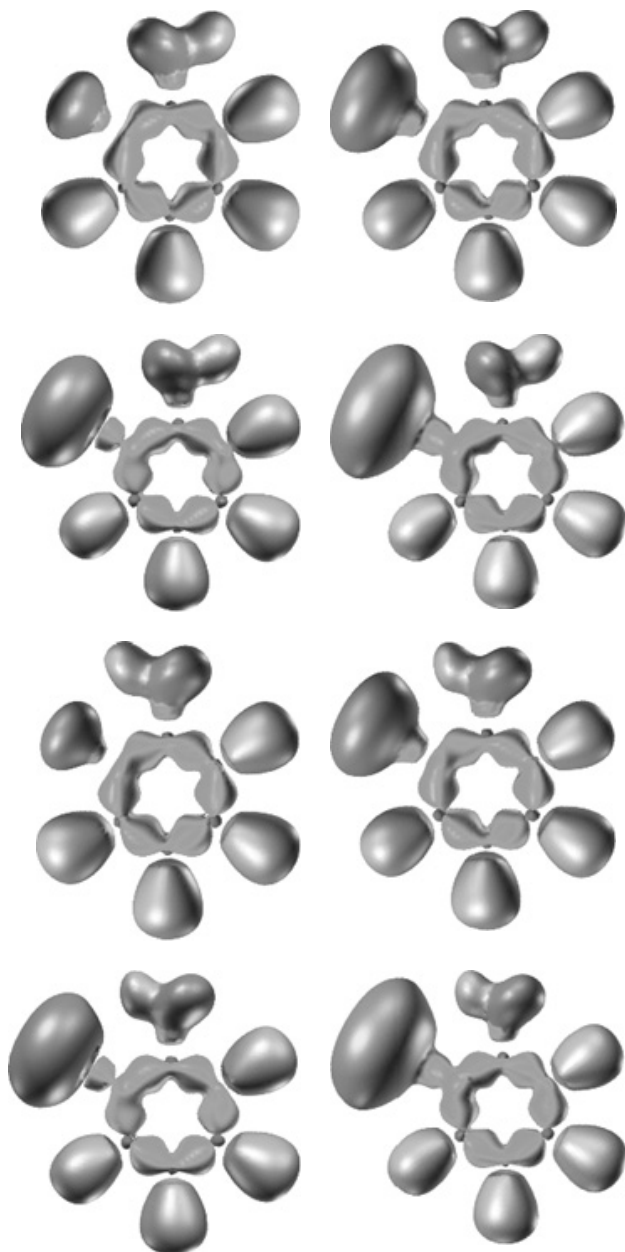


FIGURE 15 (PLATE 4). Localization domains of *ortho*-X-substituted phenols (from left to right X = F, Cl, Br, I; top—*trans* conformer, bottom—*cis* conformer). The *ELF* value defining the boundary isosurface, $\eta(\mathbf{r}) = 0.659$ corresponds to the critical point of index 1 on the separatrix between adjacent $V(\mathbf{C}, \mathbf{C})$ basins of benzene. Colour code: magenta = core, orange = monosynaptic, blue = protonated disynaptic, green = disynaptic. Adapted from Reference 220 with permission

TABLE 22. Basin populations $\bar{N}(V)$ and electrophilic substitution positional indices RI_c of *ortho*-substituted phenols

	<i>trans</i> conformation				<i>cis</i> conformation			
	F	Cl	Br	I	F	Cl	Br	I
Populations								
V(C ₁ , O)	1.54	1.54	1.58	1.52	1.52	1.55	1.57	1.51
V(C ₂ , X)	1.05	1.49	1.45	1.39	1.0	1.42	1.33	1.29
V(C ₁ , C ₆)	2.82	2.87	2.82	2.82	2.79	2.77	2.79	2.73
V(C ₁ , C ₂)	2.92	2.78	2.80	2.74	2.97	2.85	2.80	2.82
V(C ₆ , C ₅)	2.90	2.96	2.94	2.93	3.01	2.98	2.97	2.95
V(C ₅ , C ₄)	2.97	2.86	2.86	2.89	2.90	2.75	2.76	2.80
V(C ₄ , C ₃)	2.76	2.86	2.83	2.96	2.78	2.97	2.97	2.92
V(C ₃ , C ₂)	2.98	3.05	2.83	2.96	2.99	3.04	3.0	3.04
Net transfer	0.43	0.46	0.16	0.26	0.52	0.44	0.37	0.34
Positional indices								
RI_1	0.047	0.040	0.039	0.043	0.044	0.036	0.035	0.039
RI_2	0.100	0.082	0.076	0.072	0.113	0.099	0.094	0.092
RI_3	0.010	0.0	-0.001	0.002	0.009	0.00	-0.001	0.013
RI_4	0.010	0.012	0.013	0.018	0.011	0.013	0.014	0.009
RI_5	0.0	-0.006	-0.007	-0.003	0.0	-0.007	-0.008	-0.004
RI_6	0.035	0.037	0.037	0.042	0.020	0.022	0.023	0.028

Values taken from Reference 220 with permission.

V(C₆, X) populations are close to their values in the corresponding halobenzene; however, there is a small electron transfer towards this basin for X = F, whereas the iodine atom undergoes an opposite effect. With respect to phenol, the regioselectivity of the electrophilic substitution is softened because as the OH and X = F, Cl, Br groups are both *ortho-para* directors, they contribute in opposite directions. As all the positional indices of C₆H₅I are positive, they are enhanced in the *trans ortho*-iodophenol. The additive rule works satisfactorily for all positions as the largest discrepancy between estimated and calculated value does not exceed 0.002.

In the *cis* conformer, the charge transfer towards the V(C₁, O) basin is close to that calculated for the *trans* partner, as the population difference between the two conformers is of the order of the precision of the employed integration procedure. Within the OH group, the formation of the intramolecular hydrogen bond yields a small decrease of *ca* 0.005 *e*, whereas the V(O) basin population is increased by almost the same amount of electron density. The V(C₆, X) populations are always significantly lower for the *cis* conformer than in the *trans* one; the difference increases from F to Br. This should be due to the formation of the intramolecular hydrogen bond which enhances the electron donation towards the V(X) basins. With respect to the basin population criterion, the V(C₆, X) basin appears to be more perturbed than the V(C₁, O) one, and we could therefore expect that the additivity of the reactivity indices no longer holds for the *cis* conformer because the halogen atom is perturbed in this case. Indeed, the maximum deviation between the estimated and calculated indices does not exceed 0.002 in the *trans* case while it is ten times larger for the *cis* conformer. The overall charge transfer towards the aromatic ring is always less than the sum of the substituent contributions arising from phenol and benzene halides, and it is larger for the *cis* conformer.

The strength of the intramolecular hydrogen bond can be estimated within the *ELF* analysis by the core valence bifurcation index $\vartheta\text{AHB}^{275}$. This index is defined as the

difference between the values of *ELF* calculated at the index 1 critical point of the separatrix of the $V(A, H)$ and $V(B)$ basin and at the core valence boundary of the proton donor moiety. It is nicely correlated with the proton donor stretching frequency, namely negative values indicate a weak hydrogen bonding such as in the $FH \cdots N_2$ complex whereas positive values indicate stronger hydrogen bonds such as in $FH \cdots NH_3$. For the *cis ortho*-fluoro-, chloro- and bromo-phenols, we find the following values of the core valence bifurcation index: -0.06 , -0.02 and -0.01 , respectively. These values correspond to very weak or weak hydrogen bonds. On the other hand, they show that the hydrogen bond strength increases from F to Br, which is counterintuitive if one considers the halogen electronegativity. However, it completely explains the order reported in equation 5. This also indicates that the strength of the intramolecular hydrogen bond is driven by geometrical strains which hamper the formation of these bonds with the lightest halogens. A similar conclusion is drawn in Subsection III.A (see also Figure 12) although from a different point of view.

b. The meta-substituted phenols. Figure 16 displays the localization domains of the *trans* and *cis meta*-substituted phenols whereas quantitative information is provided by Table 23. In these derivatives the interaction of the two substituents is expected to be weaker than in the *ortho* case. The $V(C_1, O)$ basin population is smaller than its value in phenol for all molecules except *cis* iodophenol. In the latter case the discrepancy could be due to the use of a large core pseudopotential on the iodine atom (in practice, the *ELF* analysis requires the explicit presence of core basins, at least determined by a small core pseudopotential). On the halogen side, the $V(C_4, X)$ basin populations are also smaller (except for iodine) than in halobenzene. There is a net enhancement of the electron donation towards the ring which is evidenced by the calculated charge transfer which is larger than the value given by an additive assumption.

Except for iodine, the additivity of the electrophilic positional indices is nicely verified. With respect to phenol, the indices of the carbon in *ortho* and *para* positions are noticeably increased whereas that of carbon C_3 is more negative, because it corresponds to a *meta* position for both substituents.

c. The para-substituted phenols. In the *para*-substituted phenols presented in Figure 17, the two substituents act in the opposite directions. From Table 24 it becomes clear that the substitution of the hydrogen atom by a *para*-halogen induces a small increase in the $V(C, O)$ basin population with respect to phenol as well as in the $V(C, X)$ populations with respect to halobenzene. The additive estimate of the electrophilic substitution positional indices is verified (except in some cases for iodine). As expected, the orientational effects are smoothed.

The population of the $V(C, H)$ basins are all close to 2.10 within the accuracy of the integration scheme, and therefore it is not possible to draw any conclusion about their behaviour.

The *ELF* population analysis enables one to show the following cooperative trends, which are in agreement with chemical intuition:

(i) In the *ortho*- and *para*-substituted species, the $V(C, O)$ population is increased with respect to phenol.

(ii) In the *ortho*- and *para*-substituted species, the orientational effects are weakened except for *ipso* positions.

(iii) In the *meta*-substituted species, the $V(C, O)$ and the orientational effects are enhanced.

(iv) The formation of the intramolecular hydrogen bond in the *ortho* species softens the additivity of the orientational effects.

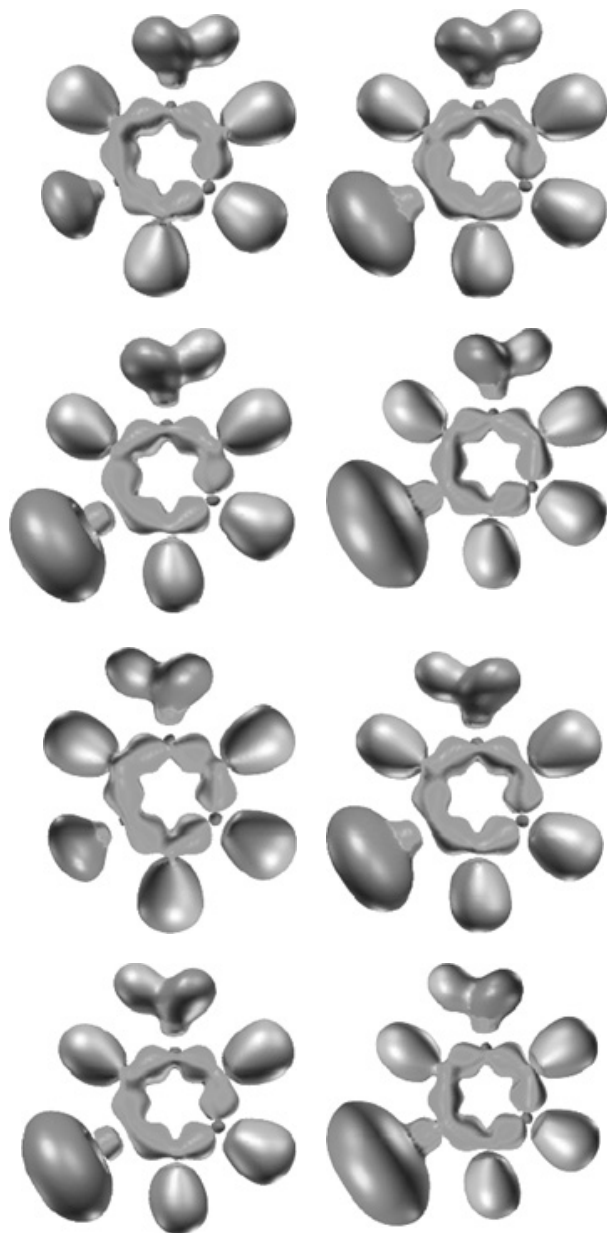


FIGURE 16 (PLATE 5). Localization domains of *meta*-X-substituted phenols (from left to right X = F, Cl, Br, I; top—*trans* conformer, bottom—*cis* conformer). The *ELF* value defining the boundary isosurface, $\eta(\mathbf{r}) = 0.659$ corresponds to the critical point of index 1 on the separatrix between adjacent V(C, C) basins of benzene. Colour code: magenta = core, orange = monosynaptic, blue = protonated disynaptic, green = disynaptic. Adapted from Reference 220 with permission

TABLE 23. Basin populations $\bar{N}(V)$ and electrophilic substitution positional indices RI_c of *meta*-substituted phenols

	<i>trans</i> conformation				<i>cis</i> conformation			
	F	Cl	Br	I	F	Cl	Br	I
Populations								
V(C ₁ , O)	1.44	1.46	1.47	1.49	1.49	1.47	1.49	1.65
V(C ₃ , X)	0.97	1.45	1.45	1.40	1.0	1.45	1.45	1.39
V(C ₁ , C ₆)	2.86	2.80	2.77	2.64	2.79	2.76	2.73	2.70
V(C ₁ , C ₂)	2.72	2.84	2.84	3.05	3.03	3.03	3.02	2.85
V(C ₆ , C ₅)	2.95	2.95	2.93	3.05	2.99	2.96	3.02	3.02
V(C ₄ , C ₃)	2.85	2.80	2.74	2.77	2.92	2.91	2.89	2.69
V(C ₃ , C ₂)	3.16	2.98	3.01	2.91	2.82	2.77	2.76	3.03
Net transfer	0.61	0.38	0.34	0.34	0.58	0.36	0.41	0.31
Positional indices								
<i>RI</i> ₁	0.027	0.028	0.029	0.035	0.027	0.028	0.029	0.035
<i>RI</i> ₂	0.044	0.035	0.034	0.050	0.048	0.049	0.048	0.036
<i>RI</i> ₃	0.069	0.051	0.044	0.041	0.070	0.052	0.045	0.040
<i>RI</i> ₄	0.033	0.023	0.023	0.026	0.033	0.024	0.023	0.025
<i>RI</i> ₅	−0.012	−0.010	−0.010	−0.005	−0.013	−0.011	−0.010	−0.004
<i>RI</i> ₆	0.047	0.042	0.040	0.029	0.033	0.027	0.025	0.044

Values taken from Reference 220 with permission.

Finally, some of the unexpected results revealed for iodophenols warn against the use of large core pseudopotentials in the *ELF* analysis. It is noteworthy that the analysis of the topology of the *ELF* enables us to predict favoured protonation sites with the help of a ‘least topological change principle’²⁷⁶ which will be discussed in a following section.

D. Some Representatives of Substituted Phenols

We conclude this Section with a few words on nitrophenols and cyanophenols (CP or NCC₆H₄OH). For instance, the experimental *K_a* value for the proton separation of *p*-NCC₆H₄OH in both the ground and excited electronic states measured in solution²⁷⁷ is higher than that of phenol by one order of magnitude. This implies that cyanophenols may form much stronger hydrogen bonds. And this fact has been particularly confirmed by an observation²⁷⁸ of sharp vibronic bands in the R2PI spectrum with the electronic origin at *ca* 35410 cm^{−1} of the complex of *p*-NCC₆H₄OH with two water molecules. Cyanophenols are also rather convenient compounds for ultrafast experimental studies²⁷⁹. The *p*-NCC₆H₄OH in its ground state has been discussed theoretically²⁸⁰ and its vibrational spectrum has been collected by Varsanýi¹⁶⁷. Recently, *ab initio* calculations of *p*-cyanophenol have been performed in its ground and first excited states²⁸⁰. Strong evidence of the existence of a conical intersection in the excited state of *p*-cyanophenol following the proton dissociation coordinate has been shown¹¹⁵. The LIF and IR/UV double-resonance experiments have also been conducted on the hydrogen-bonded complexes between *o*-CP and one or two water molecules, combined with B3LYP/cc-pVTZ calculations^{281, 282}.

Figure 18 displays the optimized geometries of cyanophenols where it is seen particularly that the *cis ortho*-CP has a relatively weak intramolecular hydrogen bond. Similar

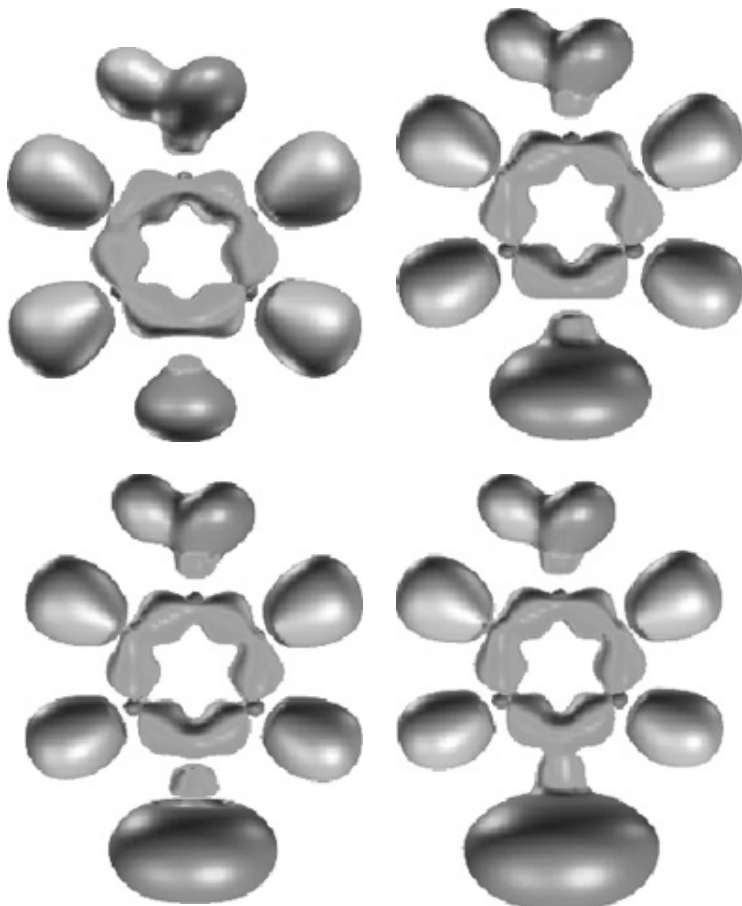


FIGURE 17 (PLATE 6). Localization domains of *para*-X-substituted phenols (from left to right X = F, Cl, Br, I). The *ELF* value defining the boundary isosurface, $\eta(\mathbf{r}) = 0.659$ corresponds to the critical point of index 1 on the separatrix between adjacent V(C, C) basins of benzene. Colour code: magenta = core, orange = monosynaptic, blue = protonated disynaptic, green = disynaptic. Adapted from Reference 220 with permission

to Subsection III.A, we can estimate its energy of formation as the energy difference between the *cis ortho*- and *trans ortho*-CPs which, at the present computational level, is 10.0 kJ mol^{-1} after including ZPVE corrections. It is worthwhile to deduce the order of stability of cyanophenols similar to that given in equation 12. We thus obtain equation 27, where the values are given in kJ mol^{-1} :

$$cis\ o \overset{2.8}{>} p \overset{4.4}{>} cis\ m \overset{0.75}{\approx} trans\ m \overset{2.0}{>} trans\ o \quad (27)$$

It shows that, energetically, all cyanophenols fall into the interval of stability between the *cis ortho*- and *trans ortho*-CPs. Some characteristic vibrational modes are collected in Table 25 accompanied by their assignments based on the PEDs.

TABLE 24. Basin populations $\bar{N}(V)$ and electrophilic substitution positional indices RI_c of *para*-substituted phenols

	F	Cl	Br	I
Populations				
$V(C_1, O)$	1.52	1.60	1.56	1.62
$V(C_4, X)$	1.0	1.53	1.47	1.41
$V(C_1, C_2)$	2.98	2.87	2.85	2.74
$V(C_1, C_6)$	2.68	2.66	2.68	2.80
$V(C_2, C_3)$	2.96	3.01	3.0	3.02
$V(C_3, C_4)$	3.0	3.0	2.99	2.69
$V(C_5, C_6)$	3.06	3.13	3.10	3.02
Net transfer	0.57	0.48	0.43	0.35
Positional indices				
RI_1	0.040	0.033	0.032	0.036
RI_2	0.035	0.037	0.037	0.027
RI_3	0.010	0.001	0.0	0.002
RI_4	0.090	0.075	0.071	0.066
RI_5	0.008	0.0	-0.001	0.003
RI_6	0.020	0.022	0.022	0.042

Values taken from Reference 220 with permission.

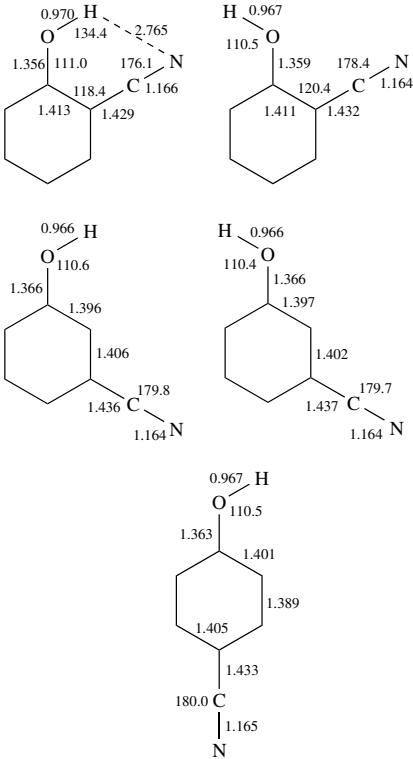


FIGURE 18. The B3LYP/6-31+G(d,p) geometries of cyanophenols in the ground electronic state. Bond lengths are in Å, bond angles in degrees

TABLE 25. Characteristic vibrational modes of cyanophenols, *p*-nitrophenol and pentachlorophenol. Frequencies are given in cm^{-1} and IR activities in km mol^{-1}

<i>para</i> -cyanophenol			
	Freq.	IR	PED, %
ν_{OH}	3823	87	ν_{OH} (100)
τ_{OH}	366	118	τ_{OH} (95)
ν_{CO}	1303	130	ν_{CO} (55)
<i>cis ortho</i> -cyanophenol			
	Freq.	IR	PED, %
ν_{OH}	3764	81	ν_{OH} (100)
τ_{OH}	438	112	τ_{OH} (91)
ν_{CO}	1281	49	ν_{CC} (29) ν_{CO} (25) β_{CH} (24)
	1341	11	β_{CH} (18) ν_{CO} (18) ν_{CC} (24)
<i>trans ortho</i> -cyanophenol			
	Freq.	IR	PED, %
ν_{OH}	3826	81	ν_{OH} (100)
τ_{OH}	351	117	τ_{OH} (94)
ν_{CO}	1294	27	ν_{CO} (30) ν_{CC} (27) β_{CH} (16)
<i>cis meta</i> -cyanophenol			
	Freq.	IR	PED, %
ν_{OH}	3826	70	ν_{OH} (100)
τ_{OH}	339	118	τ_{OH} (92)
ν_{CO}	1309	95	ν_{CO} (33) β_{CC} (14) β_{CH} (22)
	954	16	ν_{CO} (19) ν_{CC} (42) β_{CC} (10)
<i>trans meta</i> -cyanophenol			
	Freq.	IR	PED, %
ν_{OH}	3828	75	ν_{OH} (100)
τ_{OH}	332	118	τ_{OH} (93)
ν_{CO}	1306	57	ν_{CO} (30) β_{CC} (14) β_{CH} (11) ν_{CC} (10)
	953	46	ν_{CO} (18) ν_{CC} (29)
<i>para</i> -nitrophenol			
	Freq.	IR	PED, %
ν_{OH}	3821	96	ν_{OH} (100)
τ_{OH}	382	119	τ_{OH} (94)
ν_{CO}	1305	188	ν_{CO} (54)
Pentachlorophenol			
	Freq.	IR	PED, %
ν_{OH}	3688	96	ν_{OH} (100)
τ_{OH}	429	108	τ_{OH} (93)
ν_{CO}	1454	149	ν_{CO} (27) ν_{CC} (40)

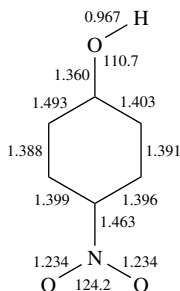


FIGURE 19. The B3LYP/6-31+G(d,p) geometry of *para*-nitrophenol in the ground electronic state. Bond length are in Å, bond angles in degrees

Figure 19 displays another representative of substituted phenols, namely *p*-nitrophenol, whose history of discovery was mentioned in Section I. A knowledge of its structure and IR spectrum is important for the study of inter- and intra-molecular interactions via a variety of spectroscopic methods.

To our knowledge, the first theoretical study of *p*-nitrophenol, at HF/3-21G computational level, was conducted in 1988²⁸³. The molecular structure of *o*-nitrophenol^{284, 285} and its IR spectra in the gas phase, solution and solid²⁸⁶ were reported. For *p*-nitrophenol, only the IR spectrum was available in the solid state²⁸⁷. Recently, a thorough study²⁸⁸ of *p*- and *o*-nitrophenols using B3LYP/6-31G(d,p) calculations has been reported which consists, first, in obtaining their geometries and, second, in calculating the harmonic vibrational frequencies and making their assignments for *p*-nitrophenol. In Table 25, we collect the key harmonic vibrational modes of *p*-nitrophenol together with their PED analysis.

Finally, we briefly mention pentachlorophenol (PCP), which is the most complex substituted phenol whose structure is reported so far in the present review and which is widely used in studies on the hydrogen bonding abilities of phenols. Its optimized geometry is demonstrated in Figure 20 and Table 25 lists its characteristic vibrational modes (cf. Reference 289). Except for the vibrations involving the OH and OD bonds, agreement between experimental and calculated values exists for the fundamental wavenumbers between 3600 and 400 cm⁻¹. The infrared spectra between 3600 and 10000 cm⁻¹ have also been studied and the overtones or combination bands were assigned by comparing the spectra of both isotopomers PCP-OH and PCP-OD. The anharmonicities of the OH

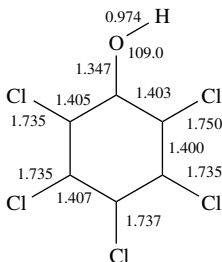


FIGURE 20. The B3LYP/6-31+G(d,p) geometry of pentachlorophenol in the ground electronic state. Bond lengths are in Å, bond angle in degrees

and OD stretching modes were determined and the binary or ternary combinations characterized by the highest coupling constants, and the highest intensities are those involving the OH and CO vibrations²⁸⁹.

IV. ENERGETICS OF SOME FUNDAMENTAL PROCESSES

A. Protonation

Protonation is a simple but important chemical process. The primary protonated form is usually a pivotal intermediate that guides the subsequent steps of an entire chemical transformation. Biomolecules such as DNA and proteins can often exist in numerous protonated forms. In a molecular system having several basic sites, the protonation usually turns out to be regioselective yielding predominantly one protonated species. The attachment of proton to a molecule A is quantified by its proton affinity, $PA(A)^{290}$, which is defined as the negative standard enthalpy (ΔH°) of the reaction $A + H^+ \rightarrow AH^+$. The PA is a measure of the basicity of the molecule which is one of the fundamental concepts in chemistry. In the most general sense, basicity is the ability of a substance to accept a positive charge. In the Lewis definition, the charge is transferred by gain or loss of an electron pair. In the Brønsted definition, the charge is transferred by gain or loss of a proton; therefore, the basicity is conventionally defined as the negative standard free energy (ΔG°) of the protonation reaction. Although the PA of a functional group is definitely influenced by the presence of substituents, any given functional group is more or less characterized by a certain range of proton affinities and a simple comparison of their values could often allow the most favoured protonation site of a polyfunctional substrate to be determined.

Let us consider in some detail the protonation of the parent phenol, a series of monohalogenated phenols (XC_6H_4OH , $X=H, F, Cl, Br, I$), and for a further control, the fluoroanisoles, $FC_6H_4OCH_3$. The interaction of the alkali metal cations including Li^+ , Na^+ and K^+ is also probed. In what follows, only the processes taking place in the gaseous phase are considered.

1. Protonation of phenol

Phenol contains both phenyl and hydroxyl functional groups. While the PA of the phenyl moiety could be estimated from that of benzene, the PA of water provides an estimate for that of the hydroxyl group. The experimental $PA(H_2O)^{291}$ is well established at $697 \pm 4 \text{ kJ mol}^{-1}$ whereas the PA of benzene²⁹² is experimentally evaluated as 753 kJ mol^{-1} . In other words, the $PA(C_6H_6)$ exceeds the $PA(H_2O)$ by as much as 56 kJ mol^{-1} . Such a difference suggests that the preferential protonation of phenol should occur on the ring moiety, even though it is not always true²⁹³. In reality, the experimental gas-phase $PA(PhOH)$ of $816\text{--}818 \text{ kJ mol}^{-1}$, as determined by either pulsed ion cyclotron resonance equilibrium experiments²⁹⁴ or high pressure mass spectrometry²⁹⁵ (for a recent compilation, see Reference 296), turns out to be substantially larger than those mentioned above, implying that the OH group markedly affects the protonation of the phenyl moiety. In fact, it was demonstrated experimentally that the gas-phase phenol protonation occurs predominantly on the ring, and the oxygen PA is about $55\text{--}84 \text{ kJ mol}^{-1}$ smaller than the carbon PA^{297} . These findings were subsequently supported by *ab initio* MO calculations^{298,299}. The O-protonated form was calculated to lie 81 kJ mol^{-1} higher in energy than its *para*-C-protonated isomer²⁹⁹. Recently, the existence of at least two protonated phenol isomers corresponding to proton attachment at oxygen and at the aromatic ring has been confirmed convincingly by using IR spectroscopy³⁰⁰.

In contrast to these gas-phase findings, the oxygen protonation was found to be favoured in various solutions²⁹⁷. The influence of the solvent is known to be a crucial factor determining the strength of bases. In some cases, the relative basicity ordering is even reversed by external effects.

The presence of a hydroxyl group induces four different positions on the ring susceptible for an electrophilic attack, namely the *ipso*-C₁, *ortho*-C₂, *meta*-C₃ and *para*-C₄ carbons, relative to the hydroxyl position, and one of these carbon centres will show the largest attraction for the proton. For the sake of convenience, the term '*ortho*-protonation' stands hereafter for a protonation occurring at the carbon C₂ etc. All theoretical methods agreed with each other in predicting the *para*-position as the most favourable protonation site^{298–300} followed by the *ortho* position with a rather small difference of ca 10 kJ mol⁻¹. The *meta*-protonated phenol is placed ca 60 kJ mol⁻¹ above the *para*-counterpart, whereas the *ipso*-protonated species lies consistently much higher in energy. The difference between the PAs of both *meta*-C₃- and O-protonated forms is calculated to be small, approximately 15 kJ mol⁻¹^{298–300}.

At the B3LYP/6-311++G(d,p) + ZPE level of theory, the local PAs of phenol at different sites are evaluated in kJ mol⁻¹ as follows: 820 for *para*-C₄, 809 for *ortho*-C₂, 757 for *meta*-C₃, 699 for *ipso*-C₁ and 743 for oxygen²⁹⁹. The coupled-cluster CCSD(T) approach in conjunction with the 6-311++G(d,p) basis set yields a PA(C₄) of 819 kJ mol⁻¹. When using an appropriate basis set, the calculated PAs thus compare reasonably well with the experimental value quoted above.

The potential energy surface (PES) of the protonated phenol species possesses seven local energy minima all displayed in Figure 21, which vividly illustrates the migration of the excess proton between the adjacent heavy atoms. This portion of the energy surface also includes four transition structures (TS) for 1,2-hydrogen migrations. Starting from the highest-energy *ipso*-protonated form, the excess H⁺ almost freely migrates to the *ortho*-protonated form passing through a small barrier of 8 kJ mol⁻¹ described by TS₃. The barriers for proton migration between the other adjacent carbon atoms are substantially larger, viz. 31 kJ mol⁻¹ for the *meta*-to-*para* (TS₁) and 45 kJ mol⁻¹ for the *meta*-to-*ortho* migration (TS₂). The activation barrier governing the *ipso*-to-oxygen migration amounts to 121 kJ mol⁻¹ (TS₄). The corresponding transition frequencies of 773i, 869i, 960i and 1599i cm⁻¹, respectively, are assigned to the vibrational modes of the excess migrating proton. The large energy separation between the *para*-C₄ and O-protonations clearly demonstrated in Figure 21 constitutes a key difference from the protonation process in aniline (C₆H₅NH₂) where both the *para*-C₄- and N-protonated species have comparable energy content^{301–303}. Nevertheless, a substantial energy barrier of 159 kJ mol⁻¹ for H-shift has been found separating the O-protonated phenol from its nearest C-isomers. This result provides us with a rationalization for the recent experimental observations using IR spectroscopic techniques³⁰⁰. It appears that in this experiment, protonation initially occurs at several positions, but eventually only the O- and one C-protonated form were stabilized and spectroscopically detected. Due to the ease with which the proton scrambled around the ring, it is rather difficult to observe, for example, a *meta*-form even though it is thermodynamically more stable than the O-isomer. In contrast, the latter was able to resist unimolecular rearrangements, thanks to the more difficult oxygen-to-carbon proton migration (Figure 21), and thus it lived long enough to be detectable within the time frame of an IR experiment.

The regioselectivity of the gas-phase protonation of phenol can be understood in simple terms of its resonance structures. Drawing them, we may figure out that a positive π -charge of the protonated form is mainly localized in the *para*- and *ortho*-positions with respect to the protonation site. If the OH group is attached to one of these positions, the relevant molecule is then described by four resonance structures, resulting in the positive π -charge

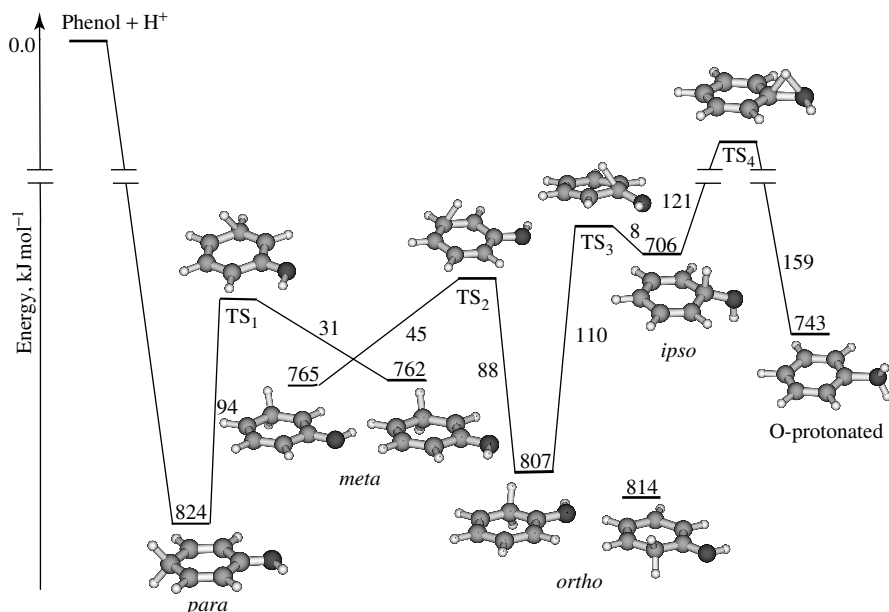
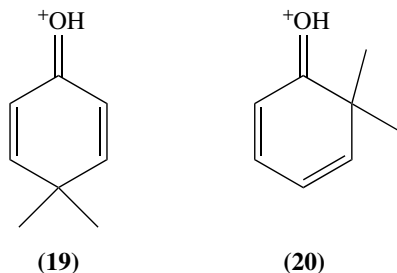


FIGURE 21. Portion of the potential energy surface of the protonated phenol showing the proton migration between the adjacent heavy atoms. Values given in kJ mol^{-1} were obtained from B3LYP/6-31+G(d,p)+ZPE computations²⁹⁹. Adapted from Reference 299 with permission

to be distributed over all atoms. Otherwise, only three structures are allowed. The presence of a positive charge in direct conjugation with the oxygen atom favours the electron density shift from the oxygen lone pairs to the ring and strengthens a stabilization of the arenium ion. Spectroscopically, it is manifested in a blue-shifting $\Delta\nu_{\text{CO}}$ of the fundamental mode 13 with the dominant contribution of the ν_{CO} stretching vibration which accompanies a shortening of the CO bond (Δr). In particular, the calculated Δr and $\Delta\nu_{\text{CO}}$ take the following values: 0.06 Å and 112 cm^{-1} in *para*-, 0.06 Å and 46 cm^{-1} in *ortho*- and 0.03 Å and 27 cm^{-1} in *meta*-protonated phenol. The other indicative frequency shifts showing the contribution of the resonance structures with the doubly-bonded oxygen atom, i.e., **19** and **20**, are associated with the OH stretching and torsional vibrations. The contribution of both structures **19** and **20** is expected to weaken the OH bond and shift the corresponding ν_{OH} mode to lower frequencies. Also, it likely determines the torsional barrier describing the rotation of the OH group around the single conjugated CO bond^{304,305} and therefore increases the τ_{OH} frequency. The low-energy *para*- and *ortho*-protonated structures reveal the most pronounced and rather similar red shifts of the ν_{OH} mode by 89 cm^{-1} and 93 cm^{-1} , and also the blue shifts of the τ_{OH} mode by 281 cm^{-1} and 277 cm^{-1} , respectively. This implies participation of the lone pairs of oxygen in stabilizing the arenium ion that leads to increase in the PA of the phenyl moiety. The *meta*-protonation shifts the corresponding vibrations by only 30 cm^{-1} and 69 cm^{-1} compared to those in the neutral molecule. A similarity in frequency shifts of the ν_{OH} and τ_{OH} modes in both *para*- and *ortho*-protonated structures and also in their relative energies suggests that the regioselectivity of the protonation of phenol is primarily governed by resonance factors.



2. Proton affinities of halophenols

The calculated PAs for mono-fluorinated phenols listed in Table 26, obtained by using the B3LYP/6-31+G(d,p)+ZPE level, are found to be in reasonable agreement with the recent ion cyclotron resonance data³⁰⁶, namely 797 kJ mol⁻¹ (expt. 788 kJ mol⁻¹) for 2-fluorophenol, 813 kJ mol⁻¹ (expt. 802 kJ mol⁻¹) for 3-fluorophenol and 787 (expt. 776 kJ mol⁻¹) for 4-fluorophenol, and thus approach the experimental PA with a quasi-systematic overestimation of *ca* 10–12 kJ mol⁻¹. To our knowledge, no experimental PAs of Cl-, Br- and I-substituted phenols have been available so far.

For the 2- and 3-halophenols, the *para*-position remains the most attractive protonation site, irrespective of the nature of the X-atom, followed by two *ortho*-positions, C₆ and C₂, respectively. All structures protonated at these sites lie within 20 kJ mol⁻¹ above the corresponding global C₄ minima (Table 26). The other sites are less accessible for protonation. As envisaged by the classical resonance model, the lower-energy protonated structures always have the OH and X groups in the *para*- and *ortho*-positions relative to the protonation site. Among them, the structures where the OH group is attached in *para* and the X atom in *ortho* reach the global minimum on the PES of a given X-substituted protonated phenol, featuring the largest PAs in the whole series, viz. 813 kJ mol⁻¹ in 3-fluorophenol,

TABLE 26. The B3LYP/6-31+G(d,p) proton affinities (kJ mol⁻¹) of halogenated phenols^a

Protonation site Substitution	C ₁	C ₂	C ₃	C ₄	C ₅	C ₆	O
2-F	711	749	764	797	761	784	731
3-F	672	802	683	813	732	804	721
4-F	709	787	753	756	—	—	729
2-Cl	700	756	757	801	760	790	715
3-Cl	679	798	699	815	735	811	724
4-Cl	709	789	756	771	—	—	727
2-Br	702	763	760	806	763	795	736
3-Br	683	801	716	818	738	815	727
4-Br	713	792	759	784	—	—	728
2-I	710	791	767	813	769	803	743
3-I	691	807	—	823	746	820	730
4-I	719	791	765	816	—	—	731

^a Atoms numbering is shown in Chart 1. In *meta*-fluorophenols, the OH bond is leaned away from the substituent, and in all other *meta*-substituted phenols, towards it, providing the most stable neutral structures. In case of *para*-X-phenols, two pairs of structures with the protonation sites on C₂–C₆ and C₃–C₅ atoms, respectively, are energetically close. Values taken from Reference 299.

815 kJ mol⁻¹ in 3-chlorophenol, 818 kJ mol⁻¹ in 3-bromophenol, and 823 kJ mol⁻¹ in 3-iodophenol. Such behaviour can in part be accounted for by a better conjugation of the oxygen lone pairs with the ring compared to those of the X groups.

The 3-X-phenols (X=Cl, Br, I) protonated at the C₄ and C₆ positions are nearly isoenergetic; their PAs are equal to 815 and 811 kJ mol⁻¹ in 3-chlorophenol, 818 and 815 kJ mol⁻¹ in 3-bromophenol, and 823 and 820 kJ mol⁻¹ in 3-iodophenol, whereas the C₂-protonated species lie slightly higher in energy due to a steric repulsion with the OH group.

In 4-halophenols (X =F, Cl, Br), the excess proton tends to reside in *ortho*-positions. On the other hand, in *para*-iodophenol, the protonated structure with both I and the excess H⁺ residing in the *para*-site has the lowest energy.

As for a correlation between PAs and molecular properties, Table 27 lists the characteristic frequencies of the hydroxyl torsional τ_{OH} and stretching ν_{OH} vibrational modes in the neutral and protonated fluorophenols. The τ_{OH} vibration is directly related to distortions in the π -electronic system which was demonstrated experimentally for a wide variety of substituted phenols³⁰⁷. The π -electron donor substituents at the *para*-position lower the τ_{OH} frequency compared to unsubstituted phenol, while the π -electron acceptor substituents act in the opposite way. In neutral fluorophenols, the τ_{OH} mode is centred at 304 cm⁻¹ for *para*-fluorophenol, 330 cm⁻¹ for *meta*-fluorophenol and is blue-shifted to 411 cm⁻¹ for *ortho*-fluorophenol due to the hydrogen bonding (see Table 27; 330 cm⁻¹ in unsubstituted phenol). The τ_{OH} frequency is blue-shifted upon protonation depending on the protonation site. In *para*- and *ortho*-protonated phenols which are resonance-stabilized via the structures with the doubly-bonded oxygen atom of the types **19** and **20** exhibiting the highest PA, these shifts are very pronounced and yield values of 317 cm⁻¹ in the C₆-protonated *para*-fluorophenol, 283 cm⁻¹ in C₂-protonated, 264 cm⁻¹ in C₄-protonated and 231 cm⁻¹ in C₆-protonated *meta*-fluorophenols. In *meta*-protonated structures, the blue shift of the τ_{OH} becomes smaller, viz. 2 cm⁻¹ in *para*-fluorophenol and 70 cm⁻¹ in *meta*-fluorophenol. In *ortho*-fluorophenols, the effect of the protonation site on τ_{OH} is less evident due to its interplay with the effects of hydrogen bonding.

The ν_{OH} frequency behaves in a similar manner with respect to the protonation site, although shifts are in the opposite direction. By analogy with the torsional frequency, the maximal shifts are found in *para*- and *ortho*-protonated structures, viz. 98 cm⁻¹ in C₆-protonated *para*-fluorophenol, 93 cm⁻¹ in C₂-protonated, 84 cm⁻¹ in C₄-protonated and 76 cm⁻¹ in C₆-protonated *meta*-fluorophenols. In the hydrogen-bonded systems, both the hydrogen bonding and the distortions in the π -electronic system caused by protonation behave coherently in weakening of the OH bond and thus shifting the ν_{OH} to lower frequencies. The predicted red shifts of the ν_{OH} mode in these systems become even more pronounced: 116 cm⁻¹ in C₄-protonated and 110 cm⁻¹ in C₆-protonated 2-fluorophenols.

In the case of 3-X-phenols, the X-protonated structures are local minima, but they are consistently above the high-energy *ipso*-protonated phenols, except for 3-iodophenol in which an *ipso*-protonation is less favourable by 13 kJ mol⁻¹ than an I-protonation. The calculated PAs for the X-protonated 3-halophenols are the following: 613 kJ mol⁻¹ for 3-fluorophenol, 676 kJ mol⁻¹ for 3-chlorophenol, 680 kJ mol⁻¹ for 3-Br-phenol and 704 kJ mol⁻¹ for 3-iodophenol, using the same level of theory.

It is well known that in halobenzenes, the *para*-position relative to the halogen is the more basic site and the *meta*-position the least basic³⁰⁸. The higher activity for the *para*-position in fluorobenzene results from the need to add a proton to a position that is not disfavoured by the σ -electron withdrawal by fluorine atom, due to its strong inductive effect. The effect is smaller for chlorine, bromine and iodine. Thus when there is competition between the hydroxy group and a halogen atom in directing the ring protonation,

TABLE 27. Frequencies (cm^{-1}) of the torsional and stretching vibrations in the protonated and unprotonated fluorophenols²⁹⁹

Structure ^a	τ_{OH}	ν_{OH}	Structure ^a	τ_{OH}	ν_{OH}	Structure ^a	τ_{OH}	ν_{OH}
	411	3802		330	3831		304	3833
	399	3780		613	3738		306	3809
	684	3686		594	3747		621	3735
	370	3780		400	3798			
	655	3692		561	3755			

^aThe first structure refers to the neutral fluorophenol. The other species are protonated fluorophenols at different positions.

as in the case of halophenols, the outcome turns out to be in favour of the hydroxy group which, as discussed above, consistently leads to a C₄-protonation (Table 26).

3. Proton affinities of anisole and fluoroanisoles

Anisoles are phenol derivatives in which the OH is replaced by the OCH₃ group. As expected, anisole reveals the same protonation pattern as phenol, although all of its local PAs appear to be larger, namely 845 kJ mol⁻¹ in *para*-C₄-protonation, 836 kJ mol⁻¹ in *ortho*-C₆-protonation and 780 kJ mol⁻¹ in *meta*-C₃-protonation. Similarly, a correlation

has been observed between the local PAs and the C–O bond shortening (Δr) and the blue-shifting ($\Delta \nu_{\text{CO}}$) of the fundamental mode with the dominant contribution of ν_{CO} vibration. The Δr and $\Delta \nu_{\text{CO}}$ changes take the following values: 0.03 Å and 28 cm^{-1} in C₃-protonated anisole, 0.07 Å and 103 cm^{-1} in C₄-protonated anisole, 0.03 Å and 29 cm^{-1} in C₅-protonated anisole and finally 0.07 Å and 81 cm^{-1} in C₆-protonated anisole²⁹⁹.

The PAs of fluoroanisoles are equal to 820 kJ mol^{-1} (expt. 807³⁰⁶) for 2-fluoroanisole, 835 kJ mol^{-1} (expt. 826³⁰⁶) for 3-fluoroanisole and 809 kJ mol^{-1} (expt. 796³⁰⁶) for 4-fluoroanisole. An average overestimation of ca 12 kJ mol^{-1} by the B3LYP/6-31+G(d,p)+ZPE calculations can again be noted²⁹⁹.

4. Two views on the protonation regioselectivity

It is now legitimate to pose the question as to whether there exists a clear-cut but simple theoretical approach to predicting the protonation regioselectivity solely on the basis of molecular properties of the neutral substrate. Theoretical chemists persist in their continuing endeavour to search for such a reactivity index. The relative gas-phase acidity and basicity data collected in the last several decades have been analysed and correlated with a variety of atomic and molecular parameters. Examples include the atomic charges, charge-induced dipole field or polarizabilities, electrostatic potentials surrounding a base, core ionization energies or 1s-orbital energies, electronegativities, hybridization, bond energies, electron affinities etc. The main idea is to design a way of partitioning the molecular charge distribution into atomic properties that show acceptable correlations with PA^{309–315}. The most representative approach is the atom-in-molecule theory³⁰⁹. Use of the components of wave functions constructed by either multi-configurational³¹³ or spin-coupled³¹² methods was also put forward in support of an interpretation in terms of resonance structures. However, all these approaches to identifying the protonation sites either were not quite successful^{314–315} or could not be extended to a larger sample of compounds³¹⁵. We will consider two of the most recent attempts including the use of the topological analysis based on the electron localization function (*ELF*)^{272, 273, 316, 317}, discussed in Section III.C, and the density functional theory-based reactivity descriptors, in both a global and a local sense^{301, 302, 318–340}.

As seen above, the topology of the *ELF* suggests that the most favoured protonation site can be found by using a ‘least topological change principle’^{275, 317} which states that:

- (i) the protonation occurs in the most populated, accessible valence basin for which there is the least topological change of the electron localization function, and
- (ii) in the protonated base, the V(B,H) population cannot be noticeably larger than 2.5 electrons.

In all cases, except for *ortho*-Cl and *ortho*-Br phenols, it is the V(O,H) basin which is favoured over the V(X) basin. In the two aforementioned molecules, the intramolecular hydrogen bond is strong enough to perturb the topology of the halogen valence shell having three basins, and the *ELF* predicts that the favoured protonation site is one of the most populated V(X) halogen basins. In other words, the *ELF* could correlate the relative basicities between heteroatoms but is apparently unable to account for the preference of the ring *para*-C₄ carbon in the protonation process²²⁰.

We now turn to the reactivity indices defined within the framework of density functional theory (DFT). The validity and applicability of these indices have been discussed in several recent studies by different groups^{301, 302, 318–340}. This is a different way of decomposing a molecular electronic distribution into global and/or local indices coupled with an account of the frontier molecular orbitals. Starting from the electronegativity equalization principle³¹⁸, the global descriptors such as ‘group hardness’ and ‘group electronegativity’

were defined³¹⁹ and correlated with PAs. Nevertheless, their scope of applicability was quite limited. More recently, the more local descriptors, including the Fukui function, local atomic softness or even orbital softness, have been employed in order to interpret the protonation sites^{299, 301, 302}. The definitions^{320, 321} and evaluations^{322–325} of DFT-based reactivity indices are well established.

The condensed Fukui functions f_k of a k th atom in a molecule with N electrons are defined by equations 27a and 27b:

$$f_k^+ = [q_k(N+1) - q_k(N)] \quad \text{for nucleophilic attack} \quad (27a)$$

$$f_k^- = [q_k(N) - q_k(N-1)] \quad \text{for electrophilic attack} \quad (27b)$$

where q_k is the electronic population of atom k in the molecule under consideration. The local softness parameter can then be defined as $s_k^i = f_k^i \times S$ in which i stands for + or -. Within the finite difference approximation³²², the global softness, S , can be approximated by

$$S = 1/(\text{IE} - \text{EA})$$

where IE and EA are the first vertical ionization energy and electron affinity of the molecule, respectively.

The local softness has been applied with much success in interpreting and predicting the regio-selectivities of different types of organic reactions including radical additions³²⁶, nucleophilic additions^{327–329}, pericyclic $[2+1]$ ^{330–333}, $[2+2]$ ³³⁴ and $[3+2]$ ^{335–341} additions, hydrogen shifts³⁴² and internal rotations.^{343, 344}

In the parent phenol for which the local indices are summarized in Table 28, the values for the C₅ and C₆ atoms are also close to those for C₃ and C₂, respectively, and

TABLE 28. Calculated local softnesses of phenol

Property	B3LYP/cc-pVTZ
vert-IE (eV)	8.45
vert-EA (eV)	-1.66
S^a	2.69
s_k^+	
C ₁	0.04
C ₂	0.39
C ₃	0.25
C ₄	0.31
O	0.12
s_k^-	
C ₁	0.08
C ₂	0.36
C ₃	-0.04
C ₄	0.83
O	0.48
s_k^-/s_k^+ ratio	
C ₁	1.94
C ₂	0.92
C ₃	-0.17
C ₄	2.64
O	3.91

^a S is the global softness. The Fukui functions f_k can be obtained using $s_k = f_k \cdot S$.

thus omitted for the sake of simplification. In the present case, the *local softness for electrophilic attack* s^- is to be used to probe the protonation mechanism, that is, the larger the local softness, the more basic the site. It is clear that the C₄ carbon atom bears the largest softness ($s^- = 0.83$), a value much larger than that of oxygen ($s^- = 0.48$). While the C₂ carbon has a significant softness ($s^- = 0.36$), the C₁ and C₃ atoms do not show much affinity for electrophiles. These observations are in accord with the proton affinities discussed above which unambiguously indicate the preferential protonation at the C₄ carbon of phenol, followed by that at C₂ carbon and oxygen. Table 28 lists the s_k values and the quantities s_k^-/s_k^+ and shows that *the latter ratio also does not hold true for phenol protonation*. In fact, the oxygen atom is characterized by the largest ratio followed by C₄. Among the ring carbon atoms, while C₄ has the largest ratio (which is correct), C₁ has a larger ratio than C₂ (which is not correct according to the calculated PAs).

The calculated local softnesses and Fukui functions of the fluoro- and chloro-substituted phenols (values of s_k^-) suggest the following protonation ordering (versus the real ordering found from calculated proton affinities).

- | | |
|---|--|
| (a) Fluorophenols: 2-F: O > C ₄ > C ₆ | versus C ₄ > C ₆ > C ₃ > C ₅ > C ₂ > O, |
| 3-F: C ₄ > C ₆ > O | versus C ₄ > C ₆ > C ₂ > C ₅ > O, |
| and 4-F: O > C ₄ > C ₆ > C ₂ | versus C ₂ > C ₄ > C ₃ > O. |
| | |
| (b) Chlorophenols: 2-Cl: C ₄ > O > C ₆ | versus C ₄ > C ₆ > C ₅ > C ₃ ≈ C ₂ > O, |
| 3-Cl: C ₄ > C ₆ > O | versus C ₄ > C ₆ > C ₂ > C ₅ > O, |
| and 4-Cl: O > C ₆ > C ₂ | versus C ₂ > C ₄ > C ₃ > O. |

In comparison with the calculated PAs mentioned above, a few points are worth noting²⁹⁹:

(i) The local softnesses of atoms having different atomic numbers cannot be compared to each other (for example, a comparison of a carbon and an oxygen atom is not relevant). Similarly to the shortcomings of net atomic charges or electrostatic potentials^{314, 315, 345, 346}, this local descriptor is apparently unable to differentiate the relative basicities of heteroatoms. A comparable conclusion was drawn from an analysis of the *orbital local softnesses*^{302, 342}. Such behaviour differs somewhat from that of the *ELF* discussed in Section III.C.

(ii) The local softness behaves more regularly among the ring carbon atoms. In fact, for both 2-X and 3-X phenols, the local softness points towards a *para* protonation in agreement with explicit computations of PAs. While for 4-Cl the local softness correctly predicts the preference of C₆ and C₂, the situation is more confusing in 4-F where the s^- values of all carbons are similar to each other, with a marginally larger value for C₄ followed by C₆ and C₂ (if oxygen is omitted).

(iii) The s_k^-/s_k^+ ratio is nowhere able to unravel the preferable protonation site.

(iv) There is no correlation between the absolute values of local softnesses with the PAs at the ring carbon centres.

These drawbacks of either *ELF* or DFT-based indices raise the question as to whether it is meaningful to use the local properties of reactants in distinguishing the protonation of atoms of different nature. Similar to the case of two different atoms, such as O and C, when a X-substituent strongly modifies the electronic environment of the carbon, a perturbative treatment could also no longer be applied to the C(H) and C(X) centres.

Although the local softness includes, by definition, both the differences of frontier orbitals of the neutral substrate and the differential electron densities between the neutral and ionized states, as expressed in the global softness and Fukui functions, the actual computations of these quantities suffer from some severe practical limitations²⁹⁹.

In summary, neither the *ELF* nor the DFT-based reactivity indices are capable of accurately predicting the most preferably protonated sites of phenols as well as the order of the local PAs. Similar to the many well-known static indices, their performance is expected to be limited in other classes of compounds as well. Thus the discovery of a good protonation index remains a formidable challenge for theoretical chemists. The difficulty lies in the fact that any quantitative correlation between a molecular property and the PAs of a series of compounds is based on the assumption that the relaxation energy involved should practically be constant for the entire series. After all, the proton is strongly electrophilic and very hard, and its approach polarizes the whole medium due to its small size and basically modifies the molecular and electronic structure of the substrate. As the local indices are usually defined at unperturbed neutral substrates, it is obvious that they are not sensitive enough to predict the realistic situations characterized by drastic changes following the protonation process.

5. Interaction of phenol with Li^+ , Na^+ and K^+

Properties of the complexes of alkali metal cations with various bases are important in understanding ion–molecule interactions, solvation effects, biomedical and physiological phenomena related to ion channels and relevant in medical treatments. Reliable experimental bond dissociation enthalpies, and thereby gas-phase alkali ion affinities, could now be obtained using various mass spectrometry techniques such as the Fourier-transform ion cyclotron resonance (FT-ICR), collision-induced dissociation and photodissociation methods. However, these methods do not provide direct information on the adduct structures.

The Li^+ cation exhibits a vacant p-orbital and its interaction with benzene occurs with the π -electrons giving rise to a symmetrical bridging complex in which the cation is placed on the C_6 axis, about 2.0–2.1 Å from the centre of the ring³⁴⁷. When approaching phenol, the cation could thus associate either with the ring or the oxygen lone pair. It has been argued that both the ion–dipole and polarizability interactions would strongly favour an alignment of the cation along the dipole axis of the compound³⁴⁸. Indeed, calculations point out that, in contrast to the protonation, the lithiation occurs preferentially at the position of the oxygen lone pair of phenol. The heavier alkali cations Na^+ and K^+ show a similar behaviour. The resulting complexes are nearly planar with a marginal torsion of the hydroxyl hydrogen atom. Some selected geometrical parameters are displayed in Figure 22. Significant lengthening of the C–O bond (up to 0.05 Å) is found upon complexation. The oxygen–cation distances are longer in the ring complexes. At the B3LYP/6-311++G(*d*, *p*)+ZPE level of theory, the alkali cation affinities of phenol amount to 149, 101 and 68 kJ mol^{−1} for Li^+ , Na^+ and K^+ , respectively. Thus, the heavier the cation, the smaller the binding energy and the weaker the ion–phenol complex becomes.

There is only a small charge transfer in the complexes in which the alkali metal retains from 0.75 to 0.95 electronic unit of its original positive charge. This supports the general view that ion–molecule bonding is due to a predominantly electrostatic interaction with a large contribution from the bond dipole.

B. Deprotonation

The Brønsted acidity of a molecule is its capacity to give up a proton. It can be expressed either by the equilibrium constant, the $\text{p}K_{\text{a}}$ value, the change of standard free energy ($\Delta G_{\text{T}}^{\circ}$) or simply the energy of the deprotonation reaction: $\text{AH} \rightarrow \text{A}^- + \text{H}^+$. The acidities of phenols were measured experimentally^{349–351}, including a series of 38 *meta*-

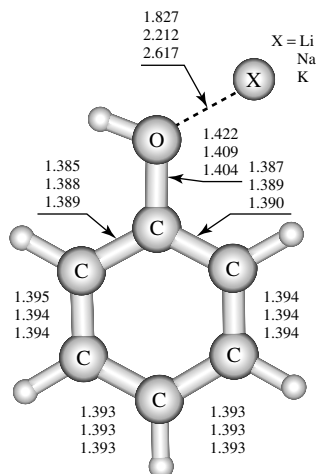


FIGURE 22. Selected B3LYP/6-311++G(d,p) geometrical parameters of the complexes between phenol and alkali metal cations. Bond lengths are in Å

and *para*-substituted phenols using the ion cyclotron resonance (ICR) equilibrium constant method³⁵¹. Theoretical evaluations of acidity usually involve energy calculations of both the neutral substrates and conjugate anions.

1. Phenolate anion

Geometries and vibrational frequencies of phenolate anion (PhO^-) in the ground, triplet and excited states were analysed in details^{115,352–361}. Figure 23 displays selected optimized geometrical parameters of the free PhO^- in both lowest-lying singlet and triplet electronic states. Although several crystal structures of phenolates have been reported^{362–364}, different degrees of aggregation and solvation prevent a direct comparison. The geometry of PhO^- is quite close to that of the benzyl anion (PhCH_2^-). In both cases the

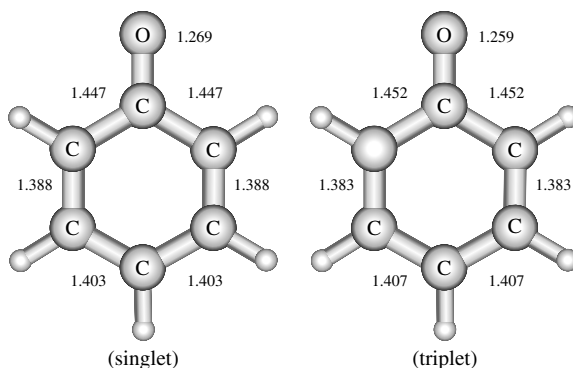


FIGURE 23. Selected (U)B3LYP/6-311++G(d,p) optimized bond lengths (Å) of the phenolate anion in both lowest-lying singlet and triplet states

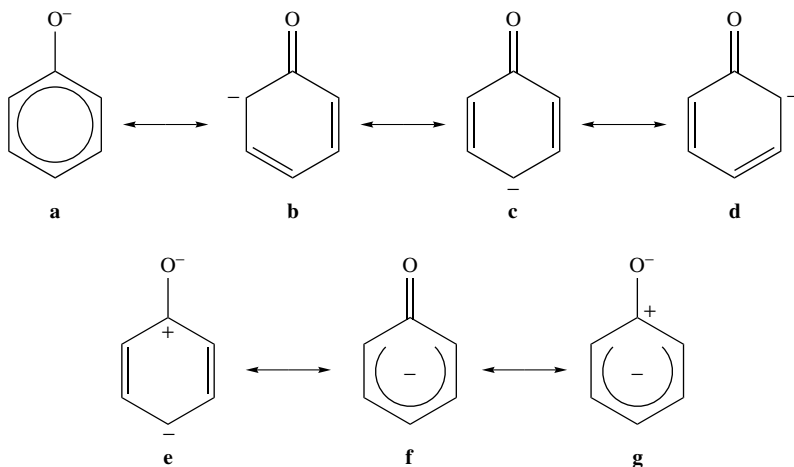


CHART 4. Resonance hybrids of the phenolate ion

p - π delocalization apparently causes a small bond alternation (up to 0.06–0.07 Å) in the anion ring. On this simple basis, PhO^- has thus *ca* 60% of the aromatic character of PhOH ³⁵⁶. The C–O distance of 1.27 Å of the anion lies between those of 1.37 Å in PhOH and 1.22 Å in *para*-benzoquinone, giving the CO bond of PhO^- a partial double-bond character which could be understood in terms of simple resonance structures (Chart 4)^{357, 358}. Considering the geometry, a quinonoid resonance form **c** with alternating double and single CC bonds may well be a depiction of PhO^- .

Since the charges on oxygen are -0.9 electron and on the *ipso*-carbon C_1 $+0.5$ electron, the dipolar forms are also expected to contribute significantly to the electronic structure of the anion. A certain similarity exists between the phenolate and enolate anions regarding the C–O distances. Quantum chemical calculations^{115, 353, 358, 360} of vibrational frequencies for free PhO^- in the ground state did show some discrepancies with experimental data^{365, 366}. While IR frequencies determined using DFT methods compare reasonably with the FTIR results in the case of the modes ν_4 and ν_5 , the frequency of the C–O stretching mode is overestimated in all calculations. In addition, large deviations were also found for most modes on isotopic ^{13}C and ^{18}O shifts, as well as on relative IR intensities. Using appropriate scaling factors on computed frequencies at different levels of theory led to the estimated values of 1594, 1495 and 1353 cm^{-1} for the modes ν_4 , ν_5 and ν_6 , respectively. While the former two are close to the IR absorption peaks at 1585 (or 1592) and 1483 cm^{-1} , the latter deviates from the observed ν_6 value of 1273 cm^{-1} by a larger amount of 80 cm^{-1} . Multi-reference CASSCF(10,10) calculations resulted equally in a CO bond distance of 1.285 Å and a ν_6 frequency of 1450 cm^{-1} . Thus, the discrepancy between experiment and theory cannot be attributed to a failure of quantum chemical methods, but presumably results from the formation of a complex of PhO^- with either solvent molecules or counterions, weakening the CO bond and inducing a down shift of the corresponding stretching mode. This point will be considered in a subsequent paragraph.

The delocalization of the negative charge from the oxygen to the ring affects the aromaticity of the latter. The magnetic properties of the ring carbons show in fact some marked changes upon deprotonation. Using the GIAO-HF/6-311+G(d,p) method, the

^{13}C NMR chemical shifts (δ in ppm) of phenol and phenolate anion are calculated as follows³⁵²:

$$\begin{aligned} & \text{C}_1:156 \text{ (PhOH)}/182 \text{ (PhO}^-), \text{ C}_2:111/115, \text{ C}_3:131/132, \text{ C}_4:118/91, \\ & \text{C}_5:133/132 \text{ and } \text{C}_6:115/115. \end{aligned}$$

The C_1 (shielded) and C_4 (deshielded) atoms obviously experience the largest variations. The proton chemical shifts remain almost unchanged, varying by less than 2 ppm.

The nucleus-independent chemical shifts (NICS)³⁶⁷, calculated as the negative of the absolute magnetic shieldings at ring centres, could be used as a probe for aromaticity. While the phenol in-plane NICS(0) value of -10.8 is greater than that of benzene (-9.7), the NICS value for PhO^- is much smaller (-6.3), only about 58% of the phenol value. This reduction in aromaticity is apparently due to the predominance of the quinoidal structure having alternate CC distances c (Chart IV). It is worth noting that while the PhOH NICS(1) of -11.3 is only slightly larger than the corresponding NICS(0), the PhO^- NICS(1) of -7.6 is larger than its NICS(0) counterpart. This indicates a larger concentration of π -electrons in the anion.

The decreasing aromaticity in the anion is also manifested in a smaller magnetic susceptibility exaltation (Λ)³⁶⁸, which is defined as the difference between the bulk magnetic susceptibility (χ_M) of a compound and the susceptibility ($\chi_{M'}$) estimated from an increment system for the same structure without cyclic conjugation ($\Lambda = \chi_M - \chi_{M'}$ in units of ppm cgs). Thus, the value $\Lambda = -9.1$ for PhO^- is equal to only 59% of the $\Lambda = -15.5$ for phenol. The computed values for the diamagnetic susceptibility anisotropy (χ_{anis}) follow the same trend, indicating that PhO^- has actually about 60% of the aromaticity of PhOH ³⁵².

It is perhaps interesting to examine here the NICS values for a series of halogenophenols. The influence of one halogen atom on the PhOH NICS is already noticeable: F increases it by 0.2 (-11.0 in *ortho*-F-phenol) whereas Cl reduces it by 1.3 (-9.6 in *ortho*-Cl-phenol) and Br reduces it further by 1.5 (-9.3 in *ortho*-Br-phenol). The effect of multiple X-substituents is appreciable in increasing the NICS to -13.0 in 2,4-di-F- and -14.6 in 2,4,6-tri-F-phenol. The 2,4-di-Cl and 2,4,6-tri-Br species have NICS values approaching that of PhOH . Although the halogen effect is quantitatively more important in phenolates, the trend of the variations is parallel to that in the neutral series, suggesting a significant effect of fluorine.

The electron affinity of the phenoxy radical has received considerable attention. Experimentally, a 2.36 eV upper limit was obtained in 1975³⁶⁹. Later, the UV photoelectron spectroscopy of PhO^- was recorded³⁷⁰ from which an adiabatic ionization energy $\text{IE}_a(\text{PhO}^-) = 2.253 \pm 0.006$ eV was determined. This low value implies that the valence excited states of phenolate are autoionizing. Evidence for an autoionizing state was found at about 3.5 eV in the photoelectron experiment³⁷⁰ and at 3.65 eV (340 nm) in the photodetachment spectrum³⁶⁹. In other words, there is no evidence for singlet excited states of PhO^- below the ionization threshold. The S_1 and S_2 states belong to the A_1 and B_1 irreducible representations of the C_{2v} symmetry group and can be labelled as 1L_a and 1L_b , respectively. Both S_1 and S_2 excited states of PhO^- were calculated to have comparable vertical energies^{115, 356, 361}. Recent large CASPT2 computations^{357, 371, 372} suggested an adiabatic $S_1 \leftarrow S_0$ energy gap of about 3.69 eV³⁵⁷. The latter is further increased to 4.2 eV in aqueous medium, thus corresponding to a blue shift of 1817 cm^{-1} . Experimentally, the first two peaks in the phenolate UV absorption spectrum in aqueous solution are located at 4.32 and 5.30 eV³⁷³. Molecular dynamics simulations on excited states in solvents were also carried out³⁷¹. A comparison of the oscillator strengths of both states

seems to indicate that the 1A_1 state, which enjoys a much larger stabilization following geometry relaxation, actually corresponds to the lower-lying state (at least in aqueous solution) of the anion. There is thus a reversed ordering of excited singlet 1L_a and 1L_b states in going from phenol to its conjugate anion. The inversion of singlet states is further confirmed in cyanophenols, irrespective of the substitution position¹¹⁵.

While the S_0 and S_2 (1B_1) states are characterized by a similar charge distribution, they strongly differ from the S_1 (1A_1). A large amount of negative charge (0.45 e) was estimated to be transferred from the oxygen to the ring centre upon the $S_1 \leftarrow S_0$ transition corresponding to a $\pi^* \leftarrow n$ character. This fact allows for the qualitative deprotonation behaviour of both diabatic states 1L_a and 1L_b to be understood in terms of electrostatic interactions when the O–H distance becomes sufficiently large. The approach of the positive charge to the anion does not modify the transition energy of 1L_b due to the small difference in both ground and excited state dipole moments. In contrast, the 1L_a transition energy changes, due to a significant charge transfer in the anion, reducing the negative charge on oxygen. At a certain O–H distance, both states eventually cross each other implying that, in a reduced symmetry, namely C_s rather than C_{2v} along the proton dissociation coordinate, a conical intersection in the excited states of phenol becomes possible. The centre of such a conical intersection, if it exists, should be located on the C–O axis at a distance of *ca* 2.6 Å from the oxygen atom. Although these features need to be confirmed by more accurate calculations than those reported¹¹⁵, it seems that the presence of an avoided crossing along the physically relevant O–H direction, and a conical intersection along the C–O approach of the proton, is of importance per se, as well as, more generally, in the dynamics of the excited state proton transfer reaction from phenol to, for example, water.

The lowest-lying PhO^- triplet state shows marginal deviations from planarity. Some important geometrical features of the T_1 state of the parent are also shown in Figure 23. It is of particular importance that the C–O distance remains almost unchanged with respect to the corresponding singlet state, and that the ring keeps the quinoidal shape (Figure 23). At the B3LYP/6-311++G(d,p)+ZPE level, the $T_1 \leftarrow S_0$ energy gaps are calculated to be around 2.4–2.5 eV for PhO^- and the $p\text{-XC}_6\text{H}_4\text{O}^-$ anions. These values are slightly larger than the corresponding ionization energies. The triplet anion has not yet been experimentally observed. The T_1 state is readily formed with a dominant configuration arising from a single excitation from the ground state, and rapidly undergoes autodetachment.

The lower-lying singlet and triplet excited states of PhO^- in the environment of photoactive yellow proteins (PYP) were recently simulated by placing point charges to represent the electrostatic field of the seven amino acids and explicit interaction of the anion with two water molecules to account for the hydrogen bonds³⁵⁷. The most interesting results are that while the hydrogen bonds were found to exert a minor influence for the lower-excited states of the embedded PhO^- , the electrostatic environment of the PYP protein is essential in providing the dominant stabilization, shifting the lowest singlet excited state below the first ionization energy of the system. This effect is also reinforced by a substantial increase of about 4 eV in the anion ionization energy, on passing from the free PhO^- to the protein-bound anion, and then further increasing by up to 0.9 eV for the protein-bound anion–water complex. This feature is significant as it approaches more closely the spectral data for biological chromophores in their native environments.

In halophenolate anions, the *meta* isomers (Figure 24) turn out to be consistently the more stable ones followed by the *ortho* and *para* derivatives, irrespective of the nature of the substituents. The effect is more pronounced in fluoro-anions where the *meta* isomer is about 16 kJ mol^{−1} more stable than the *ortho* counterpart (Figure 25). This energy gap is reduced to 7 and 6 kJ mol^{−1} in chlorinated and brominated phenolate anions, respectively. The energy differences between the *ortho*- and *para*-anions are rather small (*ca* 2 kJ mol^{−1}). On the other hand, the phenolate anion (charge at oxygen) is calculated

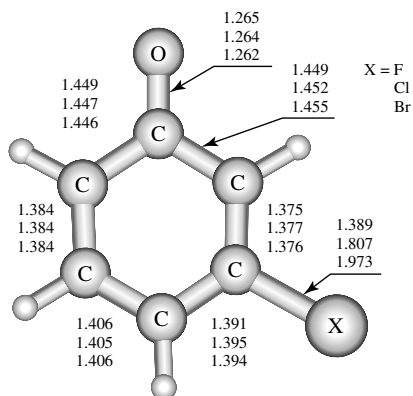


FIGURE 24. Selected B3LYP/6-311++G(d,p) optimized bond lengths (Å) of the metahalophenolate anions in their ground singlet state

to be remarkably more stable than the ring carbon anions by a large amount ranging from 150 to 200 kJ mol⁻¹.

Within the series of ring carbanions (Figure 25), the *ortho*-anions situated at the C₂ positions relative to the hydroxy group (except for *o*-FC₆H₄OH where the anion is on C₆) are found to be favoured regardless of halogen position. This is no doubt due to the strong interaction between the OH-hydrogen and the negatively charged carbon centre. This implies that the *ortho*-carbon is the most acidic atom within the ring, and this fact has also been verified even in the case of the electron-donating methyl group³⁷⁴. Bearing in mind that the *para*-carbon constitutes the most basic ring centre (cf. the preceding section), the difference can be understood by the fact that a ring deprotonation is overshadowed by its σ -electron skeleton whereas a ring protonation is rather directed by its π -electron distribution. Overall, the deprotonation energies (DPE) of polysubstituted benzenes apparently follow a simple and transparent additivity of the independent substituent effects, implying these DPEs could be deduced using the pre-determined increments of monosubstituents³⁷⁴.

Regarding the ionization energies of phenolate ions, or conversely the electron affinities of phenoxy radicals (XPhO•), calculated results of some simple substituted species are summarized in Table 29. Density functional theory, in particular when using the hybrid B3LYP functionals, could reproduce the EAs of aromatic radicals with an absolute error of 0.03 eV with respect to the experimental estimates^{358, 359}. As substituents on the ring, the halogen atoms tend to increase this quantity by up to 0.4 eV, in the decreasing order: *meta* > *ortho* > *para* position, relative to the value for the parent radical. In contrast, OH and NH₂ groups on the *para*-C₄ position of the phenolate ion consistently reduce the ionization energy by 0.25 and 0.50 eV, respectively³⁵⁹.

2. Gas-phase acidities

A convenient measure of the gas-phase acidity is the proton affinity (PA) of the anion, or conversely, the deprotonation energy (DPE) of the acid. For the parent phenol, the experimental value can be deduced from equation 28 for the PA of phenolate,

$$\text{PA}(\text{PhO}^-) = \text{IE}(\text{H}) + D(\text{PhO-H}) - \text{EA}(\text{PhO}^\bullet) \quad (28)$$

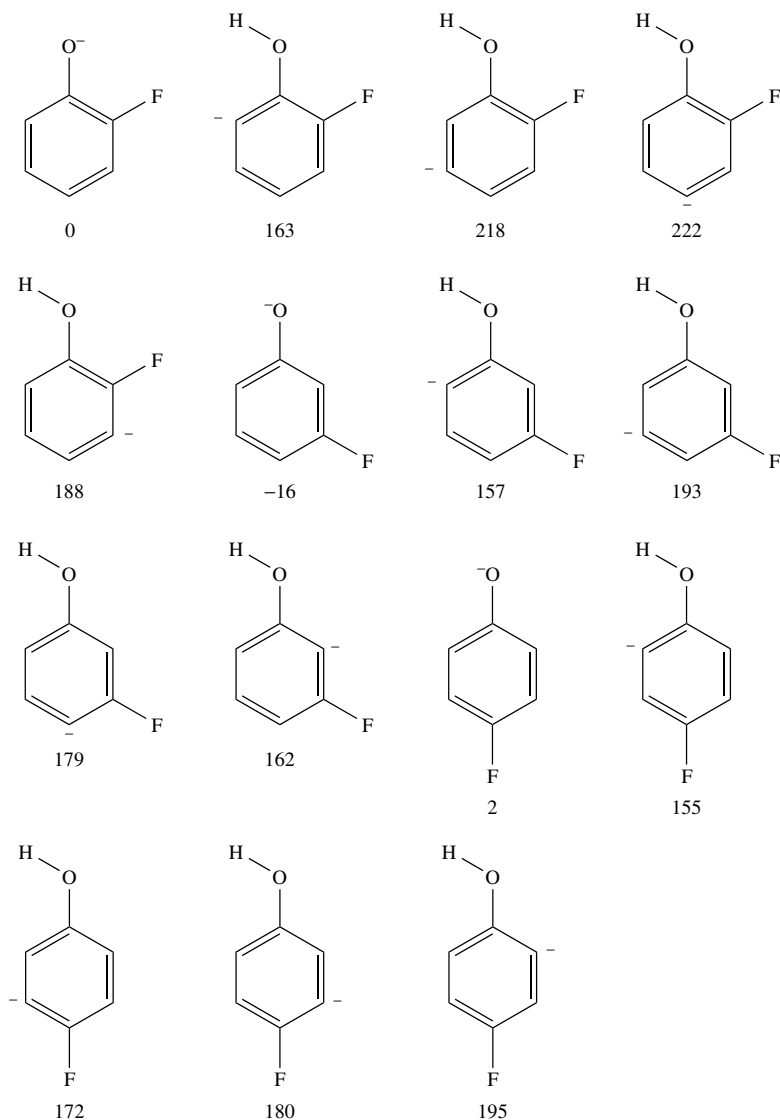


FIGURE 25. Relative energies (in kJ mol^{-1}) obtained from B3LYP/6-311++G(d,p)+ZPE calculations of different isomers of fluorophenolate ions

where $\text{IE}(\text{H}) = 13.606 \text{ eV}$ is the ionization energy of the hydrogen atom and $\text{EA}(\text{PhO}^{\bullet}) = 2.253 \text{ eV}$ is the electron affinity of the phenoxy radical³⁷⁰. The PA is thus dependent on $D(\text{PhO}-\text{H})$, being the $\text{PhO}-\text{H}$ bond energy. Taking the most recent recommended value of $D(\text{PhO}-\text{H}) = 3.838 \text{ eV}$ ³⁷⁵, we obtain $\text{PA}(\text{PhO}^-) = \text{DPE}(\text{PhOH}) = 15.191 \text{ eV}$, which is slightly larger than the value of 15.169 eV in an earlier compilation³⁷⁶. Indeed,

TABLE 29. Ionization energies of halophenolate anions

Phenolate anion	IE _a (eV) ^a
Phenolate	2.23 (2.25)
<i>o</i> -Fluorophenolate	2.40
<i>m</i> -Fluorophenolate	2.52
<i>p</i> -Fluorophenolate	2.27
<i>o</i> -Chlorophenolate	2.52
<i>m</i> -Chlorophenolate	2.61
<i>p</i> -Chlorophenolate	2.45
<i>o</i> -Bromophenolate	2.57
<i>m</i> -Bromophenolate	2.64
<i>p</i> -Bromophenolate	2.50

^aValues were obtained from B3LYP/6-311++G(d,p)+ZPE. In parentheses is the experimental value taken from Reference 370.

TABLE 30. Deprotonation energy (DPE)^a of phenol derived from various levels of the calculation method

Level of theory ^b	DPE (eV)
B3LYP/6-311++G(d,p)	14.98
B3LYP/6-311++G(3df,2p)	14.90
MP2/6-311++G(d,p)	15.05
MP2/6-311++G(3df,2p)	14.94
CCSD(T)/6-311++G(d,p)	15.17
CCSD(T)/6-311++G(3df,2p)	15.10
Experiment ^c	15.20

^aIncluding zero-point energies (ZPE).

^bGeometries were optimized at B3LYP/6-311++G(d,p) level.

^cExperimental value, see text.

calculated values in Table 30 provide a support for this estimate with the DPE of phenol lying in the range of 15.1–15.2 eV. In the gas phase, phenol is thus by far more acidic than water (DPE = 16.95 eV) and methanol (16.50 eV), but slightly less acidic than formic acid (14.97 eV) and acetic acid (15.11 eV). Phenol also has a greater acidity than vinyl alcohol (DPE = 15.51 eV) thanks to a more extensive delocalization of the negative charge in the phenolate ion and a greater polarizability of the larger phenyl group.

Results derived from coupled-cluster calculations for halophenols are summarized in Table 31. It is remarkable that even the small variations due to substituents (as detected by experiments³⁵¹) are correctly reproduced by the calculations. Accordingly, the *meta*-halophenols are consistently more acidic than the *para*-counterparts, in contrast to the pattern found for the cyano (CN) group, another strong electron-withdrawing one which tends to reduce the DPE to 14.56, 14.64 and 14.48 eV for *ortho*-, *meta*- and *para*-cyanophenols. The gas-phase acidity scale of cyanophenols is thus *para* > *ortho* > *meta*.

The effect of fluorine substitution on phenol acidities was examined in detail^{351, 377, 378}. Through a charge analysis, the F-effect could classically be explained by invoking both resonance and induction effects. In the *meta* position, the halogen tends to stabilize preferentially the phenolate anion due to the resonance effects, resulting in a smaller

TABLE 31. Deprotonation energies of halophenols

Phenol	DPE	
	(calc, eV) ^a	(expt, eV) ^b
Phenol	15.10	15.20
<i>o</i> -Fluorophenol	14.98	
<i>m</i> -Fluorophenol	14.85	14.97
<i>p</i> -Fluorophenol	15.00	15.10
<i>o</i> -Chlorophenol	14.88	
<i>m</i> -Chlorophenol	14.80	14.89
<i>p</i> -Chlorophenol	14.84	14.94
<i>o</i> -Bromophenol	14.85	
<i>m</i> -Bromophenol	14.74	
<i>p</i> -Bromophenol	14.80	

^a Calculated values from CCSD(T)/6-311++G(3df,2p)+ZPE based on B3LYP/6-311++G(d,p) geometries and frequencies.

^b Based on the DPE(phenol) = 15.2 eV and relative acidities given in Reference 351.

DPE and a greater acidity. This pattern is confirmed by the energies of fluorophenolate anions shown in Figure 24 pointing towards a greater stability of the *meta*-derivatives.

The characteristics emphasized above for the halogens and the cyano group are actually relevant to other substituents as well. Indeed, it has been shown³⁷⁷ that the effects of substituents on acidities are largely dominated by those occurring in the phenolate anion and only marginally by those in neutral phenol. Substituents which interact favourably in the *meta* position of phenol act unfavourably in the *para* position (the halogens), and vice versa (the cyano group). Both π and σ charge transfers are important in determining interaction energies. The σ acceptance by a substituent stabilizes OH and O⁻ more effectively at the *para* position than at the *meta* position, due to a π -inductive mechanism. Stabilization by π acceptors and destabilization by π donors are the results of direct π delocalization, which is inherent of the *para* substituents (see also Reference 380). On the one hand, groups exhibiting a competition of both π -donating and σ -accepting effects, such as NH₂, OH and F, cause an increase in acidity at the *meta* position and a decrease at the *para* one (except for F). On the other hand, accepting groups such as CN, CHO, NO₂ and CF₃ provide an enhanced acidity following either *meta* or *para* substitution, with a preference for the *para* position³⁷⁷. There is also little evidence for direct steric strain in the series of *ortho*-phenols³⁷⁹.

Overall, the acidities of the substituted phenols are largely determined by the stabilization of the corresponding phenolate ions, i.e. the energies of the phenolate HOMOs. There is a similarity between the substituent effect on the latter and the LUMOs of substituted benzenes; both can be understood by simple perturbative PMO treatment³⁸¹.

From a more quantitative point of view, it is more difficult to achieve accurate computations for DPEs than for PAs of neutral substrates, because molecular anions are involved in the former case. However, when using second-order perturbation theory (MP2), a coupled-cluster theory (CCSD(T)) or a density functional theory (DFT/B3LYP), in conjunction with a moderate atomic basis set including a set of diffuse and polarization functions, such as the 6-311++G(d,p) or cc-aug-pVDZ sets, the resulting DPE errors appear to be fairly systematic. To some extent, the accuracy rests on a partial but uniform cancellation of errors between the acid and its conjugate base. Therefore, use of appropriate linear regressions between experimental and calculated values allows the DPEs for new members of the series to be evaluated within the ‘chemical accuracy’ of ± 0.1 eV or ± 10 kJ mol⁻¹.

3. Acidity in solution

The situation is more complex for the acidities in condensed phases. The relevant quantities are rather estimated using a thermodynamic cycle³⁸² involving the experimental gas-phase PAs and solvation free energies for the neutral species along with the observed aqueous pK_a values. Using this approach, the experimental hydration free energy of the phenoxide ion³⁸² was estimated to be -301 kJ mol^{-1} , which is far larger than the corresponding value of -28 kJ mol^{-1} found for phenol^{383, 384}.

On the other hand, while the basic features of neutral solvation energies could, in general, be fairly well reproduced by continuum solvent models, similar treatments of the anions are less successful. Theoretical approaches to the solvation usually involve a combination of quantum and classical mechanical methods. The molecular responses in the presence of solvent are often handled classically. The most important ingredients in determining solvation energies are the charge distribution and dipole moment of the solute. Evaluation of the electron distribution and dipole moments of charged species is quite troublesome, as they are also quite sensitive to the polarity of the environment. As a consequence, the errors committed on predicted solvation energies for most of the anions are significantly larger than for the neutrals, and this makes quantitative prediction for pK_a values a more difficult task³⁷¹. Similar to the treatment of electron correlation in polyatomic systems, modelling of the impact of the surrounding medium on different entities could hardly be carried out in a balanced way. A small error in the electrostatic terms for long-range interactions easily leads to a large variation in the relative scale. In addition, the difficulties associated with modelling also arise from the account for non-electrostatic interactions, that include among others the cavitation, dispersion and repulsion terms. In practice, a good fit between experimental and theoretical estimates for a category of acids could be established and the predicted values might be useful in establishing, in particular, the acidity order³⁸⁵.

These general remarks could be applied to the phenol acidities in the aqueous phase that were studied using different combined theoretical methods for evaluating free energies of solvation^{115, 374, 378, 385}. In fact, the relative acidities were reproduced with variable success. For example, while excellent agreement was obtained for the *ortho*-fluorophenol, a larger error of 12 kJ mol^{-1} was seen for the *para* isomer³⁷⁸. Similarly, experimental acidity trends of both ground and excited singlet states were found for phenol and cyanophenols, but the calculated differences between the ground and excited state pK_a values were only in qualitative agreement with experimental results, with errors up to 4 pK_a units¹¹⁵.

Nevertheless, the analysis of the charge distribution and hydration behaviour revealed some interesting features. The effect of fluorine substitution on the charge density was found to be not greatly perturbed by the presence of an aqueous solution. The changes in the charge distribution upon substitution are found to be similar in both gaseous and aqueous phases. Thus the observed attenuation of the F-effect on phenol acidities in solution is likely to arise from a hydrophobic shift introduced by the substituent, which finally balances the effects on the hydration free energies of phenol and its conjugate anion.

The enhanced phenol acidity in excited states will be discussed in a subsequent section.

4. Correlation between intrinsic acidities and molecular properties

Understanding substituent effects on molecular properties in a quantitative way has long been a goal of physical organic chemistry and dates back to the 1930s with the introduction of the Hammett σ constants³⁸⁶. For phenol derivatives, a variety of correlations have in fact been established between their physical properties in different forms^{349–351, 387–391}. The general-purpose Hammett constants yield a reasonable representation of the acidities. A decreasing value of DPE corresponds to an increasing acidity, and hence an increasing

value of σ_p^- . We consider here in particular the correlations involving the intrinsic phenol acidities with quantum chemical reactivity descriptors.

The most obvious property related to acidity is the atomic charge on the acidic hydrogen of the neutrals^{389–391} and on the deprotonated oxygen of the anions^{390, 391}. Use of the atomic charges derived from either the simple Mulliken population analyses, $Q_M(H)$ and $Q_M(O^-)$, or the more advanced natural orbital population analyses, $Q_N(H)$ and $Q_N(O^-)$, leads to linear regression equations with acidities³⁹¹, expressed in terms of pK_a , of the type shown in equations 29a and 29b,

$$pK_a = -aQ(H) + b \quad (29a)$$

$$pK_a = -cQ(O^-) + d \quad (29b)$$

where Q is either Q_M or Q_N . A more positively charged hydrogen corresponds to a more acidic hydrogen and is arguably associated with lower pK_a values. In the same manner, delocalization of the negative charge of the phenolate oxygen tends to impart stability to the anion, favouring its formation and increasing the acidity. It is crucial to have a consistent atomic charge definition in order to describe the acid–base properties of the hydroxy group. Correlations between relative acidities and changes in the dipole moments were also attempted³⁸⁷, but the regression was not very good.

For a given family of compounds, there exists a certain relationship between the proton affinity and the core ionization energy of the atom which is protonated^{392–395}. The latter could be approximated by the 1s-orbital energy, $\varepsilon(1s)$, of the relevant atom of the conjugate anion, which is relatively stable with respect to the small variations in the basis sets. Calculations³⁸⁹ demonstrated that for phenol derivatives, a linear relationship (equation 30) equally exists:

$$PA(X-C_6H_4O^-) = -A \cdot \varepsilon(O_{1s}) + B \quad (30)$$

in which $\varepsilon(O_{1s})$ are the oxygen core orbital energies.

The acidity is expressed above in terms of the PA of the anion. The basicity of the anion somehow describes the ease with which core electrons are removed. In fact, both quantities depend on two terms, namely the electrostatic potential at the site to which the proton is to be attached, and the ease with which the positive charge can be delocalized over the entire substrate by rearrangement of valence electrons.

The first term is known as the inductive effect and is determined by the charge distribution of the initial base. The electrostatic potential minima around the basic centres, V_{min} , needs to be considered. In view of the reasonable behaviour of atomic charges for a series of simple XC_6H_4OH , a good correlation was found between $V_{min}(\text{oxygen})$ and σ_p^- , and thereby the acidities. This was verified with $X = H, F, CH_3, NH_2, CN, CF_3, NO$ and NO_2 ³⁸¹. Because the experimental σ_p^- were determined in aqueous solutions or in water/alcohol mixtures, their good correlation points out again that the substituent effects in phenolate ions in the gas phase and solution are linearly related. Good interpolations could therefore be made without using solvent models to evaluate unknown or uncertain σ_p^- values.

The second term, known as the relaxation or polarization, depends on the polarizability of the surrounding entity. An inductive effect which favours removal of an electron is expected to hinder the removal of a proton. It is thus logical that there is a negative correlation between the PA of the anion and the core-ionization energy. The higher the core-ionization energy, the lower the PA and the stronger the acid. This view points out the importance of considering both electrostatic and relaxation terms when evaluating the PAs.

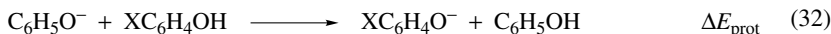
In the same vein, the acidity could equally be related to the first ionization energy (IE), which can be estimated from the HOMO energy given by Hartree–Fock wavefunctions. Good linear relationships (equation 31) have been obtained between acidities and frontier orbital energies,

$$\text{p}K_{\text{a}} = C \cdot \varepsilon(\text{HOMO}) + D \quad (31)$$

No strong correlations could be found for either the $\varepsilon(\text{LUMO})$ or the absolute hardness (η), or the absolute electronegativity (χ) defined in the previous section. The poor result for the LUMO energies is probably due to their incorrect evaluation using the Hartree–Fock wavefunctions. Calculations³⁹⁰ revealed that when the acidity of a *para*-substituted phenol decreases, its electronegativity (χ) decreases and its global hardness (η) increases. Conversely, an increasing basicity of the phenolate anion induces an increasing global hardness. This is in line with the original proposal³⁹⁶ that basicity bears a direct relationship to the hardness of a base. Nevertheless, because the hardness is a global property, it cannot fully account for the changes in basicity/acidity, which is rather a site-specific problem. In fact, the changes in the hardness do not follow a regular pattern and the regression coefficients are lower than those involving other parameters³⁹¹.

The local descriptors for the oxygen centre, including the Fukui function (f_{O}^{-}) and local softness (s_{O}^{-}) whose definitions are given in the preceding section (equation 27), are expected to perform better for this purpose. Both indices tend to increase upon increasing basicity of the anion. Linear relationships were obtained for both indices with $\text{p}K_{\text{a}}$ with higher correlation coefficients³⁹¹. This supports the view that the basicity of phenolate ions depends on how the oxygen negative charge could be delocalized into the ring. If the charge cannot be delocalized, the base is getting destabilized and becomes more basic, and vice versa. As a consequence of an increasing oxygen charge, its nucleophilic Fukui function (f_{O}^{-} , always positive) and condensed softness (s_{O}^{-}) also increase, implying that the oxygen centre becomes more polarizable and softer, in the sense of the original softness definition³⁹⁶.

A more direct measure of changes in acidity could be determined using the relative proton transfer between substituted phenolate ions and phenol^{377, 391} (equation 32)



A positive value of ΔE_{prot} indicates that the substituted phenol is less acidic than phenol itself, and vice versa. As a correlation descriptor, ΔE_{prot} performs quite well, giving again a linear relationship with $\text{p}K_{\text{a}}$.

5. Alkali metal phenolates

The structures, energies and reactivities of polar organometallic species are often determined by the metal counterions. Solvation and aggregation also influence their stability and mechanism in condensed phases. The largely dominating electrostatic interactions of both ions outweigh the other modes of stabilization of the anions such as π -delocalization, hyperconjugation, polarization and inductive effects, and basically modify the behaviour of the ion pair relative to the free anion. Phenolate ions with different alkali metal gegenions also show varying reactivity, which has been attributed to the structural changes in the presence of the metal. A case in point is the Kolbe–Schmitt reaction³⁹⁷ in which sodium phenolate is carboxylated by CO_2 mostly in the *ortho*-position whereas potassium phenolate yields predominantly a *para*-carboxylation product. Charge localization due to the metal ion tends to reduce the stabilization energies of phenolate ion. The metallation reactions (equation 33)



are much less exothermic than those involving OH^-/PhO^- , amounting to -34 , -51 , -54 , -59 and -52 kJ mol^{-1} for $\text{M} = \text{Li}$, Na , K , Rb and Cs , respectively (values obtained at B3LYP/6-311++G(d,p)+ZPE)³⁵² as compared with that of -173 kJ mol^{-1} for free PhO^- . This emphasizes that the presence of the metal cation in a contact pair counteracts the stabilization of the free anion³⁹⁸. Similar behaviour was observed for the analogous enolate anions³⁵². The metal ions in the ion pair retain a near unit positive charge ($+0.97$ to $+0.99$) pointing towards the pure ionic $\text{M}-\text{O}$ bonds. Such electrostatic charge localization is no doubt responsible for a higher oxygen charge in the ion-paired species³⁹⁹.

The geometrical parameters of the $\text{PhO}-\text{M}$ species are displayed in Figure 26. The $\text{C}-\text{O}-\text{M}$ moiety is actually linear. The $\text{C}-\text{C}$ distance is shortest in phenol, longest in free phenolate anion and intermediate in metallated compounds. The bond angle around the *ipso*-carbon, $\text{C}_6\text{C}_1\text{C}_2$, is smallest in free phenolate ion [114° , charge $q(\text{C}_1) = 0.50$] and largest in phenol [120° , $q(\text{C}_1) = 0.38$]. The corresponding angles in $\text{PhO}-\text{M}$ lie in between, ranging from 118° for $\text{M} = \text{Li}$ [$q(\text{C}_1) = 0.43$] to 116° for Rb [$q(\text{C}_1) = 0.46$]. Both the angle and charge at the *ipso*- C_1 atom are somehow related to each other. Even at large $\text{M}-\text{O}$ distances, the charge localizing effect remains effective because the electrostatic interaction energies decrease with the inverse of the distance, $d(\text{M}-\text{O})^{-1}$. Even at a distance $d = 4$ Å, the negative charge on oxygen is already increasing (-0.97), suggesting that the counterion effect is significant in solvent-separated ion pairs.

The magnetic properties of C_1 and C_4 ring atoms are most affected by ion pairing. The calculated $\delta(^{13}\text{C})$ chemical shifts in ppm [obtained from GIAO-HF/6-311+G(d,p) calculations] in $\text{PhO}-\text{M}$ vary as follows:

$$\delta(\text{C}_1): \text{M} = \text{Li}: 167 \text{ (expt: 168)}, \text{Na}: 171, \text{K}: 180, \text{Rb}: 180,$$

$$\text{Cs}: 179 \text{ and free anion: } 182.$$

$$\delta(\text{C}_4): \text{M} = \text{Li}: 111 \text{ (expt: 115)}, \text{Na}: 108, \text{K}: 106, \text{Rb}: 106,$$

$$\text{Cs}: 107 \text{ and free anion: } 91.$$

Deshielding of the atom C_4 in the ion-paired structures is thus obvious. The chemical shifts of other carbon atoms remain almost unchanged upon deprotonation or ion pairing.

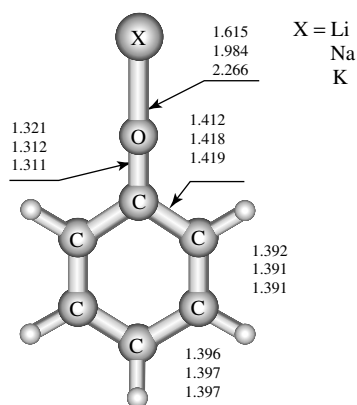


FIGURE 26. Selected B3LYP/6-311++G(d,p) optimized bond lengths (Å) of some alkali metal phenolates in their ground singlet state

The NICS(0) values of the alkali phenolates increase down the group from -9.9 in Li, -9.2 in Na, -8.8 in K, -8.0 in Rb, -7.5 in Cs and -6.3 for free phenolate anion. Thus the charge localization is still effective for cesium phenolate, which has a more aromatic character than the free anion. The other criteria yield a similar pattern³⁵². The loss of aromaticity in the free phenolate anion, 60% of the neutral phenol, due to a $p-\pi$ delocalization discussed above, could largely be restored by ion pair formation with alkali metal cations, thanks to a charge localization effect of the latter.

We now turn back to the CO stretching frequency (ν_6), where there is a discrepancy between observed and computed values (Section IV.B.1). Calculations³⁵³ indicated that the C–O bond length is only slightly elongated by 0.012 Å upon complexation of PhO^- with a water molecule. Such anion–molecule interactions induce only a weak downshift of at most 13 cm^{-1} for modes containing significant CO character. In contrast, as seen in Figure 26, the C–O distances are lengthened to a larger extent (up to 0.047 Å) following interaction with Li^+ , Na^+ and K^+ , and now have a more significant single-bond character (1.31 – 1.32 Å). The scaled frequencies of the mode ν_6 are calculated at 1310 , 1306 and 1290 cm^{-1} in PhOLi , PhONa and PhOK , respectively [B3LYP/6-311++G(d,p) values]. Complexation with the heavier ion induces a larger downshift of the C–O stretching ν_6 mode, up to 53 cm^{-1} with the K^+ counterion. The latter values thus become closer to the experimental value^{365,366} of 1273 cm^{-1} than that derived from free PhO^- . More important perhaps is the fact that the ν_6 frequency is now associated with the most intense IR absorption in this region, in agreement with the FTIR data³⁶⁶. However, the theoretical overestimation of the C–O stretching mode frequencies remains significant, and some of the ^{13}C and d_5 isotope shifts are still large³⁵³. This suggests that an oligomer of the complex may actually be formed in solution and is responsible for the larger frequency downshift. Dimers and tetramers of lithium enolates⁴⁰⁰ and lithium phenolates⁴⁰¹ have in fact been found experimentally.

Finally, it is noteworthy that, along with phenol, phenolate anion has been used as the simplest model to mimic the active site of the tyrosine protein residues. Its interaction with thiol (CH_3SH), a model of the cysteine side chain of glutathione, was studied using *ab initio* calculations⁴⁰² in order to examine the role of active site tyrosine in glutathione S-transferases. The location of the key proton of the enzyme–glutathione binary complex, O–H–S, was predicted to be near the phenolic oxygen, and this proton position could be manipulated by changing the acidity of the tyrosine. This could be accomplished either by introducing a substituent, such as a fluorine atom, on the phenol moiety, or by changing the protein environment. The hydrogen bond between phenolate anion and thiol is very strong (up to 80 kJ mol^{-1}) and the phenol OH group in the residue of the enzyme complexed by a water molecule in a mutant is related to the notion of substrate-assisted catalysis⁴⁰³. In conclusion, the use of PhOM species in order to initiate polymerization and/or to catalyse the chain growth in polycarbonates has been studied³⁵⁴.

C. Electronic Excitation

Although the valence $\pi-\pi^*$ excitation spectra of benzene derivatives have been extensively studied over the past 65 years both experimentally and theoretically, much less is known about that of phenol, apart from its lowest excited state. In general, absorption and fluorescence spectroscopy of a benzene ring can be used to detect its presence in a larger compound and to probe its environment. While the relative constancy of the valence $\pi-\pi^*$ excitation spectrum allows a qualitative identification of spectral bands by a correspondence with those in free benzene, detailed quantitative differences could indicate the nature of substituents, ligands or medium. Key information on substituted benzene includes the excitation energies, transition moments and their direction, and electrostatic

properties of the excited states. Although experimental transition dipole directions could be determined by aligning the molecule in a crystal or stretched film, their interpretation is not straightforward and needs the help of accurate calculations.

Thus, knowledge of the transition moment direction of a phenol band could help in interpreting the fluorescence spectrum of a tyrosine chromophore in a protein in terms of orientation and dynamics. The absorption spectrum of the first excited state of phenol was observed around 275 nm with a fluorescence peak around 298 nm in water. The tyrosine absorption was reported at 277 nm and the fluorescence near 303 nm. Fluorescent efficiency is about 0.21 for both molecules. The fluorescent shift of phenol between protic and aprotic solvents is small, compared to indole, a model for tryptophan-based protein, due to the larger gap between its first and second excited states, which results in negligible coupling⁴⁰⁴.

A mono-substituted benzene has traditionally a number of singlet excited valence states, or pairs of states, of $\pi^* \leftarrow \pi$ type. The valence $\sigma^* \leftarrow \pi$ or $\pi^* \leftarrow \sigma$ excitations require much larger energies. Below the first ionization level, a number of Rydberg $\pi^* \leftarrow \pi$ and $\sigma^* \leftarrow \pi$ states could also be expected. Each open-shell singlet state also has a triplet companion situated at slightly lower energy. The corresponding vacuum UV singlet spectrum can be subdivided into three bands, the first denoted as 1L_b centered at about 2600 Å, the second 1L_a at *ca* 2050 Å and the third 1B band at *ca* 1850 Å⁴⁰⁵. Note that the notations 1L_b and 1L_a mean that their dipole transition moment are approximately perpendicular and parallel, respectively, to the main axis.

The lower-lying singlet states of phenol exhibit a $^1A'$ symmetry. As mentioned above, the lowest 1L_b band of phenol was well established experimentally to have an origin at 4.507 eV (275 nm or 36349 cm⁻¹ with an oscillator strength $f = 0.02$)¹¹⁸. This first singlet excited state S_1 closely corresponds to the covalent $^1B_{2u}$ state of benzene and has a transition dipole in the x direction. The vertical 1L_a absorption due to the second excited state S_2 was found at 5.82 eV⁴⁰⁶, whereas the corresponding adiabatic value was estimated at 5.77 eV (with $f = 0.13$)¹¹⁹ and is correlated to the more ionic $^1B_{1u}$ state of benzene. The identity of the third excited state of phenol inducing the appearance of its 1B band was more problematic^{119, 406}, but it now appears that the observed band, centred at *ca* 6.66 eV, arises from the lower component of a splitting of the degenerate benzene $^1E_{1u}$ state and is associated with a fairly large transition moment ($f = 1.1$)¹¹⁹. A small and static splitting of this band is usually found in most mono-substituted benzenes with approximately equal intensities. As for the benzene $^1E_{2g}$ band, CASSCF/CASPT2 calculations^{119, 407, 408} revealed a significantly larger splitting giving two components centred now at 7.14 and 7.72 eV. Although the E_{2g} states are formally characterized as covalent, they are in reality strongly mixed with a multitude of higher states.

The Rydberg states have not yet been detected experimentally, but CASPT2 calculations^{119, 408} indicated the existence of at least six $\pi^* \leftarrow \pi$ Rydberg states that range from 6.3 to 7.6 eV and arise from the promotion of 3π and 4π electrons to $3p$ and $3d$ orbitals. There are also no less than twelve $\sigma^* \leftarrow \pi$ Rydberg states ranging from 5.8 to 7.8 eV.

The measured rotational constants of the first excited S_1 state¹²⁷ suggested rather moderate changes of the geometrical parameters upon electronic excitation. The $S_1 \leftarrow S_0$ excitation tends to enlarge the carbon ring and reduce the C–H and C–O bond lengths. The O–H bond length and the C–O–H bond angle are almost invariant upon excitation. The constants vary as follows: S_0/S_1 (in MHz): A; 5650/5314; B; 2619/2620; and C; 1782/1756. Multi-reference CASSCF computations reproduced these quantities reasonably well and suggest a planar structure^{114, 115, 126, 139, 356, 372, 407, 408}. In particular, the CASSCF(8,7)⁴⁰⁷ study provided the rotational constants of $A = 5338$, $B = 2572$ and $C = 1736$ MHz for phenol S_1 . The changes in rotational constants could be understood as arising from a deformation of the molecule in the S_1 state along the in-plane mode

6a or mode 8a. CASSCF geometry optimizations^{126, 372, 407, 408} showed a rather modest shortening of 0.006 Å of the CO distance and a somewhat more important lengthening of 0.03 Å of all CC bonds. Nevertheless, a comparison between the dispersed fluorescence spectrum of phenol and its Franck–Condon simulation¹¹⁴ indicated that the CC bond length actually increases on average by 0.027 Å, whereas the CO bond distance decreases by 0.023 Å upon excitation. The most significant geometrical relaxation could also be deduced from the experimentally observed intensity pattern.

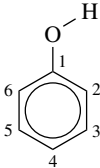
For the second excited S_2 state of phenol, a quite different geometry was found with larger variations of up to 0.11 Å for the CC bond lengths and the COH bond angle (opening by 10°), and a non-negligible shortening of 0.02 Å of the CO bond (relative to phenol S_0). This suggests a considerable charge delocalization from the oxygen into the ring.

The S_1 vibrational frequencies were also observed^{153, 156, 169, 409} and analysed in detail by means of quantum chemical computations^{114, 115, 126, 139, 356, 372, 407, 408}. Frequency shifts up to 100 cm⁻¹ were detected for in-plane modes. While the $\sigma(\text{OH})$ mode decreases from 3656 to 3581 cm⁻¹, the CH-stretching modes 20a and 20b increase from 3087 and 3070 to 3186 and 3136 cm⁻¹, respectively, following excitation. Out-of-plane modes show much more scrambling in going from S_0 to S_1 , and several original modes⁴⁰⁹ needed to be re-assigned¹¹⁴. In particular, the Kekule mode 14 should have a larger wave number in the S_1 state (1572 cm⁻¹) than in the S_0 state (1343 cm⁻¹). This mode has CH-bending and CC-stretching character in the ground state but becomes a CC-stretching plus a small component of the OH-bending mode in the excited state. The relaxation of the OH-stretching vibrations in the S_1 – S_0 transition could also be followed in examining the IR-UV double resonance spectra recorded after pumping to the OH stretching level⁴¹⁰. These techniques provided us with valuable information on the intramolecular vibrational redistribution (IVR) of the corresponding vibrations.

The phenol dipole moment remains almost unchanged upon excitation to S_1 but shows a marked variation in S_2 , in line with a more ionic character of the latter. The ratio of oscillator strengths for both S_2 and S_1 transitions amounts to 6.6 and, as evidenced by the $\langle z^2 \rangle$ values, both valence excited states have no relevant mixing with Rydberg states. Cyanophenols show a similar behaviour where the S_1 charge distribution is close to the ground state and the S_2 counterpart appears to have an appreciable charge transfer from the oxygen¹¹⁵.

Solvent effects were found to have minimal influence on the excitation energies of phenol in aqueous solution using a quantum Monte Carlo simulation³⁷², which is in line with experimental observations on its absorption spectra⁴¹¹. Reaction field calculations of the excitation energy also showed a small shift in a solution continuum, in qualitative agreement with fluorescent studies of clusters of phenol with increasing number of water molecules^{412a}. The largest fluorescent shift of 2100 cm⁻¹ was observed in cyclohexane.

In substituted phenols, the excited S_1 states are again dominated by the LUMO \leftarrow HOMO and LUMO + 1 \leftarrow HOMO – 1 transitions and the corresponding excitation energies apparently differ from that of phenol by, at most, 0.6 eV. Results obtained using time-dependent density functional theory computations in conjunction with a systematic empirical correction are recorded in Table 32. CASSCF(8,7) calculations on both S_0 and S_1 of monochlorophenols^{412b} also point to a similar trend. The frontier orbital energies are only weakly but uniformly stabilized by the halogens or the cyano group, or else they are destabilized by electron-donor groups such as methyl. While the fluorine atoms do not exert any significant effect, multiple substitutions by chlorine and bromine induce a significant decrease in the transition energies^{412b}. The chlorine atom makes the C–O bond shorter and the methyl group makes a marginal modification; the cyano shows a detectable effect when introduced at the 2-*ortho* position.

TABLE 32. Lowest excitation energies of substituted phenols^a


	$S_1 \leftarrow S_0$ Transition energy (eV)
Phenol	4.5 (4.5)
2-F	4.5
3-F	4.5
4-F	4.3
2,3-di-F	4.6
2,4-di-F	4.3
2,5-di-F	4.5
2,6-di-F	4.5
4,5-di-F	4.3
2,4,5-tri-F	4.3
2,4,6-tri-F	4.4
2,3,4,6-tetra-F	4.4
2,3,4,5,6-penta-F	4.5
2-Cl	4.4
3-Cl	4.4
4-Cl	4.2
2,3-di-Cl	4.3
3,4-di-Cl	4.1
4,6-di-Cl	4.1
3,4,5-tri-Cl	4.0
2,4,6-tri-Cl	4.0
2,3,4,6-tetra-Cl	3.9
2,3,4,5,6-penta-Cl	3.8
2-Br	4.3
3-Br	4.4
4-Br	4.2
2,3-di-Br	4.2
2,4-di-Br	4.0
2,5-di-Br	4.2
2,6-di-Br	4.2
2,4,6-tri-Br	3.9
2-CH ₃	4.5
3-CH ₃	4.5
4-CH ₃	4.4
2-CN	4.2 (4.2)
3-CN	4.3
4-CN	(4.5)

^aEstimated values using TD-DFT/B3LYP/6-311++G(d,p) calculations and a systematic correction based on a comparison of the calculated and experimental values for phenol. Experimental values are in parentheses.

The acidities of phenols were found to be greatly increased upon electronic excitation. Due to a change of about 40 kJ mol⁻¹ in the free energy of deprotonation, phenol is intrinsically 7 pK_a units more acidic in the S_1 than in the S_0 state in the gas phase. Similarly, intermolecular proton transfer in solution from an S_1 excited phenol to, e.g., a solvent base is typically characterized by a pK_a value of some 6–7 units less than that of the corresponding ground state. In aqueous solution, the pK_a of phenol amounts to 10.0 in the ground state and 3.6 in the S_1 state.

It is natural to ask whether the enhanced acidity in the excited state arises from an electronic effect of the neutral acid or from the product anion. As seen in Section IV.B above, it has been shown in various ways^{377, 413} that the changes in ground-state acidity resulting from several substitutions are due to the corresponding phenolate anions. The same argument could equally be applied to the difference between ground- and excited-state acidities. The pK_a modification could be understood by the fact that the gas-phase proton affinity of the phenolate anion, a measure of the phenol acidity, amounts to 15.2 eV in the ground state but decreases to 14.3 eV in the S_1 state⁴¹⁴. This anion also has a large blue shift of the vertical excitation energy (1800 cm^{-1}) in solution. Monte Carlo simulations³⁷² demonstrated that the excited states of phenol and phenolate anion are better solvated than the ground states by *ca* -2 and -11 kJ mol^{-1} in water, respectively. The experimental value $pK_a = 3.6$ of phenol in the S_1 state in solution is likely to arise from a cancellation of the intrinsic energy difference (*ca* 50 kJ mol^{-1}) of the excitation energy of phenol and phenolate anion, and by the differential solvent spectral shift (*ca* 25 kJ mol^{-1}). The energetic outcome leads to a change of -5 in the pK_a value, which is roughly in accord with the experimental estimate³⁷³.

It has been observed that the magnitude of the electrostatic potential (V_{\min}) around the oxygen atom undergoes a much larger reduction for the anions than for the neutrals in going from S_0 to S_1 ¹¹⁵. In other words, from a purely electrostatic point of view, the increase in S_1 phenol acidity can better be understood by the fluctuations of the phenolate anions.

Relatively little is known about the phosphorescent phenol⁴¹⁵. The experimental T_1-S_0 transition energy was found at 28500 cm^{-1} , confirming that the triplet state is, in general, lower in energy than its singlet counterpart³⁵⁶. The selected optimized geometrical parameters of the lowest triplet T_1 state of phenol is displayed in Figure 27. The molecule is no longer planar but shows a small ring deformation with stretched and compressed CC distances, and a marginal out-of-plane OH torsion.

The quenching mechanism of the first excited states of phenol and phenolate anion differ significantly from each other. The fluorescent neutral S_1 state lies substantially higher in energy than T_1 and could be inhibited from quenching by the energy gap (*ca* 8000 cm^{-1}) as well as the small one-electron spin-orbit coupling. At the anion- S_1 geometry, both

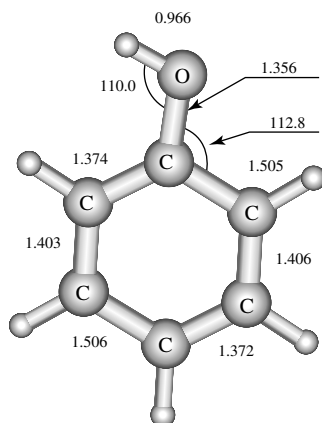


FIGURE 27. Selected UB3LYP/6-311++G(d,p) optimized parameters of the lowest triplet state of phenol. Bond lengths are in Å, bond angles in deg

singlet and triplet states of the anion are shown to be dominated by the same electronic configuration, thus allowing for a direct spin-orbit coupling³⁵⁶. As a consequence, the lifetime for fluorescence is short in the anion.

At the neutral- S_0 geometry, the spin-orbit coupling is expected to increase, but there was no evidence of a change in the fluorescence efficiency as a function of the excitation energy in the first singlet excited band⁴¹⁶. Quenching in the singlet S_1 state to the T_1 triplet was reported⁴¹⁷. The weak spin-orbit coupling is likely to account for an observation of the neutral triplet. In this case the corresponding anion triplet is not observed, due to the fact that its energy is larger than the electron affinity of the phenoxy radical and it is readily autodetached.

Finally, the phenol super-excited states, which are electronic states of neutral species with energy above the first ionization energy, were also identified at about 9 eV above the ground state^{418, 419}. Some of these super-excited states could be mapped spectroscopically out on a picosecond and femtosecond time scale.

D. Ionization

Owing to their relatively low ionization energies (IE) of *ca* 8.0–8.5 eV, phenols are also good electron donor solutes. Recent experimental studies of phenols in non-protic solvents^{420–423} showed that ionized solvent molecules react with phenol to yield not only phenol radical cations by electron transfer, but also phenoxy radicals by hydrogen transfer. An obvious question is whether, under these conditions, the latter radicals were formed from ionized phenols rather than by direct hydrogen abstraction, because proton transfer reactions could be facilitated upon ionization. This also raises a question about the influence of solvent properties, both by specific and non-specific interactions, on the mechanism and kinetics of deprotonation processes^{424, 425}.

Gas-phase properties of a molecule have, by definition, an intrinsic character and they could be modified by the environment. Although the formation and reactions of gaseous ionized phenol **21** (cf. Chart 5) and its cyclohexa-2,4-dienone isomer **22** have been studied in numerous ionization and mass spectrometric studies^{182, 426–438}, thermochemical parameters of these isomers^{439–447} as well as information on other non-conventional isomers, such as the distonic ion **23**, were rather scarce. Conventional cations of analogous aromatic systems ($X-C_6H_5$)⁺ and their distonic isomers generated by simple 1,2-hydrogen shifts within the ring were demonstrated to be observable gas-phase species^{448–451}. In addition, the mechanism of the CO-loss upon phenol ionization has only recently been unraveled⁴⁵².

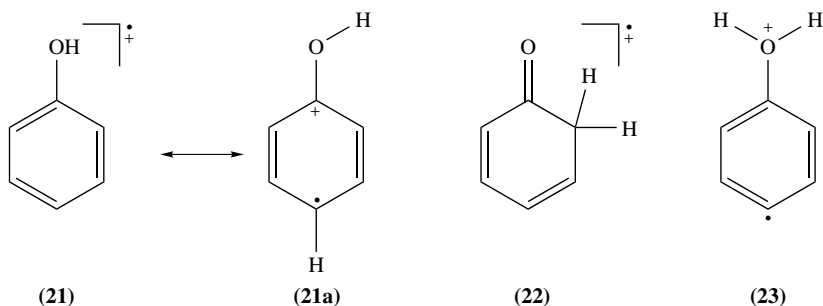


CHART 5. Two isomers of phenol radical cation

1. Molecular and electronic structure of phenol radical cation

The molecular structure, vibrational frequencies and spin densities of ionized phenol **21** in its ground and lower-lying excited electronic states have been investigated intensively using different MO and DFT methods^{138, 168, 182, 425, 426, 453}. For the purpose of comparison, Figure 28 shows again a selection of (U)B3LYP/6-311++G(d,p) geometrical parameters of both neutral and ionized structures (c.f. Table 5). The lowest-energy electronic state of **21** exhibits a planar geometry and a $^2A''$ symmetry arising from removal of an electron from the π -system; therefore, its ground state can be qualified as a $^2\Pi$ -state. Following such an ionization, the quasi-equal C–C bond (1.40 Å) framework in the neutral phenyl ring becomes longer (1.43 Å) and shorter (1.37 Å) bonds. The latter distance becomes now closer to that of a typical C=C double bond (1.35 Å). Although the absolute changes in the bond lengths vary with the methods employed, they consistently point out that the C–O bond is shortened in going from 1.37 Å in the neutral to 1.31 Å in the ionized phenol, but it remains longer than that of a typical C=O double bond (1.22 Å)¹³⁸. Such distance changes can be understood from the shape of the HOMO of neutral phenol as displayed in Figure 5. Accordingly, the C–O bond is characterized by antibonding orbital 2p-lobes; therefore, electron removal is expected to shorten the C–O distance. The same argument could be applied to the changes in the ring C–C distances. In fact, electron removal from the bonding C₆–C₁–C₂ and C₃–C₄–C₅ components leads to bond stretching, whereas a decrease in the antibonding C₂–C₃ and C₄–C₅ components results in bond compression. Because the unpaired electron occupies a π -orbital and exerts a marginal effect on the σ framework, the C–H and OH distances are not significantly affected and the COH bond angle opens by only 4° upon ionization (cf. Figure 28). Although the changes in geometry are a clear-cut manifestation of the oxidation, it is not possible to correlate these alterations completely with all the accompanying intramolecular reorganization energies⁴⁵⁴. This reorganization is global rather than a local phenomenon.

To some extent, the geometry confers on the phenol ion a quinone-like distonic character as seen in **21a** (Chart 5) in which the charge and radical centres are located at two different sites. This picture is supported by the charge distribution according to the Mulliken population analysis suggesting that the *para*-C₄ carbon of the ring bears the largest

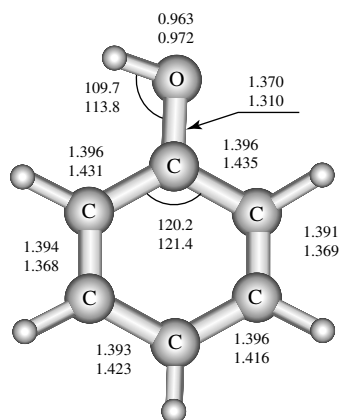


FIGURE 28. Selected (U)B3LYP/6-311++G(d,p) bond distances (Å) and angles (deg) of the neutral ($^1A'$, upper values) and ionized ($^2A''$, lower values) phenol. See also Table 5

part of the excess electron spin (*ca* 0.5 *e*). The positive charge is, as expected, delocalized over the entire ring skeleton but with a substantial part on the oxygen region^{138, 168}.

Bear in mind that the HOMO-1 is equally a phenyl orbital with the 2p(π)-lobes centred on the *ortho* and *meta* carbon atoms (Figure 5). As a consequence, ejection of an electron from this orbital is expected to yield a $^2\Pi$ excited state of phenol ion in which the C₂–C₃ and C₅–C₆ distances likely become longer than the corresponding values in neutral phenol whereas the C–O distance likely remains unchanged. Removal of an electron from the HOMO-2 again leads to a $^2\Pi$ excited state. The HOMO-3 of phenol is the first in-plane orbital (*a'*) thus leading to a $^2A'$ excited state of phenol ion.

The recorded He(I) and He(II) photoelectron spectra of phenol^{443–447} contain several peaks ranging from 8.56 to 22.67 eV. It appears that the reported value of 8.56 eV⁴⁴³ is actually the first phenol vertical IE whereas that of 8.47 eV⁴⁴⁴ corresponds to its first adiabatic IE_a. Geometry relaxation of the vertical ion results in a small stabilization. For comparison, note that the IE_a(phenol) is computed to be 8.37 and 8.42 eV using B3LYP and CCSD(T), respectively, in conjunction with the aug-cc-pVTZ basis set. This leads to a standard heat of formation of $\Delta H_f^\circ(\mathbf{21}) = 724 \pm 6 \text{ kJ mol}^{-1}$ ⁴⁴¹.

The vertical lowest-lying excited state A^2A'' of phenol radical cation **21** lies only 0.72 eV above the ground X^2A'' state whereas the vertical B^2A'' state is identified at 2.96 eV from the photoelectron spectrum⁴⁴³. MCSCF/FOCI computations⁴⁵⁵ yielded a value of 3.32 eV (373 nm) for this vertical transition. A recent photoinduced Rydberg ionization spectroscopic study⁴²⁶ revealed a gap of 2.62 eV (21129 cm^{–1}), which is assigned to the *B*-state of **21**. Geometry relaxation apparently induces a larger stabilization in this *B*-state. Electronic spectra of the phenolcation–water complex also suggested a certain transition in this region⁴⁵⁶.

Coupled-cluster CCSD(T)/6-311++G(d,p) electronic energy computations of the $^2A'$ state using the $^2A''$ ground-state geometry leads to an estimation of 3.6 eV for the vertical $C^2A' \leftarrow X^2A''$ transition, which compares reasonably well with the PE of 3.37 eV⁴⁴³. The lowest-lying quartet state of phenol ion was found to be a dissociative state giving a triplet phenyl cation plus OH radical that lie about 5.3 eV above the ground-state $^2A''$. Overall, the calculated results point towards the following energy ordering of electronic states of **21**: $X^2A''(0.0) < A^2A''(0.5) < B^2A''(2.6) < C^2A'(3.1)$, where values given in parentheses are energy gaps in eV.

A deprotonation of the phenol ion giving the phenoxy radical **21** \rightarrow C₆H₅O \cdot (2B_1) + H⁺ is a barrier-free endothermic scission. Due to the small size of the proton, the stabilizing through-bond delocalization during the cleavage, if any, is likely to be small⁴⁴¹. The process is characterized by a DPE of 857 kJ mol^{–1} (at 0 K) and 863 kJ mol^{–1} (at 298 K) derived from B3LYP computations. The latter value compares well with the experimental proton affinity of 860 kJ mol^{–1} previously determined for the phenoxy radical⁴⁴². This is by far smaller than the corresponding value of neutral phenol, DPE(PhOH) = 1464 kJ mol^{–1} (15.16 eV), discussed above. Electron removal from a neutral system tends to facilitate effectively its deprotonation. For the sake of comparison, remember that the PAs (0 K) of phenol and anisole amount to PA(phenol) = 820 kJ mol^{–1} and PA(anisole) = 842 kJ mol^{–1} (cf. Section IV.A). From a technical point of view, the hybrid density functional B3LYP method appears to provide the most accurate DPE values¹³⁸.

The effect of substituents on the DPE and IE also depends on their nature and position. For a series of mono-halophenol ions, the DPEs (in kJ mol^{–1}) calculated using the B3LYP/6-311++G(d,p)+ZPE level are as follows:

F:	<i>ortho</i> :	843;	<i>meta</i> :	840;	<i>para</i> :	849.
Cl:	<i>ortho</i> :	852;	<i>meta</i> :	848;	<i>para</i> :	861.
Br:	<i>ortho</i> :	858;	<i>meta</i> :	853;	<i>para</i> :	867.

Relative to the value of 857 kJ mol^{-1} for **21**, fluorine consistently tends to reduce the DPE up to 17 kJ mol^{-1} , whereas chlorine and bromine could either enhance or reduce it by *ca* 10 kJ mol^{-1} . The *meta*-C₃ position is peculiar in having the smallest DPE, irrespective of the nature of the halogen. This is due to the fact that the *meta*-X-phenol radical cation corresponds to the least stable isomer within each series, lying up to 20 kJ mol^{-1} above the most stable *para*-C₄ counterpart. In the *ortho* position, the *cis*-C₂ conformer is more stable than *trans*-C₆ and energetically close to the *para*-C₄ one. A direct consequence of the lower stability of the *meta*-X-phenol ions is the higher IE_a of the corresponding neutral molecules whereas the *para*-X-phenols, on the contrary, exhibit the smallest IE_a . The IE_a s of the series of mono-halophenols are evaluated as follows (bearing in mind that the relevant value for the parent phenol is actually 8.48 eV):

F:	<i>ortho</i> :	8.68;	<i>meta</i> :	8.70;	<i>para</i> :	8.48.
Cl:	<i>ortho</i> :	8.61;	<i>meta</i> :	8.63;	<i>para</i> :	8.39.
Br:	<i>ortho</i> :	8.55;	<i>meta</i> :	8.57;	<i>para</i> :	8.32.

The observed changes in both quantities could partly be rationalized in classical terms of electron-donating and electron-withdrawing effects^{439, 440}.

We now turn to the hyperfine coupling constants (hfcc) of **21** that were determined using EPR spectroscopy techniques⁴⁵⁷. It is believed that these properties could be used with enough accuracy to distinguish phenol radical cations from phenol radicals in tyrosine-derived species¹³⁸. Isotropic hfcc values are a sensitive measure of the electronic spin distribution, as they are directly proportional to the spin density at the position of nucleus N, $\rho(r_N)$. According to the McConnell relation⁴⁵⁸, the spin density at the H nucleus is well known to depend on the spin polarization of the $\sigma(\text{C}-\text{H})$ electrons by virtue of the unpaired carbon π -electron density. Therefore, it suggests the repartition of the excess electron among the ring carbon atoms. Measured hfcc values included 5.3, 0.8 and 10.7 Gauss for the protons at the C₂, C₃ and C₄, respectively. This agrees qualitatively with the spin distribution from simple resonance terms, where the highest spin density is on the *para*-C₄, followed by the *ortho* C₂ and C₅ carbons. The values for the hydroxyl proton, ¹³C and ¹⁷O hfcc values, as well as the sign of spin polarization at each proton were not reported⁴⁵⁷.

Table 33 lists the hfcc values calculated at the UB3LYP/6-311++G(d,p) level for both phenol radical cation and phenoxy radical. A few points are noteworthy.

(i) There are significant differences between the hfcc values of both doublet species which are perfectly distinguishable on the basis of this spectroscopic parameter. Protonation of the symmetrical phenoxy radical induces some large shifts on the ¹³C constants, in particular the *ipso*-carbon, and to a lesser extent the *ortho*-carbons. The odd-alternate pattern of spin densities is thus more pronounced in the radical cation than in the radical.

(ii) A large asymmetry is manifested in the hfcc values of ion **21**.

(iii) Calculated hfcc values for **21** agree qualitatively with the EPR results mentioned above. Thus the calculated $a(\text{H}_4) = -9.9 \text{ G}$, $a(\text{H}_2) = -4.1 \text{ G}$ and $a(\text{H}_3) = 0.7 \text{ G}$ are close to the experimental magnitude of 10.7, 5.3 and 0.8 G, respectively.

(iv) Calculations reveal a substantial hfcc for the hydroxyl proton (-6.9 G).

The difference in structural and bonding properties of both neutral and ionized species also manifests itself strongly in their vibrational motions. Most of the 11 experimentally measured vibrational frequencies for **21** and 10 frequencies for its deuteriated analogue **21-d5** correspond to the CH bending, CC and CO stretching⁴²⁵. The highest frequency observed at 1669 cm^{-1} was assigned to a CC stretching mode (the Wilson 8a mode) and the lowest frequency of 169 cm^{-1} describes an out-of-plane ring torsion. No surprises were noted in the measured isotopic frequency shifts; all modes of **21** shift to lower frequencies

TABLE 33. Hyperfine coupling constants (G) of phenoxy radical and phenol radical cation^a

Atom	Phenoxy radical Isotropic Fermi Contact Couplings	Phenol radical cation 21 Isotropic Fermi Contact Couplings
C-1	-12.5	-2.5
C-2	6.6	1.6
C-3	-8.8	-6.4
C-4	10.3	10.0
C-5	-8.8	-7.4
C-6	6.6	2.8
O	-7.3	-6.9
H(C-2)	-6.7	-4.1 (5.3) ^b
H(C-3)	2.6	0.7 (0.8)
H(C-4)	-8.8	-9.9 (10.7)
H(C-5)	2.6	1.5
H(C-6)	-6.8	-5.0
H(O)		-6.9

^aResults obtained from UB3LYP/6-311++G(d,p).^bIn parentheses are experimental values from Reference 424.

upon deuteration and the largest observed frequency shift of -359 cm^{-1} appears for a CH bending motion. Calculations¹³⁸ have helped to reassign several observed bands⁴²⁵. Most importantly, the band observed at 1500 cm^{-1} is due to the CO stretching (rather than a CC stretching as originally assigned) and the band at 1395 cm^{-1} to a CH bending (rather than a CO stretching).

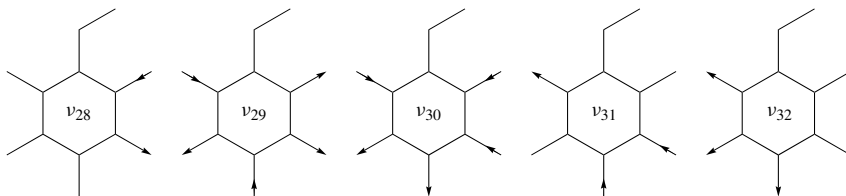
Although the atomic masses remain unchanged, the force constants, frequencies and normal modes are modified significantly upon electron loss. We note that the most important shifts arise from the C–O–H torsion mode (upshift of 256 cm^{-1}), the C–O–H bending (downshift of 57 cm^{-1}) and the CO stretching (upshift of 101 cm^{-1}). It is possible not only to identify these changes, but also to quantify them in terms of the percentage of a neutral mode present in that of the ion by making use of a vibrational projection analysis technique¹⁶⁸. Figure 29 displays a qualitative graphic representation of the hydrogen displacements in the C–H stretching normal modes calculated for both neutral and ionized phenol. While the highest and lowest C–H stretching modes of **21** are clearly assignable to the respective modes of phenol, the middle three modes show a higher degree of changes and mixing.

2. Relative energies of the $(\text{C}_6\text{H}_6\text{O})^{*+}$ radical cations

There are obviously a large number of possible isomers of phenol ion. Let us consider only the isomers where the six-membered ring framework is preserved. Starting from **21**, one hydrogen atom could be displaced from either O or one C atom to another atom and this exercise results in the creation of the various isomeric groups presented in Figure 30: group 1 includes ions having a CH_2 group at the *para* (C_4) position, group 2 at the *meta* (C_3), group 3 at the *ortho* (C_2) and group 4 at the *ipso* (C_1) and oxygen positions.

Calculated energies relative to the phenol ion given in Figure 30 indicate that **21** represents the most stable form among the six-membered ring group of isomers. Keto-forms **22** and **24** are low-lying isomers which are situated 146 and 133 kJ mol^{-1} , respectively, above **21**. This energy ordering within the pair **21** and **22** (or **24**) is reminiscent of that encountered for simple keto–enol tautomers^{459, 460}. For example, ionized vinyl alcohol

Phenol



Phenol Radical Cation

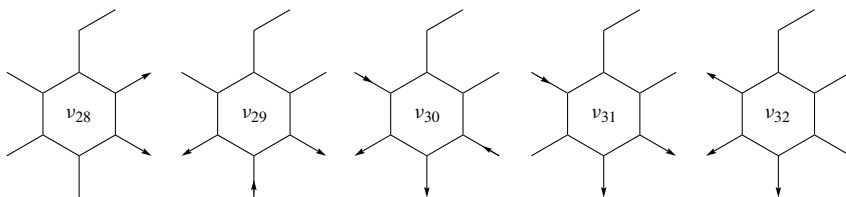


FIGURE 29. Qualitative graphic representation of the hydrogen displacements in the C–H stretching normal modes calculated for both neutral and ionized phenol

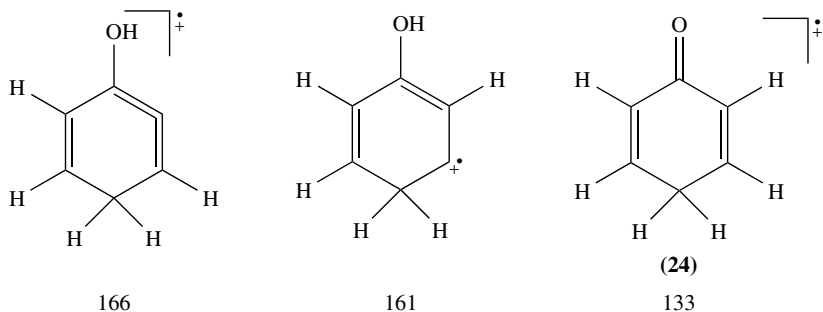
is significantly more stable (about 60 kJ mol^{-1}) than its keto ion counterpart^{461, 462}. The difference in energy observed here between ionized phenol and its keto tautomers is, however, more pronounced; this point will be examined below. The distonic oxonium species **23** (Chart 5) belongs to the high-energy group of isomers; its energy, relative to **21**, equals 241 kJ mol^{-1} . The distonic species **25** (Figure 30) turns out to be the lowest lying isomer of group 2. This situation is opposite to the situation met in the ionized aniline system in which the ammonium distonic ion is found to be only 80 kJ mol^{-1} above ionized aniline³⁰³. The other *meta*- and *ortho*-distonic ions have similar energy and are separated from each other by high-energy barriers for 1,2-hydrogen shifts (Chart 6).

In order to evaluate the effect of ionization on the relative stabilities of phenol isomers, a selected set of neutral species is considered whose relative energies are displayed in Figure 31. It is remarkable that, in the neutral state, only three six-membered ring structures are in a *ca* 70 kJ mol^{-1} energy range, namely phenol **26** and its keto-forms **27** and **28**. The carbene, allene or biradical isomeric forms are strongly destabilized and lie more than 200 kJ mol^{-1} above **26**. In contrast, the five-membered ring containing a ketene or a ketone moiety are only 90 to 140 kJ mol^{-1} above phenol. As expected, phenol **26** is more stable than its tautomers **27** and **28**, and this is partly at the origin of the large difference in stability of the corresponding ionized species. In fact, in the phenol series, the aromaticity renders the enol tautomer more stable; this situation is opposite to that observed in the aliphatic series. For example, neutral acetaldehyde is *ca* 40 kJ mol^{-1} below its enol form, namely the vinyl alcohol^{459, 461}. After removal of one electron, the enol structure becomes more stable than the keto form by 60 kJ mol^{-1} as recalled above⁴⁶². This stability reversal is due to the large difference in IE_a values between the two structures, namely 9.14 eV for vinyl alcohol and 10.23 eV for the acetaldehyde, in keeping with the fact that it consists of a $\pi_{\text{C}=\text{C}}$ ionization in the former case and an ionization of an oxygen lone pair in the latter. A comparable situation arises for the phenol ($\text{IE} = 8.5 \text{ eV}$) and its keto tautomers **27** and **28** ($\text{IE} = 10.8 \text{ eV}$). This difference, added to the difference in energy between the neutral molecules (in favour of the phenol molecule), explains the large energy gaps of **22** and **24** with respect to **21**.

3. The $(\text{C}_6\text{H}_6\text{O})^{*\,+}$ potential energy surface (PES)

The essential features of the portion of the $(\text{C}_6\text{H}_6\text{O})^{*\,+}$ PES starting from **21** were constructed and illustrated schematically in Figure 32. The shape of the most interesting intermediates are defined in Figure 33 and X/Y denotes a transition structure (TS) linking two equilibrium radical cation structures X and Y. The ion fragments $\text{C}_5\text{H}_6^{*\,+}$ resulting from elimination of CO, labelled as **31**, **33**, **38**, **40** and **43** in Figure 32, are omitted for the sake of simplicity. Their actual shape can easily be deduced from the structures of

Group 1



Group 2

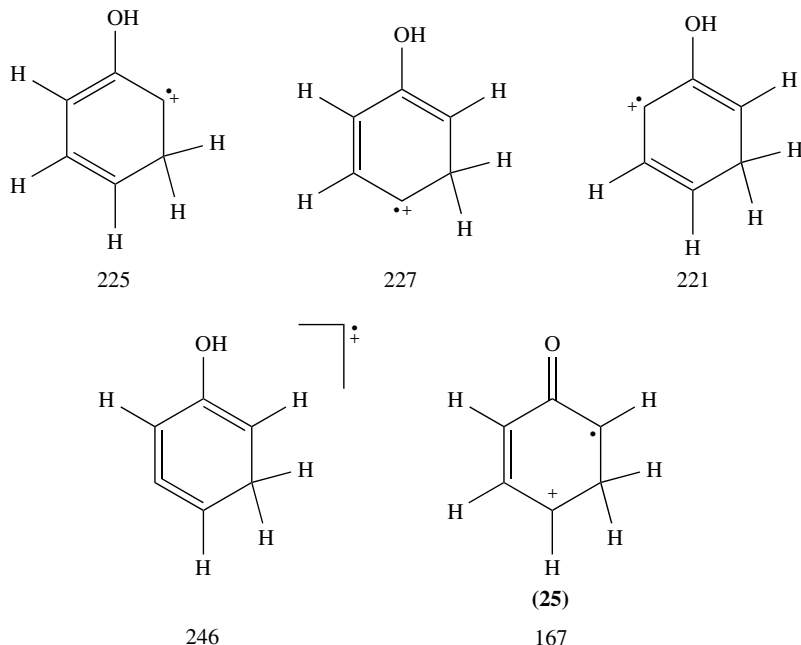
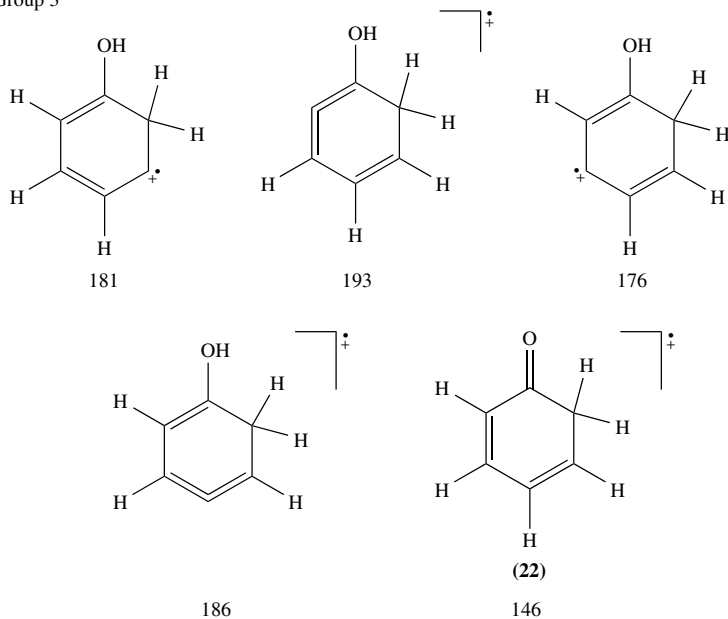


FIGURE 30. Relative energies of selected isomers of phenol radical cation containing a six-membered ring. Values given in kJ mol^{-1} relative to **21** were obtained from UB3LYP/6-311++G(d,p)+ZPE calculations. Adapted from Reference 452 with permission

Group 3



Group 4

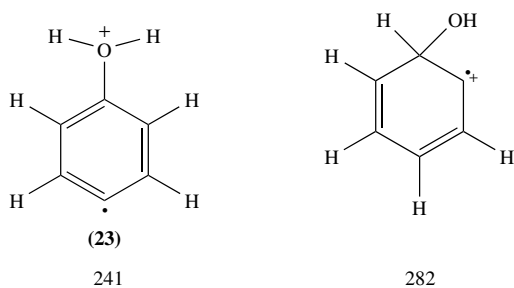


FIGURE 30. (continued)

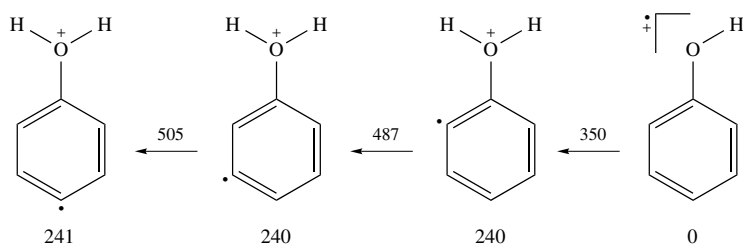


CHART 6. B3LYP/6-311++G(d,p)+ZPE energies (in kJ mol^{-1}) of the oxonium dicationic isomers and the transition structures connecting them relative to phenol ion **21**. Adapted from Reference 452 with permission

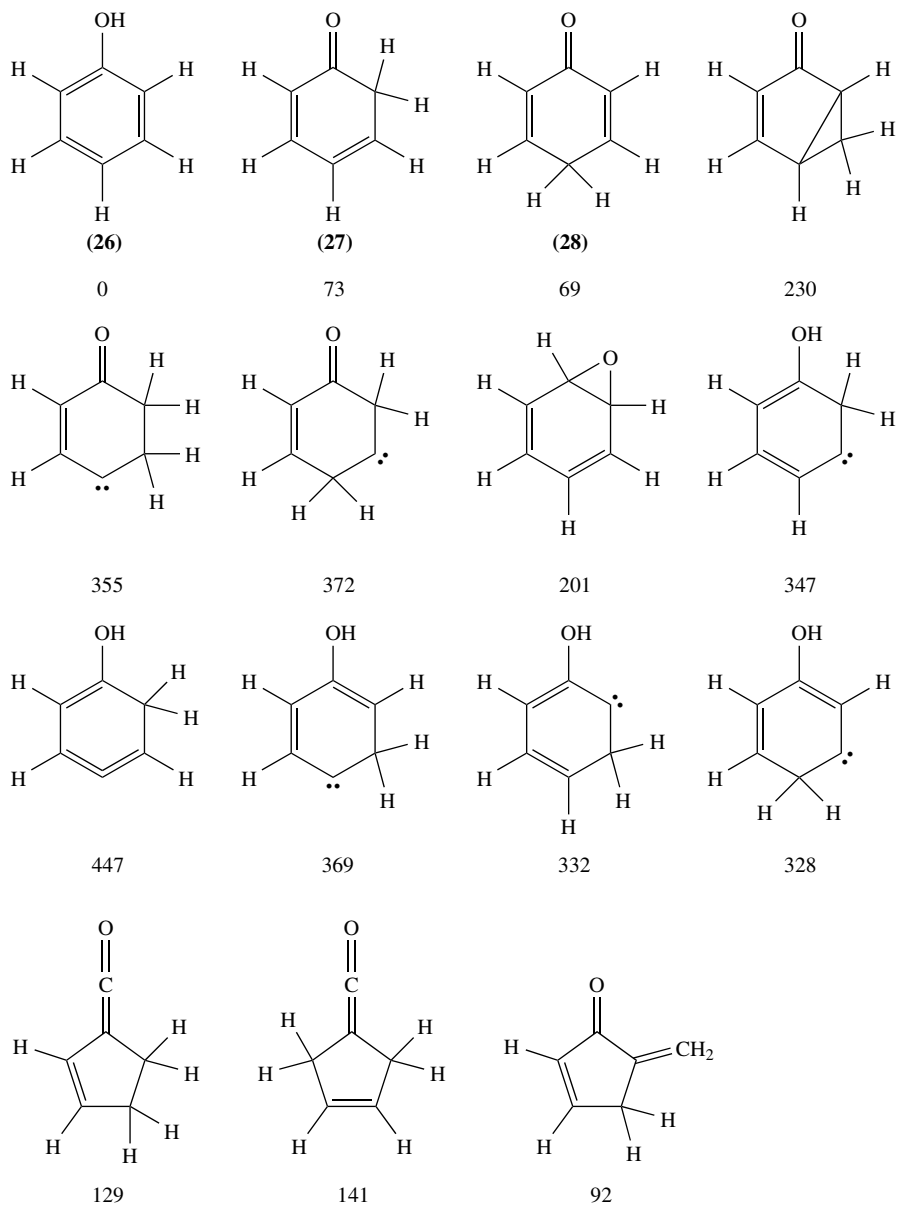


FIGURE 31. Relative energies of selected isomers of neutral phenol. Values given in kJ mol^{-1} were obtained from B3LYP/6-311++G(d,p)+ZPE calculations. Adapted from Reference 452 with permission

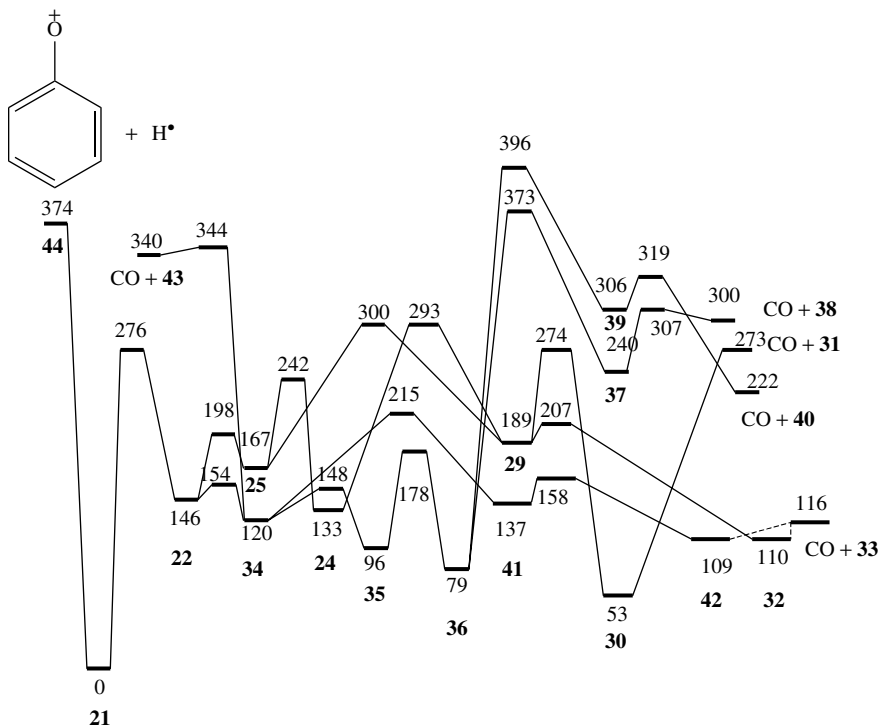


FIGURE 32. Schematic representation of the $(\text{C}_6\text{H}_6\text{O})^{+\bullet}$ potential energy surface showing the rearrangements of phenol radical cation leading to a CO loss. Relative energies given in kJ mol^{-1} were obtained from B3LYP/6-311++G(d,p)+ZPE calculations. Adapted from Reference 452 with permission

the corresponding radical cations **30**, **32**, **37**, **39** and **11**, respectively. The phenoxy cation **44**, results from hydrogen loss from the phenol radical cation **21**.

The numerous reaction pathways found in Figure 32 invariably lead to an elimination of CO giving $(\text{C}_5\text{H}_6)^{+\bullet}$ ion fragments (m/z 66). The PES can be divided into two distinct parts: while the first part involves the three cyclohexanone ion isomers **22**, **24** and **25**, the second consists in the conversion of the cyclic keto-ions into either the various open-chain distonic forms **34** (or its conformers **35** and **36**), **37** and **39**, or the five-membered cyclic derivatives **29**, **30** and **41**. There are also some weak hydrogen bond complexes between CO and the CH bond of ionized cyclopentadienes such as **32** and **42**.

The first step thus corresponds to a 1,3-hydrogen shift via the transition structure (TS) **21/22** which is associated with a rather high energy barrier of 276 kJ mol^{-1} relative to the phenol radical cation **21**. The corresponding energy barrier for the neutral system amounts to 278 kJ mol^{-1} . Thus, there is practically no reduction in the barrier height following ionization, in contrast to the case of the propene ion⁴⁶³. It appears that, once formed, the keto ion **22** easily undergoes a ring opening via TS **22/34** yielding the open-chain distonic ketene radical cation **34**. The successive 1,2-hydrogen shifts within the ring can also give **25** and finally the most stable keto form **24**. From here, the six-membered cyclic framework could be converted into the five-membered ring **29** lying 189 kJ mol^{-1} above

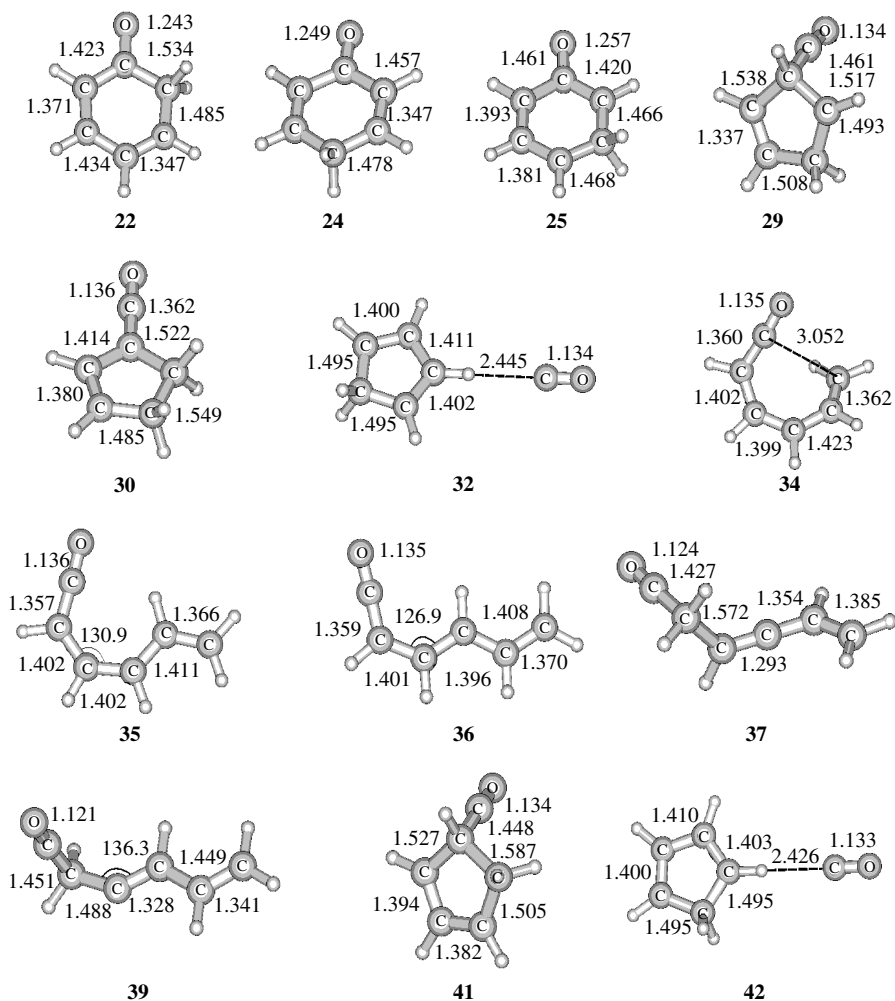


FIGURE 33. Selected B3LYP/6-311++G(d,p) geometric parameters of the $(\text{C}_6\text{H}_6\text{O})^{*+}$ equilibrium structures considered. Bond distances are given in Å and bond angles in deg. Adapted from Reference 452 with permission

21 by direct one-step rearrangements via the TSs **24/29** and **25/29**. From **29**, an almost spontaneous CO loss with an energy barrier of only 18 kJ mol⁻¹ could thus occur, giving the complex **32**, which dissociates to the fragment products CO + cyclopentadiene ion **33**, 116 kJ mol⁻¹ less stable than phenol ion **21**.

Although the ketene ring **30** is found to be only 53 kJ mol⁻¹ above **21** and by far more stable than acetyl ion **29**, it turns out that the CO loss from an indirect process, finally giving the five-membered ion **31**, namely **29** → **30** → (CO + **31**), constitutes a substantially more difficult route. It is apparent from Figure 32 that the cyclic isomer **29** could be a possible intermediate in the CO-eliminative process of phenol cation **21**. Nevertheless,

the high energy content of both TSs **24/29** and **25/29** at 293 and 300 kJ mol⁻¹, respectively, above **21** but actually 20 kJ mol⁻¹ above the TS **21/22** for the initial 1,3-hydrogen shift, makes the rearrangement through **29** less competitive than other routes. The latter is, however, more favoured than a hydrogen atom elimination characterized by a dissociation energy of 374 kJ mol⁻¹ for a direct O–H bond cleavage (Figure 32).

The alternative route comprises the open-chain ketene ion **34** and its conformers **35** and **36** formed by ring opening of the ketone ion **22**. From here, the super-system could either rearrange to the open-chain acetyl cations **37** and **39** or undergo a cyclization, forming back the five-membered ring **41** which is significantly more stable than **37** and **39** (137, 240 and 306 kJ mol⁻¹ above **21**, respectively). Figure 32 clearly points out that the CO loss via **41** is beyond any doubt the lowest energy route⁴⁵².

Figure 34 illustrates the lowest energy rearrangement path for the CO-loss process of ionized phenol. It involves, in a first step, the enol–keto conversion **21**–**22**. Starting from **22**, a ring opening leads to structure **34** which, in turn, by ring closure produces ion **41**. A direct and concerted isomerization **22** → **41** was not found⁴²⁸. The CO loss from **41** involves the slightly stabilized ion/neutral intermediate **42**. The rate-determining step of the overall process **21** → **22** → **34** → **41** → **42** → (CO + C₅H₆⁺) is the 1,3-hydrogen shift **21/22**.

The processes suggested by calculations are in good agreement with experimental mass spectrometric studies^{429–435} which demonstrated that the CO loss (*m/z* 66) corresponds to the least energy demanding fragmentation. Furthermore, it was found earlier that the kinetic energy released during the CO loss from the keto ion **22** was less than that involved during the dissociation of the phenol ion **21** itself⁴³⁴. This is clearly in keeping with the potential energy profile presented in Figure 34. The appearance energy of the [M–CO]⁺ ions has been determined by time-resolved electron impact⁴³⁵ and photoionization⁴³⁶ experiments and by photoelectron photoion coincidence⁴⁴⁴.

From a comparison of the data and after consideration of the kinetic shift, an energy threshold of 11.4 ± 0.1 eV at 298 K has been deduced. Considering an adiabatic ionization energy value of 8.47 ± 0.02 eV^{444, 464} and a correction for the 298 K enthalpy of ca 0.1 eV for the phenol, the energy barrier separating **21** from its fragments is thus ca 3.0 ± 0.15 eV, i.e. 290 ± 15 kJ mol⁻¹. This value is in excellent agreement with the calculated 0 K energy barrier **21** → **22** of 276 kJ mol⁻¹.

It may be noted that the energy amount involved in the CO-loss process is by far smaller than that needed for a deprotonation of phenol cation as mentioned above, namely 857 kJ mol⁻¹. This suggests that the ease with which a deprotonation of phenol radical cations occurs in different solutions^{419, 423, 424} was likely to arise from either a specific participation of the solvent molecules in the supermolecule or a strong continuum effect.

4. Mass spectrometric experiments

The state-of-the-art mass spectrometric experiments described below were designed to search for a possible production of (C₆H₆O)⁺ isomers, such as dehydrophenyloxonium ions or cyclohexadienone ions. They were performed on a large-scale tandem mass spectrometer of E₁B₁E₂qC₃E₃B₂cE₄ geometry (E stands for electric sector, B for magnetic sector, q for a radio-frequency-only quadrupole collision cell and c for the ‘conventional’ collision cell)^{465, 466}. The following three MS experiments have been carried out:

(a) First, both 4-bromophenol (**45**) and 4-bromoanisole (**46**) were protonated in the chemical ionization ion source. It was expected that collisional debromination of protonated 4-bromophenol (**47**) could be an interesting source of a distonic isomer of ionized phenol if protonation takes place at oxygen. Alternatively, phenol ions should be produced in the case of ring protonation. The same behaviour was expected for protonated 4-bromoanisole (**48**).

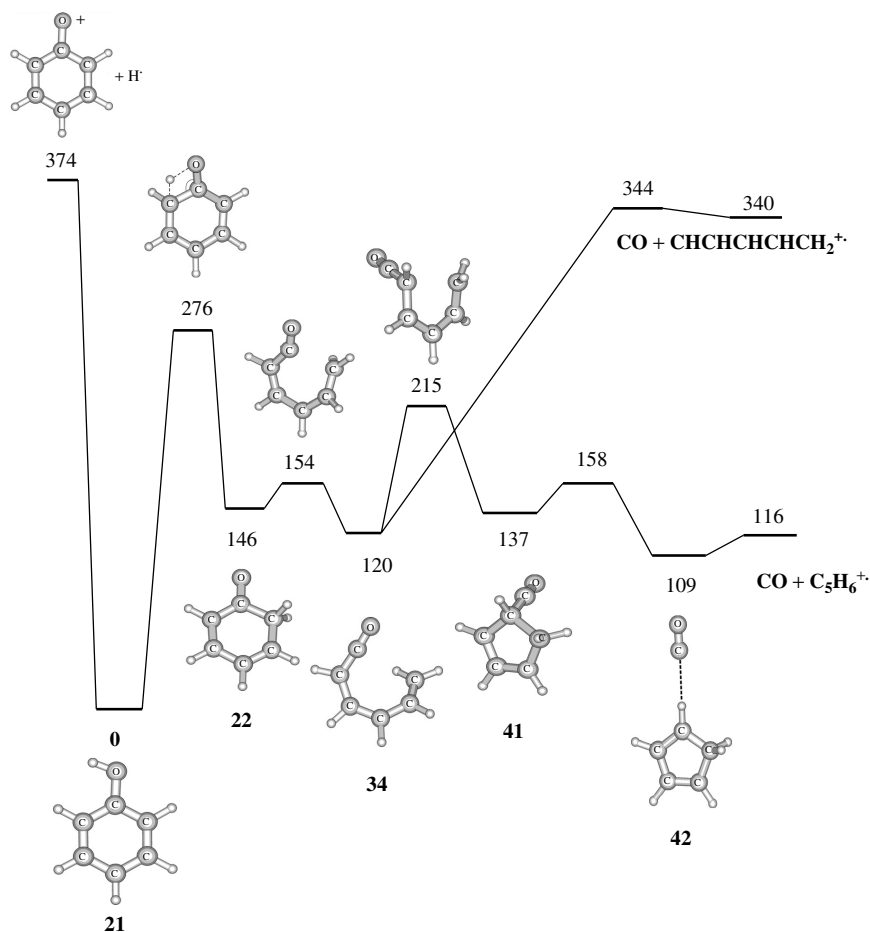


FIGURE 34. Schematic representation of the $(\text{C}_6\text{H}_6\text{O})^{\bullet+}$ potential energy surface showing the lowest energy path for CO loss of phenol radical cation. Relative energies given in kJ mol^{-1} were obtained from B3LYP/6-311++G(d,p)+ZPE calculations. Adapted from Reference 452 with permission

The high-energy collisional activation (CA) spectra of the $\text{C}_6\text{H}_6\text{O}^{\bullet+}$ ions (m/z 94) or $\text{C}_7\text{H}_8\text{O}^{\bullet+}$ ions (m/z 108) were recorded and the resulting spectra depicted in Figure 35 were found identical to the corresponding spectra of ionized phenol or anisole, respectively.

This observation is in line with the preferential protonation at the ring, not at the oxygen atom, of phenol or anisole (cf. Section IV.A). Distonic dehydro-oxonium ions **50** are therefore not generated in these chemical ionization experiments, in line with the fact that they are more than 200 kJ mol^{-1} less stable than ions **49** (Chart 7). A major fragmentation of ions **50** should be a loss of HOH or ROH with the production of benzyne ions (m/z 76), but the relative intensity of this peak is not increased, thus confirming that ions **50** are not produced to a significant extent in the protonation–debromination sequence.

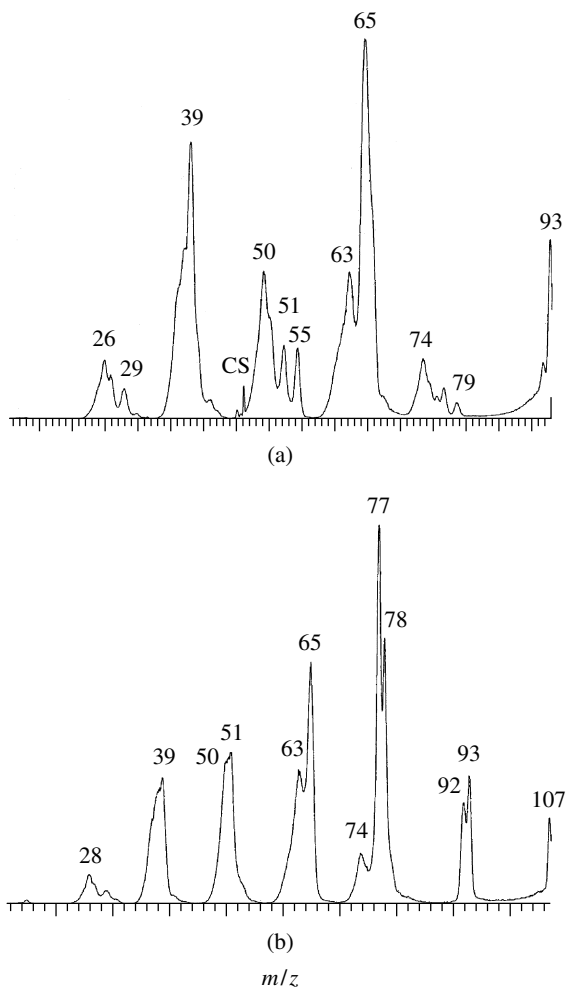


FIGURE 35. CA spectra of (a) $[MH-Br]^+$ radical cations (nitrogen collision gas) generated by low-energy collisional activation (argon collision gas) of mass-selected protonated 4-bromophenol **47**, and (b) protonated 4-bromoanisole **48**. CS refers to a charge stripping. Adapted from Reference 452 with permission

Such behaviour clearly contrasts with the case of 4-iodoaniline, where protonation in a chemical ionization source occurred not only on the ring but also on the nitrogen atom⁴⁵⁰. Nitrogen protonation was indicated by ion–molecule reactions with dimethyl disulphide consecutive to collisional dehalogenation (FT-ICR experiments)⁴⁶⁷ or by an increase in the intensity of the peak at m/z 76 following high-energy collisional activation⁴⁵⁰.

(b) Given the fact that a ring protonation was identified in the preceding experiment, unsubstituted anisole was also protonated under methane chemical ionization conditions with the expectation that if the methyl group could subsequently be expelled collisionally

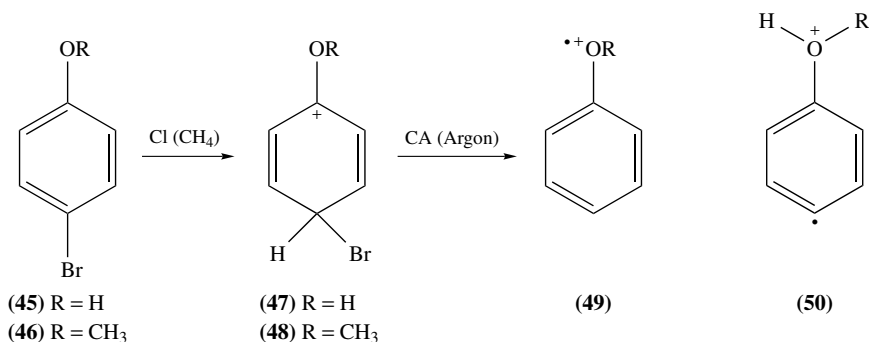


CHART 7. Protonation and Debromination

within the quadrupole collision cell, a cyclohexadienone radical ion (*ortho* **22** and/or *para* **24**) should be produced. The protonation occurs on the ring as indicated by the experiments described above on 4-bromoanisole and a demethylation was indeed a prominent fragmentation of the protonated anisole (Figure 36a), but the CA spectrum of the re-accelerated m/z 94 ions (Figure 36b) was found identical to the CA spectrum of the phenol radical cations, not to that of cyclohexadienone ions.

A similar observation has also been made using another MS/MS/MS experiment, where the demethylation step was realized in the high kinetic energy regime. Demethylation of protonated anisole is evaluated to be less endothermic by about 146 kJ mol^{-1} if ionized phenol **21** was formed rather than ionized cyclohexadienone **22** (cf. Chart 8, where values given are estimated heats of formation).

Computations on the interconversion of protonated anisoles indicate that the demethylation of the latter invariably involves formation of its O-protonated form and ends up with the production of **21**. The O-protonation is about 57 kJ mol^{-1} less favoured than the ring *para*-C₄ protonation and the entire process is associated with an energy barrier of 232 kJ mol^{-1} relative to the most stable protonated form, a value comparable to that required for a direct C–O bond cleavage of O-protonated anisole.

(c) In the last experiment, 2-hydroxybenzaldehyde (salicylaldehyde) was submitted to electron ionization. Due to an *ortho* effect, carbon monoxide is, *inter alia*, expelled from the metastable molecular ions (MIKE spectrum, the concerned field-free region being the quadrupole cell, Figure 37a). The CA spectrum of the m/z 94 ions detected in the mass spectrum (Figure 37b) is depicted in Figure 37c. This spectrum indicates that these ions are actually *not* phenol ions. Moreover, when the m/z 94 ions are generated collisionally in the quadrupole, the CA spectrum is very significantly modified (Figure 37d) with the appearance of an intense signal at m/z 76, corresponding to a loss of water.

In summary, a debromination of protonated 4-bromophenol and 4-bromoanisole essentially produces phenol and anisole radical cations, respectively; no less conventional molecular ions were detected. Similarly, collisional demethylation of protonated anisole gives rise to ionized phenol. Only an electron ionization of salicylaldehyde appears to produce an *ortho*-oxonium distonic isomer of the phenol ion. Quantum chemical calculations suggest predominant stability of **21** lying at least 130 kJ mol^{-1} below the other six-membered isomers. Its preponderant fragmentation is a CO loss occurring via different intermediates, namely its keto six-membered ring, open-chain ketene and five-membered cyclopentadiene isomers. The rate-determining step corresponds to the enol–ketone interconversion of the phenol ion with a barrier height of 276 kJ mol^{-1} relative to phenol ion,

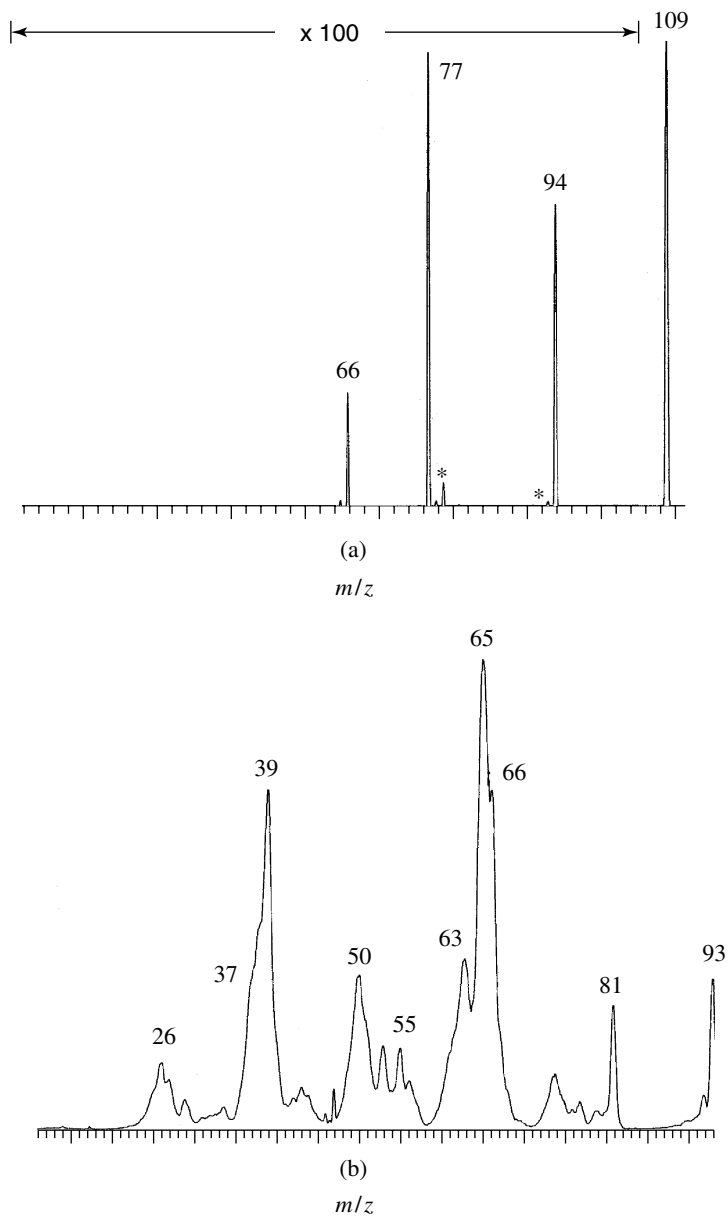


FIGURE 36. (a) MIKE spectrum of protonated anisole m/z 109 and (b) CA (nitrogen) spectrum of the m/z 94 ions. Adapted from Reference 452 with permission

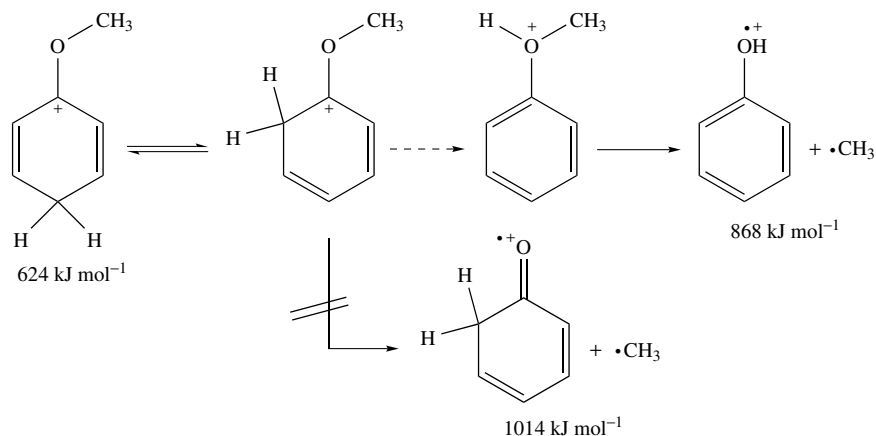
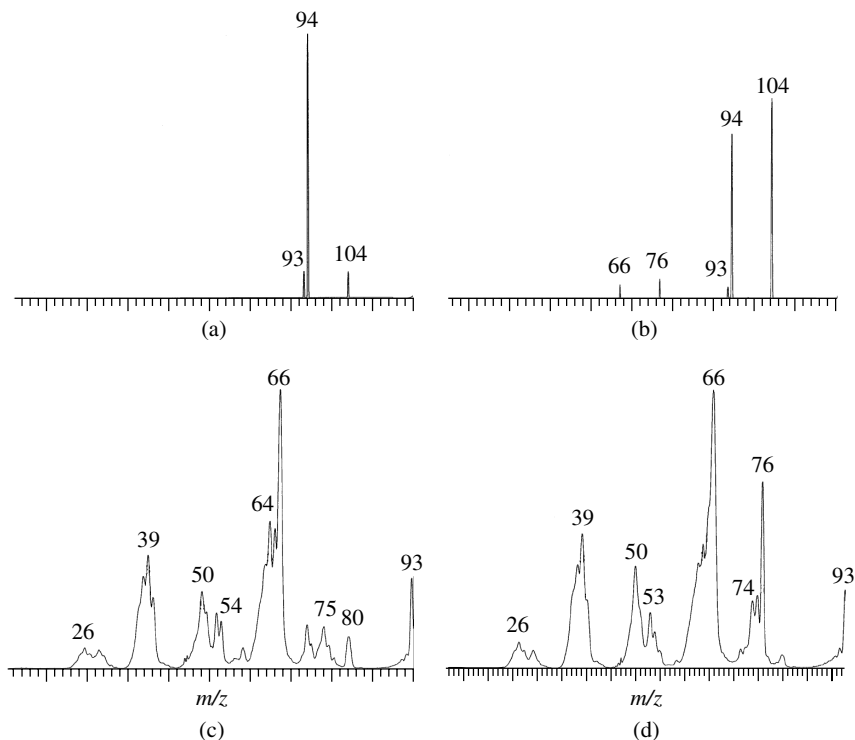


CHART 8. Protonation of anisole

FIGURE 37. (a) MIKE and (b) CA spectra of the m/z 122 ions of ionized salicylaldehyde (peaks at m/z 121, *ca* $5 \times$ more intense, not shown), and (c) and (d) CA (nitrogen) spectra of the m/z 94 ions produced in these conditions. Adapted from Reference 452 with permission

which is markedly smaller than that required for hydrogen atom loss or deprotonation. This suggests that the solvent plays an important role in assisting the deprotonation of phenol ions in non-polar media.

5. Keto–enol interconversion

As discussed in a previous section, thanks to the aromatic stabilization, the phenol–cyclohexadienone pair thus represents a specific case in which the enol form is actually more stable than its keto tautomers. Hydrogen transfer from oxygen to carbon indeed disrupts the phenyl ring and this disfavors the ketone form. However, the latter intervene as crucial intermediates during the phenol decomposition, in the oxidative metabolism of aromatic compounds (the ‘NIH-shift’), in the reactions of arene oxides, the photo-Fries rearrangement, the Kolbe–Schmitt and the Reimer–Tiemann reactions^{184, 185, 468}. Both cyclohexa-2,4-dien-1-one **27** and cyclohexa-2,5-dien-1-one **28** have been generated experimentally by flash photolysis of appropriate precursors in aqueous solution. Based on kinetic results, logarithms of the equilibrium constants for the enolization **27** → **26** and **28** → **26** were evaluated to be $pK_E(\mathbf{27}, 25^\circ\text{C}) = -12.73$ and $pK_E(\mathbf{28}, 25^\circ\text{C}) = -10.98$. Combination with the acidity constant of phenol **26** also defines the acidity of both ketones which are characterized as strong carbon acids with $pK_a(\mathbf{27}) = -2.89$ and $pK_a(\mathbf{28}) = -1.14$, all with errors of ± 0.15 . The common conjugate base is the phenolate anion discussed in a preceding section. Both ketone forms disappeared by proton transfer to the solvent with estimated lifetimes of $\tau(\mathbf{27}) = 260 \mu\text{s}$ and $\tau(\mathbf{28}) = 13 \mu\text{s}$ ⁴⁶⁸.

Let us remember that the energy difference between phenol **26** and both keto isomers **27** and **28** amount to 73 and 69 kJ mol^{-1} , respectively (Figure 31). The contribution of entropy is small, amounting to $\Delta S = -9$ and $-1 \text{ J mol}^{-1}\text{K}^{-1}$, for both ketonization reactions, respectively, and this also leads to an estimate for the equilibrium constant of the enolization, pK_E , ranging from -12 to -13 , of the same order of magnitude as the experimental results in aqueous solution^{186, 187, 469}. It should be stressed that such similarity of values in both gaseous and condensed phases should not be considered as an ‘agreement’ and need to be treated with much caution, due to the fact that the solvent effect on the equilibrium has not been taken into account.

The results discussed above clearly demonstrate that the keto–enol energy difference is further enlarged upon ionization at the expense of the keto form (Figure 34), due to the higher IE_a of the latter, namely 804 kJ mol^{-1} for **26** and 878 kJ mol^{-1} for **27**. Figure 38a shows a remarkable effect of the methyl substituent on the energy differences. Although the group placed either at the *meta* or *para* position does not induce large changes in the relative energies of the neutral species (a reduction of $3\text{--}5 \text{ kJ mol}^{-1}$), it strongly modifies those in the ionized state, in particular in the *para*-substituted system: the IE_a of phenol is effectively reduced whereas the IE_a of cyclohexadienone has increased. This results in a further destabilization of 18 kJ mol^{-1} of the ionized ketones.

The phenomenon is also manifested, albeit to a lesser extent, in the amino-substituted pairs as illustrated in Figure 38b. In this system, the IE_a s are substantially decreased due to the presence of the amino group, which confers an ‘aniline’ character to the ionized species.

It is also well known that the keto–enol equilibrium is modified fundamentally in aqueous solution due to the specific interaction of solvent molecules with the substrates through hydrogen bonds^{470–472}. Calculated results summarized in Figure 39a indicate that the keto–enol equilibrium is markedly modified in the bimolecular neutral systems in which each tautomer interacts with one water molecule. In particular, the energy barrier for hydrogen transfer from oxygen to carbon is reduced appreciably, in going from

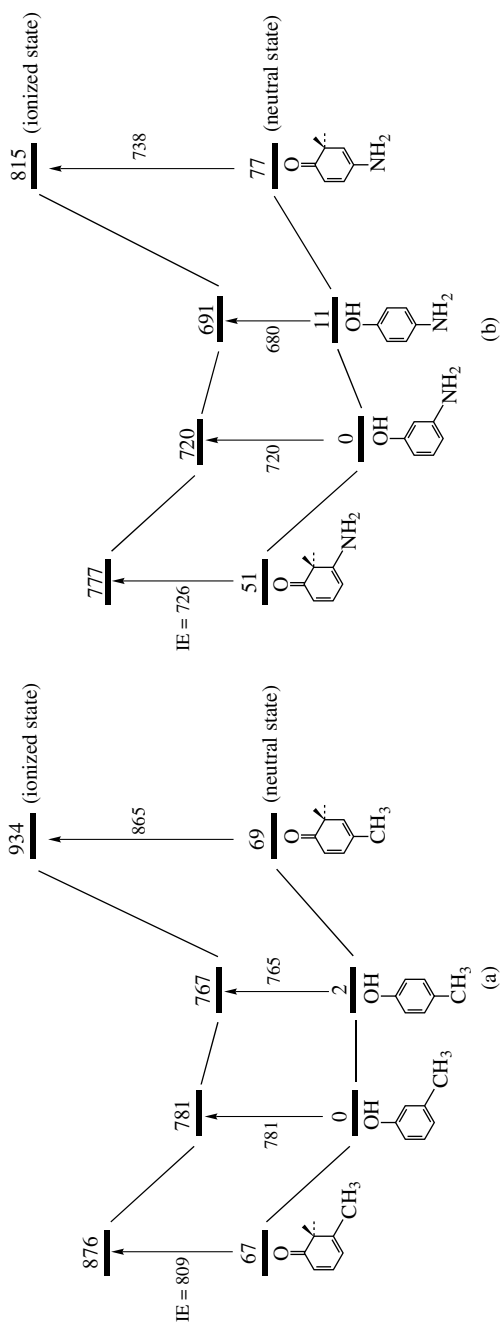


FIGURE 38. Relative and ionization energies of *meta*- and *para*-X-substituted phenol and cyclohexa-2,4-dienone: (a) X = methyl and (b) X = NH₂. Values given in kJ mol⁻¹ were obtained from B3LYP/6-311++G(d,p)+ZPE computations

175 kJ mol⁻¹ in the unimolecular system to 76 kJ mol⁻¹ in the water-assisted hydrogen transfer. The displacement of the equilibrium in favour of the enol form is further accentuated in the ionized counterparts in which the ionized keto form virtually disappears. The relevant calculated results are illustrated in Figure 39b.

We also mention that the ionized phenol–water complex has been observed and examined in depth^{113, 455, 473–476}. Complexes of phenol radical cation with ammonia⁴⁷⁷ and molecular nitrogen⁴⁷⁸ have also been produced. The existence of an intramolecular hydrogen bond in *ortho*-substituted phenol radical cations has also been demonstrated⁴⁷⁹.

E. The O–H Bond Dissociation

1. Phenoxyl radicals

Owing to the relatively facile oxidation of phenols, phenoxyl radical (PhO•) and their substituted derivatives occur widely in nature and are involved in many biological and industrial processes as crucial intermediates⁴⁸⁰. The phenoxyl radical is a simple prototype of a substituted aromatic radical and a model for tyrosyl radicals [TyrO• = *p*–(H₂N)(CO₂H)CHCH₂C₆H₄O•] in oxidized proteins. Tyrosyl radicals were found as stable cofactors in several metalloenzyme active sites including ribonucleotide reductase R2 protein⁴⁸¹, cytochrome *c* peroxidase, prostaglandin synthase⁴⁸², and the oxygen evolving complex of photosystem II⁴⁸³. Covalently modified analogues of TyrO• were detected in galactose oxidase⁴⁸⁴ and amine oxidase⁴⁸⁵. While the biological function of these radicals is not always well established, they are believed to form covalent cross-links between DNA and proteins⁴⁸⁶, to be involved in the catalytic cycles of a number of biosynthetic reactions and to serve as an electron transfer intermediate in photosynthesis⁴⁸³.

Phenoxyl derivatives also play a primordial role in the antioxidant activities of the phenolic components of Vitamin E⁷⁶. Because phenols are produced in the early stage of high temperature oxidation of benzenes, phenoxyl radicals are again postulated as key intermediates in the combustion of many aromatic compounds that are used as additives in lead-free fuels due to their high octane value⁴⁸⁷. In spite of their highly reactive nature which precluded direct structure determinations, a plethora of careful spectroscopic studies of phenoxyl radicals have been scattered throughout the literature. A considerable amount of information on the structure and properties of PhO• has thus been gained from numerous experimental electron paramagnetic resonance (EPR)^{457–459, 488, 489}, vibrational (IR, resonance Raman)^{490–498} and absorption (UV, visible)^{416, 499–506} spectroscopy studies.

a. Electronic structure. The unsubstituted PhO• radical exhibits a C_{2v} point group symmetry. The unpaired electron is expected to reside in a π -orbital which is anti-symmetric with respect to the two-fold axis and the reflection in the molecular plane. In this case, the notation of the corresponding irreducible representations depends on the choice of axes. Depending on whether the molecular plane is taken to be the first or the second plane of reflection, the ground state is denoted 2B_2 or 2B_1 . In the literature both labels 2B_1 ^{359, 455, 507–514} and 2B_2 ^{507, 508} have been used equally. Although this is a simple symmetry notation problem, it might cause a certain confusion!

We adopt here an axis convention in which the ground state of the phenolate anion (PhO⁻) is described by the following basic orbital configuration: ... (13a₁)² ... (8b₂)² ... (3b₁)² (1a₂)². The reference configurations for the 2A_2 , 2B_1 and 2B_2 electronic states of the neutral radical can hence be formed from this, making an electron hole in the 1a₂, 3b₁ and 8b₂ orbitals, respectively. The shapes of the singly-occupied orbitals b₁, b₂ and a₂ are displayed in Figure 40. Numerous *ab initio* calculations^{509, 510, 514} have indicated that, within this notation, the ground state π radical has 2B_1 symmetry. We are mainly concerned with the nature of the electronic states.

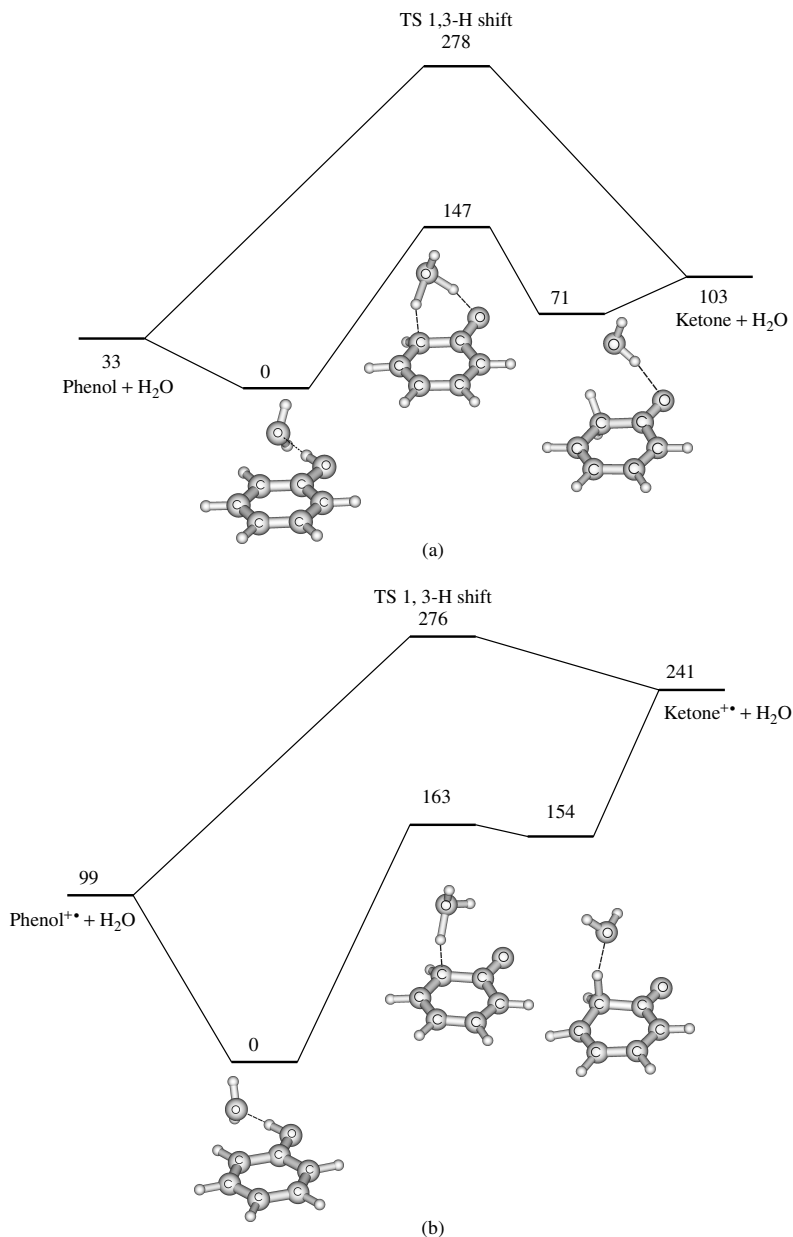


FIGURE 39. Schematic potential energy profiles showing the interconversion between phenol and cyclohexa-2,4-dienone in free and water-assisted systems: (a) in the neutral state and (b) in the ionized state. Values given in kJ mol⁻¹ were obtained from B3LYP/6-31G(d,p)+ZPE computations

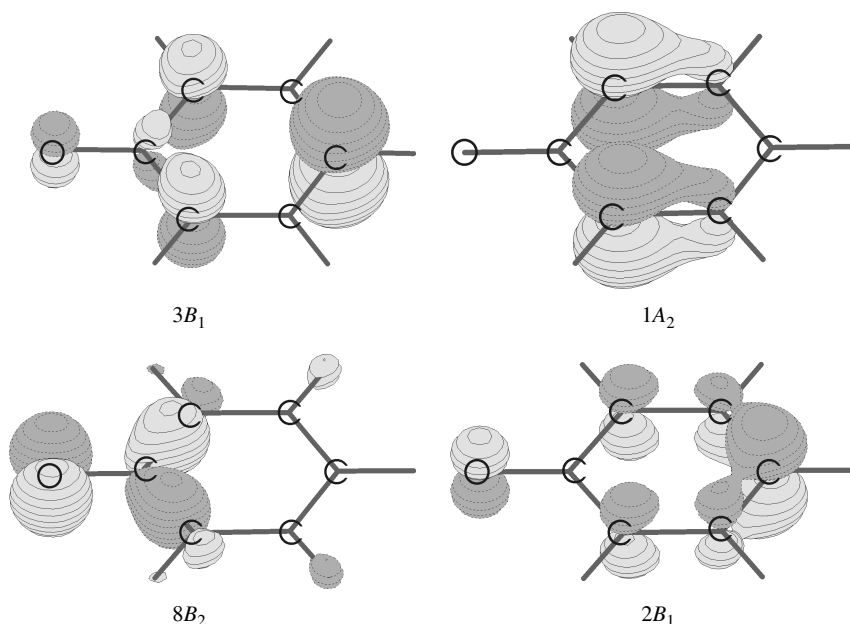


FIGURE 40. A representation of four different singly-occupied orbitals (SOMO) of the phenoxyl radical in the corresponding electronic states

Several electronic excitations have been identified experimentally. The early gas-phase absorption spectra^{499, 500} showed bands with λ_{max} at 395 nm (3.1 eV) and 292 nm (4.2 eV). A subsequent experimental study in a nitrogen matrix observed the analogues of these bands and an additional higher energy band with λ_{max} at 240 nm (5.2 eV)⁵⁰¹. A weak and broad band was detected in the 600 nm region with a peak centred at 611 nm (2.0 eV) and several other regularly spaced peaks whose spacings of about 500 cm^{-1} were presumably due to a vibrational progression^{416, 502–506}. An ultraviolet photoelectron spectroscopy study³⁷⁰ suggested, however, that the first excited state of phenoxyl radical appears rather at 1200 nm (1.06 eV). The identity of the 600 nm absorption band of PhO^\bullet and some of its derivatives was the subject of a subsequent study⁵⁰⁷ which also used the calculated transition energies and oscillator strengths to help the assignments.

When comparing all the available observed absorption bands and the energies calculated using the multi-reference CASSCF methods with large active space^{510, 515}, the following assignments of the observed transitions can be proposed: (i) the band at 1200 nm is due to the $1^2B_2 \leftarrow X^2B_1$ transition, (ii) 611 nm to $1^2A_2 \leftarrow X^2B_1$, (iii) 395 nm to $2^2B_1 \leftarrow X^2B_1$, (iv) 292 nm to $2^2B_2 \leftarrow X^2B_1$ and finally (v) 240 nm to $2^2A_2 \leftarrow X^2B_1$.

A possible problem concerns the transition $2^2B_2 \leftarrow 2^2B_1$, which is symmetry forbidden under C_{2v} symmetry and might cast doubt on the assignment of the 292 nm band. Experimentally, this band was observed to be weak and the relevant peak is almost completely obscured by the strong peak centred at 240 nm⁵⁰³. The CASSCF excitation energies were found to be overestimated by up to 0.5 eV, indicating the importance of dynamic electron correlation for a reasonable description of the excited states. Calculations on PhO^\bullet using small atomic basis sets turned out to give incorrect results.

b. Geometry and vibrational frequencies. There has been a persistent disagreement over the CO bond length of PhO \cdot and its stretching frequency^{353, 358–360, 370, 455, 508–519}. Indeed, values ranging from 1.22 Å to 1.38 Å were reported for the CO distance from a variety of wave functions. While both CASSCF(9,8)⁵¹⁰ and UMP2⁵¹⁵ treatments, in conjunction with various basis sets, resulted in a short distance of 1.22–1.23 Å, density functional methods yielded a consistently longer distance of 1.25–1.28 Å^{358, 359} (cf. Figure 41). Despite a variance between CASSCF and DFT results which might be due to the choice of the active spaces in CAS computations, it seems reasonable to admit that the CO distance in the radical is close to the length typical of a double bond (1.23 Å in *p*-benzoquinone), which is also in line with the inference from the observed CO stretching frequency⁴⁹⁸. As in the phenolate anion, PhO \cdot possesses a quinoidal structure with alternating long (1.45 and 1.40 Å) and shorter (1.37 Å) CC distances (Figure 41). The geometries of the neutral and the anion are in fact quite similar, with a noticeable difference being an increase in the C₆C₁C₂ angle of about 3° from the anion to the radical (cf. Figure 23, Section IV.B.1). The geometrical parameters remain almost unchanged upon halogenation, irrespective of the substitution position of the halogen (Figure 2). Even the *p*-amino^{509, 512} or *p*-methoxy⁵¹⁷ phenoxyl radicals, having a strong π -donor group, also do not represent a special case; their structure is found to be similar to that of the parent radical with very small modifications of the parameters.

In the lower-lying excited states, the molecular frame remains planar (Figure 42). The 2B_2 state has a longer CO distance, stretched up to 0.13 Å, becoming close to that of a single bond. In going from the ground state to the 2A_2 state, the C₂C₃ distance also increases by 0.09 Å whereas the change of the CO remains small. This could be understood in examining the shape of the corresponding singly-occupied orbitals involved in the electronic transition⁵⁰⁹. In both excited states, the CCC bond angles deviate significantly

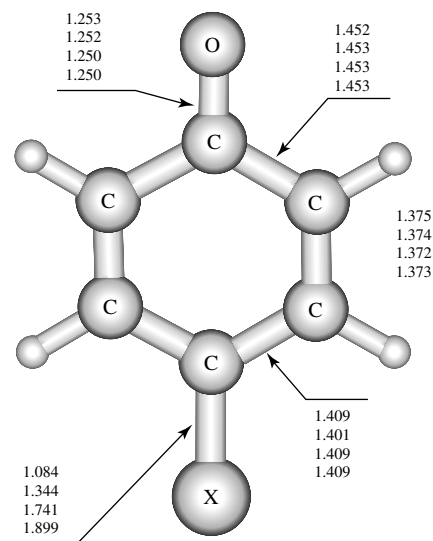


FIGURE 41. A comparison of the distances (in Å) for the phenoxyl radical and its *para*-halogenated derivatives. The entries are X = H (upper), F, Cl and Br (lower). Values were obtained from UB3LYP/6-311++G(d,p) optimizations

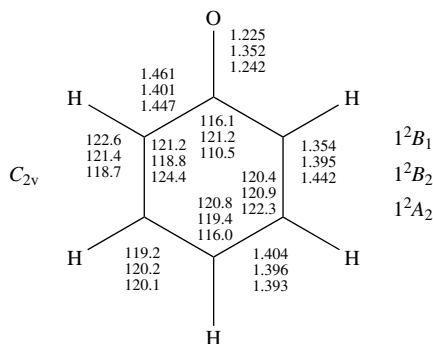


FIGURE 42. Comparison of the bond distances (Å) and angles (deg) of three lowest-lying electronic states of phenoxyl radical. Values obtained from UMP2/6-31G(d,p) optimizations

from the benzene value of 120° . Remarkably, all the CC distances of the 2B_2 state are close to 1.4 Å. All these changes suggest that the aromaticity of the benzene ring is probably preserved in 2B_2 but not in either 2B_1 or 2A_2 states.

The C_{2v} symmetry of PhO^\bullet leads to 21 in-plane modes (11 a_1 and 10 b_2) and 9 out-of-plane modes (3 a_2 and 6 b_1). The assignment of the associated frequencies was also the subject of considerable discussion among experimental^{492–498} and theoretical^{358, 359, 498, 509–518} chemists, in particular as regards the location of the CO stretching frequency. The resonance Raman spectra were observed^{492–494} for the phenoxyl- h_5 , phenoxyl-2,4,6- d_3 and phenoxyl- d_5 isotopomers. Thus, ten in-plane fundamental vibrations including eight totally symmetric a_1 modes and two non-symmetric b_2 modes were observed and now assigned. These fundamental vibrations are sketched in Figure 43 along with the experimental frequencies. High level calculation^{358, 359, 498, 510, 514, 518} agreed on the identity and absolute values of most of these modes. There is now a large consensus that the band observed near 1505 cm^{-1} , characterized by the strongest intensity in the resonance Raman spectra, should be assigned to a primary CO stretching, whereas the band centred at 1398 cm^{-1} , which was assigned earlier to the CO stretch³¹, corresponds rather to the CC stretch. The observed band near 1552 cm^{-1} is confirmed to arise from the C=C stretching vibration. These assignments were further supported by the downshifts upon deuteration and the larger shift of the C=C stretch relative to the CO stretch (the CO stretch occurs at 1487 cm^{-1} in phenoxyl-2,4,6- d_3 and 1489 cm^{-1} in phenoxyl- d_5). In addition, it was found that the resonance Raman spectrum for near-resonance with the excited 2^2B_1 state is dominated by the CO stretch mode⁵¹⁰. As mentioned above, the latter state is responsible for the absorption band centred at 400 nm. This finding was believed to lend further support for the assignment of the CO stretch band at 1505 cm^{-1} .

A correlation between the CO bond properties in the closed-shell molecules (single and double bonds) was proposed to estimate the bond lengths and stretching frequencies of open-shell phenoxyl radicals⁵¹². Nevertheless, while it is possible to estimate the CO force constants using the Badger-type relations, it is difficult to relate them to the experimental frequencies that do not represent the stretching of a single bond.

The CC and CO vibrations are also sensitive to the molecular environment by virtue of electrostatic and hydrogen bonding interactions. The frequencies of phenoxyl and tyrosyl radicals complexed by macrocyclic ligands⁵¹⁴ and generated *in vivo*⁵¹⁶ were measured by resonance Raman and FTIR techniques. Thus a selective enhancement of the vibrational CC and CO stretch modes of the phenoxyl chromophores in metal-coordinated radical

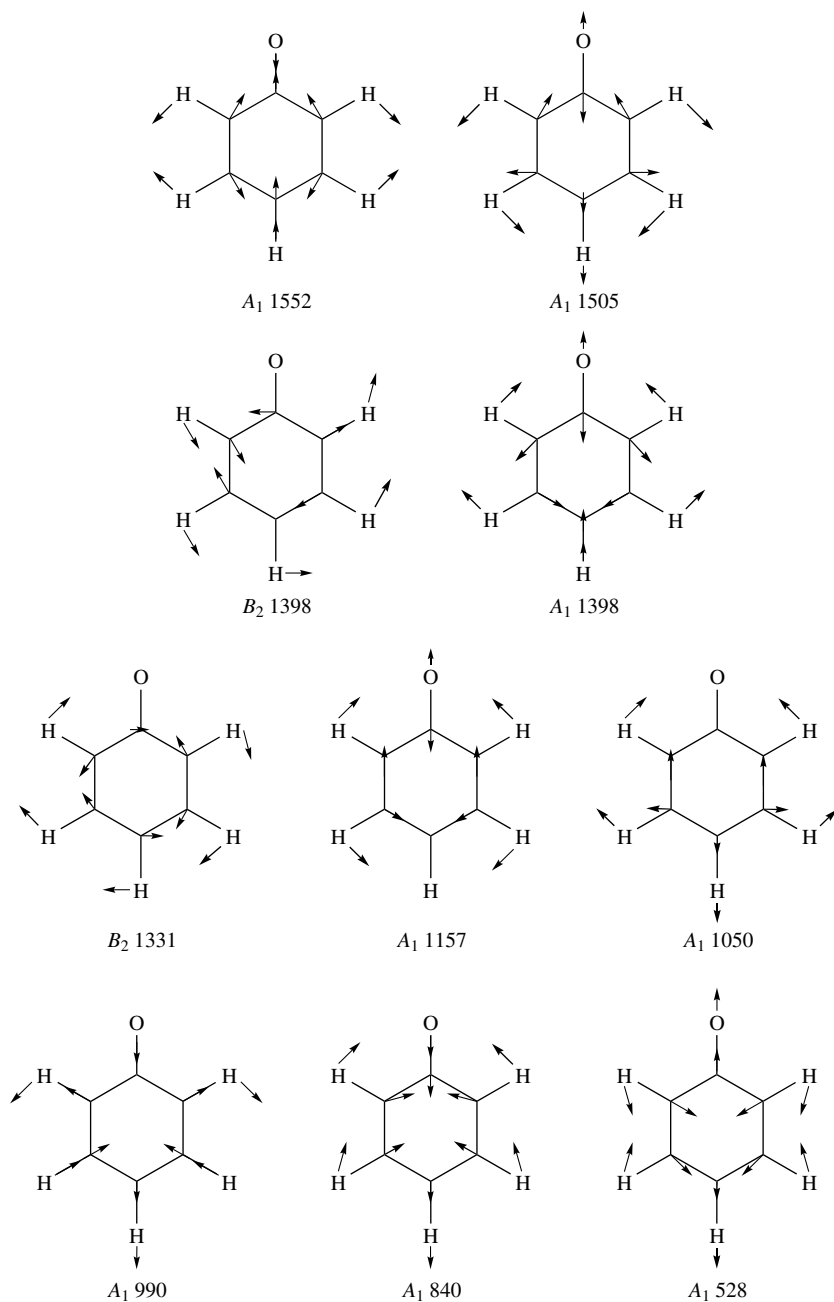


FIGURE 43. In-plane vibrational modes of phenoxyl radical and the experimental frequencies (values in cm^{-1})

complexes was achieved upon excitation in resonance with the transition at 410 nm. The CO stretch mode is found at 1505 cm^{-1} in aqueous alkaline solution, but at 1518 cm^{-1} for neutral pH^{514} , which indicates a certain H-bonding interaction with water molecules. These CC and CO modes are of special interest in as much as they could be used as sensitive spectral indicators for the semi-quinoidal structural and electronic properties of the coordinated phenoxyl radicals. Accordingly, an upshift of these frequencies should reflect an increased double bond character of the bonds, which in turn is paralleled by a contraction of the bond distance and also by a decrease in the spin density at the oxygen atom. For example, the $\text{C}=\text{C}$ frequency increases in the order: PhO^\bullet (1562 cm^{-1}) $< p\text{-CH}_3\text{C}_6\text{H}_4\text{O}^\bullet$ (1578 cm^{-1}) $< p\text{-CH}_3\text{OC}_6\text{H}_4\text{O}^\bullet$ (1595 cm^{-1}).

It is remarkable that the CO stretch frequencies calculated using DFT methods for free substituted phenoxyl radicals are invariably underestimated by $25\text{--}45\text{ cm}^{-1}$ with respect to the experimental values observed *in vivo* or in metal-coordinated complexes. This led to a proposition that the phenoxyl and related tyrosyl radicals exist as ion complexes *in vitro*⁵¹⁶. Computations on model systems such as PhO-M^+ or $\text{PhO-(H}_2\text{O)}_2$ provide some support for this view. In spite of the fact that the CO distance is somewhat lengthened following complexation with an alkali metal cation ($\text{M} = \text{Li}^+, \text{Na}^+, \text{K}^+$; see geometrical parameters displayed in Figure 44), the resulting CO stretching frequency turns out to be enhanced by $60\text{--}70\text{ cm}^{-1}$ relative to the uncomplexed system, likely due to the underlying electrostatic interaction. Specific H-bonding interaction of the radical with water molecules also induces an enhanced CO stretching, but to a lesser extent, by about 30 cm^{-1} .

c. Spin densities. The EPR spectrum of PhO^\bullet has been studied in considerable detail, and the different sets of experimental hyperfine splitting constants (hfcc values) obtained for hydrogen atoms^{457–459, 488, 489} consistently offered the following picture: $a(\text{ortho-H}_2) = 6.6\text{--}6.9\text{ G}$, $a(\text{meta-H}_3) = 1.8\text{--}1.9\text{ G}$, and $a(\text{para-H}_4) = 10.1\text{--}10.2\text{ G}$.

In general, density functional methods in conjunction with the unrestricted formalism could satisfactorily reproduce the characteristics of the spin distribution and the

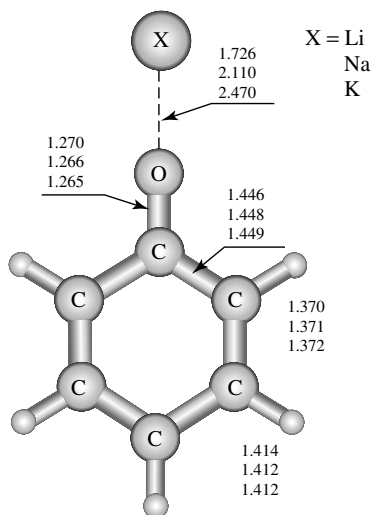


FIGURE 44. Comparison of the distances (Å) in phenoxyl radical—alkali cation complexes. The entries are $\text{X} = \text{Li}^+$ (upper), Na^+ and K^+ (lower), UB3LYP/6-311++G(d,p) values

experimental values within the errors of at most $\pm 15\%$, depending on the basis set employed^{511, 517, 518}. For example, the popular UB3LYP/6-311++G(d,p) method provides the following values, including the occurrence of negative spin densities on both *ortho* and *para* hydrogens: $a(\text{H}_2) = -6.8$ G, $a(\text{H}_3) = 2.6$ G and $a(\text{H}_4) = -8.8$ G. This constitutes a good performance bearing in mind that the spin densities at nuclei (Fermi contact terms) are known to be difficult to determine from molecular orbital wave functions (due to the cusp problem and spin contamination in UHF references). Calculations⁵¹⁸ showed that the corrections for vibrational averaging and polarization by the solvent are rather small. While a negligible correction (< 0.1 G) was estimated for the vibrational effect, a slight reduction of at most 0.6 G is due to the effect of a bulk solvent.

The spin density on oxygen $a(\text{O})$ is calculated to vary from -8 to -10 G. Nevertheless, the lack of a significant coupling at the oxygen site in radical–radical reactions is consistent with a dominant odd-alternate cyclic resonance structure in which the radical centre is displaced into the ring. The absolute hfcc values are only moderately changed upon the introduction of a halogen substituent into the benzene ring. The largest effects are found for a fluorine substitution at the *meta* position, which induces a decrease of 0.7 G on $a(\text{H}_2)$ and an increase of 0.4 G on $a(\text{H}_4)$. The methyl substituent also induces a marginal effect. As a consequence, spin densities of the phenoxyl side-chain in TyrO• radicals are very close to those of free PhO•. There is thus no evidence for a spin delocalization onto the tyrosyl peptide chain⁵¹³.

The general trend found earlier⁵¹⁹ for the aromatic hydrogen hfcc values is confirmed, namely $a(\text{H}_4) > a(\text{H}_2) > a(\text{H}_3)$. In view of the empirical McConnell relationship, the spin population on the adjacent carbon atoms could be taken to be proportional to the hfcc values of hydrogen atoms bound to them. Thus, the experimental hfcc values of phenoxyl radical show much larger spin density on the *para* and *ortho* carbons ($\rho_{\text{para}}/\rho_{\text{ortho}} = 1.5$) than on the *meta* carbon ($\rho_{\text{para}}/\rho_{\text{meta}} = 5.3$). While calculations are able to account for the ratio of *para* and *ortho* carbons, the trend for the *meta* carbon spin densities is not consistent with that suggested by the McConnell relationship.

As for a possible reason for this disagreement, we consider the spin densities in terms of different components⁵¹⁸. In general, the spin densities can be decomposed into three contributions: (i) a delocalization, or direct term which is always positive, (ii) a spin polarization or indirect term, arising from the singly-excited configurations and (iii) a correlation term originating from the contribution of higher excitations^{520, 521}. The spin polarization term arises from the fact that the unpaired electron interacts differently with the two electrons of a spin-paired bond; the exchange interaction is only operative for electrons with parallel spin. The shorter average distance between parallel spin than between antiparallel spins leads to a spin polarization illustrated by the map of spin densities in the molecular plane (Figure 45) whose sign is governed by some general rules⁵²⁰. Because the molecular plane is actually the nodal plane of the SOMO, the only contribution to spin density at nuclei should come from indirect spin polarization terms. The latter can again be decomposed into different first-order and second-order components. As the SOMO (b_1) is mainly localized on *ortho* and *para* carbon atoms leading to large π -spin populations on these atoms, large positive spin densities are thus induced at the corresponding nuclei and negative short-range hfcc values at *ortho* and *para* hydrogens. The positive spin population at an *ortho* carbon induces for its part a negative spin population at the *meta* carbon (first-order effect) and thereby a positive but weak (of second-order character) spin density at the *meta* hydrogen. The same mechanism is operative for the *para* carbon, yielding an additional contribution to the *meta* hydrogen. Overall, the *meta* hydrogens receive non-negligible positive spin densities resulting from cumulative second-order effects. If the oxygen atom was replaced by a more electronegative group, the hfcc values of *ortho* and *para* hydrogens would increase whereas the hfcc values of *meta* hydrogen would remain roughly unchanged due to cancellation of effects.

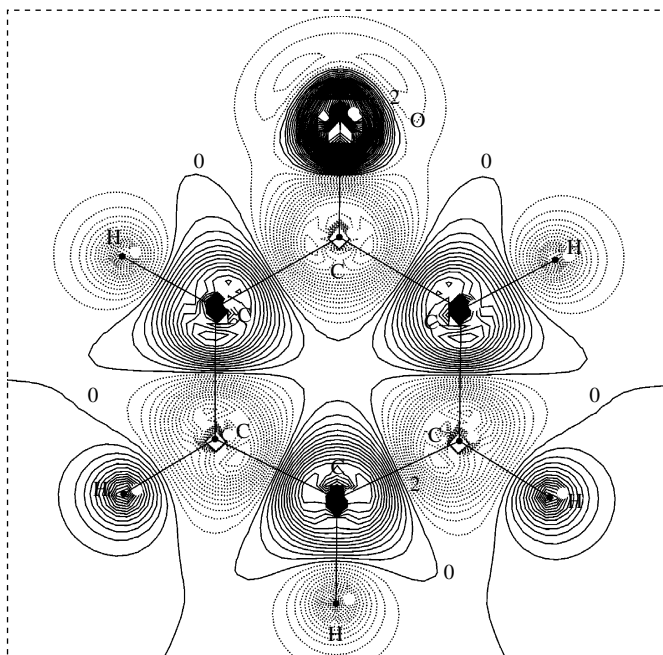


FIGURE 45. Isocontour spin density plot in the molecular plane of phenoxyl radical. Contour levels are spaced by 0.0005 a.u.

The McConnell relationship⁵²⁰ basically converts spin population due to delocalization (direct term) into spin polarization (indirect term). It could strictly be applied to the first-order spin polarization effects and thus correctly account for the *ortho* and *para* carbon ratio spin densities of phenoxyl radical from hydrogen hfcc values. On the contrary, it could hardly be applied to more subtle second-order mechanism such as is the case of *meta* carbon and hydrogen atoms, and this is the probable reason for the disagreement revealed above. In the unrestricted spin formalism (UHF, UB3LYP), the spin polarization is directly included in the wave function together with delocalization. As a consequence of the unavoidable spin contamination by higher spin states, unrestricted methods tend to overestimate the spin polarization terms. That is the likely reason for a larger calculated value of the hfcc of the *meta* hydrogen compared with the observed values.

d. Decomposition of phenoxy radical. Under combustion conditions, this radical undergoes a thermal decomposition whose primary products are found to be cyclopentadiene radical (C_5H_5) and carbon monoxide⁴⁸⁷. Two mechanisms have been proposed^{21, 522} to rationalize the decarbonylation. Results of kinetic measurements, thermochemical considerations²¹ and quantum chemical computations of the potential energy surfaces^{523, 524} concur with each other and point towards the dominance of the molecular mechanism depicted in Figure 46. In brief, this involves the formation of the bicyclic intermediate **A** via the transition structure **TS-A**, followed by an α -CC bond cleavage via **TS-B** yielding the five-membered ring **B**. Finally, the elimination of the CO moiety from **B** through **TS-C**, producing the main products **C**, is an obvious

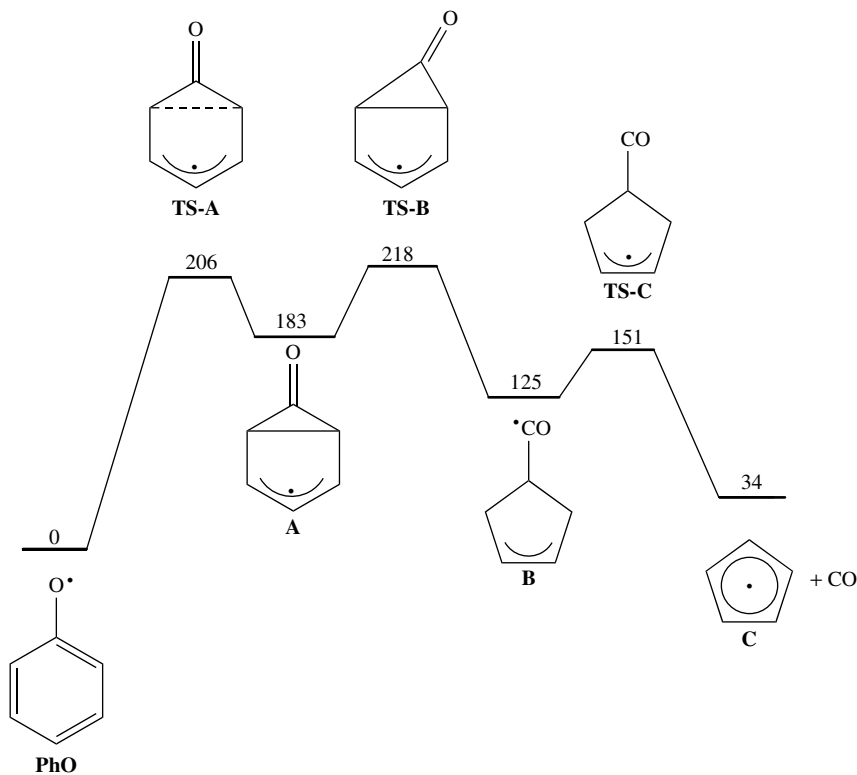


FIGURE 46. A schematic potential energy profile showing the CO elimination from phenoxyl radical. Relative energies, given in kJ mol⁻¹, were obtained from CASPT2/CASSCF(8,7)/6-311G(d,p)+ZPE computations. Adapted from Reference 524 with permission

step with low energy barrier. The rate-determining step corresponds to the formation of the five-membered cycle **B**. Using a modified G2M scheme based on coupled-cluster energies⁵²⁴, the transformation is associated with an energy barrier of 218 kJ mol⁻¹, which is significantly larger than the experimental estimate of 184 kJ mol⁻¹²¹. Note that the first step $\text{PhO}^\bullet \rightarrow \text{A}$ is a symmetry-forbidden process, which could take place either via a non-symmetrical transition structure or through an avoided crossing mechanism. The energy barrier in both cases are close to each other (205 kJ mol⁻¹) and slightly smaller than for the rate-controlling step. The mechanism found for the PhO^\bullet decomposition is thus comparable to, but simpler than, the decarbonylation of the phenol radical cation discussed in a previous section. The key intermediate in both cases is in fact a high-energy five-membered cyclic species. Kinetic evaluations using the RRKM method in conjunction with the computed energetic and geometric parameters yielded rate constants close to the experimental values, especially for temperatures below 1200 K.

Let us also mention that interest in atmospheric chemistry and combustion chemistry of PhO^\bullet led to a number of theoretical studies of its reactions with simple radicals such as atomic oxygen⁵²⁵, HOO^\bullet radical⁵²⁶, NO and NO₂ radicals^{527, 528} and molecular oxygen⁵²⁸. In all cases, computation of the potential energy surfaces has helped a great

deal in the interpretation of reaction mechanisms and/or provided necessary parameters for appropriate kinetic analyses.

2. Antioxidant activity of phenols

a. The O–H bond dissociation energies. As discussed in previous sections, the adiabatic electron affinity and the proton affinity of phenoxyl radical were determined quite reliably and they amount to $EA_a(\text{PhO}^\bullet) = 2.25 \text{ eV}^{370}$ and $PA(\text{PhO}^\bullet) = 860 \text{ kJ mol}^{-1 442}$, respectively. The substituent effect on the PAs has been examined in a previous section. Note also that a *para*-methyl group induces an increase of 20 kJ mol^{-1} on the proton affinity of phenoxyl radicals⁵²⁹. Concerning the adiabatic ionization energy, a tentative value of 8.56 eV was suggested⁵²⁹. Nevertheless, our high-level coupled-cluster computations revealed that this value is likely somewhat too low and suggested a higher value of $IE_a(\text{PhO}^\bullet) = 8.8 \pm 0.2 \text{ eV}^{530}$.

Combination of the phenol acidity $\Delta H_{\text{acid}}(\text{PhOH}) = 1458 \pm 8 \text{ kJ mol}^{-1}$ and the EA value given above yields the gas-phase bond dissociation energy of phenol $BDE(\text{PhO–H}) = 362 \pm 8 \text{ kJ mol}^{-1 124, 370}$. Photoacoustic calorimetry studies in various solvents having different hydrogen-bond accepting properties provided values ranging from 360 to $369 \text{ kJ mol}^{-1 191, 531}$. A spectroscopic ESR equilibrium method for measuring differences in BDEs of substituted phenols yielding transient phenoxyl radicals led to a value of $369 \text{ kJ mol}^{-1 532}$. The BDE is thus not very sensitive to the environmental properties.

Use of the above values together with the standard heats of formation $\Delta H_f^\circ(\text{PhOH}) = -96 \pm 1 \text{ kJ mol}^{-1}$ and $\Delta H_f^\circ(\text{H}) = 218 \text{ kJ mol}^{-1}$ leads to the heats of formation $\Delta H_f^\circ(\text{PhO}^\bullet) = 48 \pm 8 \text{ kJ mol}^{-1}$ for the neutral radical, and $\Delta H_f^\circ(\text{PhO}^+) = 897 \pm 8 \text{ kJ mol}^{-1}$ for the cation.

The quantity $BDE(\text{PhO–H})$, which constitutes a measure of the O–H bond strength, is by far smaller than $BDE(\text{HO–H}) = 498 \text{ kJ mol}^{-1}$, which is well established for water. Its magnitude is closer to that of $BDE(\text{C–O})$ in phenyl ethers⁵³³. Electron donor groups such as CH_3 and CH_3O tend to cause destabilization in phenols, but stabilization in the corresponding phenoxyl radicals and the combined effect usually lead to a markedly reduced $BDE(\text{O–H})$. An electron-withdrawing group has the opposite effect. Use of a multiple substitution of electron donor groups results in substantial O–H bond weakening due to the radical stabilizing effect. The BDE of α -tocopherol, the major and bioactive component of vitamin E, was measured by photoacoustic calorimetry to be 40 kJ mol^{-1} lower than that of phenol obtained by the same technique¹⁹¹. Similarly, the value for δ -tocopherol, which is the minor and least bioactive component, was measured to be 10 kJ mol^{-1} larger than that of the α -component. Thus, a small difference of 10 kJ mol^{-1} on the BDEs of the phenolic bond already makes a marked variation on the bioactivity¹⁹¹. Amino groups in the *ortho* position appear to induce a large O–H bond weakening of more than 59 kJ mol^{-1} and thus represent a peculiar group.

In general, the effect that a substituent exerts on the phenoxyl radical is by far more important than that on the corresponding phenol. An empirical equation⁵³⁴ relating the differences in phenolic O–H strengths (in kJ mol^{-1}) to the sums of the σ -constants for all the ring substituents has been proposed (equation 34),

$$\Delta BDE(\text{O–H}) = 30 \left[\sum (\sigma_{\text{ortho}}^+ + \sigma_{\text{meta}}^+ + \sigma_{\text{para}}^+) \right] - 2 \quad (34)$$

where the relationship $\sigma_{\text{ortho}}^+ = 0.66\sigma_{\text{para}}^+$ is presupposed. A simple group additivity scheme also allowed the BDE to be evaluated with high accuracy^{116, 192}. This quantitative consideration confirms the ease with which substituted phenols lose their phenolic hydrogens

and points towards the main reason for their inherent antioxidant activities. The BDEs should thus be used as a reliable primary indicator in the search for novel antioxidants more active than vitamin E^{116, 140, 192, 198, 201}.

The radical stabilization energies (RSE) in a compound of the type ROH can be defined as

$$\text{RSE}(\text{ROH}) = \text{BDE}(\text{O-H})_{\text{ref}} - \text{BDE}(\text{O-H})_{\text{ROH}}$$

When taking the value $\text{BDE}(\text{O-H})_{\text{ref}}$ of 440 kJ mol^{-1} in a saturated alcohol as reference, $\text{RSE}(\text{PhOH})$ is found to be 80 kJ mol^{-1} , which is in line with the view that in PhO^\bullet is rather a resonance-stabilized radical in which the radical center is not fully centered on the oxygen atom. Regarding the substituent effects, a few general remarks can be noted: (i) In substituted radicals, the stability is influenced not only by the polar effect but also by the spin delocalization. While the polar contribution is related to the ability of the substituent to delocalize the lone pair on the phenolic oxygen, the spin delocalization is more characteristic of the radical stabilization. (ii) There are various approaches for estimating both effects using isodesmic reactions or charge distributions (electrostatic potentials, spin densities)^{125, 193}. It has been found that the polar contribution is more important than the spin delocalization. (iii) For electron donor groups, both effects tend to stabilize the radical. (iv) In contrast, electron-withdrawing groups considerably destabilize the radical by virtue of the polar effect; although the spin delocalization tends to stabilize it, the destabilizing polar effect remains dominant. In this regard, the difference in reactivity between the isoelectronic phenoxyl (PhO^\bullet) and benzyl (PhCH_2^\bullet) radicals resides in the fact that oxygen is a strong π -acceptor whereas methylene is a poor electron-withdrawing group. As a result, the stability of the benzyl radicals is less sensitive to the polar effect of a substituent.

b. Antioxidant activities. The reaction of molecular oxygen with organic molecules under mild conditions is usually referred to as autooxidation. It can be represented by the following simplified reaction scheme (equations 35–39).



While reaction 36 is very fast, having a rate constant of $ca\ 10^9 \text{ M}^{-1} \text{ s}^{-1}$, reaction 38 is much slower at $10^1 \text{ M}^{-1} \text{ s}^{-1}$. All organic materials exposed to the air undergo oxidative degradation. Reduction of the rate of such degradation utilizing low concentrations of ‘antioxidants’ is important for all aerobic organisms and for many commercial products. In this respect, phenols turn out to represent a primordial family of antioxidants. Their activity arises from their ability to trap chain-carrying peroxy radicals by donating the phenolic hydrogen atom (reaction 39), which is a much faster reaction than the attack of the peroxy radicals on the organic substrate (reaction 37), thanks to the smaller $\text{BDE}(\text{PhO-H})$ values as discussed above.

The idea that autooxidation affects humans (and other mammals) was put forward in the mid-1950s by the so-called free-radical theory of ageing⁵³⁵. It was suggested that ageing is the result of endogenous oxygen radicals generated in cells during the normal course

of metabolism, disrupting the structure of biopolymers and resulting in cellular damage. This theory provided a mechanistic link between the metabolic rate and ageing. This link was noticed nearly a century before, when it was observed that animals with higher metabolic rates often have a shorter life span. A careful analysis further demonstrated that production of free radical species rather than metabolic rates provides the strongest correlation with longevity⁵³⁶.

The relevant free radicals can be either produced endogenously as a consequence of metabolic activities or generated from different environmental sources such as ionizing radiation, ultraviolet light, chemotherapeutics, inflammatory cytokines or environmental toxins⁵³⁷. The balance of free-radical production and antioxidant defence determines the degree of oxidative stress. When the stress is severe, survival depends on the ability of the cell to resist the stress and to repair or replace the damaged molecules. If the oxidative stress and the ability to respond appropriately is important for ageing, then it follows that factors that increase resistance to stress should have anti-ageing benefits and lead to enhanced life span. After many years of research, it has been shown that mammalian maximum life span cannot be significantly increased with antioxidants, but the mean life span for mammals can be increased. In the light of these results, a 'disease-specific free-radical theory of ageing'⁵³⁷ has been formulated, in which free radicals are involved in the etiology and development of many of the chronic diseases that contribute to shorten the (maximum) life span potential for a species. For humans, these chronic diseases particularly include atherosclerosis, emphysema and cancer.

At this point the antioxidants which are expected to protect key cell components from damage intervene by scavenging free radicals and are therefore to attenuate—in part—the diseases. Much progress has been achieved in our understanding of the role played by antioxidants in the maintenance of optimal health. It is now well established that vitamin E is the major lipid soluble, peroxy radical-trapping chain-breaking antioxidant in human blood plasma^{76, 538, 539} and in normal and cancerous tissues⁵⁴⁰.

The naturally occurring vitamin E consists of four components, namely α , β , γ and δ tocopherols (TOH). These four molecules, which differ from each other by the number and position of methyl groups attached to the phenol ring, reveal a rather different antioxidant activity. The following results show that the ordering of antioxidant activity of the tocopherols *in vitro*⁵⁴¹ is $\alpha > \beta$, $\gamma > \delta$, which is almost the same order as their *in vivo* activities ($10^4 \cdot k_4$ values in $\text{M}^{-1} \text{s}^{-1}$ are 320 for α -TOH, 130 for β -TOH, 140 for γ -TOH and 44 for δ -TOH).

In other words, the α -TOH is the most active component of the vitamin E, responsible for its high antioxidant activity. The reason for this phenomenon could be found in the difference in BDE(O—H) values discussed above.

c. Features of hydrogen atom abstraction from phenols. In order to have a deeper appreciation of the remarkable aptitude of vitamin E as antioxidant⁵⁴¹, the details of the mechanism of reaction 39 will be examined.

Let us consider Figure 47, which vividly shows the reaction profile of the hydrogen atom abstraction (reaction 39) from structurally related model compounds—phenols with various numbers of methyl groups in the ring—by the simplest peroxy radical $\cdot\text{OOCH}_3$. In the case of the parent phenol **I**, the classical reaction barrier separating the reactant and product H-bonded complexes amounts to 28 kJ mol^{-1} , whereas the two minima of the corresponding H-atom double-well potential are nearly isoenergetic. The presence of methyl groups in the phenol ring stabilizes the phenoxyl radicals, lowers the barrier and makes the reaction certainly exothermic. In particular, substitution of two methyl groups in the *ortho* positions reduces the reaction barrier by about 8 kJ mol^{-1} , whereas a third CH_3 group in the *meta* position decreases it further by *ca.* 3.0 kJ mol^{-1} . Invoking the Hammond

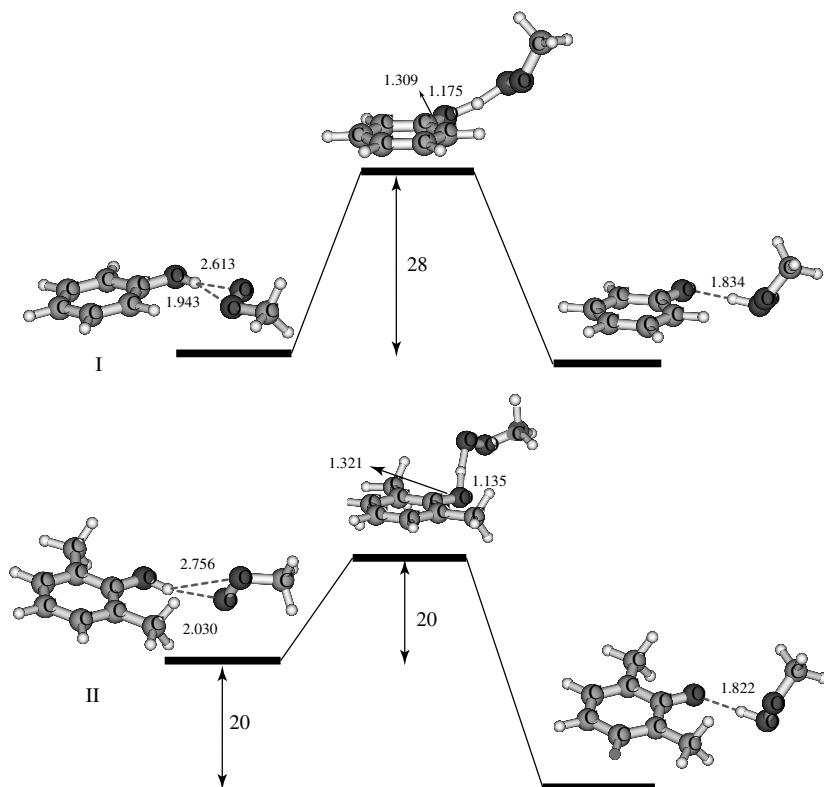


FIGURE 47. Schematic energy profiles illustrating the hydrogen abstraction reaction of a peroxy radical $\text{CH}_3\text{OO}^\bullet$ with (I) phenol and (II) 2,6-dimethylphenol. Relative energies (given in kJ mol^{-1}) were obtained from UB3LYP/6-31+G(d,p)+ZPE calculations. Adapted from Reference 551 with permission

postulate, one can in fact relate the stability of the phenoxyl radical to the stability of the transition state structure. In the case of 2,6-dimethylphenol **II**, the corresponding phenoxyl radical is stabilized with respect to the parent molecule by 20 kJ mol^{-1} and the transition state structure is more reactant-like than the counterpart of the unsubstituted phenol and occurs at the phenolic C—O and O—H distances of 1.321 Å and 1.135 Å (cf. 1.309 Å and 1.175 Å in phenol **I**, respectively).

What make other structural factors of α -TOH such a good antioxidant? Extensive investigation on the effect of various substituents on the k values for reaction 39 in simple phenols⁵⁴² led to the conclusion that the ‘best pattern’ of substituents in the phenol ring required to facilitate this reaction is optimally the methoxy group residing in the *para* and four methyl groups in the remaining positions. Many years later, it was found that 4-methoxy-2,3,5,6-tetramethylphenol, which structurally approximates α -TOH, is actually a much less active compound than all tocopherols^{76, 538}. A clue that helps us to rationalize this marked difference is provided by the X-ray structures of related molecules⁷⁶. The oxygen’s π -type lone pair of the methoxy group can stabilize the phenoxyl radical by resonance overlap with its singly-occupied molecular orbital and the degree of such interaction depends on the angle (θ) between this pair and aromatic π -orbitals.

Knowing the extremely important role of phenolic antioxidants in both biological and commercial systems, extensive experimental and theoretical studies have been conducted in the past on these species^{543–552}. However, an unambiguous understanding of the physical mechanism of the reaction of phenols with free radicals was hindered by insufficient knowledge about the potential energy surface of reaction 39. By analyzing the geometries displayed in Figure 47, one can easily see that while the minimum-energy hydrogen-bonded complexes are characterized by a planar orientation of the phenol OH group, in transition state structures this bond is twisted out-of-plane. Such twisting occurs due to the fact that the TSs for such reactions are formed by the avoided crossing of two lower-lying electronic states of phenoxyl radical, which takes place at some angle τ between the OH bond and the aromatic ring plane, while the in-plane reaction pathway ($\tau = 0$) is characterized by the intersection of these surfaces⁵⁵¹. In view of this fact, it is interesting to note that the barrier to internal rotation of the OH group (V_τ) which partly contributes to the activation barrier of reaction 39 is also influenced by a stereoelectronic effect of the lone pair of the *para*-alkoxy oxygens. When the latter is oriented perpendicular to the ring, the overlap is maximal and resonance structures with the doubly bound methoxyl oxygen prohibit a simultaneous conjugation of phenolic OH group with the ring, which results in decreasing V_τ . Correlations of V_τ and k values for reaction 39 with known or expected θ were established experimentally⁵⁵².

V. HYDROGEN BONDING ABILITIES OF PHENOLS

A. Introductory Survey

Molecular design requires detailed knowledge of hydrogen bond strengths, at least as much as knowledge of the polar atoms participating in such bonding. Phenol is rather specific in this respect because it involves the phenolic oxygen atom which is usually regarded as a major hydrogen acceptor due to its lone pairs. However, on comparison, for example, with furan, the hydrogen bond ability of phenol is determined by the degree of delocalization of the oxygen lone pair electrons into the π -system of the phenol ring.

On the other hand, phenols as proton donors actually occupy a very particular position among organic acids due to the well-known fact that by changing the substituents in the phenyl ring, we can readily regulate, almost continuously pK_a values from 10 to 0. For example, 4-CH₃OC₆H₄OH is characterized by a pK_a equal to 10.21. Furthermore, we are also able to record readily the extent of proton transfer because it evokes a change in the electronic spectrum of phenol. The long-wavelength 1L_b phenolic band is rather sensitive to the hydrogen bond formation. The stronger the hydrogen bond, the stronger the bathochromic shift and hyperchromic effects, and after the proton transfer, a further bathochromic shift and increase in intensity take place on increasing the charge separation. The largest bathochromic shifts of the 1L_b bands are observed for free phenolic anions. The UV-VIS spectra of hydrogen-bonded complexes with phenols reflect not only the proton transfer process, but also a continuous displacement of the proton along the hydrogen bond bridge⁵⁵³.

The literature on the hydrogen-bonded complexes of phenols with various proton acceptors and the corresponding proton transfer equilibria covers literally thousands of papers. First of all, it is worth mentioning the monograph by Davies²⁰², the reviews by Zeegers-Huyskens and Huyskens²¹⁰ and by Müller and coworkers⁵⁵³. Several groups^{203–209, 554–573} made important contributions to elucidate the nature of the hydrogen bonding and proton transfer in complexes with phenols. Hydrogen-bonded complexes with phenol have been the subject of numerous studies at both experimental (e.g. molecular beam spectroscopy^{164, 409, 412, 574–591}) and theoretical levels. Surveying briefly the achievements in this area, we would like to mention that the

hydrogen-bonded complexes of phenol with proton-accepting molecules such as ethers and alcohols are known to shift the spectra to longer wavelengths from that of the parent phenol by 200–400 cm⁻¹, depending on the proton-accepting strength of the bases^{33, 553, 574, 592–596}. Clusters of phenols with ammonia^{473, 577, 597} and amines have been studied^{125, 164, 473, 550, 568, 577, 588, 598–607}. Among these studies, it is worth mentioning a recent work⁶⁰⁸ using BLYP/6-31G(d,p) calculations on complexes of ammonia with phenol, and its *p*-nitro, pentafluoro-, 2,6-difluoro-, 4-nitro- and 2-fluoro-4,6-dinitro derivatives. Under complexation with ammonia, these phenol derivatives show a growing acidity which, as expected, may lead to proton transfer in the gas phase, but which was observed in solution and the condensed phase. Alas, contrary to the growing acidity due to the p*K*_a change from 9.95 to 2, no proton transfer along the hydrogen bond O–H···N towards ammonia has been predicted. Interestingly, the interaction between the very strong proton sponge bases and phenols was studied in non-aqueous solutions using UV-VIS and IR spectroscopy⁶⁰⁹. The present survey continues in Table 34.

Mannich bases formed from formaldehyde, secondary amines and *ortho*-derivatives of phenol and Schiff bases derived from aromatic *ortho*-hydroxyaldehydes are treated as rather convenient model systems to study intramolecular proton transfer^{25, 621, 647–676}.

The hydrogen bonded clusters of phenol with water and methanol have been investigated rather thoroughly, both experimentally and theoretically, for several reasons. The key reason is that they can be considered as model systems for larger aggregates. We will discuss phenol–water clusters in Section V.B while the discussion of the phenol–methanol clusters will only be confined to listing the corresponding references^{474, 574, 575, 596, 677–679} (note that the complex between PhOH and the NH₂ radical has recently been studied⁶⁸⁰). We will tell a more exciting story about hydrogen bonding between phenol and acetonitrile, and two brief stories about a very short O–H···N hydrogen bond recently determined in the 1:1 crystalline adduct of 2-methylpyridine and pentachlorophenol and about the hydrogen-bonded complex of phenol and benzonitrile. Before doing so, let us start with some interesting observations.

Phenol may also interact with some molecules directly via its aromatic ring due to a so-called π -bonding. For instance, spectroscopic measurements have revealed that phenols form π -bonded complexes in their ground electronic states with rare gas atoms (Rg) and methane^{164, 576, 681–686}. On the other hand, phenols form only hydrogen bonds with ligands such as, CO and N₂ which have nonvanishing dipole and/or quadrupole moment^{164, 478, 686–688}. As shown recently⁶⁸⁹ in IR experiments and *ab initio* calculations, phenol cation may form two stable complexes with Ar: one is hydrogen bonded whereas the other is π -bonded. The former occupies the global minimum. A similar situation occurs with the phenol cation–N₂ complex.

If phenol forms hydrogen-bonded complexes with some molecules, it is natural to study proton transfer along these hydrogen bonds if the proton transfer PES has a double-well character. However, it has been stressed that an enhanced p*K*_a of the hydrogen-bonded complex upon electron transfer favours a concerted proton-coupled electron-transfer mechanism⁶⁹⁰. It implies that after electron transfer, a double-well proton potential is converted to a single minimum potential corresponding to proton transfer. For instance, recent *ab initio* studies of the radical cation complexes of phenol with water^{476, 691} and molecular nitrogen⁴⁷⁸ gave group distances which are substantially shorter compared to those in neutral complexes. This suggests⁶⁹⁰ that the proton PES might have a vanishing or rather small barrier. Adding more water molecules to the phenol–water cation radical complexes leads to the stabilization of the proton-transferred forms¹¹³. Regarding hydrogen-bonded complexes of phenol with ammonia, only the proton-transferred structures were found to be stable^{472, 597}.

TABLE 34. References for some experimental and theoretical data on the hydrogen-bonding ability of phenol and its derivatives. The pK_a value of phenol and its derivatives is indicated in parentheses

Phenol	Hydrogen bond partner ^a	Method of study	Reference
Phenol (9.94)	<i>N,N</i> ,9-Trimethyladenine	IR	610
	1,10-Phenanthroline derivatives	IR	611
	Pyridine, 3-I-pyridine	IR	611, 612 ^b
	Conjugated imines	IR	613
	BIPA	IR	614
	PCA	IR	615
	<i>N</i> -Heterocyclic bases	IR	616
	Triethyl thiophosphate	IR	617
	Caffeine, 1,3-dimethyluracil	IR	618
	Pyridazine, pyrimidine, pyrazine	IR	619, 620
	<i>N,N</i> -DMBA, <i>N</i> -BMA	IR	621
	Dioxane, water, methanol, dimethyl ether, cyclohexene, benzene, tetrahydrofuran	Fluorescence excitation spectra	574
	(HCOOH) _{<i>n</i>} <i>n</i> = 1, 2	R2PI, IR-UV, DF HF/6-31G(d,p)	622
	(CH ₃ COOH) _{<i>n</i>} <i>n</i> = 1–4	R2PI, IR-UV, DF HF/6-31G(d,p)	623
	Phenoxides, TMA oxide	IR	624
	Ethanol	DF	33, 574
	Acetonitrile	IR	612
	TMA	IR, B3LYP/6-31G(d,p)	625
	Methanol	IR	626, 627
	Quinuclidine	IR, NMR	628
	<i>N</i> -Mono- and <i>N,N'</i> -dioxides	IR	629–631
	TMA <i>N</i> -oxide	IR	632, 633
	TMA acetate	IR	634, 635
		PhOH rotational coherence spectroscopy + B3LYP/6-31G(d)	636
4-F-Phenol	Bathocuproine	IR	611
	Triethyl thiophosphate	IR	617
	Pyridazine, pyrimidine, pyrazine	IR	619
4-Cl-Phenol	<i>N</i> -Heterocyclic bases	IR	616
	Triethyl thiophosphate	IR	617
	<i>N,N</i> -DMBA, <i>N</i> -BMA	IR	621
	<i>n</i> -Propylamine	IR	637 ^c

(continued overleaf)

TABLE 34. (continued)

Phenol	Hydrogen bond partner ^a	Method of study	Reference
3-Br-Phenol (9.03)	<i>N,N</i> ,9-trimethyladenine	IR	610
	Conjugated imines	IR	613
	BIPA	IR	614
	PCA	IR	615
	Caffeine, 1,3-dimethyluracil	IR	618
	Pyridazine, pyrimidine, pyrazine	IR	619
4-Br-Phenol (9.34)	<i>N,N</i> ,9-trimethyladenine	IR	610
	1,10-Phenanthroline derivatives	IR	611
	Conjugated imines	IR	613
	BIPA	IR	614
	PCA	IR	615
	Triethyl thiophosphate	IR	617
	Caffeine, 1,3-dimethyluracil	IR	618
	<i>N,N</i> -DMBA, <i>N</i> -BMA	IR	621
3,4-di-Cl-Phenol (8.58)	<i>N,N</i> ,9-trimethyladenine	IR	610
	Bathocuproine	IR	611
	Conjugated imines	IR	613
	BIPA	IR	614
	PCA	IR	615
	Triethyl thiophosphate	IR	617
	Caffeine, 1,3-dimethyluracil	IR	618
	pyridazine, pyrimidine, pyrazine	IR	619
3,5-di-Cl-Phenol (8.18)	<i>N,N</i> ,9-Trimethyladenine	IR	610
	Bathocuproine	IR	611
	BIPA	IR	614
	PCA	IR	615
	Triethyl thiophosphate	IR	617
	Caffeine, 1,3-dimethyluracil	IR	618
3,4,5-tri-Cl-Phenol (7.75)	<i>N,N</i> ,9-Trimethyladenine	IR	610
	Bathocuproine	IR	611
	BIPA	IR	614
	PCA	IR	615
	Triethyl thiophosphate	IR	617
	Caffeine, 1,3-dimethyluracil	IR	618
Pentachlorophenol	Pyridine betaine	X-ray, FTIR	638
	4-Methylpyridine	MNDO, PM3	639
	4-Acetylpyridine	AM1, PM3	640
	Formaldehyde	NMR	641
	Pyrimidine derivatives	IR	642

TABLE 34. (continued)

Phenol	Hydrogen bond partner ^a	Method of study	Reference
2-NO ₂ –Phenol (7.17)	Methanol	IR, NMR	643–645
3-NO ₂ –Phenol (8.28)	Pyridazine, pyrimidine, pyrazine	IR	619
4-NO ₂ –Phenol (7.15)	BIPA	IR	614
	TMA	IR, PM3	646
2,4-di-NO ₂ –Phenol	Methanol	IR	644

^a BIPA = *trans*-butenylidene-isopropylamine; PCA = 1-pyrrolidinecarboxaldehyde; *N,N*-DMBA = dimethylbenzylamine; *N*-BMA = benzylidenemethylamine; TMA = trimethylamine.

^b For pyridine.

^c See Reference 573 for a recent review.

B. Phenol–(Water)_{*n*}, 1 ≤ *n* ≤ 4 Complexes

1. Introduction

Knowledge of the potential energy surface of a molecular complex is always a key goal in the study of its vibrational pattern and dynamics. The PES of the interaction of water clusters with phenol is rather particular for several reasons. The prime reason is that phenol–water complexes are formed via hydrogen bonds and can thus be treated as prototypes for hydrogen-bonded aromatic systems and models of diverse important chemical and biological processes such as, e.g., solute–solvent interactions involving a participation of hydrogen bonds.

Hydrogen-bonded phenol–water complexes PhOH(H₂O)_{*n*} (≡ PhOH-*w_n*) have been thoroughly studied experimentally^{122, 164, 175, 412, 574, 578, 580, 585–587, 590, 596, 692–719} by standard spectroscopic methods, particularly by laser-induced fluorescence, resonance-enhanced multiphoton ionization, high-resolution UV spectroscopy, single vibronic level dispersed fluorescence and hole burning spectroscopy. The mass-selected multiphoton ionization studies^{585–587, 693, 694} of these complexes with *n* ≤ 4 suggested that the ground-state global minimum structure of PhOH(H₂O)₂ is realized when water molecules form a ring (defined hereafter as *S*₂)^{164, 412, 574, 578, 585–587, 596, 692–702}. A comparison of the spectra of the PhOH(H₂O)_{1–3} complexes led to the conclusion that these three complexes should not be treated as a sequence of additive derivatives and, moreover, that they might even have different geometries^{585–587}. Two-colour photoionization and cluster ion dip spectroscopy of PhOH(H₂O)_{*n*≤4} were carried out^{590, 708} showing the existence of two isomers of PhOH(H₂O)₄. The Raman spectrum of PhOH(H₂O)₁ was also observed¹⁶⁴.

The infrared (IR) and Raman UV double-resonance spectroscopy of PhOH(H₂O)_{*n*≤4} in the OH-stretching vibration region was also studied^{580, 703–705}. These studies led to the conclusion that, on the one hand, the symmetric water *v*₁ and phenolic OH-stretching (*v*_{OH}) vibrations are downshifted considerably upon the formation of phenol–water complexes (compared with those inherent for bare water and phenol molecules). On the other hand, the antisymmetric *v*₃ vibration of the water molecule is only weakly affected. This results in the appearance of a transparent ‘window’ region⁷⁰⁴ in the IR spectrum

of $\text{PhOH}(\text{H}_2\text{O})_{n=2-4}$ which widens as n increases, having a width of $ca\ 280\text{ cm}^{-1}$ for $n = 4$, and disappears in the spectrum of the $\text{PhOH}(\text{H}_2\text{O})_5$ complex²⁰³. An explanation was proposed⁷⁰⁴ for the origin of the ‘window’ region by the presence of the cyclic S_n arrangements of water molecules in these complexes with $n \leq 4$. Interestingly, these authors also observed a completely different IR pattern for $\text{PhOH}(\text{H}_2\text{O})_4$ in the region of the OH-stretching vibrations where four bands fall into the ‘window’ region^{704, 705}. It has been particularly suggested that such a pattern is attributed to the second isomer of $\text{PhOH}(\text{H}_2\text{O})_4$ ⁵⁹⁰ which might have a substantially different structure of water molecules compared to the cyclic structure⁷⁰⁵. A recent resonant two-photon ionization study⁶⁹⁷ of $\text{PhOH}(\text{H}_2\text{O})_{2-5}$ and $\text{PhOH}-d-(\text{D}_2\text{O})_{2-5}-d_1$ complexes led to the conclusion that this second isomer of $\text{PhOH}(\text{H}_2\text{O})_4$ might have a non-cyclic, more compact water arrangement that can only be expected for cage-, prism-, boat- and book-like structures of water clusters around PhOH (for the nomenclature of water cluster structures see, e.g., References 720–723 and references therein). This is somewhat similar to the book-like structure of water molecules in the global-minimum $\text{PhOH}(\text{H}_2\text{O})_5$ complex, where one water molecule forms an anchor-type π H-bond with the aromatic ring^{700, 702}.

The first *ab initio* calculations of $\text{PhOH}(\text{H}_2\text{O})_1$ were performed at the Hartree–Fock (HF) level^{699, 701} and the second-order correlated Møller–Plessett (MP2) level¹²¹ with the 6-31G(d,p) basis set within a frozen core (\equiv fc) approximation^{404, 724–726}. Density functional B3LYP calculation of $\text{PhOH}(\text{H}_2\text{O})_n$ was recently carried out by different groups^{473, 727}. The ground-state $\text{PhOH}(\text{H}_2\text{O})_2$ complex was first optimized in 1994–1995^{696, 710} (see also References 113 and 725–728). The structure and vibrations of $\text{PhOH}(\text{H}_2\text{O})_3$ in the singlet ground and its first excited state, and the lowest triplet state were investigated by two groups^{695, 711} at the HF/6-31G(d,p) computational level who reported that several local minima on the ground-state PES of $\text{PhOH}(\text{H}_2\text{O})_3$ are situated above the global-minimum structure with the cyclic S_3 water arrangement by 33.5–58.5 kJ mol^{-1} .

Theoretical study of the $\text{PhOH}(\text{H}_2\text{O})_n$ complexes calculated preliminarily at the HF/6-31G(d) computational level⁷²⁹ suggested that the ‘window’ region originates from the spectra of the $\text{PhOH}(\text{H}_2\text{O})_4$ isomer with the cyclic water structure S_4 . Another, experimentally observed IR pattern of $\text{PhOH}(\text{H}_2\text{O})_4$ does not fit the theoretical spectra of any complex found in the study and may probably be attributed to a mixture of certain complexes with more compact water arrangements. The proton-transferred $\text{PhOH}(\text{H}_2\text{O})_4$ complex suggested earlier^{704, 705} as a possible candidate for the second isomer was subsequently rejected^{697, 701, 730}. This problem remains unsolved.

We performed a rather thorough search of the ground-state PES of the $\text{PhOH}(\text{H}_2\text{O})_{n=3,4}$ complexes in the vicinity of the global minimum. We describe here the lower-energy minimum structures and offer a new, hopefully sound explanation of the origin of two different ‘window’ patterns in the IR spectra of the $\text{PhOH}(\text{H}_2\text{O})_4$ complex⁷³¹. Actually, the ‘window’ region measures the strength of hydrogen bonding: the larger the ‘window’, the stronger the bonding⁷³². We also use a canonical indication of the strength of hydrogen bonding in terms of the stretching vibration ν_σ of the hydrogen-bond bridge²⁶⁶ although the blue-shifted torsion vibration τ_{OH} of phenol can be applied for this purpose as well.

The present section is organized in the following manner. Computational methodology is outlined elsewhere^{733, 734}. In Section V.B.3, we briefly report two lowest-energy structures of $\text{PhOH}(\text{H}_2\text{O})_{n=1,2}$ and their theoretical spectra. Section V.B.4 demonstrates the existence of five lower-energy structures on the PES of $\text{PhOH}(\text{H}_2\text{O})_3$ lying above the global minimum by less than 12.5 kJ mol^{-1} . On the one hand, this shows a rather rich landscape of the PES of $\text{PhOH}(\text{H}_2\text{O})_3$ in comparison to the reported PES⁷¹¹ and the three lower-energy structures found later⁷²⁹ at the same computational level and located within 27.8 kJ mol^{-1} above the PES bottom. On the other hand, it also reveals a novel

structure where one of the water molecules forms a so-called π hydrogen bond with the π -electrons of the phenol ring. Such a structure partly resembles the analogous structure named as Leg2 type and found for the benzene–water complex^{735, 736}. Section V.B.5 considers ten lower-energy local minimum structures of the $\text{PhOH}(\text{H}_2\text{O})_4$ complex compared with the five reported in Reference 729 and located in nearly the same interval of energies, 15.9 kJ mol^{-1} , above the global energy minimum. This section provides a novel interpretation^{704, 705, 731} of the experiments on the existence of two different IR patterns in the IR spectra of this complex and confirms other observations⁵⁹⁰.

2. Interaction of phenol with water

We know already that the chosen computational methods accurately describe the properties of phenol, particularly its vibrational spectrum. The frequencies of the OH stretching vibrations of phenol and water molecule are collected in Table 35. It is interesting to note that the HF/A frequency of 4118 cm^{-1} assigned to the ν_{OH} stretching vibration of bare phenol corresponds to its highest frequency. Therefore, it can be treated as the most accepting mode of phenol. Moreover, this frequency lies between the frequencies of the ν_1 (4070 cm^{-1}) and ν_3 (4188 cm^{-1}) OH-stretching vibrational modes of water molecules (equation 40),

$$\nu_1 \overset{48}{<} \nu_{\text{OH}} \overset{70}{<} \nu_3 \quad (40)$$

Here, a value above the inequality sign indicates the corresponding frequency difference in cm^{-1} between its left- and right-hand side quantities. Notice that the first difference $\Delta\nu = \nu_{\text{OH}} - \nu_1$ is 48 cm^{-1} .

3. The most stable complexes of mono- and dihydrated phenol

Phenol is certainly more acidic than water and, for this reason, the energetically most favourable binding site of phenol is with its OH group acting as a hydrogen bond donor. Such a phenol donor–water acceptor structure, hereafter designated as $\text{PhOH-}w_1\text{-1}$ and shown in Figure 48, lies at the bottom of the PES of $\text{PhOH}(\text{H}_2\text{O})_1$. Its binding energy of 30.8 kJ mol^{-1} calculated at the HF/A level rises to 39.9 kJ mol^{-1} when the MP2(sp)/A calculation is carried out (see Table 36). Note that the latter value agrees with the binding energy of 38.9 kJ mol^{-1} obtained at the MP2 level in conjunction with the D95* Dunning basis set⁴⁷³. Due to the donor function of the phenolic O–H group in $\text{PhOH-}w_1\text{-1}$, its bond length is slightly elongated by 0.006 \AA compared to that in bare phenol. The oxygen atoms are calculated to be 2.901 \AA apart from each other, which correlates rather well with the experimental separation of $2.93 \pm 0.02 \text{ \AA}$ ⁶⁹⁷ or 2.88 \AA ⁶⁹⁹, and also with the HF/6-31G(d,p) result of 2.90 \AA ¹⁷⁵. The O–H \cdots O₁ hydrogen bond is practically linear: the corresponding angle $\angle\text{OHO}_1$ is 174.1° (the MP2/A value is 175.3°). The phenolic hydrogen donation to the water molecule only affects the geometries of the composing partners.

However, a major effect of the hydrogen bond in the $\text{PhOH-}w_1\text{-1}$ complex is anticipated to occur in its vibrational spectrum. It is primarily manifested by a significant red shift of *ca* 109 cm^{-1} as compared with ν_{OH} of bare phenol. Furthermore, the IR intensity of ν_{OH} gradually increases by a factor of 6.6. The HF/A red shift agrees rather satisfactorily with the experimental results^{703, 705}, showing a red shift of 133 cm^{-1} . Notice that the MP2/6-31G red shift amounts to 186 cm^{-1} ⁷²⁹ whereas its B3LYP/DZP value is larger and equal to 244 cm^{-1} ¹¹³. The stretching vibrations of water are predicted to be much less affected. More specifically, its ν_1 and ν_3 frequencies are changed by only 1 and

TABLE 35. The OH-stretching frequencies (in cm^{-1}) of water and phenol, and phenol–water_{1,2} complexes calculated via the HF/A and MP2/A (in parentheses) computational methods. Infrared intensity is in km mol^{-1} , Raman (R) activity in $\text{\AA}^4 \text{amu}^{-1}$

	ν_1			ν_3			ν_{OH}		
	Frequency	IR	R	Frequency	IR	R	Frequency	IR	R
H ₂ O	4070.0 3658 ^a	18	76	4188.2 3756 ^a	58	39			
PhOH							4118.1 3657 ^b	81	79
							4197.2 (3881.8) ^c	84 (53)	
PhOH- <i>w</i> ₁₋₁	4068.6 (3764.1)	22 (18)	69	4182.0 (3897.4)	102 (81)	54	4008.9 (3597.8)	537 (645)	144
	3650 ^b			3748 ^b			3524 ^b		
PhOH- <i>w</i> ₁₋₂	4057.2	94	89	4170.2	134	41	4114.3	94	73
PhOH- <i>w</i> ₂₋₁	3973.2 (3560.7)	308 (419)	47	4147.1 (3846.9)	121 (99)	81	3916.6 (3420.9)	393 (501)	156
	4021.7 (3662.7)	237 (282)	58	4154.7 (3850.2)	137 (69)	40			

^aExperimental frequencies of water are taken from Reference 738.

^bExperimental frequencies for phenol and phenol–water clusters are taken from References 704 and 705. See also Table 10 for the phenol vibrational modes.

^cCalculated frequency at the HF/6-31G(d,p) and MP2/6-31G(d,p) (in parentheses) levels (cf. Table 10).

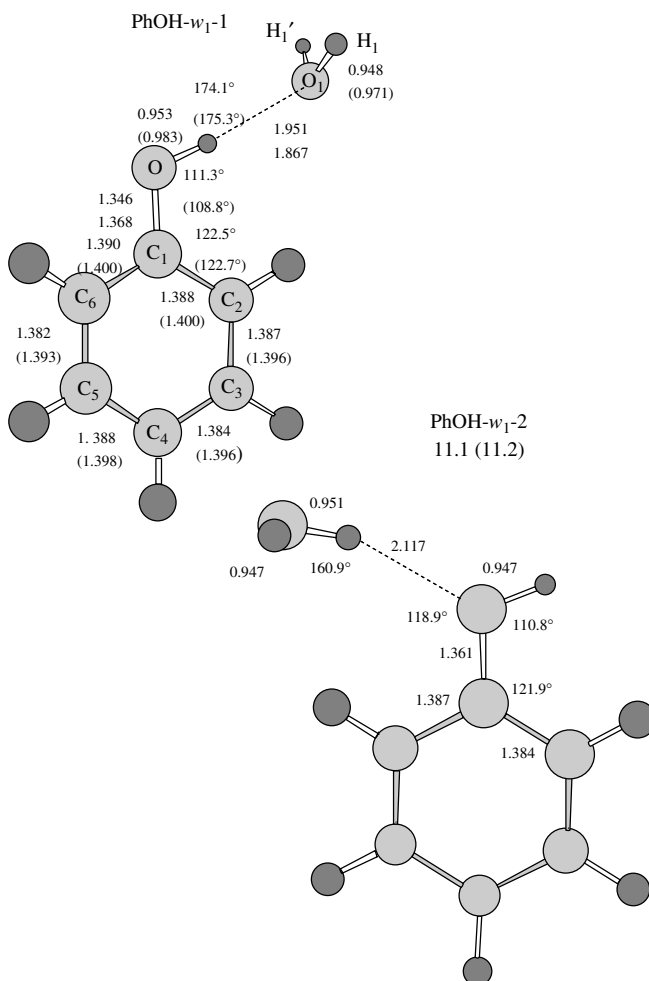


FIGURE 48. Two lower-energy structures of the phenol–water₁ complex. The HF/A bond lengths are in Å. The geometrical parameters of the global minimum structure are paired: the first value corresponds to the HF/A level while the MP2/A value is given in parentheses. The HF/A relative energy with respect to the global minimum structure PhOH- w_1 -1 is given in kJ mol⁻¹. Its MP2(sp)/A analogue is followed in parentheses. Numbering of the carbon atoms of phenol is as in Chart 1. Adapted from Reference 731 with permission

6 cm⁻¹, respectively. Besides, their IR intensities increase by 4 and 44 km mol⁻¹ whereas the Raman activity decreases by 7 Å⁴ amu⁻¹ for ν_1 and increases by 15 Å⁴ amu⁻¹ for ν_3 . Therefore, we may conclude that the hydrogen-bond donation of phenol to the water molecule in the global minimum energy PhOH- w_1 -1 structure has the following effects. It decreases the phenolic OH stretching vibration and breaks the order of the OH frequencies of the isolated phenol and water deduced in equation 40 in such a way that the phenolic

TABLE 36. Relative energies, ZPVEs, enthalpies (in kJ mol^{-1}) and entropies (in $\text{cal mol}^{-1} \text{K}^{-1}$) of $\text{PhOH}(\text{H}_2\text{O})_n$ complexes. Relative energy of $\text{PhOH}(\text{H}_2\text{O})_n$ is defined as $-[\text{E}(\text{PhOH}(\text{H}_2\text{O})_n) - n \times \text{E}(\text{H}_2\text{O})]$. The relative energies with respect to structure 1 of the phenol-water_n complex are also given^{a,b,c}

$\text{PhOH}(\text{H}_2\text{O})_n$	$\Delta\text{Energy}_{\text{HF}}$	$\Delta\text{Energy}_{\text{MP2}(\text{op})}$	ZPVE	$\Delta\text{Enthalpy}$	$\Delta\text{Entropy}$
$\text{PhOH}-w_1-1$	30.75	39.92	0.0	0.0	0.0
$\text{PhOH}-w_1-2$	19.66	28.70	-0.13	10.84	3.26
$\text{PhOH}-w_2-1,2$	43.64	61.92	0.0	0.0	0.0
$\text{PhOH}-w_3-1,2$	48.74	63.81	0.0	0.0	0.0
$\text{PhOH}-w_3-3,4$	46.57	61.25	-0.63	1.88	-6.02
$\text{PhOH}-w_3-5$	45.06	59.45	-0.46	3.14	-11.97
$\text{PhOH}-w_3-6$	37.70	51.38 (10.296 ^d)	-2.34	9.62	-12.18
$\text{PhOH}-w_4-1$	40.04	51.71	0.0	0.0	0.0
$\text{PhOH}-w_4-2$	33.81	52.17 (-4.56 ^a ; -4.92 ^b ; -0.29 ^c)	-2.22 (4.48 ^c)	7.24	-26.69
$\text{PhOH}-w_4-3$	33.52	53.56 (-3.72 ^a ; 1.88 ^c)	-2.18 (4.56 ^c)	5.36	-30.08
$\text{PhOH}-w_4-4$	33.68	51.25 (-2.30 ^a ; 2.80 ^b ; 3.89 ^c)	-0.08 (1.38 ^c)	6.52	-15.94
$\text{PhOH}-w_4-5$	33.26	50.38	0.33	6.82	-12.38
$\text{PhOH}-w_4-6$	36.11	49.87	-0.96	4.56	-8.91
$\text{PhOH}-w_4-7$	35.56	49.87	0.42	5.27	-7.28
$\text{PhOH}-w_4-8$	34.73	49.33	-1.17	5.77	-12.76
$\text{PhOH}-w_4-9$	37.66	48.12	1.05	1.97	10.96
$\text{PhOH}-w_4-10$	28.62	38.99	0.42	11.30	8.62
$\text{PhOH}-w_4-11$	21.55	36.02	1.46	17.99	4.60

^aMP2/A.

^bMP2/A⁺.

^cB3LYP/A. Values taken from Reference 731 with permission.

OH stretching vibration is characterized by a lower wavenumber than ν_1 (equation 41),

$$\begin{aligned} \text{Expt: } \nu_{\text{OH}} &< \nu_1^a < \nu_3^a \\ \text{HF/A: } \nu_{\text{OH}} &< \nu_1^a < \nu_3^a \\ \text{MP2/A: } \nu_{\text{OH}} &< \nu_1^a < \nu_3^a \end{aligned} \quad (41)$$

where the superscript *a* stands for an *acceptor* of hydrogen bonding, emphasizing the role of the water molecule. This merges into a ‘window’ region of *ca* 113–133 cm^{-1} width. The hydrogen bonding between phenol and the water molecule also gives rise to the hydrogen bond stretching ν_σ mounting at 158.5 (182.2) cm^{-1} (the experimental value ranges between 151 and 163 cm^{-1} ; see in particular Table 2 in Reference 473). Interestingly, the torsional mode τ_{OH} of phenol is blue-shifted substantially to 719.3 (775.5) cm^{-1} (the B3LYP/D95* value⁴⁷³ is 447 cm^{-1}).

The next lowest energy local minimum on the PES of $\text{PhOH}(\text{H}_2\text{O})_1$ is occupied by the $\text{PhOH-}w_1\text{-2}$ structure shown in Figure 48. Here, phenol acts as an acceptor of the hydrogen bond and, compared to the hydrogen bond donor structure, it is less favourable, by 1.11 kJ mol^{-1} at the HF/A level⁷²⁹. The energy gap between $\text{PhOH-}w_1\text{-1}$ and $\text{PhOH-}w_1\text{-2}$ decreases slightly to 10.8 kJ mol^{-1} after ZPVE correction and increases to 11.2 kJ mol^{-1} when both structures are recalculated at the MP2(sp)/A level.

It is particularly unfavourable that the $\text{O-H}\cdots\text{O}_1$ bond length elongates by 0.12 Å in $\text{PhOH-}w_1\text{-2}$ compared to that in $\text{PhOH-}w_1\text{-1}$, and appears more bent by 13.2°. The hydrogen bond in this case also causes the elongation of the C–O bond by *ca* 0.1 Å compared to its value in bare phenol. In both mentioned structures, there is a very weak interaction between the oxygen atom of the water molecule and the *ortho* hydrogen atom of the phenol ring that is indicated by the corresponding distances of 2.875 Å and 2.727 Å for $\text{PhOH-}w_1\text{-1}$ and $\text{PhOH-}w_1\text{-2}$, respectively. The rotational constants and the total dipole moment of both reported $\text{PhOH-}w_1$ structures are gathered in Table 37. As seen there, the hydrogen-bond donor structure is more polar than the hydrogen-bond acceptor structure. There is still another feature which distinguishes the two studied structures of phenol with a water molecule from each other: if, in the global minimum energy structure, the oxygen atom of a water molecule resides in the phenol plane, in $\text{PhOH-}w_1\text{-2}$, on the contrary, it lies out-of-plane forming a dihedral angle of 95.0°. We explain this by the directionality of the lone pair of the phenolic oxygen. It implies that there are actually two isomers of $\text{PhOH-}w_1\text{-2}$: one where the oxygen atom of a water molecule is placed above the phenol ring and the other where it lies below it. Such a feature remains if more water molecules interact with phenol. We consider this as one of the reasons for the appearance of π hydrogen bonding after adding a sufficient number of water molecules to phenol: the cyclic arrangement of water molecules becomes exhausted and the energetic favour turns to 3D water patterns.

Compared with $\text{PhOH-}w_1\text{-1}$, the symmetric ν_1 and asymmetric ν_3 vibrations in $\text{PhOH-}w_1\text{-2}$ are red shifted by 13 and 18 cm^{-1} while the phenol ν_{OH} stretching vibration is downshifted by only 4 cm^{-1} . Therefore, the stretching IR pattern of $\text{PhOH-}w_1\text{-2}$ appears to be that given in equation 42

$$\nu_1^d < \nu_{\text{OH}} < \nu_3^d \quad (42)$$

Notice that the IR pattern inherent for isolated phenol and water molecules (equation 40) is nearly retained in the $\text{PhOH-}w_1\text{-2}$ structure. The H-bond vibrational mode $\nu_\sigma = 125.5 \text{ cm}^{-1}$ is lower than in $\text{PhOH-}w_1\text{-1}$, implying that the hydrogen bonding in the $\text{PhOH-}w_1\text{-1}$ structure is stronger.

TABLE 37. Theoretical rotational constants A , B and C (in GHz) and total dipole moment (in D) of $\text{PhOH}(\text{H}_2\text{O})_n$ complexes calculated via the HF, MP2^a and B3LYP^b methods in conjunction with basis set A

$\text{PhOH}(\text{H}_2\text{O})_n$	A	B	C	Dipole
PhOH- w_1 -1	4.38507	1.08337	0.87222	3.92
	4.25523 ^a	1.11400 ^a	0.88657 ^a	3.89 ^a
PhOH- w_1 -2	4.09796	1.11817	0.88142	3.56
PhOH- w_2 -1	2.70968	0.73097	0.63654	1.15
	2.53870 ^a	0.83238 ^a	0.75134 ^a	1.10 ^a
PhOH- w_3 -1	1.94209	0.50448	0.42647	1.16
	1.89925 ^a	0.54336 ^a	0.46239 ^a	1.14 ^a
PhOH- w_3 -3	1.91922	0.51563	0.44259	1.13
PhOH- w_3 -5	1.86586	0.52443	0.45787	1.52
PhOH- w_3 -6	1.45663	0.69364	0.59343	1.98
	1.46994 ^a	0.78406 ^a	0.66417 ^a	1.94 ^a
PhOH- w_4 -1	1.31037	0.37687	0.31183	0.96
	1.21338 ^a	0.44044 ^a	0.36928 ^a	1.17 ^a
	1.32264 ^b	0.41360 ^b	0.34133 ^b	1.25 ^b
PhOH- w_4 -2	1.14775	0.53379	0.47190	2.58
	1.11526 ^a	0.70260 ^a	0.61283 ^a	2.34 ^a
	1.21478 ^b	0.57219 ^b	0.49779 ^b	2.55 ^b
PhOH- w_4 -3	1.51720	0.43861	0.41398	3.55
	1.55673 ^a	0.49177 ^a	0.46151 ^a	3.82 ^a
	1.59183 ^b	0.46947 ^b	0.44238 ^b	3.69 ^b
PhOH- w_4 -4	1.21216	0.51396	0.45024	2.48
	1.25108 ^a	0.56229 ^a	0.50145 ^a	2.92 ^a
	1.29591 ^b	0.54344 ^b	0.48837 ^b	2.42 ^b
PhOH- w_4 -5	1.18647	0.52433	0.45296	1.73
PhOH- w_4 -6	1.58475	0.34963	0.30846	3.23
PhOH- w_4 -7	1.03920	0.52807	0.49064	1.11
PhOH- w_4 -8	1.14855	0.47892	0.40965	2.35
PhOH- w_4 -9	1.26070	0.37569	0.310086	0.92
PhOH- w_4 -10	1.26992	0.35619	0.31544	2.37
PhOH- w_4 -11	1.13115	0.49384	0.47181	1.56

Values taken from Reference 731 with permission.

Let us now proceed to the PES of $\text{PhOH}(\text{H}_2\text{O})_2$ whose lower-energy portion is displayed in Figure 49. Two ring isomers, $\text{PhOH-}w_2$ -1 and $\text{PhOH-}w_2$ -2, reside at its global energy minimum. They are equivalent because $\text{PhOH-}w_2$ -2 is obtained from $\text{PhOH-}w_2$ -1 by applying the reflection relative to the phenol plane. In these structures, the OH group of phenol acts bifunctionally, both as the hydrogen-bond donor and acceptor. The three hydrogen bonds in $\text{PhOH-}w_2$ -1 are rather bent, as indicated by the values of the corresponding $\text{O-H}\cdots\text{O}$ angles: 143.59° , 149.66° and 156.14° taken clockwise. The hydrogen bond formed between the phenol hydrogen-bond acceptor and the water molecule donor (w_{ad1}) is quite long and comprises 2.138 \AA , although the corresponding oxygen–oxygen separation of 2.96 \AA is reasonable and shorter than in $\text{PhOH-}w_1$ -2. The other O–O distances are typical for such hydrogen bonds: $r(\text{O}-\text{O}_2)=2.813 \text{ \AA}$ and $r(\text{O}_1-\text{O}_2)=2.848 \text{ \AA}$.

Five calculated OH-stretching vibrations of the $\text{PhOH-}w_2$ -1 structure are presented in Table 35. By analogy with the $\text{PhOH-}w_1$ -1 complex, the hydrogen-bonded phenolic ν_{OH} vibration is red-shifted significantly by 202 cm^{-1} and its IR intensity is enhanced by a factor of 4.9 while its Raman activity only doubles. The other four vibrations are simply assigned to the ν_1 and ν_3 of water molecules w_{ad1} and w_{ad2} , although their collective nature (essential for larger water clusters) should be noted. One pair of them, ν_1^{ad1} and

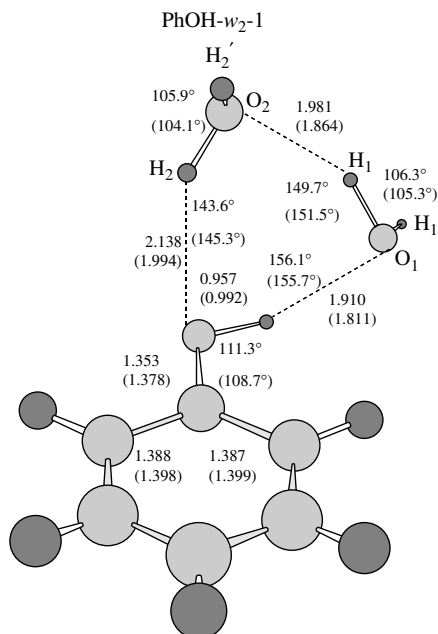


FIGURE 49. The lowest-energy structure of the phenol–water₂ complex. Bond lengths are in Å. The geometrical parameters are paired: the former value corresponds to the HF/A level while the MP2/A value is given in parentheses. Adapted from Reference 731 with permission

ν_3^{ad1} , at 3973.2 and 4147.1 cm^{-1} , corresponds to symmetric and asymmetric stretchings of the water molecule w_{ad1} , accepting the phenolic hydrogen bond and donating the hydrogen bond to water dimer. The other one, ν_1^{ad2} and ν_3^{ad2} , centred at 4021.7 and 4154.7 cm^{-1} , describes the symmetric and asymmetric OH-stretching vibrations of the water molecule w_{ad2} , donating the hydrogen bond to phenol and accepting the other one from w_{ad1} . Altogether, they are red-shifted and considerably enhanced compared with the similar vibrations in water and monohydrated phenol. Summarizing, the IR stretching region assumes the pattern shown in equation 43,

$$\begin{aligned}
 \text{Expt: } \nu_{\text{OH}} &< \nu_1^{ad1} < \nu_1^{ad2} < \nu_3^{ad1} < \nu_3^{ad2} \\
 \text{HF/A: } \nu_{\text{OH}} &< \nu_1^{ad1} < \nu_1^{ad2} < \nu_3^{ad1} < \nu_3^{ad2} \\
 \text{MP2(fc)/A: } \nu_{\text{OH}} &< \nu_1^{ad1} < \nu_1^{ad2} < \nu_3^{ad1} < \nu_3^{ad2}
 \end{aligned} \quad (43)$$

Here, we thus observe the MP2/A ‘window’ region of 184 cm^{-1} width. Compared to the value reported above for the phenol–water₁ complex and demonstrated in equation 41, it is extended by 51 cm^{-1} . It is clearly seen from Table 35 that its extension follows, first, from a further red shift by 177 cm^{-1} of the phenolic OH-stretching compared to PhOH- w_1 -1 as a result of a stronger hydrogen-bonding donation of the OH group of phenol to water dimer. Despite the fact that the corresponding ν_{σ} frequency is less by 21 cm^{-1} than in PhOH- w_1 -1, the hydrogen bonding is stronger since the phenolic O–H

bond keeps elongating by 0.009 Å. Second, the ‘window’ extension also follows from a rather substantial red shift of 203 cm⁻¹ in the water dimer, where the corresponding hydrogen-bridge stretching frequency reaches the value of 245.2 cm⁻¹. And finally, third, it stems from a strengthening of the hydrogen-bonding donation of water dimer to the lone pair electrons of the phenolic OH group as indicated particularly by the ν_σ frequency of 201.2 cm⁻¹, which exceeds the analogous one in PhOH- w_2 -1 by a factor of 1.8. Note in conclusion that the ν_1 mode of the water molecule w_{ad2} (as donor of a hydrogen bond to phenol) borders the left-hand side edge of the ‘window’ region. This is a typical feature for the cyclic arrangements of water molecules bonded to phenol. We will observe it also for the PhOH(H₂O)₃ complex in the following subsection.

4. Lower-energy structures of PhOH(H₂O)₃

Adding a third water molecule to the PhOH(H₂O)₂ complex significantly enriches the PES landscape of PhOH(H₂O)₃. This is clearly seen in Figure 50, which displays six lower-energy structures of phenol bonded to three water molecules. The global minimum is occupied by two isoenergetic structures, PhOH- w_3 -1 and PhOH- w_3 -2, converting into each other via the plane containing the CO group, and perpendicular to the phenol ring. These structures possess a closed cyclic water pattern S_3 to which the phenolic OH group simultaneously donates and accepts hydrogen bonds. A similar water pattern is inherent for the other three structures PhOH- w_3 -3, PhOH- w_3 -4 (actually the isomer of PhOH- w_3 -3) and PhOH- w_3 -5 lying within *ca* 4.2 kJ mol⁻¹ above the global minimum and reported in the present work for the first time. Their difference from the global minimum isomers originates from the flippings of the free OH groups of water molecules which can be classified by the *u* and *d* symbols⁷⁰². In this regard it is worth mentioning that the structure reported as the most energetically close to the global minimum⁷²⁹ is misplaced by 10.8 kJ mol⁻¹. By analogy with the existence of two isoenergetic global-minimum structures, there are actually three additional structures deduced from PhOH- w_3 -3, PhOH- w_3 -4 and PhOH- w_3 -5 by applying the same reflection operation of bare phenol.

Analysis of the global minimum structures in Figures 48, 49 and 50 reveals a tendency towards systematic shortening of the phenol–water hydrogen bonds upon adding an extra water molecule. The length of the phenol donor–water acceptor hydrogen bond varies from 1.95 Å in PhOH- w_1 to 1.91 Å in PhOH- w_2 and, finally, to 1.83 Å in PhOH- w_3 . This correlates fairly with recent experimental findings⁶³⁶. On the other hand, passing from PhOH- w_2 to PhOH- w_3 , the water donor–phenol acceptor phenol–water hydrogen bond decreases by 0.18 Å.

Table 38 collects seven theoretical OH-stretching vibrations of the five relevant lower-energy PhOH- w_3 structures to discuss a ‘window’ region. Inspection of Table 38 shows that they are actually gathered in two rather well separated groups. Considering the PhOH- w_3 -1 structure as an example, we find that the first group consists of four highly intense IR vibrations placed between 3835 and 3983 cm⁻¹ and describing cooperative stretching vibrations of the intra-ring OH bonds. The first two are predominantly assigned to the coupled OH-stretching vibration of phenol and its nearest-neighbour OH bond O₁–H₁ (see Figure 50). The lower of these two, corresponding to the symmetric stretch of these OH bonds, is rather Raman active and red-shifted by 283 cm⁻¹ with respect to the OH-stretching frequency of bare phenol. The other one is less red-shifted, by 223 cm⁻¹. The second group of vibrations consists of three vibrations lying between 4142 and 4148 cm⁻¹. The OH-stretching vibrations of three free OH groups of water molecules contribute predominantly to this group. They are shifted to lower wavenumbers relative to the ν_3 vibration of the water molecule by approximately 40 cm⁻¹. The separation between these

groups which determines a width of the ‘window’ region amounts to 307 cm^{-1} at the HF/A level and decreases to 267 cm^{-1} after performing the MP2/A calculation. In other words, the stretching IR pattern of the PhOH- w_3 -1 structure are those in equation 44,

$$\text{MP2/A: } \nu_{\text{OH}}^{145(109)} < \nu_1^{ad1\ 77(56)} < \nu_1^{ad2\ 83(50)} < \nu_1^{ad3\ 267(264)} < \nu_3^{ad1\ 5(4)} < \nu_3^{ad2\ 3(3)} < \nu_3^{ad3} \quad (44)$$

where the experimental spacings⁷⁰⁵ are given in parentheses.

The sixth structure of the PhOH- w_3 complex reported in the present work for the first time and displayed in Figure 50 is rather peculiar in the following sense. As shown in Figure 50, one of its water molecules accepts the phenolic OH group. Another one, $\text{O}_3\text{H}_3'\text{H}_3''$, lies above the phenol ring. It forms a so-called π hydrogen bond with the

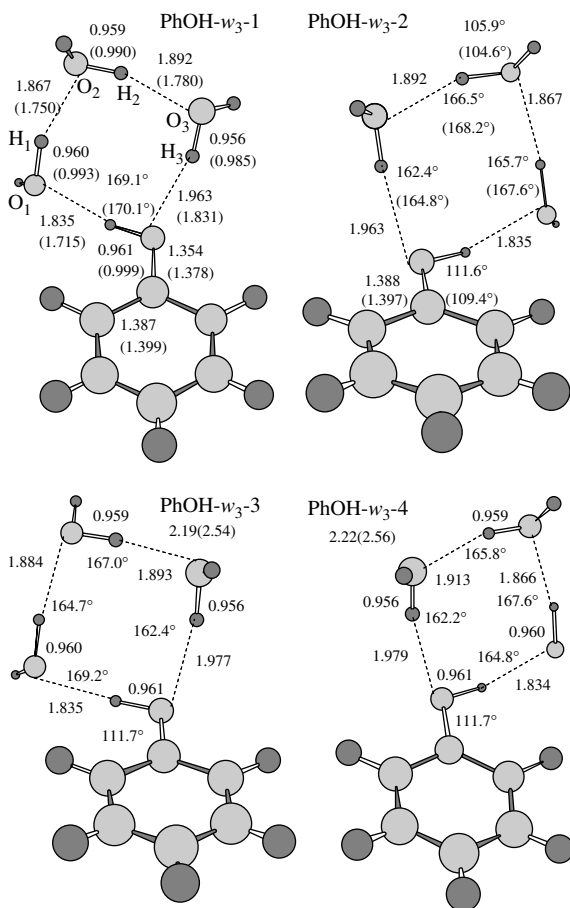


FIGURE 50. Six lower-energy structures of the phenol-water₃ complex. Bond lengths are in Å. The geometrical parameters are paired for some particular structures: the former value corresponds to the HF/A level while the MP2/A value is presented in parentheses. The HF/A [MP2(sp)/A] relative energy with respect to the global-minimum structure PhOH- w_3 -1 is given in kJ mol^{-1} . Adapted from Reference 731 with permission

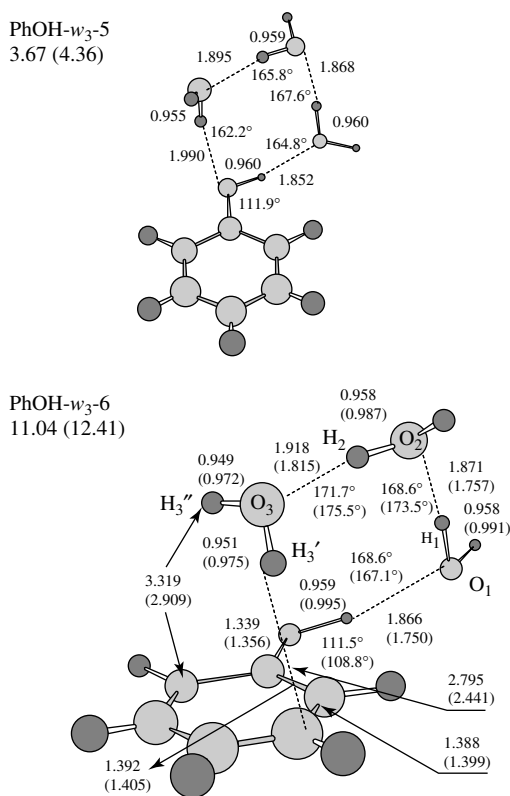


FIGURE 50. (continued)

π cloud of this ring, partly similar to the Leg2-type benzene–water structure discussed elsewhere⁷³⁶. The shortest MP2/A distance of 2.441 Å is predicted between the H_3' and the carbon atom C_3 (see Figure 50). The other one, $r(H_3''-C_3) = 2.909$ Å, almost coincides with the sum of van der Waals radii of the corresponding atoms. Compared to a free water molecule, both O–H bond lengths undergo tiny elongations, about 0.003–0.006 Å, although, contrary to the other water molecules belonging to this structure as well as to all water molecules in the aforementioned structures, the water molecule participating in the π hydrogen bonding with phenol ring has its bond angle $\angle HOH$ decreased by 1.3°. This is in turn manifested in the scissor vibrations of water molecules. If two of them, w_1 and w_2 , are characterized by the scissor frequencies ν_2 centred at 1762 and 1788 cm^{-1} , which are red-shifted by 27 and 52 cm^{-1} compared to that in water monomer, the third water molecule w_3 possesses the scissor frequency at 1742 cm^{-1} , resulting in a blue shift of 7 cm^{-1} .

The novel PhOH- w_3 -6 structure has the largest total dipole moment (1.98 D) among all reported lower-energy PhOH- w_3 structures⁷³¹. It is also a more compact structure, as follows from a comparison of the rotational constants of all PhOH- w_3 structures. Energetically speaking, PhOH- w_3 -6 is 11.0 kJ mol^{-1} (HF/A) and 10.3 kJ mol^{-1} (MP2/A) above the global minimum structure PhOH- w_3 -1. These values are modified to 8.7 and

TABLE 38. The OH-stretch frequencies (in cm^{-1}) of phenol–water₃ complexes calculated at the HF/A and MP2/A (in parentheses) computational levels. Infrared intensity is in km mol^{-1} , Raman (R) activity in $\text{\AA}^4 \text{amu}^{-1}$. Partial contributions are evaluated as the ratio of total displacements. The contribution of the first reported mode is referred to 100%

Frequency	IR	Raman	Assignment
<i>PhOH-w₃-1,2</i>			
3834.7 (3273.4)	537 (821)	213	ν_{OH} , $\nu_{\text{O}_1\text{H}_1}$ (33.8%)
3895.4 (3418.8)	602 (755)	50	$\nu_{\text{O}_1\text{H}_1}$, ν_{OH} (69.9%), $\nu_{\text{O}_2\text{H}_2}$ (56.3%)
3929.3 (3496.1)	571 (973)	43	$\nu_{\text{O}_2\text{H}_2}$, $\nu_{\text{O}_1\text{H}_1}$ (52.7%), $\nu_{\text{O}_3\text{H}_3}$ (10.1%)
3982.8 (3578.9)	418 (616)	114	$\nu_{\text{O}_3\text{H}_3}$
4142.2 (3845.4)	136 (85)	64	$\nu_{\text{O}_1\text{H}_1'}$, $\nu_{\text{O}_2\text{H}_2'}$ (11.9%)
4143.8 (3850.8)	81 (80)	65	$\nu_{\text{O}_2\text{H}_2'}$, $\nu_{\text{O}_1\text{H}_1'}$ (12.8%)
4148.3 (3853.3)	171 (107)	53	$\nu_{\text{O}_3\text{H}_3'}$
<i>PhOH-w₃-3,4</i>			
3840.2	531	219	ν_{OH} , $\nu_{\text{O}_1\text{H}_1}$ (24.5%), $\nu_{\text{O}_2\text{H}_2}$ (6.4%)
3901.4	629	49	$\nu_{\text{O}_1\text{H}_1}$, $\nu_{\text{O}_2\text{H}_2}$ (93.1%), ν_{OH} (66.5%)
3931.0	553	38	$\nu_{\text{O}_2\text{H}_2}$, $\nu_{\text{O}_1\text{H}_1}$ (82.7%)
3983.5	362	82	$\nu_{\text{O}_3\text{H}_3}$
4144.3	99	55	$\nu_{\text{O}_3\text{H}_3'}$
4145.2	110	47	$\nu_{\text{O}_1\text{H}_1'}$, $\nu_{\text{O}_2\text{H}_2'}$ (57.9%)
4146.2	129	88	$\nu_{\text{O}_2\text{H}_2'}$, $\nu_{\text{O}_1\text{H}_1'}$ (60.3%)
<i>PhOH-w₃-5</i>			
3854.9	382	215	ν_{OH} , $\nu_{\text{O}_1\text{H}_1}$ (67.2%), $\nu_{\text{O}_2\text{H}_2}$ (19.4%)
3903.9	739	30	ν_{OH} , $\nu_{\text{O}_1\text{H}_1}$ (63.4%), $\nu_{\text{O}_2\text{H}_2}$ (46.2%)
3932.0	533	48	$\nu_{\text{O}_2\text{H}_2}$, $\nu_{\text{O}_1\text{H}_1}$ (55.9%)
3988.9	333	66	$\nu_{\text{O}_3\text{H}_3}$
4141.5	115	66	$\nu_{\text{O}_2\text{H}_2'}$
4145.8	112	44	$\nu_{\text{O}_3\text{H}_3'}$
4152.5	107	52	$\nu_{\text{O}_1\text{H}_1'}$
<i>PhOH-w₃-6</i>			
3870.2 (3351.5)	459 (683)	188	ν_{OH} , $\nu_{\text{O}_1\text{H}_1}$ (74.1%)
3919.8 (3467.4)	773 (994)	33	ν_{OH} , $\nu_{\text{O}_1\text{H}_1}$ (80.3%), $\nu_{\text{O}_2\text{H}_2}$ (31.2%)
3950.9 (3549.4)	305 (462)	58	$\nu_{\text{O}_2\text{H}_2}$, $\nu_{\text{O}_1\text{H}_1}$ (25.7%)
4054.8 (3732.9)	91 (104)	56	$\nu_{\text{O}_3\text{H}_3'}$, $\nu_{\text{O}_3\text{H}_3'}$ (56.0%)
4142.2 (3841.9)	108 (72)	94	$\nu_{\text{O}_1\text{H}_1'}$
4147.9 (3858.4)	115 (76)	57	$\nu_{\text{O}_2\text{H}_2}$
4156.6 (3852.0)	99 (73)	34	$\nu_{\text{O}_3\text{H}_3'}$, $\nu_{\text{O}_3\text{H}_3'}$ (55.3%)

Values taken from Reference 731 with permission.

7.7 kJ mol^{-1} , respectively, after taking the ZPVE corrections into account. Comparing the free energies of the lower-lying PhOH-*w*₃ structures determined by their enthalpies and entropies listed in Table 36, we conclude that at $T \geq 262.8 \text{ K}$, PhOH-*w*₃-5 becomes energetically the most favourable structure. In terms of free energy, it also lies below the PhOH-*w*₃-3,4 structures when $T \geq 209.7 \text{ K}$. The latter becomes more favourable than PhOH-*w*₃-1,2 at $T \geq 315.3 \text{ K}$. At room temperature (298.15 K), the PhOH-*w*₃-6 structure is only 6.4 kJ mol^{-1} higher than PhOH-*w*₃-3,4.

Regarding the novel PhOH-*w*₃-6 structure, its seven OH-stretching vibrations are not separable into two distinct groups. It is also worth mentioning that, in contrast to the IR

stretching pattern of PhOH- w_3 -1 which spans over a region of 580 wavenumbers, the IR pattern of PhOH- w_3 -6 is somewhat narrower, about 500 wavenumbers. Its most red-shifted vibration predicted at 3870 (3352) cm^{-1} is mainly attributed to the collective stretching vibration of the phenolic OH group and the OH group of the water molecule, which plays the role of hydrogen-bond acceptor of phenol (see Table 38). This feature looks drastically different from what we have already observed for the PhOH- w_3 -1 complex, where the most red-shifted stretching vibration is essentially localized on the OH group of phenol. The second vibration of PhOH- w_3 -6, placed at *ca* 3920 (3467) cm^{-1} , is characterized by the most intense IR absorption, equal to 773 (994) km mol^{-1} , among all reported PhOH- w_3 structures. Together with the third vibration at 3951 (3549) cm^{-1} , these vibrations describe the coupled stretchings of phenolic and water OH bonds. The fourth vibrational mode with the frequency of 4055 (3733) cm^{-1} is assigned to the symmetric π -OH stretching mode of the π hydrogen-bonded $\text{O}_3\text{H}_3'$ and $\text{O}_3\text{H}_3''$ groups, whereas the corresponding π -OH asymmetric stretch amount to 4157 (3852) cm^{-1} . Their MP2/A red shifts are rather small and amount to, respectively, 41 and 63 cm^{-1} compared to a free water molecule. This is a typical feature of weak hydrogen bonds, such as we consider here as π bonds. The other vibrations of PhOH- w_3 -6 found at 4142 (3842) and 4147 (3858) cm^{-1} describe, as usual, the stretching vibrations of free OH groups of water molecules. Altogether, these seven OH-stretching vibrations give rise to the IR pattern in equation 45,

$$\text{MP2/A: } \nu_{\text{OH}}^{116} < \nu_1^{\text{ad}1}^{82} < \nu_1^{\text{ad}2}^{184} < \nu_{\text{sym}}^{\pi}{}^{99} < \nu_3^{\text{ad}1}{}^9 < \nu_{\text{asym}}^{\pi}{}^6 < \nu_3^{\text{ad}2} \quad (45)$$

On inspecting equations 44 and 45, we note a narrowing of the ‘window’ region for the π hydrogen-bonded structure PhOH- w_3 -6 compared to the conventional one with the S_3 arrangement of water molecules. This implies that some modes of the former structure might fall in the ‘window’ region of the latter. In the present case, these are two modes: one corresponds to ν_{sym}^{π} and the other to $\nu_3^{\text{ad}1}$.

In concluding this subsection, it appears that all global minimum energy structures involve water molecule(s) arranged in a ring manner. Nevertheless, it seems that such a structure for PhOH(H_2O) $_3$ becomes somewhat exhausted in the sense that a more compact arrangement of water molecules emerges. We believe that the primary reason for this is that when $n \geq 3$, the hydrogen-bond acceptor ability of the phenolic OH group becomes competitive with the π hydrogen-bond acceptor ability of the phenol ring. This is seen more transparently in the next subsection for $n = 4$ which, in a certain sense, can be treated as a border between the global minimum energy structures where water molecules are arranged into a ring ($n \leq 3$) and those where water molecules form a 3D one with π hydrogen bonding ($n \geq 5$)^{700, 702}.

5. At the bottom of PES of PhOH(H_2O) $_4$

Analysis of the PES of the interaction of phenol with four water molecules reveals eleven lower-energy structures lying within an interval of less than 15.7 kJ mol^{-1} (MP2(sp)/A) above the global minimum. They are displayed in Figure 51. The landscape of the lower-energy portion of the PES of PhOH(H_2O) $_4$ is the following.

At the HF/A level, we find that the global minimum is occupied by the PhOH- w_4 -1 structure with water molecules forming a ring S_4 via five typical hydrogen bonds. This is in fact a conventional structure already reported in the literature^{729, 730}. It is characterized by a rather small total dipole moment of 0.96 D. Moving upward on this PES, we arrive at two energetically close structures, PhOH- w_4 -3 and PhOH- w_4 -2, which are placed above the global minimum one by 4.5 and 6.3 kJ mol^{-1} , respectively, after ZPVE correction. In PhOH- w_4 -3, water molecules are arranged in a sort of cage-like pattern^{720–723} having

six typical hydrogen bonds $\text{O}-\text{H}\cdots\text{O}$ and the additional $\text{O}-\text{H}\cdots\pi$ directed downward to the phenol ring^{735–737}. In $\text{PhOH}-w_4-2$, water molecules form a S_4 -like pattern with seven hydrogen bonds characterized by the following properties: first, the water molecule w_2 participates in three hydrogen bonds and, second, w_3 also takes part in π hydrogen bonding. One of the most interesting features of these structures is the appearance of double-donor water molecules, such as w_2 in $\text{PhOH}-w_4-2$ and w_3 in $\text{PhOH}-w_4-3$. Furthermore, the $\text{PhOH}-w_4-3$ structure has a rather peculiar pair of non-bonded oxygen atoms of water molecules, O_1 and O_3 , separated from each other by 3.426 Å, a distance which is

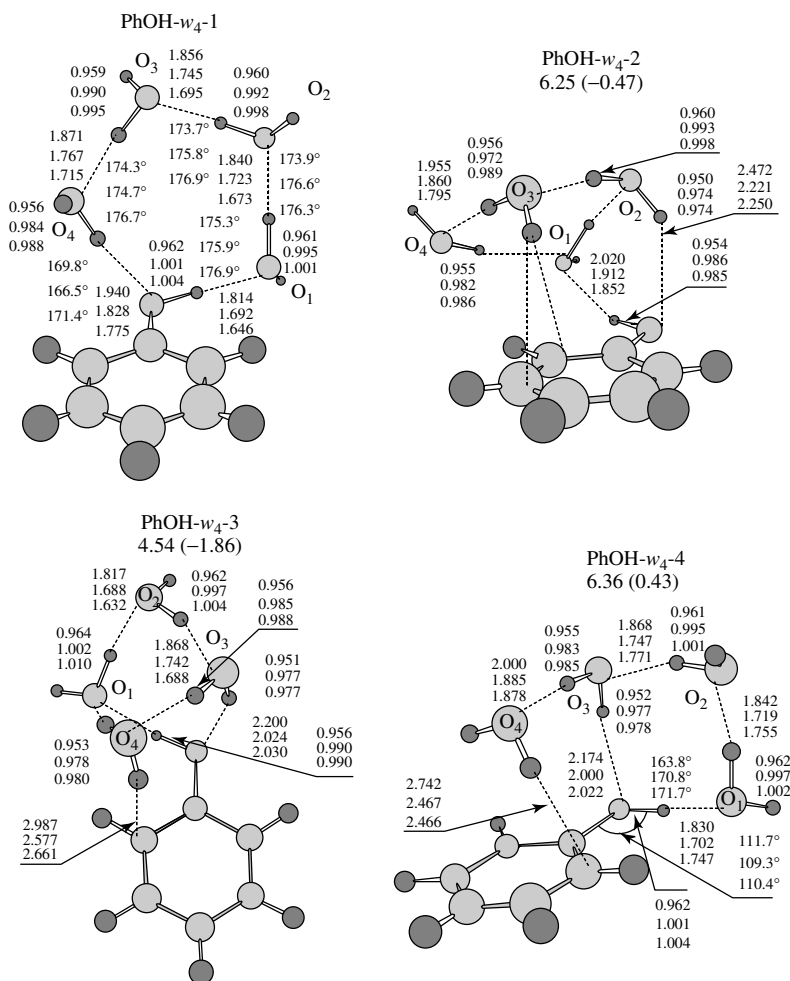


FIGURE 51. Eleven lower-energy structures of the phenol–water₄ complex. Bond lengths are in Å. The geometrical parameters are tripled for the lowest-energy structures in the following order (from the bottom to the top): the HF/A, MP2/A and B3LYP/A values. The HF/A relative energy with respect to the global-minimum structure $\text{PhOH}-w_4-1$ is given in kJ mol^{-1} . Its MP2(sp)/A analogue is followed in parentheses. Adapted from Reference 731 with permission

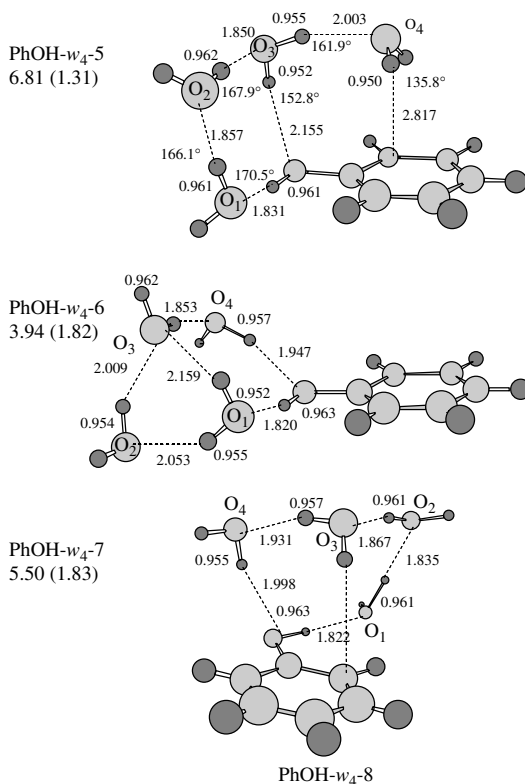


FIGURE 51. (continued)

smaller by about 0.2 Å than the first minimum of the radial oxygen–oxygen distribution function g_{oo} of liquid water widely used to define its first coordination shell⁷²³.

The next, energetically less stable structures are PhOH- w_4 -4 and PhOH- w_4 -5. They are quite remarkably different from those studied above. Three water molecules are arranged in a cyclic structure whereas the fourth one forms two π hydrogen bonds of Leg1-type with the π -electrons of the phenol ring. This water molecule resides above the phenol ring with the distances $r(\text{O}_4-\text{C}_2) = 3.35$ Å and $r(\text{O}_4-\text{C}_3) = 3.32$ Å. The energy separations of PhOH- w_4 -4 and PhOH- w_4 -5 from the global minimum are 6.4 and 6.8 kJ mol⁻¹, respectively. The remainder of the lower-energy portion of the PES of the PhOH- w_4 complex is the following. The PhOH- w_4 -6 structure has six hydrogen bonds and a total dipole moment of 3.23 D; it is 3.9 kJ mol⁻¹ above the global minimum. Its water pattern also partly resembles a book. A similar structure is also inherent for PhOH- w_4 -7 at 1.5 kJ mol⁻¹ above PhOH- w_4 -6. The next structure, PhOH- w_4 -8, is quite particular in that its OH phenolic group functions only as a hydrogen bond donor, in contrast to all other reported PhOH- w_4 structures. The PhOH- w_4 -9 structure is separated from the global minimum by 2.4 kJ mol⁻¹. Its four water molecules form a ring similar to the PhOH- w_4 -1 structure and differs from the latter by flippings of free OH groups of water molecules. A similar water pattern is seen for PhOH- w_4 -10 whereas PhOH- w_4 -11 partly mimics the PhOH- w_4 -3 structure.

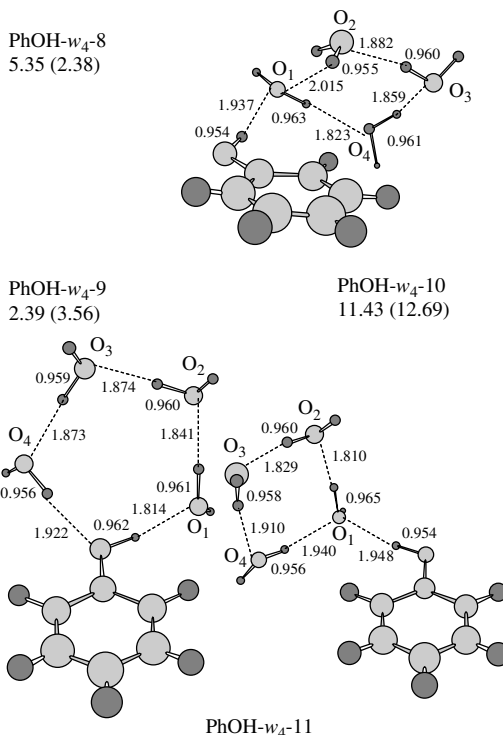
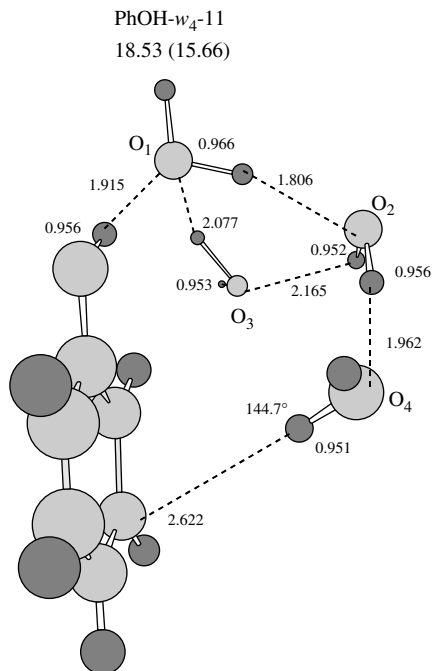


FIGURE 51. (continued)

Compared to HF/A, the MP2 and B3LYP/A PESs of $\text{PhOH}(\text{H}_2\text{O})_4$ have somewhat different topologies, which is reflected in the geometries of the phenol–water₄ complexes. For example, the MP2/A level reverses the order between the PhOH- w_4 -1–3 structures in such a way that PhOH- w_4 -2 becomes the global minimum; PhOH- w_4 -3 is only 0.8 kJ mol⁻¹ higher, and PhOH- w_4 -2 is 4.6 kJ mol⁻¹ higher (neglecting ZPVE). As for the B3LYP/A geometries, we may note that, for instance, in PhOH- w_4 -3 the oxygen atom O₄ is separated from the carbon atom C₂ of phenol by 3.410 Å whereas $r(\text{H}'_4-\text{C}_2) = 2.661$ Å. In PhOH- w_4 -2, the distances $r(\text{O}_4-\text{C}_3) = 3.345$ Å and $r(\text{H}'_4-\text{C}_2) = 2.627$ Å. The latter is smaller by about 0.3 Å than the sum of van der Waals radii of the corresponding atoms. Summarizing and taking into account that the expected margin error of the computational methods employed in the present work is *ca* ±8 kJ mol⁻¹, we conclude that these four structures PhOH- w_4 -1–4 are placed at the very bottom of the PES of $\text{PhOH}(\text{H}_2\text{O})_4$ and are actually nearly isoenergetic.

In order to interpret the experimentally determined IR pattern of phenol interacting with four water molecules, we now consider theoretical OH-stretching modes of the PhOH- w_4 -1–4 structures (Table 39). Contrary to the PhOH- w_1 -1 and PhOH- w_2 -1 structures studied above, the vibrational assignments are particular for each structure of the PhOH- w_4 complex. The most red-shifted OH-stretching vibration at 3772 (2970.1) cm⁻¹ is predicted for the PhOH- w_4 -2 structure. It is predominantly assigned to the hydrogen-stretching vibration of the O₁–H₁ ⋯ O₂ bond and is significantly enhanced by a factor

FIGURE 51. (*continued*)

of 24 in comparison with the IR intensity of the ν_1 vibration of the water molecule. The analogous OH-stretching vibration of PhOH- w_4 -3 is placed at 3798 (3008.4) cm^{-1} . It is also predominantly assigned to the symmetric hydrogen-stretching vibration of the $\text{O}_1\text{—H}_1 \cdots \text{O}_2$ and $\text{O}_2\text{—H}_2 \cdots \text{O}_3$ bonds. The corresponding asymmetric vibrational mode is found at 3874 (3201.8) cm^{-1} . Its IR intensity exceeds that of the ν_3 vibrations of the water molecule by a factor of 12. Interestingly, the phenolic OH-stretching vibration contributes only to the fourth, 3988 (3476.8) cm^{-1} , and to the third, 3958 (3394.4) cm^{-1} , vibrations of PhOH- w_4 -2 and PhOH- w_4 -3, respectively. It is therefore red-shifted by *ca* 230 and 160 cm^{-1} , respectively, from that of bare phenol and their IR intensities are increased by *ca* 4-fold.

It follows from Table 38 that the quintessential feature of OH-stretching vibrations of the PhOH- w_4 -3 and PhOH- w_4 -2 is that they are not separable into groups of vibrations. For example, in the case of PhOH- w_4 -3, the inter-vibrational separations take the following values: 75 (192), 84 (192), 26 (67), 41 (133), 71 (76), 41 (101), 6 (11) and 4 (7) cm^{-1} . We suggest that such vibrational non-separability occurs due to the cage-type arrangements of water molecules and the existence of π hydrogen bonding between one of the water molecules and the phenol ring. Such π hydrogen bonding results in that the corresponding π -OH stretching vibrations of this particular water molecule for the PhOH- w_4 -3 structure at 4024.8 (3593.9) (symmetric) and 4146.9 (3771.1) (asymmetric) cm^{-1} . Compared with the ν_1 and ν_3 stretching vibrations of the water molecule, the former is red-shifted by 45 (180) cm^{-1} whereas the latter is red shifted by 41 (144) cm^{-1} .

TABLE 39. The OH-stretch frequencies (in cm^{-1}) of phenol–water₄ complexes calculated at the HF/A and B3LYP/A (in parentheses) computational levels. Infrared intensity is in km mol^{-1} and Raman (R) activity in $\text{\AA}^4 \text{amu}^{-1}$. The partial contributions are evaluated as the ratio of the total displacements. The contribution of the first reported mode is referred to 100%

Frequency	IR	Raman	Assignment
<i>PhOH-w₄-1</i>			
3811.6 (3077.8)	724 (1260)	261	ν_{OH} , $\nu_{\text{O}_1\text{H}_1}$ (31.4%)
3869.0 (3217.1)	849 (1442)	68	$\nu_{\text{O}_2\text{H}_2}$, ν_{OH} (81.1%), $\nu_{\text{O}_1\text{H}_1}$ (60.6%), $\nu_{\text{O}_3\text{H}_3}$ (32.5%)
3898.5 (3287.7)	854 (1521)	39	$\nu_{\text{O}_1\text{H}_1}$, $\nu_{\text{O}_3\text{H}_3}$ (78.0%), $\nu_{\text{O}_2\text{H}_2}$ (21.8%)
3926.8 (3354.0)	330 (683)	73	$\nu_{\text{O}_1\text{H}_1}$, $\nu_{\text{O}_3\text{H}_3}$ (87.6%), $\nu_{\text{O}_2\text{H}_2}$ (16.1%)
3976.6 (3468.8)	314 (551)	77	$\nu_{\text{O}_4\text{H}_4}$
4140.7 (3796.0)	112 (42)	67	$\nu_{\text{O}_1\text{H}_1'}$
4143.4 (3797.5)	105 (46)	56	$\nu_{\text{O}_2\text{H}_2'}$, $\nu_{\text{O}_3\text{H}_3'}$ (19.1%)
4143.8 (3798.7)	114 (40)	39	$\nu_{\text{O}_4\text{H}_4'}$
4144.8 (3800.3)	92 (44)	70	$\nu_{\text{O}_3\text{H}_3'}$, $\nu_{\text{O}_2\text{H}_2'}$ (16.3%)
<i>PhOH-w₄-2</i>			
3771.8 (2970.1)	431 (772)	91	$\nu_{\text{O}_1\text{H}_1}$
3915.1 (3299.0)	309 (544)	52	$\nu_{\text{O}_2\text{H}_2}$
3961.7 (3429.8)	277 (315)	37	$\nu_{\text{O}_3\text{H}_3}$, $\nu_{\text{O}_4\text{H}_4}$ (90.4%)
3987.7 (3476.8)	308 (987)	55	$\nu_{\text{O}_3\text{H}_3}$, $\nu_{\text{O}_4\text{H}_4}$ (88.7%), ν_{OH} (22.7%)
4005.6 (3515.8)	416 (373)	110	ν_{OH} , $\nu_{\text{O}_4\text{H}_4}$ (18.2%)
4109.6 (3721.9)	130 (80)	33	$\nu_{\text{O}_2\text{H}_2'}$
4132.7 (3763.5)	164 (115)	47	$\nu_{\text{O}_3\text{H}_3'}$
4133.6 (3794.8)	96 (51)	95	$\nu_{\text{O}_1\text{H}_1'}$
4151.9 (3802.8)	126 (51)	80	$\nu_{\text{O}_4\text{H}_4'}$
<i>PhOH-w₄-3</i>			
3798.4 (3008.4)	448 (77)	153	$\nu_{\text{O}_1\text{H}_1}$, $\nu_{\text{O}_2\text{H}_2}$ (22.9%)
3873.6 (3201.8)	719 (1309)	36	$\nu_{\text{O}_2\text{H}_2}$, $\nu_{\text{O}_1\text{H}_1}$ (23.8%)
3957.6 (3394.4)	361 (572)	73	ν_{OH}
3983.7 (3461.4)	244 (402)	54	$\nu_{\text{O}_3\text{H}_3'}$, $\nu_{\text{O}_3\text{H}_3''}$ (16.8%)
4024.8 (3593.9)	163 (300)	54	$\nu_{\text{O}_4\text{H}_4'}$, $\nu_{\text{O}_4\text{H}_4''}$ (30.5%)
4095.7 (3670.3)	218 (247)	56	$\nu_{\text{O}_3\text{H}_3'}$, $\nu_{\text{O}_3\text{H}_3''}$ (17.9%)
4136.5 (3792.2)	111 (38)	77	$\nu_{\text{O}_1\text{H}_1'}$
4142.9 (3800.7)	112 (42)	63	$\nu_{\text{O}_2\text{H}_2'}$
4146.9 (3771.1)	122 (104)	42	$\nu_{\text{O}_4\text{H}_4''}$, $\nu_{\text{O}_4\text{H}_4'}$ (28.4%)
<i>PhOH-w₄-4</i>			
3814.1 (3064.2)	468 (815)	214	ν_{OH} , $\nu_{\text{O}_1\text{H}_1}$ (53.2%), $\nu_{\text{O}_2\text{H}_2}$ (21.8%)
3866.3 (3198.2)	1022 (1708)	24	$\nu_{\text{O}_2\text{H}_2}$, ν_{OH} (77.3%), $\nu_{\text{O}_1\text{H}_1}$ (28.1%)
3899.5 (3270.9)	379 (760)	53	$\nu_{\text{O}_1\text{H}_1}$, $\nu_{\text{O}_2\text{H}_2}$ (63.4%), ν_{OH} (12.0%)
3991.0 (3516.8)	225 (342)	54	$\nu_{\text{O}_3\text{H}_3'}$, $\nu_{\text{O}_3\text{H}_3''}$ (23.8%)
4058.1 (3691.8)	27 (156)	38	$\nu_{\text{O}_4\text{H}_4'}$, $\nu_{\text{O}_4\text{H}_4''}$ (69.6%)
4095.0 (3648.2)	218 (180)	53	$\nu_{\text{O}_3\text{H}_3'}$, $\nu_{\text{O}_3\text{H}_3''}$ (25.5%)
4139.4 (3795.8)	114 (50)	85	$\nu_{\text{O}_1\text{H}_1'}$
4145.3 (3796.9)	89 (29)	61	$\nu_{\text{O}_2\text{H}_2'}$
4163.4 (3804.6)	79 (47)	29	$\nu_{\text{O}_4\text{H}_4''}$, $\nu_{\text{O}_4\text{H}_4'}$ (62.2%)
<i>PhOH-w₄-5</i>			
3822.5	288	234	ν_{OH} , $\nu_{\text{O}_1\text{H}_1}$ (78.8%), $\nu_{\text{O}_2\text{H}_2}$ (46.2%)

(continued overleaf)

TABLE 39. (continued)

Frequency	IR	Raman	Assignment
3865.8	1227	7	$\nu_{O_2H_2}$, ν_{OH} (73.5%)
3902.7	346	54	$\nu_{O_1H_1}$, $\nu_{O_2H_2}$ (26.1%), ν_{OH} (17.1%)
3988.7	228	49	$\nu_{O_3H'_3}$, $\nu_{O_3H''_3}$ (23.9%)
4060.3	19	28	$\nu_{O_4H_4}$, $\nu_{O_4H''_4}$ (76.0%), $\nu_{O_3H'_3}$ (10.3%)
4090.7	229	58	$\nu_{O_3H'_3}$, $\nu_{O_3H'_3}$ (26.6%)
4144.8	79	68	$\nu_{O_2H'_2}$, $\nu_{O_1H'_1}$ (56.8%)
4146.1	126	99	$\nu_{O_1H'_1}$, $\nu_{O_2H'_2}$ (59.6%)
4163.5	69	25	$\nu_{O_4H'_4}$, $\nu_{O_4H_4}$ (76.7%)
<i>PhOH-w₄-6</i>			
3815.7	534	211	ν_{OH}
3866.0	906	59	$\nu_{O_2H_2}$
3972.1	514	110	$\nu_{O_3H_3}$
3992.4	145	108	$\nu_{O_4H_4}$, $\nu_{O_1H''_1}$ (32.9%)
4007.3	190	27	$\nu_{O_1H''_1}$, $\nu_{O_1H'_1}$ (48.3%), $\nu_{O_4H_4}$ (34.5%)
4088.7	252	45	$\nu_{O_1H'_1}$, $\nu_{O_1H''_1}$ (33.3%)
4140.6	112	69	$\nu_{O_2H'_2}$, $\nu_{O_3H'_3}$ (12.4%)
4141.4	165	54	$\nu_{O_3H'_3}$, $\nu_{O_2H'_2}$ (14.6%)
4154.8	128	60	$\nu_{O_4H'_4}$
<i>PhOH-w₄-7</i>			
3809.1	571	188	ν_{OH} , $\nu_{O_1H_1}$ (28.9%)
3869.4	894	46	$\nu_{O_2H_2}$, $\nu_{O_1H_1}$ (68.2%), ν_{OH} (55.6%)
3905.6	440	51	$\nu_{O_1H_1}$, $\nu_{O_2H_2}$ (84.0%)
3954.8	227	50	$\nu_{O_3H_3}$, $\nu_{O_2H_2}$ (11.5%), $\nu_{O_4H_4}$ (11.4%)
3999.4	263	51	$\nu_{O_4H_4}$
4126.9	117	60	$\nu_{O_3H'_3}$
4143.1	111	95	$\nu_{O_1H'_1}$
4148.4	101	60	$\nu_{O_2H'_2}$
4155.5	126	42	$\nu_{O_4H'_4}$
<i>PhOH-w₄-8</i>			
3824.3	302	147	$\nu_{O_1H_1}$, $\nu_{O_2H_2}$ (26.6%)
3884.9	765	40	$\nu_{O_3H_3}$, $\nu_{O_2H_2}$ (83.4%), $\nu_{O_1H_1}$ (61.5%)
3919.1	434	46	$\nu_{O_3H_3}$, $\nu_{O_2H_2}$ (94.9%)
3977.9	334	63	ν_{OH} , $\nu_{O_4H_4}$ (26.9%)
4003.4	300	90	$\nu_{O_4H_4}$, ν_{OH} (35.9%)
4131.9	202	39	$\nu_{O_4H'_4}$, $\nu_{O_1H'_1}$ (14.9%)
4135.9	81	91	$\nu_{O_1H'_1}$, $\nu_{O_4H'_4}$ (11.0%)
4142.9	130	47	$\nu_{O_2H'_2}$, $\nu_{O_3H_3}$ (14.5%)
4144.4	84	83	$\nu_{O_3H'_3}$, $\nu_{O_2H_2}$ (16.1%)
<i>PhOH-w₄-9</i>			
3817.5	732	243	ν_{OH} , $\nu_{O_1H_1}$ (33.8%)
3876.7	693	84	$\nu_{O_1H_1}$, ν_{OH} (94.2%), $\nu_{O_2H_2}$ (93.9%), $\nu_{O_3H_3}$ (34.2%)
3903.3	941	38	$\nu_{O_3H_3}$, $\nu_{O_1H_1}$ (81.5%), $\nu_{O_2H_2}$ (22.7%)
3932.0	302	60	$\nu_{O_2H_2}$, $\nu_{O_3H_3}$ (57.0%), $\nu_{O_1H_1}$ (15.3%)

TABLE 39. (continued)

Frequency	IR	Raman	Assignment
3975.6	382	107	$\nu_{O_4H_4}$, $\nu_{O_3H_3}$ (11.6%)
4142.1	105	69	$\nu_{O_1H'_1}$
4146.2	116	67	$\nu_{O_4H'_4}$, $\nu_{O_3H'_3}$ (17.9%)
4146.6	128	27	$\nu_{O_3H'_3}$, $\nu_{O_2H'_2}$ (62.9%), $\nu_{O_4H'_4}$ (37.1%)
4147.5	118	74	$\nu_{O_2H'_2}$, $\nu_{O_3H'_3}$ (55.8%)

Values taken from Reference 731 with permission.

The PhOH- w_4 -4 structure also has a rather peculiar and non-separable OH-stretching vibrational pattern. Its three most red-shifted vibrations are located at 3814 (3064.2), 3866 (3198.2) and 3900 (3270.9) cm^{-1} . Altogether, they describe the coupled OH-stretching vibrations of the trimeric water ring and the phenolic OH group. The second one is the most IR active among all OH-stretching vibrations of all reported PhOH- w_4 structures. Its IR intensity is 13 (18) times larger than that of the OH-stretching vibration of bare phenol (ν_3 of the water molecule). The symmetric and asymmetric stretches of the water molecule connecting the water ring with the terminated water molecule placed above the phenol ring are found at 3991 (3516.8) and 4095 (3648.2) cm^{-1} . Between them, at 4058 (3691.8) cm^{-1} , there exists the symmetric π OH stretch whose asymmetric vibration has the highest frequency of 4163 (3804.6) cm^{-1} . These two vibrations are separated by the OH stretches at 4139 (3795.8) and 4145 (3796.9) cm^{-1} , assigned to free OH groups of water molecules.

As we would expect, the pattern of the OH-stretching vibrations of PhOH- w_4 -1 is absolutely different from those of PhOH- w_4 -2, PhOH- w_4 -3 and PhOH- w_4 -4 and resembles the typical S_4 pattern of the PhOH- w_1 , PhOH- w_2 and PhOH- w_3 -1–5 structures. It is clearly seen from Table 39 that the nine OH-stretching vibrations of the PhOH- w_4 -1 structure are well separated into two groups in that way forming the ‘window’ region of width about 164 (327) cm^{-1} . Note that the B3LYP/A width agrees satisfactorily with the experimental one⁷⁰⁵. The former group spans the region between 3812 (3077.8; expt: ca 3135⁷⁰⁵) and 3977 (3468.8; expt: 3430⁷⁰⁵) cm^{-1} and consists of five rather IR and Raman active OH-stretching vibrations assigned to the coupled stretches of the water ring and phenolic OH groups. Its highest OH-stretching vibration is dominantly composed of the hydrogen stretch of the water molecule donating the hydrogen bond to phenol. The latter group is rather narrow with a width of only 4 (4) cm^{-1} . The OH-stretching vibrations of free water OH groups contribute to this group. Its lowest wavenumber stretch at 4141 (3796.0) cm^{-1} corresponds to the free OH group of the water molecule which accepts the phenolic hydrogen bond.

Summarizing the B3LYP/A IR patterns in the stretching region of the four most energetically stable structures PhOH- w_4 -1, PhOH- w_4 -2, PhOH- w_4 -3 and PhOH- w_4 -4, we illustrate them in equation 46.

$$\begin{aligned}
 \text{PhOH-}w_4\text{-1: } & \nu_{\text{OH}}(3077.8) <^{139} \nu_1^{ad2}(3217.0) <^{81} \nu_1^{ad13'}(3287.7) <^{66} \\
 & \nu_1^{ad13''}(3354.0) <^{115} \nu_1^d(3468.8) <^{327} \nu_3^{ad1}(3796.0) <^2 \\
 & \nu_3^{ad2}(3797.5) <^1 \nu_3^d(3798.7) <^2 \nu_3^{ad3}(3800.3) \\
 \text{PhOH-}w_4\text{-2: } & \nu_1^{ad1}(2970.1) <^{319} \nu_1^{add2}(3299.0) <^{131} \nu_1^{add3}(3429.8) <^{47} \\
 & \nu_1^{add3,ad4}(3476.8) <^{39} \nu_{\text{OH}}(3515.8) <^{106} \nu_3^{add2}(3721.9) <^{42} \\
 & \nu_3^\pi(3763.5) <^{31} \nu_3^{ad1}(3794.8) <^8 \nu_3^{ad4}(3802.8)
 \end{aligned}$$

$$\begin{aligned}
\text{PhOH-}w_4\text{-3: } & \nu_1^{ad1}(3008.4) <^{193} \nu_1^{ad2}(3201.8) <^{192} \nu_{\text{OH}}(3394.4) <^{67} \\
& \nu_1^{add3}(3461.4) <^{133} \nu_{\text{sym}}^{\pi}(3593.9) <^{76} \nu_3^{add3}(3670.3) <^{101} \\
& \nu_{\text{asym}}^{\pi}(3771.1) <^{21} \nu_3^{ad1}(3792.2) <^9 \nu_3^{ad2}(3800.7) \\
\text{PhOH-}w_4\text{-4: } & \nu_{\text{OH}}(3064.2) <^{134} \nu_1^{ad2}(3198.2) <^{73} \nu_1^{ad1}(3270.9) <^{246} \\
& \nu_1^{add3}(3516.8) <^{131} \nu_3^{add3}(3648.2) <^{44} \nu_{\text{sym}}^{\pi}(3691.8) <^{104} \\
& \nu_3^{ad1}(3795.8) <^1 \nu_3^{ad2}(3796.9) <^8 \nu_{\text{asym}}^{\pi}(3804.6). \quad (46)
\end{aligned}$$

The ‘window’ region of the PhOH- w_4 -1 structure spreads from 3468.8 to 3796.0 cm^{-1} and covers an area of 327 cm^{-1} (the experimental value is 281 cm^{-1} ⁷⁰⁵). It follows from equation 46 that, in this region, the isomer PhOH- w_4 -4 has four OH-stretching modes placed at 3516.8, 3648.2, 3691.8 and 3795.8 cm^{-1} . PhOH- w_4 -3 also has four OH-stretching modes there, i.e. 3593.9, 3670.3, 3771.1 and 3792.2 cm^{-1} , whereas PhOH- w_4 -2 exhibits five modes: 3476.8, 3515.8, 3721.9, 3763.5 and 3794.8 cm^{-1} . In other words, the PhOH- w_4 -3 and PhOH- w_4 -4 have precisely that number of vibrational modes which was revealed experimentally ^{704, 705}. Due to theoretical and experimental uncertainties, the structure PhOH- w_4 -2 might also be included into this class. Therefore, these three lower-energy structures of phenol with four water molecules characterized by the formation of the π hydrogen bond are likely referred to as the class of structures revealed in Reference 590. It is worth mentioning that the lowest stretching mode of the non-ring structure of PhOH(H_2O)₄ is calculated 73 cm^{-1} below the analogous mode in the ring S_4 structure PhOH- w_4 -1 ⁷⁰⁵. It then follows from equation 46 that PhOH- w_4 -2 and PhOH- w_4 -3 have a similar feature, i.e. 108 and 69 cm^{-1} , respectively.

In order to obtain some insight into the formation of the π hydrogen bonding in the PhOH- w_4 -2–PhOH- w_4 -4 structures in terms of the molecular orbital (MO) or electron density patterns, we draw in Figure 52 the lowest unoccupied molecular orbital (LUMO), the highest one (HOMO) and HOMO-1 of the PhOH- w_4 -4 structure. As seen vividly there, the π hydrogen bonding between the π cloud of the phenol ring and the water molecule w_4 reshapes the HOMO-1, HOMO and LUMO of bare phenol and slightly lowers the HOMO-1 orbital energy but, on the contrary, raises the orbital energies of the HOMO and LUMO by *ca* 0.2 eV. For example, we observe a small portion of the charge transfer from the HOMO-1 to the s orbital of the hydrogen atoms of this water molecule and to the lone pairs of the oxygen atom. This raises their population to 0.06 for H and to 0.15 for O and results in the appearance of a small hollow in the HOMO-1 of bare phenol precisely in the front of the water molecule w_4 . A slightly smaller charge, *ca* 0.13, is transferred from the π -HOMO of phenol to the lone pair MO of the oxygen atom, whereas a substantial charge transfer from the LUMO to the s MO of the oxygen atom of the water molecule is predicted by the present B3LYP/A level.

What are the essential conclusions of the present subsection? As we have already mentioned above, the last decade was unprecedentedly successful, primarily from the experimental point of view, in studying the interaction between phenol and water molecules. In particular, it was discovered that phenol favours a 2D ring type of arrangement of water molecules if there are less than *three* water molecules and, on the contrary, the 3D ring type if these are *five* or more water molecules. It was therefore thought that *four* looks like the ‘magic’ number for the phenol–water_{*n*} interaction, and this was really a sort of exclusive number thanks, first of all, to the experimental work by different groups ^{590, 704, 705} who revealed experimentally the existence of the phenol–water₄ isomer with a 3D arrangement



FIGURE 52. The shape (contour spacing of 0.008 e au^{-3}) of the highest occupied (HOMO), lowest unoccupied (LUMO) and HOMO-1 of the complex $\text{PhOH-w}_4\text{-4}$ using the B3LYP/A wave function; ε denotes the orbital energy

of water molecules. They showed that it was only one particular isomer which is capable of explaining the puzzling ‘window’ region in the IR stretching spectra. Logically, the ‘magic’ of the number *four* stems from the fact that this is just the borderline where the 2D water pattern ($n \leq \text{three}$) meets the 3D pattern ($n \geq \text{five}$). The analysis of the potential energy surface of the phenol–water₄ complex conducted above and its juxtaposition with the PESs of the phenol–water_{1–3} complexes demonstrates vividly this point of view.

C. Hydrogen Bonding between Phenol and Acetonitrile

1. Introductory foreground

Acetonitrile (ACN) possesses some unique properties, such as a high dielectric constant (35.95) and the solubilization of many inorganic and organic materials.^{738, 739} It is actually one of the few simple aprotic solvents miscible in water at any ratio. X-ray diffraction studies of pure acetonitrile revealed that ACN molecules do not strongly interact with themselves and are only weakly associated via dipole–dipole interaction⁷⁴⁰. The IR spectrum of pure acetonitrile includes two major bands placed at 2257 and 2295 cm^{-1} ⁷⁴⁰. The former, called ν_2 , originates from the $\text{C}\equiv\text{N}$ stretching mode while the latter is a combination band composed of the CCH bend ν_3 and C–C stretch ν_4 modes⁷⁴¹.

For the last forty years the acetonitrile molecule was, and still is, a ‘work horse’ in many laboratories worldwide, in experimental studies of the hydrogen bonding with nitriles. It is obvious that ACN possesses two sites for accepting a hydrogen bond: the one on the lone-pair electrons of the nitrogen atom (σ -bonding) and the other on the $\text{C}\equiv\text{N}$ triple bond (π -bonding). The hydrogen bond formation in phenol–nitrile systems was initially examined by several authors^{742–745} in inert solvents such as CCl_4 or C_2Cl_4 ^{746–750} who all recorded that their IR spectra contain an additional band placed on the low-frequency side of the free phenol O–H stretching band $\nu(\text{OH})$ as the concentration of the nitrile increases. The $\Delta\nu(\text{OH})$ shift varies from 148.5 cm^{-1} at 0.119 M of ACN to 156.5 cm^{-1} when the ACN concentration reaches 0.687 M⁷⁴². These authors then suggested that this new band results from the O–H stretching mode of a hydrogen-bonded complex involving the OH group of phenol and the nitrogen atom of the nitrile. It was at that time when the existence of a 1:1 complex between phenol and nitrile in inert solvents was postulated^{743, 744}. The appearance of an unusual blue shift of the $\text{C}\equiv\text{N}$ stretching vibration by about 12.5 cm^{-1} was noted⁷⁴² when the nitrogen atom of the nitrile group is complexed with the OH group of phenol, implying a σ -type hydrogen bonding between the nitrogen lone pair and the phenol OH. The increased frequency of the $\text{C}\equiv\text{N}$ stretching vibration in the complex gave rise to a shoulder on the high-frequency side of the $\text{C}\equiv\text{N}$ peak.

At nearly the same time, on the basis of the well-known Buckingham formula describing the frequency shift in a medium⁷⁵¹, it was deduced^{752, 753} that if the fundamental stretching mode $\nu(\text{OH})$ of free phenol in the gas phase is fitted at 3655 cm^{-1} , it must be extrapolated in the phenol–acetonitrile complex to 3540 cm^{-1} , and therefore the red shift due to complexation becomes equal to 115 cm^{-1} . This value looks much smaller than expected²⁰⁹ although, as we have already mentioned, a red shift of 148.5–156.5 cm^{-1} was found⁷⁴² and similar red shifts of 152⁷⁴⁵ and 160⁷⁴⁶ cm^{-1} were also detected. The origin of the frequency shift of the $\nu(\text{OH})$ mode of phenol was also noted⁷⁵⁴ in the phenol–ACN complex from 3460 to 3409 cm^{-1} on increasing the concentration of acetonitrile from 0.19 to 100% in CCl_4 (interestingly, the change proceeds stepwise: between 0.19 and 0.39% no shift was detected, between 0.78 and 1.8% it is equal to –5 cm^{-1} , a further dilution to 4% results in –10 cm^{-1} etc.). It is not entirely clear and suggests a possible formation of 2:1 phenol–acetonitrile complexes due to the increased basicity of the oxygen atom of phenol. A similar trend was recently observed⁷⁵⁵ for the pentachlorophenol–acetonitrile complex. Such a puzzling effect has not been so well appreciated by theoreticians despite the fact that it still annoys the experimentalists, although it is worth recollecting the mid-1980’s theoretical work⁷⁵⁶ (see also References 757–759) which suggested that the most favourable hydrogen bond formation with nitriles occurs via σ -type hydrogen bonding. However, this is not the case with the hydrogen-bonded complexes of water with benzonitrile, where the π -bonding is slightly superior over the σ -type⁷²⁹—we could actually agree with some authors⁷⁴³ that ‘benzonitrile... is found to be anomalous’. Nevertheless, other

authors concluded that this is just the case for hydrogen bonding with nitriles^{746, 757–759}, and also a quite recent B3LYP/6-31G(d,p) study⁶¹² of the phenol–acetonitrile and phenol–pyridine complexes mainly focused on the anharmonicity contribution to their dipole moments.

Summarizing, what else we can tell the reader from a theoretical point of view? There are certainly some as yet unclear points related to routine use of quantum chemical programs for obtaining the optimized structure of the 1:1 complex between phenol and acetonitrile and somehow exploring the calculated frequencies to discuss, again routinely, agreement between experiment and theory. It seems as if what remains is the existence of the 2:1 complex and its structure and the puzzling dependence of the shift of the $\nu(\text{OH})$ mode of phenol on the ACN concentration although, impressed by the rampant experimentalists arguments, this was likely a way to almost nowhere and does not deserve to be published at all. Nevertheless, we have performed a rather exhaustive search⁷⁶⁰ of the PES of the phenol–acetonitrile interaction and its results and the consequent attempt to explain the experiments is presented below⁷⁶¹.

2. Phenol–acetonitrile complex

The PES of the interaction of the phenol and acetonitrile molecules consists of two lower-energy minimum structures⁷⁶¹ displayed in Figure 53. The first, named PhOH-ACN-1, is the conventional structure which has been explored by experimentalists for four decades. It occupies the global minimum on that PES and is characterized by a binding energy $E_{\text{HB}}^{(1)}(\text{PhOH-ACN})$ of 22.3 kJ mol⁻¹ (see Table 40). It agrees fairly with the experimental value of 18.8 kJ mol⁻¹ for the reported enthalpy of formation^{746, 757}. The BSSE correction comprises only 0.7 kJ mol⁻¹ and is hereafter neglected. The second minimum-energy structure, PhOH-ACN-2, is reported here for the first time and placed higher by 16.5 kJ mol⁻¹, and therefore has a binding energy $E_{\text{HB}}^{(2)}(\text{PhOH-ACN})$ of 5.8 kJ mol⁻¹.

If the conventional structure is formed due to the typical medium-strength hydrogen bond between the OH group of phenol and the lone pair of the nitrogen atom of acetonitrile, respecting all canonical though still somewhat loosely defined rules¹⁷³ which will be later thoroughly discussed, the structure PhOH-ACN-2 is quite peculiar in the sense that its formation is provided by two weaker bonds which could also be referred to with some caution as some sort of hydrogen bonds. One of them is a C–H...O hydrogen bond between the methyl group of acetonitrile and the oxygen atom of phenol, while the other seems to be much weaker and is formed between the π -electrons of the C \equiv N bond of acetonitrile and the CH group of phenol. The fact that this is affirmatively a π hydrogen bond is confirmed by the value of the bonding angle $\angle \text{C–H–N} = 79.1^\circ$.

Let us first analyse by a routine procedure what are the substantial changes in the geometries of the precursors⁷⁶² and their characteristic vibrational modes which accompany the formation of the σ -type O–H...N hydrogen bond between phenol and acetonitrile. Obviously, this is primarily the elongation of the O–H bond length by 0.008 Å as manifested in a red shift of the $\nu(\text{OH})$ stretching vibration by 158 cm⁻¹ (in fair agreement with the experimental values^{742, 745}) and a significant enhancement of its IR activity, viz. from 57 km mol⁻¹ in phenol to 873 km mol⁻¹ in PhOH-ACN-1 (Table 41). The formed hydrogen bond has a typical length of 1.997 Å and is rather linear with a bond angle $\angle \text{OHN}$ of 171.6°. The hydrogen-bond stretching vibration $\nu_\sigma(\text{O–H...N})$ appears at 111.7 cm⁻¹. It is also worth mentioning two lower-frequency modes centred at 59.0 and 69.5 cm⁻¹, referring to the hydrogen-bond bending motions and originating due to the molecular dipole rotation, by analogy with the band at 90 cm⁻¹ in the phenol–pyridine complex⁶¹².

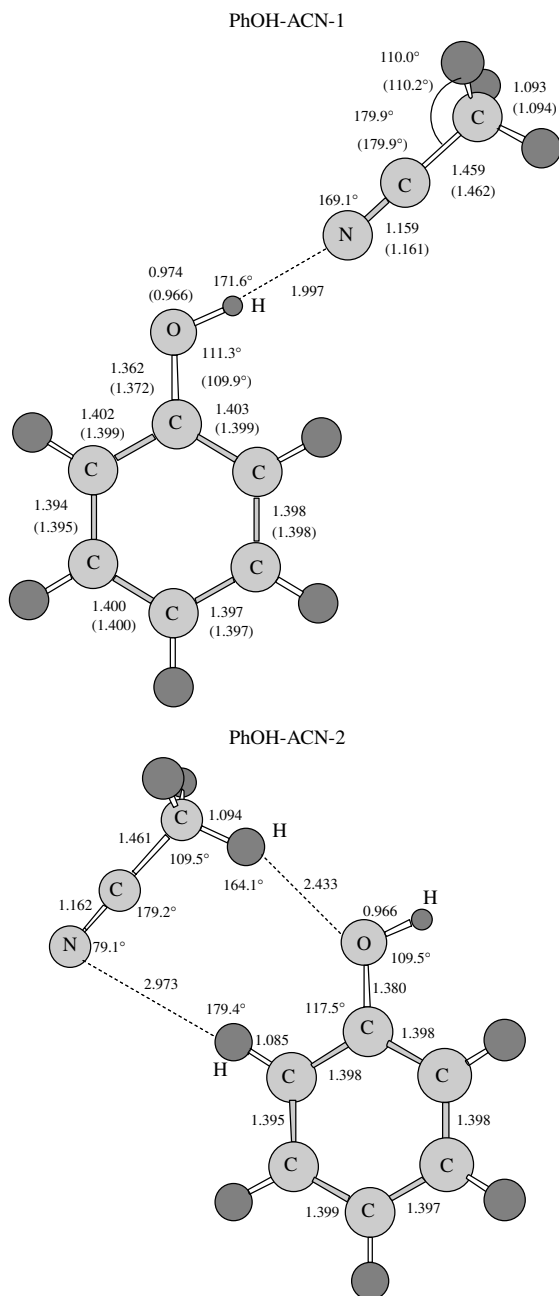


FIGURE 53. Complexes of phenol with acetonitrile. The bond lengths are in Å. Values in parentheses correspond to the optimized geometries of the free phenol and acetonitrile molecules. Adapted from Reference 761 with permission

TABLE 40. Some key features of 1:1 phenol–acetonitrile complexes

Feature	PhOH-ACN-1	PhOH-ACN-2
–Energy + 440, hartree	0.269694	0.262872
ZPVE + kJ mol ^{−1}	396.83	395.46
E_{HB} , kJ mol ^{−1}	22.3 (21.6) ^a	5.77 (5.65) ^a
Dipole moment, D	6.77	4.86
Frequencies, cm ^{−1} and IR intensities, km mol ^{−1}		
$\nu_{\sigma}(\text{N} \cdots \text{H}-\text{C})$	—	35 (7)
$\nu_{\sigma}(\text{O} \cdots \text{H}-\text{C})$	—	81 (13)
$\nu_{\sigma}(\text{N} \cdots \text{H}-\text{O})$	112 (4) [117 (4)] ^c	—
$\tau(\text{OH})$ 330 (115) ^b	645 (98) [596 (106)] ^c	323 (108)
$\nu(\text{C}-\text{O})$ 1284 (95) ^b	1300 (94) [1397(68)] ^c	1270 (96)
$\nu(\text{C}\equiv\text{N})$ 2364 (12) ^b	2378 (32)	2359 (13)
$\nu(\text{C}-\text{H} \cdots \text{O})$ 3137 (1) ^b	—	3135 (3)
$\nu(\text{C}-\text{H} \cdots \text{N})$ 3213 (5) ^b	—	3217 (3)
$\nu(\text{OH})$ 3831(57) ^b	3673 (873) [3679 (850)] ^c	3826 (53)

^aBSSE corrected.^bIn the free phenol and acetonitrile molecules.^cThe theoretical B3LYP/6-31G(d,p) results⁷³¹.

TABLE 41. Some key features of the stable complexes of phenol with two acetonitrile molecules

Feature	PhOH-ACN ₂ -1	PhOH-ACN ₂ -2
–Energy + 573, hartree	0.045325	0.039648
ZPVE + kJ mol ^{−1}	519.20	518.12
–Enthalpy + 572, hartree	0.832155	0.825477
Entropy, kJ mol ^{−1}	559.6	645.5
E_{HB} , kJ mol ^{−1}	44.60	30.75
Dipole moment, D	1.97	10.89
Quadrupole, D·Å	75.9 61.5 81.2	71.0 56.6 81.2
Polarizability, au	178.3 134.5 82.0	170.8 139.8 82.8
Frequencies, cm ^{−1} and IR intensities, km mol ^{−1}		
$\nu_{\sigma}(\text{O} \cdots \text{H}-\text{C})$ ^a	96 (3)	91 (12)
$\nu_{\sigma}(\text{N} \cdots \text{H}-\text{O})$ ^a	138 (12)	121 (5)
$\tau(\text{OH})$	681 (58)	660 (83)
$\nu(\text{C}-\text{O})$	1293 (90)	1289 (85)
$\nu(\text{C}\equiv\text{N})$	2357 (27) 2370 (47)	2358 (15) 2378 (36)
$\nu(\text{C}-\text{H} \cdots \text{O})$	3048 (13) 3128 (37)	3047 (31) 3129 (32)
$\nu(\text{OH})$	3587 (958)	3658 (905)

^aBoth modes are coupled to each other.

The out-of-plane bending mode mimicking the $\tau(\text{OH})$ of phenol is characterized by a frequency at 645 cm^{−1}. Less substantial changes are predicted by the present *ab initio* method in the phenol geometrical patterns in the vicinity of the OH group. The COH angle increases slightly, by 2.2°. The elongation of the C=O bond by 0.009 Å makes it weaker and causes a blue shift of the tackled $\nu(\text{C}=\text{O})$ stretching mode by 16 cm^{−1}. Interestingly, about the same elongation is predicted for a much lighter O–H bond. No significant

changes occur in the phenol bonded counterpart, except perhaps the blue-shifted $\nu(\text{CN})$ mode by 14 cm^{-1} , related to a shortening of the $\text{C}\equiv\text{N}$ triple bond by 0.002 \AA . The present value fairly matches the experimentally detected blue shift of 12.5 cm^{-1} ⁷⁴².

As we mentioned earlier, two weak hydrogen bonds play a major role in the formation of the PhOH-ACN-2 structure. Figure 53 shows the bond lengths of 2.433 and 2.973 \AA for the $\text{C-H}\cdots\text{O}$ and $\text{C-H}\cdots\text{N}$ bonds, respectively. Naturally, their stretching modes are characterized by lower frequencies, i.e. 81 and 35 cm^{-1} . If the C-H bond participating in the former bond is slightly lengthened by 0.0004 \AA , the opposite is observed for the other one for which the C-H bond becomes shorter by 0.0002 \AA . This involves the stretching mode placed at 3135 cm^{-1} (see Table 41). Participating in the π hydrogen bonding, the $\text{C}\equiv\text{N}$ bond slightly elongates by 0.001 \AA and its stretching mode $\nu(\text{CN})$ is red-shifted by about 5 cm^{-1} .

3. Phenol bonding with two acetonitrile molecules

After discovering above the existence of two lower-energy structures of phenol and acetonitrile (there are certainly more structures via formation of $\text{C-H}\cdots\text{N}$ on the periphery of the OH group, although a π complex between the methyl group of acetonitrile and the phenol ring should be firmly ruled out), we shall explain the experimental results via modelling microscopically an increase in the acetonitrile concentration. Before doing so, it is worthwhile briefly discussing the acetonitrile dimer because it may be anticipated that combining the locations of acetonitrile molecules in the PhOH-ACN-1 and PhOH-ACN-2 structures leads to their partial dimerization whenever another acetonitrile molecule is added to either PhOH-ACN-1 or PhOH-ACN-2 . The two possible structures of the acetonitrile dimer are a cyclic one whereas the other is built in a ‘head-to-tail’ manner^{763–766}. The latter ACN dimer structure seems not to be very important (it plays a role beyond the second solvation shell) and nearly twice as weak as the cyclic dimer^{763, 765, 766}. This is why we confine the present study to the cyclic dimer. Its optimized structure given in Figure 54 looks similar to that in Figure 2 of Reference 765 and in Figure 7 of Reference 763. Its binding energy is 17.1 kJ mol^{-1} and 14.1 kJ mol^{-1} after ZPVE corrections, and agrees satisfactorily with the MP2/cc-pVDZ and MP2/6-311+G(d) values^{763, 765}.

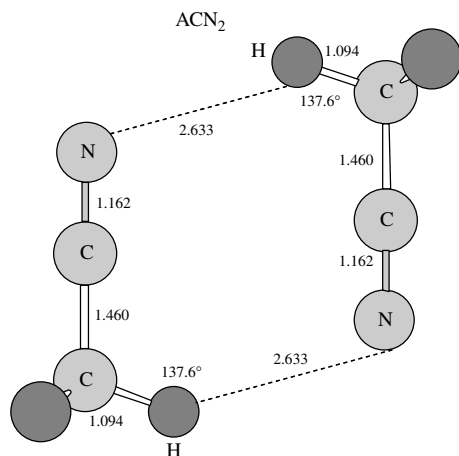


FIGURE 54. The acetonitrile dimer. Bond lengths are in \AA . Adapted from Reference 761 with permission

The cyclic ACN dimer is formed thanks to two weak $C-H \cdots N$ hydrogen bonds characterized by $N \cdots H$ bond lengths of 2.633 Å and a bond angle of 137.6° . They are manifested spectroscopically by the appearance of two far-IR bands $\nu_\sigma^{sym}(C-H \cdots N)$ and $\nu_\sigma^{asym}(C-H \cdots N)$ at 87 and 89 cm^{-1} , respectively. Two CN stretching vibrations are also organized into the symmetric and asymmetric bands placed very close to each other, at 2358.1 and 2358.9 cm^{-1} . Consequently, we conclude that the formation of the cyclic ACN dimer leads to a red shift of $\nu(C\equiv N)$ of the free acetonitrile molecule by $5\text{--}6\text{ cm}^{-1}$.

Let us now consider the lower-energy stable structures, $PhOH-ACN_2-1$ and $PhOH-ACN_2-2$, of phenol with two acetonitrile molecules. Both are displayed in Figure 55 and, when supplied by the optimized geometrical parameters, $PhOH-ACN_2-1$ possesses a partially dimerized acetonitrile moiety (see Figure 54). The former appears to be the most stable at OH with a binding energy $E_{HB}^{(1)}(PhOH-ACN_2) = 44.6\text{ kJ mol}^{-1}$ compared to the latter whose binding energy is only 30.8 kJ mol^{-1} . Increasing the temperature reverses their order due to an entropy effect, because the entropy of $PhOH-ACN_2-2$ exceeds that of $PhOH-ACN_2-1$ by 85.8 J mol^{-1} . When $T > 204\text{ K}$, the temperature at which their enthalpy difference is precisely cancelled by their entropy difference, complex $PhOH-ACN_2-2$ becomes more favourable and, at room temperature, the free-energy difference between the former and latter complexes comprises

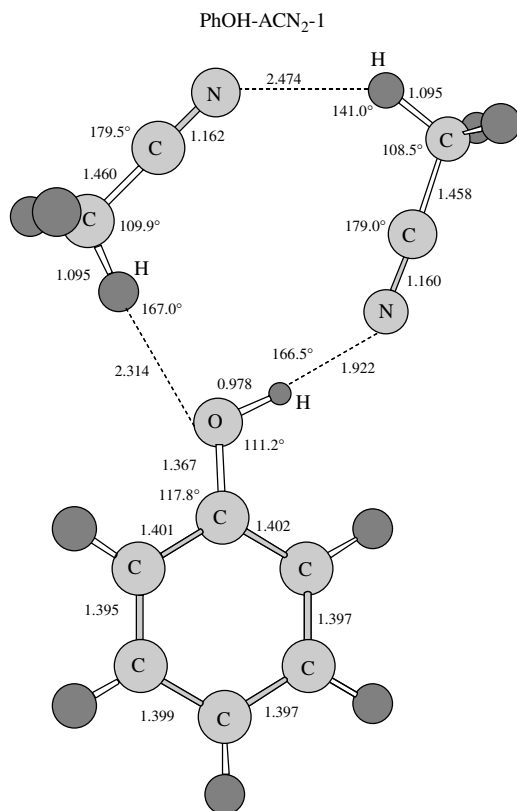


FIGURE 55. Complexes of phenol with two acetonitrile molecules. Bond lengths are in Å. Adapted from Reference 761 with permission

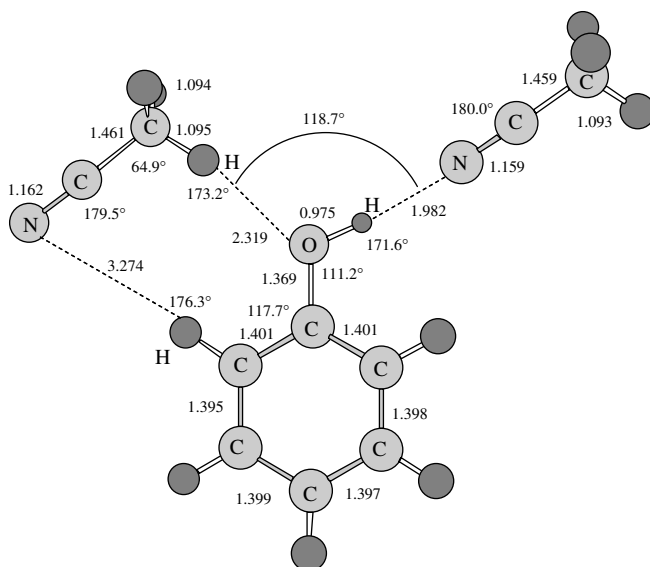
PhOH-ACN₂-2

FIGURE 55. (continued)

8.1 kJ mol⁻¹. Another effect conferring a higher stability on the complex PhOH-ACN₂-2 mostly plays a role in polar solvents such as acetonitrile, since this complex has a huge total dipole moment of 10.89 D, 5.5-fold larger than for PhOH-ACN₂-1 (their polarizabilities and quadrupole moments are nearly the same, as shown in Table 41). After clearing up the role which the complex PhOH-ACN₂-2 might play in modelling an experimental setup with increasing concentration of the acetonitrile, let us consider whether it looks somewhat peculiar in comparison to the other complex of phenol with two acetonitrile molecules. Surprisingly, it has precisely what we are looking for. It follows from Table 41 that the $\nu(\text{OH})$ stretch of phenol shifts further by 173 cm⁻¹ towards lower wavenumbers compared with the free phenol and by -15 cm⁻¹ compared to its frequency in PhOH-ACN-1. This is in line with a stepwise effect of dilution on the shift noted in the Introduction. What would also be interesting and deserves experimental verification is that the same stretch mode in PhOH-ACN₂-1 is red-shifting more strongly, by 244 cm⁻¹ compared to that in PhOH and by 86 cm⁻¹ compared to PhOH-ACN-1. Both red shifts could be ascribed to a somewhat stronger C-H...O bond formed between the methyl group of acetonitrile and the lone-pair of the phenolic oxygen in PhOH-ACN₂-1 than in PhOH-ACN₂-2. This effect weakens more the O-H bond in PhOH-ACN₂-1 which participates in the other hydrogen bonding, and it is seen in Figure 55 that the O-H bond in PhOH-ACN₂-1 is longer by 0.003 Å than that in PhOH-AC₂-2. However, why has such a tremendous shift not yet been detected experimentally? We think that the reason is that the complex PhOH-ACN₂-1 is not favourable at room temperatures and in polar solvents, and therefore an increase in the acetonitrile concentration primarily leads to the formation of the complex PhOH-ACN₂-2. Our suggestion can readily be verified by determining the location of the $\nu(\text{CN})$ bands in both complexes. As mentioned above, such mode shifts by 12 cm⁻¹ to higher frequencies in the complex PhOH-ACN-1 is in

perfect agreement with the experimental shift of 12.5 cm^{-1} ⁵⁵³. A similar shift of 13 cm^{-1} is predicted in the complex PhOH-ACN_2 -2, where it appears at the lower-frequency wing with the red shift of 7 cm^{-1} , mimicking that found in the complex PhOH-ACN -2. On the contrary, in complex PhOH-ACN_2 -1, the higher frequency band is placed by only 5 cm^{-1} aside that in the free acetonitrile molecule. Apparently, the other characteristic frequencies gathered in Table 41 might be of use to differentiate both complexes of phenol with two acetonitrile molecules.

4. A rather concise discussion

We have found the novel structure by which phenol complexes with the acetonitrile molecule. Such a structure has an absolutely different hydrogen bonding pattern, which certainly makes it less favourable on comparison with the conventional one attributed to the σ -type hydrogen bonding. A phenol–acetonitrile complex formation via π hydrogen bonding between the OH group of phenol and the $\text{C}\equiv\text{N}$ bond should be ruled out affirmatively.

However, we have shown that the novel bond formation between phenol and acetonitrile plays a role on increasing the concentration of the acetonitrile. By postulating its existence under conditions in which phenol interacts with two acetonitrile molecules, we were able to explain the experimental data that have seemed to be rather unclear during the last four decades. Moreover, we have predicted the existence of another structure formed from phenol and two molecules of acetonitrile, which is characterized by a significant downshift by 244 cm^{-1} of the $\nu(\text{OH})$ stretching mode of phenol, never observed experimentally in phenol–acetonitrile complexes. We have suggested that it is likely to exist in the gas phase and non-polar solvents at lower temperatures and showed its ‘fingerprints’ in order to facilitate its possible experimental detection.

D. Phenol–Benzonitrile Hydrogen-bonded Complex

The complex between phenol and benzonitrile is another, structurally speaking, rather complicated representative of the class of phenol–nitrile systems which are always associated by means of the π -electrons of the CN triple bond⁷³². Note that the IR spectra of a variety of phenol–nitrile systems have been reported⁷⁶⁷. Experiments on the vibrational relaxation of benzonitrile in solutions were also studied by different groups^{759, 768, 769}.

In Figure 56, we display the B3LYP/6-31+G(d,p) structure of the phenol–benzonitrile associate. It undoubtedly shows that its formation is due to a σ -type bonding between the triple bond of benzonitrile and the OH group of phenol. The energy of formation of the bond is 22.8 kJ mol^{-1} after ZPVE corrections. Noteworthy are the vibrational features of

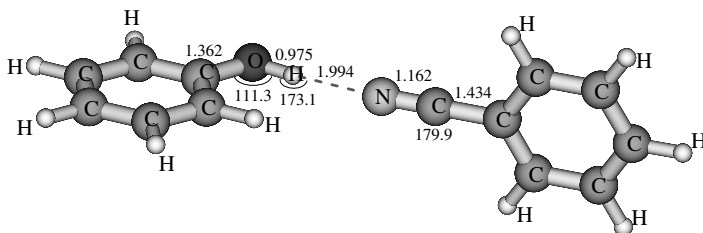


FIGURE 56. The complex of phenol with benzonitrile. Bond lengths are in Å, bond angles in deg

the studied complex. First, the ν_{CN} stretch undergoes a blue shift by 10 cm^{-1} whereas the ν_{OH} stretch of phenol is downshifted by 162 cm^{-1} . Second, the torsional mode τ_{OH} of phenol nearly doubles its frequency: 330 vs. 648 cm^{-1} .

E. A Very Short O—H . . . N Hydrogen Bond

Recently, neutron diffraction experiments⁷⁷⁰ have demonstrated the existence of a very short O—H . . . N hydrogen bond in the crystalline adduct of 2-methylpyridine and pentachlorophenol which is discussed in Subsection 4.5: the O—H bond length is equal to $1.068(7)\text{ \AA}$, the H . . . N bond length to $1.535(7)\text{ \AA}$.

Figure 57 shows the complex of 2-methylpyridine and pentachlorophenol obtained at the B3LYP/6-31G(d) computational level. It is formed due to the O—H . . . N hydrogen bond whose O—H bond length is 1.004 \AA , the H . . . N bond length is 1.795 \AA and the $\angle\text{O—H} \cdots \text{N}$ bond angle is $153.0(8)^\circ$. We also note that these two molecules in the formed complex are twisted with respect to each other by an angle of 63.3° , which resembles the experimental structure shown in Figure 1 of Reference 770. It is clear that the discrepancy between the geometry of the O—H . . . N hydrogen bond in the studied complex and in the calculation is due to the difference between the gas phase and the crystal phase.

VI. OPEN THEORETICAL PROBLEMS

In spite of the great effort made in the last several decades, a large number of problems concerning the chemistry of phenols remain open wide for theoretical studies.

The significance of the reaction of phenol with hydrogen has a number of important facets. First, the selective hydrogenation of phenol yields cyclohexanone, which is a key raw material in the production of both caprolactam for nylon 6 and adipic acid for nylon 6⁷⁷¹. Second, due to the fact that phenol is an environmental toxin⁷⁷² and phenolic waste has a variety of origins from industrial sources including oil refineries, petrochemical units, polymeric resin manufacturing and plastic units⁷⁷³, catalytic hydrogenation of phenol is nowadays the best practicable environmental option⁷⁷⁴.

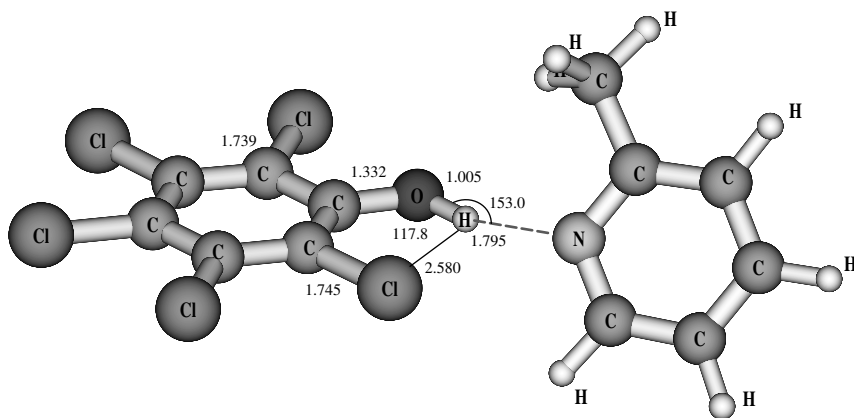


FIGURE 57. The complex of pentachlorophenol with 2-methylpyridine optimized at the B3LYP/6-31G(d) computational level. Bond lengths are in \AA , bond angles in deg

The behaviour of the tyrosyl radicals involved in different processes and environments is not yet well understood^{491, 546, 775}. Relatively little is known about the structure and selectivity of aryloxylium cations ($\text{Ar}-\text{O}^+$) that are produced in the phenolic oxidation reactions and implicated in biological processes such as isoflavone synthesis⁷⁷⁶. The thermochemistry¹⁹⁷ which is relevant to the antioxidant properties of phenols as well as the solvent effects on their reactivity^{777–780} remain also a largely under-explored topic. Finally, the structure of phenol dimers and oligomers⁷⁸¹ or even of some specific phenols⁷⁸² also deserve more attention. We expect that these problems will be subjects for theoretical research in the coming years.

VII. ACKNOWLEDGEMENTS

The authors gratefully thank Therese Zeegers-Huyskens, Asit Chandra, Sergei Bureiko, Kiran Boggavarapu, Alexander Koll, Zdislaw Latajka, Noj Malcolm, Bernard Silvi, Lucjan Sobczyk, Raman Sumathy and Georg Zundel for warm and useful discussions and suggestions. We also thank Oksana Tishchenko, Le Thanh Hung, Alexei Arbuznikov, Nguyen Thanh Loc, Alk Dransfeld, Robert Flammang, Pascal Gerbaux, Pham-Tran Nguyen-Nguyen, Guy Bouchoux, Pham-Cam Nam and Nguyen Thi Minh Hue for their great help in the preparation of this chapter at all its stages.

We are indebted to the KU Leuven Research Council for financial support through the Program for Concerted Research Action (GOA). E. S. Kryachko also thanks the “Bijzonder Onderzoeksfonds” of the Limburgs Universitair Centrum.

VIII. REFERENCES AND NOTES

1. *Quantum Chemistry Library Data Base (QCLDB)*, Japan Association for International Chemical Information, Tokyo, Japan, 2001.
2. M. J. Frisch, G. W. Trucks, H. B. Schlegel, G. E. Scuseria, M. Robb, J. R. Cheeseman, V. G. Zakrzewski, J. A. Montgomery, Jr., R. E. Stratmann, J. C. Burant, S. Dapprich, J. M. Millam, A. D. Daniels, K. N. Kudin, M. C. Strain, O. Farkas, J. Tomasi, V. Barone, M. Cossi, R. Cammi, B. Mennucci, C. Pomelli, C. Adamo, S. Clifford, J. Ochterski, G. A. Petersson, P. Y. Ayala, Q. Cui, K. Morokuma, D. K. Malick, A. D. Rabuck, K. Raghavachari, J. B. Foresman, J. Cioslowski, J. V. Ortiz, B. B. Stefanov, G. Liu, A. Liashenko, P. Piskorz, I. Komaromi, R. Gomperts, R. L. Martin, D. Fox, T. Keith, M. A. Al-Laham, C. Y. Peng, A. Nanayakkara, C. Gonzalez, M. Challacombe, P. M. W. Gill, B. Johnson, W. Chen, M. W. Wong, J. L. Andres, C. Gonzalez, M. Head-Gordon, E. S. Replogle and J. A. Pople, *GAUSSIAN 98* (Revision A.5), Gaussian Inc., Pittsburgh, PA, 1998.
3. J. J. P. Stewart, *MOPAC-7*, Quantum Chemistry Program Exchange, Bloomington, Ind., 1993.
4. (a) A. E. Reed, L. A. Curtiss and F. Weinhold, *Chem. Rev.*, **88**, 899 (1988).
(b) F. Weinhold, in *Encyclopedia of Computational Chemistry* (Ed. P. v. R. Schleyer), Wiley, Chichester, 1998, pp. 1792–1811.
5. E. D. Glendening, J. K. Badenhop, A. E. Reed, J. E. Carpenter and F. Weinhold, *NBO 4.0*, Theoretical Chemistry Institute, University of Wisconsin, Madison, 1996.
6. G. Fogarasi and P. Pulay, in *Vibrational Spectra and Structure*, Vol. 13 (Ed. J. R. Durig), Elsevier, New York, 1985.
7. S. Califano, *Vibrational States*, Wiley, New York, 1985.
8. J. M. L. Martin and K. Van Alsenoy, *GAR2PED*, University of Antwerp, Belgium, 1995.
9. S. Patai (Ed.), *The Chemistry of the Carbonyl Group*, Wiley, London, 1966.
10. E. P. Hunter and S. G. Lias, *J. Phys. Chem. Ref. Data*, **27**, 413 (1998).
11. S. A. Kafari and El-S. R. H. El-Gharkawy, *J. Phys. Chem. A*, **102**, 3202 (1998). See also S. A. Kafari, *J. Phys. Chem. A*, **102**, 10404 (1998).
12. D. Sitkoff, K. A. Sharp and B. Honig, *J. Phys. Chem.*, **98**, 1978 (1994).
13. F. J. Luque and M. Orozco, *J. Phys. Chem. B*, **101**, 5573 (1997).
14. B. Jayaram, D. Sprous and D. L. Beveridge, *J. Phys. Chem. B*, **102**, 9571 (1998).

15. J. Florián and A. Warshel, *J. Phys. Chem. B*, **101**, 5583 (1997).
16. G. Schüürmann, *Quantum Struct.-Act. Relat.*, **15**, 121 (1996).
17. J. B. Cumming and P. Kebarle, *Can. J. Chem.*, **56**, 1 (1978).
18. J. E. Bartmess, *NIST Negative Ion Database, NIST Standard Reference Database 19B, Version 3.01*, National Institute of Standards and Technology, Washington, DC, 1991.
19. M. Fujio, R. T. McIver, Jr. and R. W. Taft, *J. Am. Chem. Soc.*, **103**, 4017 (1981).
20. V. F. DeTuri and K. M. Ervin, *Int. J. Mass Spectrom. Ion. Proc.*, **175**, 123 (1998).
21. A. J. Colussi, F. Zabel and S. W. Benson, *Int. J. Chem. Kinet.*, **9**, 161 (1977).
22. D. J. DeFrees, R. T. McIver, Jr. and W. J. Hehre, *J. Am. Chem. Soc.*, **102**, 3334 (1980).
23. K. S. Peters, *Pure Appl. Chem.*, **58**, 1263 (1986).
24. F. G. Bordwell, J.-P. Cheng and J. A. Harrelson, Jr., *J. Am. Chem. Soc.*, **110**, 1229 (1988).
25. J. A. Walker and W. Tsang, *J. Phys. Chem.*, **94**, 3324 (1990).
26. See, for example, M. Kunert, E. Dinjus, M. Nauck and J. Sieler, *Chem. Ber. Recl.*, **130**, 1461 (1997) and references therein.
27. P. Ballone, B. Montanari and R. O. Jones, *J. Phys. Chem. A*, **104**, 2793 (2000).
28. F. F. Runge, *Ann. Phys. Chem.*, **31**, 65 (1834).
29. F. F. Runge, *Ann. Phys. Chem.*, **32**, 308 (1834).
30. C. F. v. Reichenbach, *Ann. Phys. Chem.*, **32**, 497 (1834).
31. G. Bugge, *Das Buch der Grossen Chemiker*, Verlag-Chemie, Weinheim, 1929.
32. J. R. Partington, *A History of Chemistry*, Vol. 4, The MacMillan Press, New York, 1972.
33. A. Laurent, *Ann. Chim. Phys.*, **63**, 27 (1836).
34. A. Laurent, *Ann. Chim.*, **iii**, 195 (1841).
35. A. Laurent, *Ann. Chim. Phys.*, **72**, 383 (1839).
36. Letter of Berzélius to Pelouze, *Ann. Chim. Phys.*, **67**, 303 (1838).
37. Letter of Berzélius to Pelouze, *Compt. Rend. Acad. Sci.*, **vi**, 629 (1838).
38. Dumas, *Compt. Rend. Acad. Sci.*, **vi**, 645 (1838).
39. Ch. Gerhardt, *Ann. Chim.*, **vii**, 215 (1843).
40. T. Lowry, *Dynamic Isomerism*, Report of the Committee, consisting of Professor H. E. Armstrong (Chairman), Dr. T. M. Lowry (Secretary), Professor Sydney Young, Dr. C. H. Desch, Dr. J. J. Dobbie, Dr. M. O. Forster and Dr. A. Lapworth, *BAAS Rep. Winnipeg* (1909), pp. 135–143 (1910). Cited in Reference 41, p. 176.
41. M. J. Nye, *From Chemical Philosophy to Theoretical Chemistry*, University of California Press, Berkeley, 1993.
42. C. Heitner and J. C. Scaiano (Eds.), *Photochemistry of Lignocellulosic Materials*, ACS Symposium Series, Vol. 531, American Chemical Society, Washington DC, 1993.
43. G. J. Leary, *J. Pulp Paper Sci.*, **20**, J154 (1994).
44. J. Emsley, *The Consumer's Good Chemical Guide. A Jargon-Free Guide to the Chemists of Everyday Life*, W. H. Freeman, Oxford, 1994.
45. J. R. Vane and R. M. Bottling (Eds.), *Aspirin and Other Salicylates*, Chapman and Hall, London, 1992.
46. See also Bayer's Aspirin web site at URL <http://www.aspirin.de>; see Hoffmann's laboratory record 10.10.1857 (source: Bayer AG).
47. *Aspirin, Molecule of the Month*, February 1996. Featured as the second molecule at MOTM site at URL <http://www.bris.ac.uk/Depts/Chemistry/MOTM/aspirin/aspirin.htm>.
48. America's 80 Billion-Aspirin Habit, *Medical Sciences Bulletin*, The Internet-Enhanced Journal of Pharmacology and Therapeutics, <http://pharminfo.com/pubs/msb/aspirin.html>.
49. Home page of the 'Aspirin Foundation of America' at URL <http://www.aspirin.org/>.
50. J. Vane, *Nature-New Biol.*, **231**, 232 (1971); *Nature*, **367**, 215 (1994); *Annu. Rev. Pharmacol.*, **38**, 97 (1998).
51. D. Picot, P. J. Loll and R. M. Garavito, *Nature*, **367**, 243 (1994); P. J. Loll, D. Picot and R. M. Garavito, *Nature Struct. Biol.*, **2**, 637 (1995).
52. P. J. Loll and R. M. Garavito, *Opin. Invest. Drugs*, **3**, 1171 (1994).
53. P. J. Wheatley, *J. Chem. Soc.*, 6036 (1964).
54. Y. Kim, K. Machida, T. Taga and K. Osaki, *Chem. Pharm. Bull.*, **33**, 2641 (1985).
55. *Cambridge Structural Database (CSD)*, *Cambridge Crystallographic Data Center*, 12 Union Road, Cambridge, CB2 1EZ, UK, 1995. Its URL <http://www.ccdc.cam.ac.uk/index.html>.
56. R. Glasser, *J. Org. Chem.*, **66**, 771 (2001).
57. M. W. Miller, *The Pfizer Handbook of Microbial Metabolites*, McGraw-Hill, New York, 1961.

58. D. A. Whiting, in *Comprehensive Organic Chemistry. The Synthesis and Reactions of Organic Compounds. Vol. 1. Stereochemistry, Hydrocarbons, Halo Compounds, Oxygen Compounds* (Ed. J. F. Stoddart), Chap. 4.2, Pergamon Press, Oxford, 1979.
59. C. Hogue, *Chem. Eng. News*, May 1, 49 (2000).
60. (a) *Nature*, **410**, 1016 (2001).
60. (b) For a recent report on the use of Agent Orange in Vietnam, see: J. M. Stellman, S. D. Stellman, R. Christian, T. Weber and C. Tomasallo in *Nature*, **422**, 681 (2003).
61. W. Karrer, *Konstitution und Vorkommen der organischen Pflanzenstoffe*, Birkhäuser, Basel, 1958.
62. T. K. Devon and A. I. Scott, *Handbook of Naturally Occurring Compounds*, Academic Press, New York, 1975.
63. R. W. Rickards, in *Chemistry of Natural Phenolic Compounds* (Ed. W. D. Ollis), Pergamon Press, Oxford, 1961, pp. 1ff.
64. A. C. Neish, in *Biochemistry of Phenolic Compounds* (Ed. J. B. Harborne), Academic Press, London, 1964, pp. 295ff.
65. A. J. Birch, in *Progress in the Chemistry of Organic Natural Products* (Ed. L. Zechmeister), Vol. 14, Springer, Vienna, 1957, p. 186.
66. E. Halsam, *The Shikimate Pathway*, Butterworths, London, 1974.
67. S. K. Erikson, J. Schadelin, U. Schmeling, H. H. Schott, V. Ullrich and H. Staudinger, in *The Chemistry of the Hydroxyl Group, Part 2*, (Ed. S. Patai), Wiley-Interscience, New York, 1971, p. 776.
68. G. J. Kasperek and T. C. Bruice, *J. Am. Chem. Soc.*, **94**, 198 (1972).
69. G. J. Kasperek, T. C. Bruice, H. Yagi, N. Kausbisch and D. M. Jerina, *J. Am. Chem. Soc.*, **94**, 7876 (1972).
70. K. B. Sharpless and T. C. Flood, *J. Am. Chem. Soc.*, **93**, 2316 (1971).
71. B. A. Diner, D. A. Force, D. W. Randall and R. D. Britt, *Biochemistry*, **37**, 17931 (1998).
72. G. Xiao, A. L. Tsai, G. Palmer, W. C. Boyar, P. J. Marshall and R. J. Kulmacz, *Biochemistry*, **36**, 1836 (1997).
73. J. D. Spikes, H. R. Shen, P. Kopeckova and J. Kopecek, *Photochem. Photobiol.*, **70**, 130 (1999).
74. L. R. Mahoney, *Angew. Chem., Int. Ed. Engl.*, **8**, 547 (1969).
75. K. U. Ingold, *Spec. Publ. Chem. Soc.*, **24**, 285 (1970).
76. G. W. Burton and K. U. Ingold, *Acc. Chem. Res.*, **19**, 194 (1986). For a current review on the anaerobic degradation of phenolic compounds, see: B. Schink, B. Phillip and J. Müller, *Naturwissenschaften*, **87**, 12 (2000).
77. E. T. Denisov and I. V. Khudyakov, *Chem. Rev.*, **87**, 1313 (1987).
78. O. Potterat, *Curr. Org. Chem.*, **1**, 415 (1997).
79. J. R. Thomas, *J. Am. Chem. Soc.*, **85**, 2166 (1963).
80. H. H. Szmant, *Organic Building Blocks of the Chemical Industry*, Wiley, New York, 1989, p. 434.
81. D. Hodgson, H.-Y. Zhang, M. R. Nimlos and J. T. McKinnon, *J. Phys. Chem. A*, **105**, 4316 (2001).
82. R. A. Marcus, *J. Phys. Chem.*, **43**, 2658 (1965).
83. D. Bittner and J. B. Howard, in *Soot in Combustion Systems and Its Toxic Properties* (Eds. J. Lahaye and G. Prado), Plenum Press, New York, 1983. See also:
(a) K. H. Becker, I. Barnes, L. Ruppert and P. Wiesen, in *Free Radicals in Biology and Environment* (Ed. F. Minisci), Chap. 27, Kluwer, Dordrecht, 1997, pp. 365–385.
(b) G. Ghigo and G. Tonachini, *J. Am. Chem. Soc.*, **120**, 6753 (1998).
84. G. I. Panov, V. I. Sobolev and A. S. Kharitonov, *J. Mol. Catal.*, **61**, 85 (1990).
85. A. M. Volodin, V. A. Bolshov and G. I. Panov, *J. Phys. Chem.*, **98**, 7548 (1994).
86. K. Yoshizawa, Y. Shiota, T. Yumura and T. Yamabe, *J. Phys. Chem. B*, **104**, 734 (2000).
87. *Chem. Eng. News*, April 6, 21 (1998). See also the recent experimental work on the Fe-silicalite catalyst for the N₂O oxidation of benzene to phenol: R. Leanza, I. Rossetti, I. Mazzola and L. Forni, *Appl. Catal. A—Gen.*, **205**, 93 (2001).
88. *Ullmann's Encyclopedia of Industrial Chemistry*, 6th edn., Wiley, New York, 2001.
89. R. K. Eikhman, M. M. Shemyakin and V. N. Vozhdaeva, *Anilinkrasochnaya Promyshl.*, **4**, 523 (1934).
90. V. Tishchenko and A. M. Churbakov, *J. Appl. Chem. (USSR)*, **7**, 764 (1934).

91. N. N. Vorozhtzov, Jr. and A. G. Oshuev, *Anilinokrasochnaya Promyshl.*, **3**, 245 (1933).
92. J.-F. Tremblay, *Chem. Eng. News*, December 11, 31 (2000). See also *Chem. Eng. News*, June 25, 78 (2001).
93. H. Hock and S. Lang, *Ber. Dtsch. Chem. Ges. B*, **77**, 257 (1944).
94. J. Wallace, in *Kirk-Othmer Encyclopedia of Chemical Technology*, Vol. 18, (Eds. J. I. Kroschwitz and M. Howe-Grant), 4th edn., Wiley, New York, 1992, pp. 592–602.
95. H.-G. Franck and J. W. Stadelhofer, *Industrial Aromatic Chemistry*, Springer, New York, 1987, pp. 146–183.
96. W. W. Kaeding, R. O. Lindblom and R. G. Temple, *Ind. Eng. Chem.*, **53**, 805 (1961).
97. W. W. Kaeding, *Hydrocarbon Process.*, **43**, 173 (1964).
98. W. W. Kaeding, R. O. Lindblom, R. G. Temple and H. I. Mahon, *Ind. Eng. Chem., Process Des. Dev.*, **4**, 97 (1965).
99. M. Taverna, *Riv. Combust.*, **22**, 203 (1968).
100. I. Donati, G. S. Sioli and M. Taverna, *Chim. Ind. (Milan)*, **50**, 997 (1968).
101. J. M. Gibson, P. S. Thomas, J. D. Thomas, J. L. Barker, S. S. Chandran, M. K. Harrup, K. M. Draths and J. W. Frost, *Angew. Chem., Int. Ed.*, **40**, 1945 (2001).
102. K. M. Draths and J. W. Frost, *J. Am. Chem. Soc.*, **116**, 399 (1994); *ACS Symp. Ser.*, **577**, 32 (1994); *J. Am. Chem. Soc.*, **117**, 2395 (1995); K. Li and J. W. Frost, *J. Am. Chem. Soc.*, **120**, 10545 (1998).
103. R. M. Badger and L. R. Zumwalt, *J. Chem. Phys.*, **6**, 711 (1938).
104. L. Pauling, *J. Am. Chem. Soc.*, **58**, 94 (1936).
105. T. Kojima, *J. Phys. Soc. Jpn.*, **15**, 284 (1960).
106. H. Forest and B. P. Dailey, *J. Chem. Phys.*, **45**, 1736 (1966).
107. T. Pedersen, N. W. Larsen and L. Nygaard, *J. Mol. Struct.*, **4**, 59 (1969).
108. N. W. Larsen, *J. Mol. Struct.*, **51**, 175 (1979).
109. G. Portalone, G. Schultz, A. Domenicano and I. Hargittai, *Chem. Phys. Lett.*, **197**, 482 (1992).
110. J. A. Pople and M. Gordon, *J. Am. Chem. Soc.*, **89**, 4253 (1967).
111. G. Keresztury, F. Billes, M. Kubinyi and T. Sundius, *J. Phys. Chem. A*, **102**, 1371 (1998).
112. D. Michalska, D. C. Bienko, A. J. Abkowicz-Bienko and Z. Latajka, *J. Phys. Chem.*, **100**, 17786 (1996).
113. S. Re and Y. Osamura, *J. Phys. Chem. A*, **102**, 3798 (1998).
114. S. Schumm, M. Gerhards, W. Roth, H. Gier and K. Kleineremanns, *Chem. Phys. Lett.*, **263**, 126 (1996).
115. G. Granucci, J. T. Hynes, P. Milli  and T.-H. Tran-Thi, *J. Am. Chem. Soc.*, **122**, 12242 (2000).
116. J. S. Wright, D. J. Carpenter, D. J. McKay and K. U. Ingold, *J. Am. Chem. Soc.*, **119**, 4245 (1997).
117. B. J. C. C. Cabrol, R. G. B. Fonesca and J. A. Martinho Sim es, *Chem. Phys. Lett.*, **258**, 436 (1996).
118. S. J. Martinez III, J. C. Alfano and D. H. Levy, *J. Mol. Spectrosc.*, **152**, 80 (1992).
119. J. Lorentzon, P.-A. Malmqvist, M. F lscher and B. O. Roos, *Theor. Chim. Acta*, **91**, 91 (1995).
120. S. Tsuzuki, H. Houjou, Y. Nagawa and K. Hiratani, *J. Phys. Chem. A*, **104**, 1332 (2000).
121. D. Feller and M. W. Feyereisen, *J. Comput. Chem.*, **14**, 1027 (1993).
122. M. Sch tz, T. B rger and S. Leutwyler, *J. Mol. Struct. (THEOCHEM)*, **276**, 117 (1992).
123. K. Kim and K. D. Jordan, *Chem. Phys. Lett.*, **218**, 261 (1994).
124. H. Lampert, W. Mikenda and A. Karpfen, *J. Phys. Chem. A*, **101**, 2254 (1997).
125. Y.-D. Wu and D. K. W. Lai, *J. Org. Chem.*, **61**, 7904 (1996).
126. S. Schumm, M. Gerhards and K. Kleineremanns, *J. Phys. Chem. A*, **104**, 10648 (2000).
127. G. Berden, W. L. Meerts, M. Schmitt and K. Kleineremanns, *J. Chem. Phys.*, **104**, 972 (1996).
128. A. L. McClellan, *Tables of Experimental Dipole Moments*, W. H. Freeman, San Francisco, 1963, p. 251.
129. A. Koll, H. Ratajczak and L. Sobczyk, *Ann. Soc. Chim. Polonorum*, **44**, 825 (1970).
130. C. J. Cramer and D. G. Truhlar, *Chem. Rev.*, **99**, 2161 (1999).
131. B. Pullman and A. Pullman, *Quantum Biochemistry*, Wiley-Interscience, New York, 1963.
132. T. A. Koopmans, *Physica*, **1**, 104 (1933).
133. R. S. Mulliken, *Phys. Rev.*, **74**, 736 (1948).
134. R. J. Lipert and S. D. Colson, *J. Chem. Phys.*, **92**, 3240 (1990).
135. K. M ller-Dethlefs and E. W. Schlag, *Annu. Rev. Phys. Chem.*, **42**, 109 (1991).

136. O. Dopfer, G. Lembach, T. G. Wright and K. Müller-Dethlefs, *J. Chem. Phys.*, **98**, 1933 (1993).
137. R. G. Neuhauser, K. Siglow and H. J. Neusser, *J. Chem. Phys.*, **106**, 896 (1997).
138. Y. Qin and R. A. Wheeler, *J. Phys. Chem.*, **100**, 10554 (1996).
139. <http://webbook.nist.gov/cgi/cbook.cgi?ID=C108952&Units=SI&Mask=20>.
140. J. S. Wright, E. R. Johnson and G. A. DiLabio, *J. Am. Chem. Soc.*, **123**, 1173 (2001).
141. R. F. W. Bader, *Atoms in Molecules. A Quantum Theory*, Clarendon, Oxford, 1990.
142. P. L. A. Popelier, *Atoms in Molecules. An Introduction*, Pearson Education, Harlow (1999).
143. R. J. Gillespie and E. A. Robinson, *Angew. Chem., Int. Ed. Engl.*, **35**, 495 (1996).
144. R. J. Gillespie and I. Hargittai, *The VSEPR Model of Molecular Geometry*, Allyn and Bacon, London, 1991.
145. E. S. Kryachko and E. V. Ludeña, *Energy Density Functional Theory of Many-Electron Systems*, Kluwer, Dordrecht, 1990.
146. N. Malcolm, Private communication, May–June, 2001. All calculations were performed using the program MORPHY 98, a topological analysis program written by P. L. A. Popelier with a contribution from R. G. A. Bone (UMIST, Manchester, U.K.).
147. K. W. F. Kohlrausch and H. Wittek, *Monatsh. Chem.*, **74**, 1 (1941).
148. M. M. Davies, *J. Chem. Phys.*, **16**, 274 (1948).
149. M. M. Davies and R. L. Jones, *J. Chem. Soc.*, 120 (1954).
150. R. Mecke and G. Rossmly, *Z. Elektrochem.*, **59**, 866 (1955).
151. J. C. Evans, *Spectrochim. Acta*, **16**, 1382 (1960).
152. J. H. S. Green, *J. Chem. Soc.*, 2236 (1961).
153. H. D. Bist, J. C. D. Brand and D. R. Williams, *J. Mol. Spectrosc.*, **24**, 402, 413 (1967).
154. H. W. Wilson, R. W. MacNamee and J. R. Durig, *J. Raman Spectrosc.*, **11**, 252 (1981).
155. N. W. Larsen and F. M. Nicolaisen, *J. Mol. Struct.*, **22**, 29 (1974).
156. H. D. Bist, J. C. D. Brand and D. R. Williams, *J. Mol. Spectrosc.*, **21**, 76 (1966).
157. J. Christoffersen, J. M. Hollas and G. H. Kirby, *Proc. Roy. Soc. London A*, **307**, 97 (1968).
158. E. V. Brown, *Opt. Spectrosc.*, **23**, 301 (1967).
159. V. N. Sarin, M. M. Rai, H. D. Bist and D. P. Khandelwal, *Chem. Phys. Lett.*, **6**, 473 (1970).
160. H. W. Wilson, *Anal. Chem.*, **46**, 962 (1974).
161. P. V. Huong, J. Lascombe and M. C. Josien, *J. Chem. Phys.*, **58**, 694 (1961).
162. E. Mathier, D. Welti, A. Bauder and Hs. H. Gunthard, *J. Mol. Spectrosc.*, **37**, 63 (1967).
163. See also different rotational studies in references 164–166.
164. G. V. Hartland, B. F. Henson, V. A. Ventura and P. M. Felker, *J. Phys. Chem.*, **96**, 1164 (1992).
165. J. H. S. Green, D. J. Harrison and W. Kynaston, *Spectrochim. Acta*, **27A**, 2199 (1971).
166. B. Nelander, *J. Chem. Phys.*, **72**, 771 (1980).
167. G. Varsanyi, *Assignments for Vibrational Spectra of 700 Benzene Derivatives*, Wiley, New York, 1974.
168. A. K. Grafton and R. A. Wheeler, *J. Comput. Chem.*, **19**, 1663 (1998).
169. W. Roth, P. Imhof, M. Gerhards, S. Schumm and K. Kleinermanns, *Chem. Phys.*, **252**, 247 (2000).
170. D. Michalska, W. Zierkiewicz, D. C. Bienko, W. Wojciechowski and Th. Zeegers-Huyskens, *J. Phys. Chem. A*, **105**, 8734 (2001).
171. G. R. Carlson and W. G. Fateley, *J. Phys. Chem.*, **77**, 1157 (1973).
172. W. G. Fateley, G. L. Carlson and F. F. Bentley, *J. Phys. Chem.*, **79**, 199 (1975).
173. G. Pimentel and A. L. McClellan, *The Hydrogen Bond*, Freeman, San Francisco, 1960.
174. O. R. Wulf and E. J. Jones, *J. Chem. Phys.*, **8**, 745 (1940) and references therein.
175. M. Schütz, T. Bürgi, S. Leutwyler and T. Fisher, *J. Chem. Phys.*, **98**, 3763 (1993).
176. D. H. Whiffen, *J. Chem. Soc.*, 1350 (1956).
177. G. Durocher and C. Sandorfy, *J. Mol. Spectrosc.*, **15**, 22 (1965).
178. M. Asselin, G. Bélanger and C. Sandorfy, *J. Mol. Spectrosc.*, **30**, 96 (1969).
179. M. Couzi and P. V. Huong, *Spectrochim. Acta*, **26A**, 49 (1970).
180. J. Davison, J. H. Gutow and R. N. Zare, *J. Phys. Chem.*, **94**, 4069 (1990).
181. M. Rospenk, N. Leroux and Th. Zeegers-Huyskens, *J. Mol. Spectrosc.*, **183**, 245 (1997).
182. S. I. Ishiuchi, H. Shitomi, K. Takazawa and M. Fujii, *Chem. Phys. Lett.*, **283**, 243 (1998).
183. M. Rospenk, B. Czarnik-Matusiewicz and Th. Zeegers-Huyskens, *Spectrochim. Acta A*, **57**, 185 (2001).

184. M. Capponi, I. Gut and J. Wirz, *Angew. Chem., Int. Ed. Engl.*, **25**, 344 (1986).
185. O. S. Tee and N. R. Inyengar, *J. Am. Chem. Soc.*, **107**, 455 (1985).
186. T. A. Gadosy and R. A. McClelland, *J. Mol. Struct. (THEOCHEM)*, **369**, 1 (1996).
187. D. Santoro and R. Louw, *J. Chem. Soc., Perkin Trans. 2*, 645 (2001).
188. K. U. Ingold and J. S. Wright, *J. Chem. Educ.*, **77**, 1062 (2000).
189. L. R. Mahoney, F. C. Ferris and M. A. DaRooge, *J. Am. Chem. Soc.*, **91**, 3883 (1969).
190. M. Lucarini, G. F. Pedulli and M. Cipollone, *J. Org. Chem.*, **59**, 5063 (1994).
191. D. D. M. Wayner, E. Lusztyk, K. U. Ingold and P. Mulder, *J. Org. Chem.*, **61**, 6430 (1996).
192. G. A. DiLabio, D. A. Pratt, A. D. LoFaro and J. S. Wright, *J. Phys. Chem. A*, **103**, 1653 (1999).
193. T. Brinck, M. Haeberlein and M. Jonsson, *J. Am. Chem. Soc.*, **119**, 4239 (1997).
194. R. M. B. dos Santos and J. A. Martinho Simões, *J. Phys. Chem. Ref. Data*, **27**, 707 (1998).
195. M. I. De Heer, H.-G. Korth and P. Mulder, *J. Org. Chem.*, **64**, 6969 (1999).
196. F. Himo, L. A. Eriksson, M. R. A. Blomberg and P. E. M. Siegbahn, *Int. J. Quantum Chem.*, **76**, 714 (2000).
197. L. J. J. Laarhoven, P. Mulder and D. D. M. Wayner, *Acc. Chem. Res.*, **32**, 342 (1999).
198. D. A. Pratt, G. A. DiLabio, G. Brigati, G. F. Pedulli and L. Valgimigli, *J. Am. Chem. Soc.*, **123**, 4625 (2001).
199. T. N. Das, *J. Phys. Chem. A*, **105**, 5954 (2001).
200. D. A. Pratt, M. I. de Heer, P. Mulder and K. U. Ingold, *J. Am. Chem. Soc.*, **123**, 5518 (2001).
201. M. Lucarini, G. F. Pedulli, L. Valgimigli, R. Amoraati and F. Minisci, *J. Org. Chem.*, **66**, 5456 (2001).
202. M. M. Davies, *Acid-Base Behaviour in Aprotic Organic Solvents*, Natl. Bur. Standards Monograph 105, Washington D.C., 1968.
203. S. Nagakura and H. Baba, *J. Am. Chem. Soc.*, **74**, 5693 (1952).
204. S. Nagakura, *J. Am. Chem. Soc.*, **76**, 3070 (1954).
205. H. Baba and S. Suzuki, *J. Chem. Phys.*, **41**, 895 (1964).
206. H. Baba, A. Matsuyama and H. Kokubun, *Spectrochim. Acta A*, **25**, 1709 (1969).
207. R. Scott, D. De Palma and S. Vinogradov, *J. Phys. Chem.*, **72**, 3192 (1968).
208. R. Scott and S. Vinogradov, *J. Phys. Chem.*, **73**, 1890 (1969).
209. R. A. Hudson, R. Scott and S. Vinogradov, *J. Phys. Chem.*, **76**, 1989 (1972).
210. Th. Zeegers-Huyskens and P. Huyskens, in *Molecular Interactions Vol. 2*, (Eds. H. Ratajczak and W. J. Orville-Thomas), Wiley, New York, 1981.
211. L. Sobczyk, *Ber. Bunsenges. Phys. Chem.*, **102**, 377 (1998).
212. L. Pauling, *The Nature of the Chemical Bond*, Cornell University Press, Ithaca, 1939.
213. O. R. Wulf and U. Liddel, *J. Am. Chem. Soc.*, **57**, 1464 (1935).
214. O. R. Wulf, U. Liddel and S. B. Hendricks, *J. Am. Chem. Soc.*, **58**, 2287 (1936).
215. G. E. Hilbert, O. R. Wulf, S. B. Hendricks and U. Liddel, *Nature*, **135**, 147 (1935).
216. O. R. Wulf and E. J. Jones, *J. Chem. Phys.*, **8**, 745 (1940).
217. O. R. Wulf, E. J. Jones and L. S. Deming, *J. Chem. Phys.*, **8**, 753 (1940).
218. G. Rossmy, W. Lüttke and R. Mecke, *J. Chem. Phys.*, **21**, 1606 (1953).
219. All computations were performed at the density functional hybrid B3LYP potential in conjunction with the split-valence 6-311++G(d,p) basis set using a GAUSSIAN 98 suit of packages. The tight convergence criterion was employed in all geometrical optimizations. Harmonic vibrational frequencies were kept unscaled. ZPVEs and thermodynamic quantities were also calculated at $T = 298.15$ K. Throughout the present section, the energy comparison was made in terms of the total energy + ZPVE.
220. B. Silvi, E. S. Kryachko, O. Tishchenko, F. Fuster and M. T. Nguyen, *Mol. Phys.*, **100**, 1659 (2002).
221. M. M. Davies, *Trans. Faraday Soc.*, **36**, 333 (1940).
222. E. A. Robinson, H. D. Schreiber and J. N. Spencer, *Spectrochim. Acta A*, **28**, 397 (1972).
223. A. W. Baker and W. W. Kaeding, *J. Am. Chem. Soc.*, **81**, 5904 (1959).
224. T. Lin and E. Fishman, *Spectrochim. Acta A*, **23**, 491 (1967).
225. See various chapters in Reference 173.
226. P. Schuster, G. Zundel and C. Sandorfy (Eds.), *The Hydrogen Bond. Recent Developments in Theory and Experiments*, North-Holland, Amsterdam, 1976.
227. A. W. Baker, *J. Am. Chem. Soc.*, **80**, 3598 (1958).
228. M. St. C. Flett, *Spectrochim. Acta*, **10**, 21 (1957).

229. H. Bourassa-Bataille, P. Sauvageau and C. Sandorfy, *Can. J. Chem.*, **41**, 2240 (1963).
230. C. Sandorfy, in *The Hydrogen Bond. Recent Developments in Theory and Experiments* (Eds. P. Schuster, G. Zundel and C. Sandorfy, Chap. 13, North-Holland, Amsterdam, 1976).
231. L. R. Zumwalt and R. M. Badger, *J. Am. Chem. Soc.*, **62**, 305 (1940).
232. M. M. Davies, *Trans. Faraday Soc.*, **34**, 1427 (1938).
233. E. A. Allan and L. W. Reeves, *J. Phys. Chem.*, **66**, 613 (1962).
234. E. A. Allan and L. W. Reeves, *J. Phys. Chem.*, **67**, 591 (1963).
235. D. A. K. Jones and J. G. Watkinson, *Chem. Ind.*, 661 (1960).
236. R. A. Nyquist, *Spectrochim. Acta*, **19**, 1655 (1963).
237. L. Radom, W. J. Hehre, J. A. Pople, G. L. Carlson and W. G. Fateley, *J. Chem. Soc., Chem. Commun.*, 308 (1972).
238. J. H. Richards and S. Walker, *Trans. Faraday Soc.*, **57**, 412 (1961).
239. S. W. Dietrich, E. C. Jorgensen, P. A. Kollman and S. Rothenberg, *J. Am. Chem. Soc.*, **98**, 8310 (1976).
240. H. H. Jaffe, *J. Am. Chem. Soc.*, **79**, 2373 (1957).
241. R. M. Badger and S. H. Bauer, *J. Chem. Phys.*, **5**, 839 (1937).
242. G. D. Hawkins, D. J. Giesen, G. C. Lynch, C. C. Chambers, I. Rossi, J. W. Storer, J. Li, P. Winget, D. Rinaldi, D. A. Liotard, C. J. Cramer and D. G. Truhlar, *AMSOLE, Version 6.6*, University of Minnesota, Minneapolis, 1997, based in part on *AMPAC, Version 2.1* by D. A. Liotard, E. F. Healy, J. M. Ruiz and M. J. S. Dewar.
243. J. J. Urban, R. L. v. Tersch and G. R. Famini, *J. Org. Chem.*, **59**, 5239 (1994).
244. O. Tishchenko, E. S. Kryachko and M. T. Nguyen, *Spectrochim. Acta A*, **58**, 1951 (2002).
245. W. Zierkiewicz, D. Michalska and Th. Zeegers-Huyskens, *J. Phys. Chem. A*, **104**, 11685 (2000).
246. F. A. Miller, *Molecular Spectroscopy*, Institute of Petroleum, London, 1969, p. 5.
247. A. B. Hollinger and H. L. Welsh, *Can. J. Phys.*, **56**, 974 (1978).
248. A. B. Hollinger and H. L. Welsh, *Can. J. Phys.*, **56**, 1513 (1978).
249. A. B. Hollinger, H. L. Welsh and K. S. Jammu, *Can. J. Phys.*, **57**, 767 (1979).
250. H. B. Jensen and S. Brodersen, *J. Raman Spectrosc.*, **8**, 103 (1979).
251. R. J. Jakobsen and E. J. Brewer, *Appl. Spectrosc.*, **16**, 32 (1962).
252. M. H. Palmer, W. Moyes, M. Speirs and J. N. A. Ridyard, *J. Mol. Struct.*, **52**, 293 (1979).
253. A. Pross and L. Radom, *Prog. Phys. Org. Chem.*, **13**, 1 (1981).
254. E. L. Mehler and J. Gerhards, *J. Am. Chem. Soc.*, **107**, 5856 (1985).
255. A. D. Becke and K. E. Edgecombe, *J. Chem. Phys.*, **92**, 5397 (1990).
256. G. N. Lewis, *J. Am. Chem. Soc.*, **38**, 762 (1916).
257. G. N. Lewis, *Valence and the Structure of Atoms and Molecules*, Dover, New York, 1966.
258. R. J. Gillespie and R. S. Nyholm, *Quart. Rev. Chem. Soc.*, **11**, 339 (1957).
259. R. J. Gillespie, *Molecular Geometry*, Van Nostrand Reinhold, London, 1972.
260. R. Thom, *Stabilité Structurale et Morphogénèse*, Interéditions, Paris, 1972.
261. R. H. Abraham and C. D. Shaw, *Dynamics: The Geometry of Behavior*, Addison Wesley, New York, 1992.
262. R. H. Abraham and J. E. Marsden, *Foundations of Mechanics*, Addison Wesley, New York, 1994.
263. A. Savin, O. Jepsen, J. Flad, O. K. Andersen, H. Preuss and H. G. v. Schnering, *Angew. Chem., Int. Ed. Engl.*, **31**, 187 (1992).
264. B. Silvi and A. Savin, *Nature*, **371**, 683 (1994).
265. A. Savin, B. Silvi and F. Colonna, *Can. J. Chem.*, **74**, 1088 (1996).
266. S. Noury, F. Colonna, A. Savin and B. Silvi, *J. Mol. Struct. (THEOCHEM)*, **450**, 59 (1998).
267. X. Fradera, M. A. Austen and R. F. W. Bader, *J. Phys. Chem. A*, **103**, 304 (1998).
268. J. Cioslowski and S. T. Mixon, *J. Am. Chem. Soc.*, **113**, 4142 (1991).
269. J. G. Ángyán, M. Loos and I. Mayer, *J. Phys. Chem.*, **98**, 5244 (1994).
270. J. F. Dobson, *J. Chem. Phys.*, **94**, 4328 (1991).
271. J. F. Dobson, *J. Chem. Phys.*, **98**, 8870 (1993).
272. H. L. Schmider and A. L. Becke, *J. Chem. Phys.*, **109**, 8188 (1998).
273. P. L. A. Popelier, *Coord. Chem. Rev.*, **197**, 169 (2000).
274. F. Fuster, A. Savin and B. Silvi, *J. Phys. Chem. A*, **104**, 852 (2000).
275. F. Fuster and B. Silvi, *Theoret. Chem. Acc.*, **104**, 13 (2000).
276. F. Fuster and B. Silvi, *Chem. Phys.*, **252**, 279 (2000).

277. S. G. Schulman, W. R. Vincent and J. M. Underberg, *J. Phys. Chem.*, **85**, 4068 (1981).
278. S. Leutwyler, T. Bürgi, M. Schütz and A. Taylor, *Faraday Discuss.*, **97**, 285 (1994).
279. R. A. Slavinskaya, Kh. Kh. Muldagaliyev and T. A. Kovaleva, *Izv. Akad. Nauk. Kaz. SSR, Ser. Khim. Engl. Transl.*, 23 (1990).
280. W. Roth, P. Imhof and K. Kleineremanns, *Phys. Chem. Chem. Phys.*, **3**, 1806 (2001).
281. P. Imhof and K. Kleineremanns, *J. Phys. Chem. A*, **105**, 8922 (2001).
282. M. Broquier, F. Lahmani, A. Zehnacker-Rentien, V. Brenner, P. Millé and A. Peremans, *J. Phys. Chem. A*, **105**, 6841 (2001).
283. P. Polizer and N. Sukumar, *J. Mol. Struct. (THEOCHEM)*, **179**, 439 (1988).
284. K. B. Borisenko, C. W. Boch and I. J. Hargittai, *J. Phys. Chem.*, **98**, 1442 (1994).
285. P. C. Chen and C. C. Huang, *J. Mol. Struct. (THEOCHEM)*, **282**, 287 (1993). See also P. C. Chen and S. C. Chen, *Int. J. Quantum Chem.*, **83**, 332 (2001).
286. A. Kovacs, V. Izvekov, G. Keresztury and G. Pongor, *Chem. Phys.*, **238**, 231 (1998).
287. Y. Kishore, S. N. Sharma and C. P. D. Dwivedi, *Indian J. Phys.*, **48**, 412 (1974).
288. A. J. Abkowicz-Bieńko, Z. Latajka, D. C. Bieńko and D. Michalska, *Chem. Phys.*, **250**, 123 (1999).
289. B. Czarnik-Matusiewicz, A. K. Chandra, M. T. Nguyen and Th. Zeegers-Huyskens, *J. Mol. Spectrosc.*, **195**, 308 (1999).
290. R. P. Bell, *The Proton in Chemistry*, Cornell University Press, Ithaca, 1959, p. 20.
291. C. Y. Ng, D. J. Trevor, P. W. Tiedemann, S. T. Ceyer, P. L. Kroebusch, B. H. Mahan and Y. T. Lee, *J. Chem. Phys.*, **67**, 4235 (1977).
292. D. Kuck, *Angew. Chem., Int. Ed.*, **39**, 125 (2000).
293. E. S. Kryachko and M. T. Nguyen, *J. Phys. Chem. A*, **105**, 153 (2001).
294. R. T. McIver, Jr. and R. C. Dunbar, *Int. J. Mass Spectrom. Ion Phys.*, **7**, 471 (1971).
295. Y. Lau and P. Kebarle, *J. Am. Chem. Soc.*, **98**, 7452 (1976).
296. (a) E. P. Hunter and S. G. Lias, *J. Phys. Chem. Ref. Data*, **27**, 413 (1998).
296. (b) For the most recent value, see G. Bouchoux, D. Defaye, T. McMahon, A. Likhohyot, O. Mó and M. Yáñez, *Chem. Eur. J.*, **8**, 2899 (2002).
297. D. J. DeFrees, R. T. McIver and W. J. Hehre, *J. Am. Chem. Soc.*, **99**, 3853 (1977).
298. M. Eckert-Maksić, M. Klessinger and Z. B. Maksić, *Chem. Phys. Lett.*, **232**, 472 (1995). For semiempirical calculations see R. Voets, J.-P. Francois, J. M. L. Martin, J. Mullers, J. Yperman and L. C. Van Poucke, *J. Comput. Chem.*, **11**, 269 (1990).
299. O. Tishchenko, N. N. Pham-Tran, E. S. Kryachko and M. T. Nguyen, *J. Phys. Chem. A*, **105**, 8709 (2001).
300. N. Solca and O. Dopfer, *Chem. Phys. Lett.*, **342**, 191 (2001).
301. R. K. Roy, F. De Proft and P. Geerlings, *J. Phys. Chem. A*, **102**, 7035 (1998).
302. N. Russo, T. Toscano, A. Grand and T. Mineva, *J. Phys. Chem. A*, **104**, 4017 (2000).
303. H. T. Le, R. Flammang, M. Barbieux-Flammang, P. Gerbaux and M. T. Nguyen, *Int. J. Mass Spectrom.*, **217**, 45 (2002).
304. G. E. Campagnaro and J. L. Wood, *J. Mol. Struct.*, **6**, 117 (1970).
305. N. W. Larsen and F. M. Nicolaisen, *J. Mol. Struct.*, **22**, 29 (1974).
306. B. Bogdanov, D. van Duijn and S. Ingemann, *Proceedings of the XX Congress on Mass Spectrometry*, Madrid, Spain, July 2000.
307. W. G. Fateley, G. L. Carlson and F. F. Bentley, *J. Phys. Chem.*, **79**, 199 (1975).
308. K. B. Wiberg and P. R. Rablen, *J. Org. Chem.*, **63**, 3722 (1998).
309. R. F. W. Bader and C. Chang, *J. Phys. Chem.*, **93**, 2946, 5095 (1989) and references therein.
310. A. Bagno and G. Scorrano, *J. Phys. Chem.*, **100**, 1536 (1996) and references therein.
311. D. Kovacek, Z. B. Maksić and I. Novak, *J. Phys. Chem. A*, **101**, 1147, 7448 (1997).
312. G. Raos, J. Gerratt, P. B. Karadakov, D. L. Cooper and M. Raimondi, *J. Chem. Soc., Faraday Trans.*, **91**, 4011 (1995).
313. M. T. Nguyen, A. F. Hegarty, T. K. Ha and G. R. De Mare, *J. Chem. Soc., Perkin Trans. 2*, 147 (1986).
314. T. K. Ha and M. T. Nguyen, *J. Mol. Struct.*, **87**, 355 (1982).
315. M. T. Nguyen and A. F. Hegarty, *J. Chem. Soc. Perkin. Trans. 2*, **2037**, 2043 (1984).
316. See the ELF analysis on protonation in Section III.C and Reference 220.
317. E. S. Kryachko and M. T. Nguyen, unpublished results.
318. R. T. Sanderson, *Polar Covalence*, Academic Press, New York, 1983.
319. A. Baeten, F. De Proft and P. Geerlings, *Int. J. Quantum Chem.*, **60**, 931 (1996).

320. R. G. Parr and W. Yang, *J. Am. Chem. Soc.*, **106**, 4049 (1984).
321. H. Chermette, *J. Comput. Chem.*, **20**, 129 (1999).
322. W. Yang and W. J. Mortier, *J. Am. Chem. Soc.*, **108**, 5708 (1986).
323. T. Mineva, N. Russo and E. Silicia, *J. Am. Chem. Soc.*, **120**, 9093 (1998).
324. P. Geerlings, F. De Proft and W. Langenaeker, *Adv. Quantum Chem.*, **33**, 301 (1999).
325. T. Mineva, N. Neshev, N. Russo, E. Silicia and M. Toscano, *Adv. Quantum Chem.*, **33**, 273 (1999).
326. A. K. Chandra and M. T. Nguyen, *J. Chem. Soc., Perkin Trans. 2*, 1415 (1997).
327. G. Raspoet, M. T. Nguyen, S. Kelly and A. F. Hegarty, *J. Org. Chem.*, **63**, 9669 (1998).
328. M. T. Nguyen, G. Raspoet and L. G. Vanquickenborne, *J. Phys. Org. Chem.*, **13**, 46 (2000).
329. M. T. Nguyen and G. Raspoet, *Can. J. Chem.*, **77**, 817 (1999).
330. A. K. Chandra, P. Geerlings and M. T. Nguyen, *J. Org. Chem.*, **62**, 6417 (1997).
331. L. T. Nguyen, N. T. Le, F. De Proft, A. K. Chandra, W. Langenaeker, M. T. Nguyen and P. Geerlings, *J. Am. Chem. Soc.*, **121**, 5992 (1999).
332. L. T. Nguyen, F. De Proft, M. T. Nguyen and P. Geerlings, *J. Chem. Soc., Perkin Trans. 2*, 898 (2001).
333. L. T. Nguyen, F. De Proft, M. T. Nguyen and P. Geerlings, *J. Org. Chem.*, **66**, 4316 (2001).
334. D. Sengupta, A. K. Chandra and M. T. Nguyen, *J. Org. Chem.*, **62**, 6404 (1997).
335. A. K. Chandra and M. T. Nguyen, *J. Comput. Chem.*, **19**, 195 (1998).
336. T. N. Le, L. T. Nguyen, A. K. Chandra, F. De Proft, M. T. Nguyen and P. Geerlings, *J. Chem. Soc., Perkin Trans. 2*, 1249 (1999).
337. A. K. Chandra and M. T. Nguyen, *J. Phys. Chem. A*, **102**, 6181 (1998).
338. A. K. Chandra, A. Michalak, M. T. Nguyen and R. Nalewajski, *J. Phys. Chem. A*, **102**, 10188 (1998).
339. A. K. Chandra, T. Uchimarui and M. T. Nguyen, *J. Chem. Soc., Perkin Trans. 2*, 2117 (1999).
340. M. T. Nguyen, A. K. Chandra, S. Sakai and K. Morokuma, *J. Org. Chem.*, **64**, 65 (1999).
341. L. T. Nguyen, F. De Proft, A. K. Chandra, T. Uchimarui, M. T. Nguyen and P. Geerlings, *J. Org. Chem.*, **66**, 6096 (2001).
342. E. Silicia, N. Russo and T. Mineva, *J. Phys. Chem. A*, **115**, 442 (2001).
343. A. Toro-Labbe, *J. Phys. Chem. A*, **103**, 4398 (1999).
344. T. Uchimarui, A. K. Chandra, S. I. Kawahara, K. Matsumura, S. Tsuzuki and M. Mikami, *J. Phys. Chem. A*, **105**, 1343 (2001).
345. M. T. Nguyen and A. F. Hegarty, *J. Chem. Soc. Perkin Trans. 2*, **1991**, 1999 (1985).
346. M. T. Nguyen and A. F. Hegarty, *J. Chem. Soc., Perkin Trans. 2*, 2005 (1985).
347. T. Fujii, H. Tokiwa, H. Ichikawa and H. Shinoda, *J. Mol. Struct. (THEOCHEM)*, **277**, 251 (1992).
348. P. Kollman and S. Rothenberg, *J. Am. Chem. Soc.*, **99**, 1333 (1977).
349. R. T. McIver and J. H. Silver, *J. Am. Chem. Soc.*, **95**, 8462 (1973).
350. T. B. McMahon and P. Kebarle, *J. Am. Chem. Soc.*, **99**, 2222 (1977).
351. M. Jujio, R. T. McIver and R. W. Taft, *J. Am. Chem. Soc.*, **103**, 4017 (1981).
352. T. Kremer and P. v. R. Schleyer, *Organometallics*, **16**, 737 (1997).
353. H. U. Suter and M. Nonella, *J. Phys. Chem. A*, **102**, 10128 (1998).
354. P. Ballone and R. O. Jones, *J. Phys. Chem. A*, **105**, 3008 (2001).
355. M. Schlosser, E. Marzi, F. Cottet, H. H. Buker and N. M. M. Nibbering, *Chem. Eur. J.*, **7**, 3511 (2001).
356. M. Krauss, O. J. Jensen and H. F. Hameka, *J. Phys. Chem.*, **98**, 9955 (1994).
357. Z. He, C. H. Martin, R. Birge and K. F. Freed, *J. Phys. Chem. A*, **104**, 2939 (2000).
358. Y. H. Mariam and L. Chantranupong, *J. Mol. Struct. (THEOCHEM)*, **454**, 237 (1998).
359. J. C. Rienstra-Kiracofe, D. E. Graham and H. F. Schaefer III, *Mol. Phys.*, **94**, 767 (1998).
360. O. Nwobi, J. Higgins, X. Zhou and R. Liu, *Chem. Phys. Lett.*, **272**, 155 (1997).
361. J. Danielsson, J. Ulicny and A. Laaksonen, *J. Am. Chem. Soc.*, **123**, 9817 (2001).
362. T. M. Krygowski, R. Anulewicz, B. Pniewska, P. Milart, C. W. Bock, M. Sawada, Y. Takai and T. Hanafusa, *J. Mol. Struct.*, **324**, 251 (1994).
363. M. Van Beylen, B. Roland, G. S. King and J. Aerts, *J. Chem. Res. (S)*, 388 (1985).
364. P. A. van den Schaff, M. P. Hogenheide, D. Grove, A. L. Spek and G. van Koten, *J. Chem. Soc., Chem. Commun.*, 1703 (1992).
365. A. Murkherjee, M. L. McGlashen and T. G. Spiro, *J. Phys. Chem.*, **99**, 4912 (1995).
366. C. Berthomieu and A. Boussac, *Biospectroscopy*, **1**, 187 (1995).

367. P. v. R. Schleyer, C. Maerker, A. Dransfeld, H. Jiao and N. R. J. van Eikema Hommes, *J. Am. Chem. Soc.*, **118**, 6317 (1996).
368. H. J. Dauben, J. D. Wilson and J. L. Laity, *J. Am. Chem. Soc.*, **90**, 811 (1968); *J. Am. Chem. Soc.*, **91**, 1991 (1969).
369. J. H. Richardson, L. M. Stephenson and J. I. Brauman, *J. Am. Chem. Soc.*, **97**, 2967 (1975).
370. R. F. Gunion, M. K. Gilles, M. L. Polak and W. C. Lineberger, *Int. J. Mass Spectrom. Ion Processes*, **117**, 601 (1992).
371. J. Gao, N. Li and M. Freindorf, *J. Am. Chem. Soc.*, **118**, 4912 (1996).
372. M. V. Vener and S. Iwata, *Chem. Phys. Lett.*, **292**, 87 (1998).
373. E. F. G. Herington and W. Kynaston, *Trans. Faraday Soc.*, **53**, 238 (1957).
374. Z. B. Maksic, D. Kovacek, M. Eckert-Maksic and I. Zrinski, *J. Org. Chem.*, **61**, 6717 (1996).
375. R. M. Borges dos Santos and J. A. Martinho Simões, *J. Phys. Chem. Ref. Data*, **27**, 707 (1998).
376. S. G. Lias, J. E. Bartmess, J. F. Liebman, J. L. Holmes, R. D. Levin and W. G. Mallard, *J. Phys. Chem. Ref. Data*, **17**, Supplement 1 (1988).
377. A. Pross, L. Radom and R. W. Taft, *J. Org. Chem.*, **45**, 818 (1980).
378. J. J. Urban, R. L. von Tersch and G. R. Famini, *J. Org. Chem.*, **59**, 5239 (1994).
379. J. Niwa, *Bull. Chem. Soc. Jpn.*, **62**, 226 (1989).
380. T. Silvestro and R. D. Topsom, *J. Mol. Struct. (THEOCHEM)*, **206**, 309 (1990).
381. S. Chowdhury, H. Kishi, G. W. Dillow and P. Kebarle, *Can. J. Chem.*, **67**, 603 (1989).
382. R. G. Pearson, *J. Am. Chem. Soc.*, **108**, 6109 (1986).
383. J. Hine and P. K. Mookerjee, *J. Org. Chem.*, **40**, 287 (1975).
384. S. Cabani, P. Gianni, V. Mollica and L. Leprori, *J. Solution Chem.*, **10**, 563 (1981).
385. W. H. Richardson, C. Peng, D. Bashford, L. Noodleman and D. A. Case, *Int. J. Quantum Chem.*, **61**, 207 (1997).
386. L. P. Hammett, *J. Am. Chem. Soc.*, **59**, 96 (1937); *Trans. Faraday Soc.*, **34**, 156 (1938).
387. J. Catalan and A. Macias, *J. Mol. Struct.*, **38**, 209 (1977).
388. W. J. Hehre, M. Taagepera, R. W. Taft and R. D. Topsom, *J. Am. Chem. Soc.*, **103**, 1344 (1981).
389. J. Catalan and A. Macias, *J. Chem. Soc., Perkin Trans. 2*, 1632 (1979).
390. F. Mendez, M. de L. Romero and P. Geerlings, *J. Org. Chem.*, **63**, 5774 (1998).
391. K. C. Gross and P. G. Seybold, *Int. J. Quantum Chem.*, **80**, 1107 (2000); **85**, 569 (2001).
392. R. L. Martin and D. A. Shirley, *J. Am. Chem. Soc.*, **96**, 5299 (1974).
393. D. W. Davis and J. W. Rabalais, *J. Am. Chem. Soc.*, **96**, 5305 (1974).
394. S. R. Thomas and T. D. Thomas, *J. Am. Chem. Soc.*, **100**, 5459 (1978).
395. G. Klopman, in *Chemical Reactivity and Reaction Paths* (Ed. G. Klopman), Wiley, New York, 1974, pp. 72–74.
396. R. G. Pearson, *Hard and Soft Acids and Bases*, Dowden, Hutchinson and Ross, Stroudsville, PA, 1973.
397. J. March, *Advanced Organic Chemistry*, Wiley, New York, 1992, pp. 546–547.
398. P. v. R. Schleyer, *Pure Appl. Chem.*, **59**, 1647 (1987).
399. C. Lambert, Y. D. Wu and P. v. R. Schleyer, *J. Chem. Soc., Chem. Commun.*, 255 (1993).
400. D. Seebach, *Angew. Chem., Int. Ed. Engl.*, **27**, 1624 (1988).
401. L. M. Jackman and B. D. Smith, *J. Am. Chem. Soc.*, **110**, 3829 (1988).
402. Y. J. Zheng and R. L. Ornstein, *J. Am. Chem. Soc.*, **119**, 1523 (1997).
403. M. Haeblerlein and T. Brinck, *J. Phys. Chem.*, **100**, 10116 (1996).
404. J. B. A. Ross, W. R. Laws, K. W. Rousslang and H. R. Wyssbrod, in *Topics in Fluorescence Spectroscopy, Vol. 3, Biochemical Applications* (Ed. J. R. Lakowicz), Plenum Press, New York, 1992, pp. 1–62.
405. J. Petruska, *J. Chem. Phys.*, **34**, 1120 (1961).
406. K. Kimura and S. Nagakura, *Mol. Phys.*, **9**, 117 (1965).
407. W. H. Fang, *J. Chem. Phys.*, **112**, 1204 (2000).
408. A. L. Sobolewski and W. Domcke, *J. Phys. Chem. A*, **105**, 9275 (2001).
409. H. Abe, N. Mikami, M. Ito and Y. Udagawa, *Chem. Phys. Lett.*, **93**, 217 (1982).
410. T. Ebata, A. Iwasaki and N. Mikami, *J. Phys. Chem. A*, **104**, 7974 (2000).
411. I. Berlman, *Handbook of Fluorescence Spectra of Aromatic Molecules*, Academic Press, New York, 1969.

412. (a) K. Fuke and K. Kaya, *Chem. Phys. Lett.*, **94**, 97 (1983).
(b) S. Hirokawa, T. Imasaka and T. Imasaka, *J. Phys. Chem. A*, **105**, 9252 (2002).
413. G. Kemister, A. Pross, L. Radom and R. W. Taft, *J. Org. Chem.*, **45**, 1056 (1980).
414. S. Martrenchard-Barra, C. Dedonder-Lardeux, C. Jouvet, D. Solgadi, M. Vervloet, G. Gregoire and I. Dimicoli, *Chem. Phys. Lett.*, **310**, 173 (1999).
415. J. E. LeClaire, R. Anand and P. M. Johnson, *J. Phys. Chem.*, **106**, 6785 (1997).
416. G. Kohler and N. Getoff, *J. Chem. Soc., Faraday Trans. 1*, **73**, 2101 (1976).
417. D. V. Bent and E. Hayon, *J. Am. Chem. Soc.*, **97**, 2599 (1975).
418. C. P. Schick and P. M. Weber, *J. Phys. Chem. A*, **105**, 3725 (2001).
419. C. P. Schick and P. M. Weber, *J. Phys. Chem. A*, **105**, 3735 (2001).
420. M. R. Ganapathi, R. Hermann, S. Naumov and O. Brede, *Phys. Chem. Chem. Phys.*, **2**, 4947 (2000); *Chem. Phys. Lett.*, **337**, 335 (2001).
421. F. G. Bordwell and J. P. Cheng, *J. Am. Chem. Soc.*, **113**, 1736 (1991).
422. O. Brede, H. Orthner, V. E. Zubarev and R. Hermann, *J. Phys. Chem.*, **100**, 7097 (1996).
423. H. Mohan, R. Hermann, S. Maunov, J. P. Mittal and O. Brede, *J. Phys. Chem. A*, **102**, 5754 (1998).
424. R. Hermann, S. Naumov, G. R. Mahalaxmi and O. Brede, *Chem. Phys. Lett.*, **324**, 265 (2000); *J. Mol. Struct. (THEOCHEM)*, **532**, 69 (2000).
425. T. A. Gadosy, D. Shukla and L. J. Johnston, *J. Phys. Chem. A*, **103**, 8834 (1999).
426. S. C. Anderson, L. Goodman, K. Krogh-Jespersen, A. G. Ozkabak and R. N. Zare, *J. Chem. Phys.*, **82**, 5329 (1985).
427. F. Borchers, K. Levsen, C. B. Theissling and N. M. M. Nibbering, *Org. Mass Spectrom.*, **12**, 746 (1977).
428. R. Caballol, J. M. Poblet and P. Sarasa, *J. Phys. Chem.*, **89**, 5836 (1985).
429. D. H. Russel, M. L. Gross and N. M. M. Nibbering, *J. Am. Chem. Soc.*, **100**, 6133 (1978).
430. D. H. Russel, M. L. Gross, J. Van der Greef and N. M. M. Nibbering, *Org. Mass Spectrom.*, **14**, 474 (1979).
431. A. Y. Van Haverbeke, R. Flammang, C. De Meyer, K. G. Das and G. S. Reddy, *Org. Mass Spectrom.*, **12**, 631 (1977).
432. A. Maquestiau, R. Flammang, G. L. Glish, J. A. Laramée and R. G. Cooks, *Org. Mass Spectrom.*, **15**, 131 (1980).
433. A. Maquestiau, R. Flammang, P. Pauwels, P. Vallet and P. Meyrant, *Org. Mass Spectrom.*, **17**, 643 (1982).
434. F. Turecek, D. E. Drinkwater, A. Maquestiau and F. W. McLafferty, *Org. Mass Spectrom.*, **24**, 669 (1989).
435. C. Lifshitz and S. Gefen, *Org. Mass Spectrom.*, **19**, 197 (1984).
436. C. Lifshitz and Y. Malinovich, *Int. J. Mass Spectrom. Ion Processes*, **60**, 99 (1984).
437. E. L. Chronister and T. H. Morton, *J. Am. Chem. Soc.*, **112**, 9475 (1990).
438. V. Nguyen, J. S. Bennett and T. H. Morton, *J. Am. Chem. Soc.*, **119**, 8342 (1997).
439. E. L. Mehler and J. Gerhards, *J. Am. Chem. Soc.*, **107**, 5856 (1985).
440. G. A. DiLabio, D. A. Pratt and J. S. Wright, *J. Org. Chem.*, **65**, 2195 (2000).
441. D. M. Camaioni, *J. Am. Chem. Soc.*, **112**, 9475 (1990).
442. S. H. Hoke, S. S. Yang, R. G. Cooks, D. A. Hrovat and W. T. Borden, *J. Am. Chem. Soc.*, **116**, 4888 (1994).
443. M. H. Palmer, W. Moyes, M. Speirs and J. N. A. Ridyard, *J. Mol. Struct.*, **52**, 293 (1979).
444. M. L. Fraser-Monteiro, L. Fraser-Monteiro, J. de Wit and T. Baer, *J. Phys. Chem.*, **88**, 3622 (1984). For recent data see: O. Dopfer, K. Müller-Dethlefs, *J. Chem. Phys.*, **101**, 8508 (1994); O. Dopfer, M. Melf and K. Müller-Dethlefs, *Chem. Phys.*, **207**, 437 (1995); T. G. Wright, E. Cordes, O. Dopfer and K. Müller-Dethlefs, *J. Chem. Soc. Faraday Trans.*, **89**, 1609 (1993); E. Cordes, E. Dopfer and K. Müller-Dethlefs, *J. Phys. Chem.*, **97**, 7471 (1993); O. Dopfer, T. G. Wright, E. Cordes and K. Müller-Dethlefs, *J. Am. Chem. Soc.*, **116**, 5880 (1994); M. C. R. Cockett, M. Takahashi, K. Okuyama and K. Kimura, *Chem. Phys. Lett.*, **187**, 250 (1991).
445. T. P. Debies and J. W. Rabalais, *J. Electron Spectrosc. Relat. Phenom.*, **1**, 355 (1972).
446. J. P. Maier and D. W. Turner, *J. Chem. Soc., Faraday Trans. 2*, **69**, 521 (1973).
447. T. Kobayashi and S. Nakakura, *Bull. Chem. Soc. Jpn.*, **47**, 2563 (1974).
448. R. Flammang, M. Barbieux-Flammang, E. Gualano, P. Gerbaux, H. T. Le, M. T. Nguyen, F. Turecek and S. Vivekananda, *J. Phys. Chem. A*, **105**, 8579 (2001).

449. R. Flammang, M. Barbieux-Flammang, P. Gerbaux, H. T. Le, F. Turecek and M. T. Nguyen, *Int. J. Mass Spectrom.*, **217**, 65 (2002).
450. R. Flammang, J. Elguero, H. T. Le, P. Gerbaux and M. T. Nguyen, *Chem. Phys. Lett.*, **356**, 239 (2002).
451. D. J. Lavorato, J. K. Terlouw, G. A. McGibbon, T. K. Dargel, W. Koch and H. Schwarz, *Int. J. Mass Spectrom.*, **179**, 7 (1998).
452. H. T. Le, R. Flammang, P. Gerbaux, G. Bouchoux and M. T. Nguyen, *J. Phys. Chem. A*, **105**, 11582 (2001).
453. C. Trindle, *J. Phys. Chem. A*, **104**, 5298 (2000).
454. S. Jakabsen, K. V. Mikkelsen and S. U. Pedersen, *J. Phys. Chem.*, **100**, 7411 (1996).
455. M. Krauss, *J. Mol. Struct. (THEOCHEM)*, **307**, 47 (1994).
456. N. Mikami, S. Sato and M. Ishigaki, *Chem. Phys. Lett.*, **202**, 431 (1993).
457. W. T. Dixon and D. Murphy, *J. Chem. Soc., Faraday Trans. 2*, **72**, 1221 (1976).
458. Y. Apeloig, in *The Chemistry of Enols* (Ed. Z. Rappoport), Chap. 1, Wiley, Chichester, 1980.
459. F. Turecek and C. J. Cramer, *J. Am. Chem. Soc.*, **117**, 12243 (1995).
460. B. J. Smith, M. T. Nguyen, W. J. Bouma and L. Radom, *J. Am. Chem. Soc.*, **113**, 6452 (1991).
461. W. Bertrand and G. Bouchoux, *Rapid Commun. Mass Spectrom.*, **12**, 1697 (1998).
462. Y. Apeloig, in *The Chemistry of Enols* (Ed. Z. Rappoport), Chap. 1, Wiley, Chichester, 1990.
463. M. T. Nguyen, L. Landuyt and L. G. Vanquickenborne, *Chem. Phys. Lett.*, **182**, 225 (1991).
464. NIST Webbook: <http://webbook.nist.gov/chemistry>.
465. R. Flammang, Y. Van Haverbeke, C. Braybrook and J. Brown, *Rapid Commun. Mass Spectrom.*, **9**, 795 (1995).
466. P. Gerbaux, Y. Van Haverbeke and R. Flammang, *J. Mass Spectrom.*, **32**, 1170 (1997).
467. L. J. Chyall and H. I. Kenttämaa, *J. Am. Chem. Soc.*, **116**, 3135 (1994); *J. Mass Spectrom.*, **30**, 81 (1995).
468. M. Capponi, I. Gut, B. Hellrung, G. Persy and J. Wirz, *Can. J. Chem.*, **77**, 605 (1999).
469. K. Mandix, A. Colding, K. Elming, L. Sunesen and I. Shim, *Int. J. Quantum. Chem.*, **46**, 159 (1993).
470. D. Delaere, G. Raspoet and M. T. Nguyen, *J. Phys. Chem. A*, **103**, 171 (1999).
471. M. T. Nguyen and G. Raspoet, *Can. J. Chem. A.*, **77**, 817 (1999).
472. G. Raspoet, M. T. Nguyen and L. G. Vanquickenborne, *J. Phys. Org. Chem.*, **13**, 46 (2000).
473. M. S. Sodupe, A. Oliva and J. Bertran, *J. Phys. Chem. A*, **101**, 9142 (1997).
474. A. Courty, M. Mons, I. Dimicoli, F. Piuze, V. Brenner and P. Millie, *J. Phys. Chem. A*, **102**, 4890 (1998).
475. R. J. Lipert and S. D. Colson, *J. Phys. Chem.*, **93**, 135 (1989); **92**, 188 (1988).
476. O. Dopfer, T. G. Wright, E. Cordes and K. Muller-Dethlefs, *J. Am. Chem. Soc.*, **116**, 5880 (1994).
477. R. J. Green, H. T. Kim, J. Qian and S. L. Anderson, *J. Chem. Phys.*, **113**, 4158 (2000).
478. S. R. Haines, W. D. Geppert, D. M. Chapman, M. J. Watkins, C. E. H. Dessent, M. C. R. Cockett and K. Muller-Dethlefs, *J. Chem. Phys.*, **109**, 9244 (1998).
479. I. Rozas, I. Alkorta and J. Elguero, *J. Phys. Chem. A*, **105**, 10462 (2001).
480. B. Halliwell and J. M. C. Gutteridge, *Free Radicals in Biology and Medicine*, 2nd edn., Oxford University Press, Oxford, 1989.
481. J. Stubbe, *Annu. Rev. Biochem.*, **58**, 257 (1989).
482. R. Karthien, R. Dietz, W. Nastainczyk and H. H. Ruf, *Eur. J. Biochem.*, **171**, 313 (1988).
483. B. Barry, M. K. El-Deeb, P. O. Sandusky and G. T. Babcock, *J. Biol. Chem.*, **265**, 20 (1990).
484. M. M. Whitakker and J. M. Whitakker, *Biophys. J.*, **64**, 762 (1993).
485. S. M. Janes, D. Mu, D. Wemmes, A. J. Smith, S. Kaus, D. Maltby, A. L. Burlingame and J. P. Klinman, *Science*, **248**, 981 (1990).
486. M. G. Simic and T. Dizdaroglu, *Biochemistry*, **24**, 233 (1985).
487. C. Y. Lin and M. C. Lin, *J. Phys. Chem.*, **90**, 425 (1986).
488. T. J. Stone and W. A. Waters, *Proc. Chem. Soc. London*, 253 (1962); *J. Chem. Soc.*, 213 (1964).
489. W. T. Dixon, M. Moghimi and D. Murphy, *J. Chem. Soc., Faraday Trans. 2*, **70**, 1713 (1974).
490. S. Un, C. Gerez, E. Elleingand and M. Fontecave, *J. Am. Chem. Soc.*, **123**, 3048 (2001).
491. T. Maki, Y. Araki, Y. Ishida, O. Onomura and Y. Matsumaru, *J. Am. Chem. Soc.*, **123**, 3371 (2001).
492. S. M. Beck and L. E. Brus, *J. Chem. Phys.*, **76**, 4700 (1982).

493. C. R. Johnson, M. N. Ludwig and S. A. Asher, *J. Am. Chem. Soc.*, **108**, 905 (1986).
494. G. N. R. Tripathi and R. H. Schuler, *J. Phys. Chem.*, **92**, 5129 and 5133 (1988); *J. Chem. Phys.*, **81**, 113 (1984); *Chem. Phys. Lett.*, **98**, 594 (1983).
495. G. N. R. Tripathi, in *Time Resolved Spectroscopy* (Eds. R. J. H. Clark and R. E. Hester), Wiley, New York, 1989, p. 157.
496. A. Mukherjee, M. L. McGlashen and T. G. Spiro, *J. Phys. Chem.*, **99**, 4912 (1995).
497. L. D. Johnston, N. Mathivanan, F. Negri, W. Siebrand and F. Zerbetto, *Can. J. Chem.*, **71**, 1655 (1993).
498. J. Spanget-Larsen, M. Gil, A. Gorski, D. M. Blake, J. Waluk and J. G. Radziszewski, *J. Am. Chem. Soc.*, **123**, 11253 (2001).
499. G. Porter and F. G. Wright, *Trans. Faraday Soc.*, **51**, 1469 (1955).
500. E. J. Land, G. Porter and E. Strachan, *Trans. Faraday Soc.*, **57**, 1885 (1961).
501. J. L. Roebber, *J. Chem. Phys.*, **37**, 1974 (1962).
502. B. Ward, *Spectrochim. Acta, Part A*, **24**, 813 (1968).
503. R. H. Schuler and G. K. Buzzard, *Int. J. Radiat. Phys. Chem.*, **8**, 563 (1976).
504. D. Pullin and L. Andrews, *J. Mol. Struct.*, **95**, 181 (1982).
505. Y. Kajii, K. Obi, N. Nakashima and K. Yohihara, *J. Chem. Phys.*, **87**, 5059 (1984).
506. H. M. Chang, H. H. Jaffe and C. A. Masmandis, *J. Phys. Chem.*, **79**, 1118 (1975).
507. V. B. Luzhkov and A. S. Zyubin, *J. Mol. Struct. (THEOCHEM)*, **170**, 33 (1988).
508. H. Yu and J. D. Goddard, *J. Mol. Struct. (THEOCHEM)*, **233**, 129 (1991).
509. R. Liu and X. Zhou, *Chem. Phys. Lett.*, **207**, 185 (1993); *J. Phys. Chem.*, **97**, 9613 (1993).
510. D. Chipman, R. Liu, X. Zhou and P. Pulay, *J. Chem. Phys.*, **100**, 5023 (1994).
511. Y. Qin and R. A. Wheeler, *J. Chem. Phys.*, **102**, 1689 (1995).
512. G. N. R. Tripathi, *J. Phys. Chem. A*, **102**, 2388 (1998).
513. Y. Qin and R. A. Wheeler, *J. Am. Chem. Soc.*, **117**, 6083 (1995).
514. R. Schnepf, A. Sokolowski, J. Muller, V. Bachler, K. Wieghardt and P. Hildebrandt, *J. Am. Chem. Soc.*, **116**, 9577 (1994).
515. P. J. O'Malley, *Chem. Phys. Lett.*, **325**, 69 (2000).
516. C. Berthomieu, C. Boullais, J. M. Neumann and A. Boussac, *Biochim. Biophys. Acta*, **1365**, 112 (1998).
517. L. A. Eriksson, *Mol. Phys.*, **91**, 827 (1997).
518. C. Adamo, R. Subra, A. Di Matteo and V. Barone, *J. Chem. Phys.*, **109**, 10244 (1998).
519. H. Fischer, *Z. Naturforsch.*, **20**, 488 (1965).
520. H. M. McConnell and D. B. Chesnut, *J. Chem. Phys.*, **18**, 107 (1958).
521. T. A. Claxton, *Chem. Soc. Rev.*, 437 (1995).
522. A. M. Schmoltner, D. S. Anex and Y. T. Lee, *J. Phys. Chem.*, **96**, 1236 (1992).
523. S. Olivella, A. Sole and A. Garcia-Raso, *J. Phys. Chem.*, **99**, 10549 (1995).
524. R. Liu, K. Morokuma, A. M. Mebel and M. C. Lin, *J. Phys. Chem.*, **100**, 9314 (1996).
525. A. M. Mebel and M. C. Lin, *J. Am. Chem. Soc.*, **116**, 9577 (1994).
526. G. Ghio and G. Tonachini, *J. Am. Chem. Soc.*, **120**, 6753 (1998).
527. F. Berho, F. Caralp, M. T. Rayez, R. Lesclaux and E. Ratajczak, *J. Phys. Chem.*, **102**, 1 (1998).
528. J. Platz, O. J. Nielsen, T. J. Wallington, J. C. Ball, M. D. Hurley, A. M. Straccia, W. F. Schneider and J. Sehested, *J. Phys. Chem. A*, **102**, 7964 (1998).
529. F. P. Lossing and J. L. Holmes, *J. Am. Chem. Soc.*, **106**, 6917 (1984).
530. M. T. Nguyen, unpublished results (2001).
531. D. D. M. Wayner, E. Luszyk, D. Page, K. U. Ingold, P. Mulder, L. J. J. Laarhoven and H. S. Aldrich, *J. Am. Chem. Soc.*, **117**, 8737 (1995).
532. M. Lucariri, P. Pedrielli, G. F. Pedulli, S. Cabiddu and C. Fattuoni, *J. Org. Chem.*, **61**, 9259 (1996).
533. W. van Scheppingen, E. Dorrestijn, I. Arends, P. Mulder and H. G. Korth, *J. Phys. Chem. A*, **101**, 5404 (1997).
534. M. Jonsson, J. Lind, T. E. Ericksen and G. Merenyi, *J. Chem. Soc., Perkin Trans. 2*, 1557 (1993).
535. D. J. Harman, *J. Geontol.*, **11**, 298 (1956); *Proc. Natl. Acad. Sci. U.S.A.*, **11**, 7124 (1981).
536. T. Finkel and N. J. Holbrook, *Nature*, **408**, 239 (2000) and references therein.
537. W. A. Pryor, in *Modern Biological Theories of Aging* (Eds. H. R. Warner, R. N. Butler and R. L. Sprott), Raven, New York, 1987, p. 89.

538. V. W. Bowry and K. U. Ingold, *Acc. Chem. Res.*, **32**, 27 (1999).
539. K. U. Ingold, A. C. Webb, D. Witter, G. W. Burton, T. A. Metcalf and D. P. R. Muller, *Arch. Biochem. Biophys.*, **259**, 224 (1987).
540. T. F. Slater, K. H. Cheeseman, C. Benedetto, M. Collins, S. Emery, S. P. Maddrix, J. T. Nodes, K. Proudfoot, G. W. Burton and K. U. Ingold, *Biochem. J.*, **265**, 51 (1990).
541. L. J. Machlin, *Vitamin E. A Comprehensive Treatise*, Marcel Dekker, New York, 1980.
542. J. A. Howard and K. U. Ingold, *Can. J. Chem.*, **40**, 1851 (1962).
543. J. A. Howard and K. U. Ingold, *Can. J. Chem.*, **41**, 1744 (1963).
544. J. A. Howard and K. U. Ingold, *Can. J. Chem.*, **41**, 2800 (1963).
545. J. A. Howard and K. U. Ingold, *Can. J. Chem.*, **42**, 1044 (1964).
546. K. Tanaka, S. Sakai, S. Tomiyama, T. Nishiyama and F. Yamada, *Bull. Chem. Soc. Jpn.*, **64**, 2677 (1991).
547. S. Tomiyama, S. Sakai, T. Nishiyama and F. Yamada, *Bull. Chem. Soc. Jpn.*, **66**, 299 (1993).
548. M. Perrakyla and T. A. Pakkanen, *J. Chem. Soc., Perkin Trans 2*, 1405 (1995).
549. M. J. Lundqvist and L. A. Eriksson, *J. Phys. Chem., B*, **104**, 848 (2000).
550. E. Mvula, M. N. Schuchmann and C. von Sonntag, *J. Chem. Soc., Perkin Trans. 2*, 264 (2001).
551. O. Tishchenko, E. Kryachko and M. T. Nguyen, *J. Mol. Struct. (THEOCHEM)*, **615**, 247 (2002).
552. G. Gilchrist, G. W. Burton and K. U. Ingold, *Chem. Phys.*, **95**, 473 (1985).
553. A. Müller, H. Ratajczak, W. Junge and E. Diemann (Eds.), *Electron and Proton Transfer in Chemistry and Biology*, Elsevier, Amsterdam, 1992.
554. G. S. Denisov and V. M. Schreiber, *Doklady Akad. Sci. USSR, (Engl. Trans.)*, **215**, 627 (1974).
555. G. S. Denisov, A. I. Kulbida and V. M. Schreiber, in *Molecular Spectroscopy*, Vol. 6, Leningrad State University, Leningrad, 1983, p. 124.
556. M. Rospenk, I. G. Rumynskaya and V. M. Schreiber, *J. Appl. Spectrosc. (USSR) (Engl. Transl.)*, **36**, 756 (1982).
557. G. S. Denisov, S. F. Bureiko, N. S. Golubev and K. Tokhadze, in *Molecular Interactions*, Vol. 2 (Eds. H. Ratajczak and W. J. Orville-Thomas), Wiley, New York, 1980, p. 107.
558. S. F. Bureiko, V. P. Oktyabrskii and K. Pihlaya, *Kinetika i Katalyz (USSR)*, **34**, 430 (1993).
559. S. F. Bureiko, N. S. Goluben, J. Mattinen and K. Pihlaya, *J. Mol. Liq.*, **45**, 139 (1990).
560. S. F. Bureiko, N. S. Golubev and K. Pihlaya, *J. Mol. Struct. (THEOCHEM)*, **480–481**, 297 (1999).
561. J. P. Dupont, J. D'Hondt and Th. Zeegers-Huyskens, *Bull. Soc. Chim. Belg.*, **80**, 369 (1971).
562. M. Rospenk and Th. Zeegers-Huyskens, *Spectrochim. Acta, Part A*, **42**, 499 (1986).
563. M. Rospenk and Th. Zeegers-Huyskens, *J. Phys. Chem.*, **91**, 3974 (1987).
564. M. Szafran, *J. Mol. Struct. (THEOCHEM)*, **381**, 9 (1996).
565. Z. Dega-Szafran, A. Kania, M. Grunwald-Wyspianska, M. Szafran and E. Tykarska, *J. Mol. Struct. (THEOCHEM)*, **381**, 107 (1996).
566. Z. Dega-Szafran and M. Szafran, *J. Chem. Soc., Perkin Trans. 2*, 897 (1987).
567. H. Ratajczak and L. Sobczyk, *J. Chem. Phys.*, **50**, 556 (1969).
568. Z. Malarski, M. Rospenk, E. Grech and L. Sobczyk, *J. Phys. Chem.*, **86**, 401 (1982).
569. H. Romanowski and L. Sobczyk, *J. Phys. Chem.*, **79**, 2535 (1975).
570. L. Sobczyk, in *Radio and Microwave Spectroscopy* (Eds. N. Piślewski and A. Mickiewicz), University Press, Poznan, 1985, p. 55.
571. M. Ilczyszyn and H. Ratajczak, *J. Chem. Soc., Faraday Trans.*, **91**, 1611, 3859 (1995).
572. M. Ilczyszyn, H. Ratajczak and K. Skowronek, *Magn. Reson. Chem.*, **26**, 445 (1988).
573. G. Zundel, *Adv. Chem. Phys.*, **111**, 1 (2000).
574. H. Abe, N. Mikami and M. Ito, *J. Phys. Chem.*, **86**, 1768 (1982).
575. H. Abe, N. Mikami, M. Ito and Y. Udagawa, *J. Phys. Chem.*, **86**, 2567 (1982).
576. N. Gonohe, H. Abe, N. Mikami and M. Ito, *J. Phys. Chem.*, **89**, 3642 (1985).
577. A. Schiefke, C. Deussen, Ch. Jacoby, M. Gerhards, M. Schmitt and K. Kleinerhmanns, *J. Chem. Phys.*, **102**, 9197 (1995).
578. A. Oikawa, H. Abe, N. Mikami and M. Ito, *J. Phys. Chem.*, **87**, 5083 (1983).
579. M. Ito, *J. Mol. Struct.*, **177**, 173 (1988).
580. T. Ebata, M. Furukawa, T. Suzuki and M. Ito, *J. Opt. Soc. Am. B*, **7**, 1890 (1990).
581. K. Fuke and K. Kaya, *Chem. Phys. Lett.*, **91**, 311 (1982).

582. K. Fuke, H. Yoshiuchi, K. Kaya, Y. Achiba, K. Sato and K. Kimura, *Chem. Phys. Lett.*, **108**, 179 (1984).
583. A. Sur and P. M. Johnson, *J. Phys. Chem.*, **84**, 1206 (1986).
584. J. L. Knee, L. R. Khundkar and A. H. Zewail, *J. Chem. Phys.*, **87**, 115 (1987).
585. R. J. Lipert, G. Bermudez and S. D. Colson, *J. Phys. Chem.*, **92**, 3801 (1988).
586. L. J. Lipert and S. D. Colson, *J. Chem. Phys.*, **89**, 4579 (1989).
587. R. J. Lipert and S. D. Colson, *Chem. Phys. Lett.*, **161**, 303 (1989).
588. D. Solgadi, C. Jouvét and A. Tramer, *J. Phys. Chem.*, **92**, 3313 (1988).
589. J. Steadman and J. A. Syage, *J. Chem. Phys.*, **92**, 4630 (1990).
590. R. J. Stanley and A. W. Castleman, *J. Chem. Phys.*, **94**, 7744 (1991).
591. G. Reiser, O. Dopfer, R. Lindner, G. Henri, K. Müller-Dethlefs, E. W. Schlag and S. D. Colson, *Chem. Phys. Lett.*, **181**, 1 (1991).
592. D. L. Gerrard and W. F. Maddams, *Spectrochim. Acta, Part A*, **34**, 1205, 1213 (1978).
593. G. Nemethy and A. Ray, *J. Phys. Chem.*, **77**, 64 (1973).
594. H. Baba and S. Suzuki, *J. Chem. Phys.*, **35**, 1118 (1961).
595. M. Ito, *J. Mol. Spectrosc.*, **4**, 106 (1960).
596. M. Gerhards, K. Beckmann and K. Kleinermanns, *Z. Phys. D*, **29**, 223 (1994).
597. M. Yi and S. Scheiner, *Chem. Phys. Lett.*, **262**, 567 (1996).
598. A. Iwasaki, A. Fujii, T. Watanabe, T. Ebata and N. Mikami, *J. Phys. Chem.*, **100**, 16053 (1996).
599. N. Mikami, A. Okabe and I. Suzuki, *J. Phys. Chem.*, **92**, 1858 (1988).
600. C. Jouvét, C. Lardeux-Dedonder, M. Richard-Viard, D. Solgadi and A. Tramer, *J. Phys. Chem.*, **94**, 5041 (1990).
601. C. Crepin and A. Tramer, *Chem. Phys. Lett.*, **156**, 281 (1991).
602. M. Ilczyszyn, H. Ratajczak and J. A. Ladd, *Chem. Phys. Lett.*, **153**, 385 (1988).
603. M. Ilczyszyn, H. Ratajczak and J. A. Ladd, *J. Mol. Struct.*, **198**, 499 (1989).
604. M. Wierzejewska and H. Ratajczak, *J. Mol. Struct. (THEOCHEM)*, **416**, 121 (1997).
605. I. Majerz and L. Sobczyk, *J. Chim. Phys.*, **90**, 1657 (1993).
606. I. Majerz, Z. Malarski and L. Sobczyk, *Chem. Phys. Lett.*, **274**, 361 (1997).
607. G. Albrecht and G. Zundel, *J. Chem. Soc., Faraday Trans. 1*, **80**, 553 (1984).
608. A. J. Abkowitz-Bieńko and Z. Latajka, *J. Phys. Chem. A*, **104**, 1004 (2000).
609. B. Brzezinski, E. Grech, Z. Malarski, M. Rospenk, G. Schroeder and L. Sobczyk, *J. Chem. Res. (S)*, 151 (1997).
610. J. De Taeye, J. Parmentier and Th. Zeegers-Huyskens, *J. Phys. Chem.*, **92**, 4555 (1988).
611. G. G. Siegel and Th. Zeegers-Huyskens, *Spectrochim. Acta, Part A*, **45**, 1297 (1989).
612. S. M. Melikova, D. N. Shchepkin and A. Koll, *J. Mol. Struct. (THEOCHEM)*, **448**, 239 (1998).
613. P. Mighels, N. Leroux and Th. Zeegers-Huyskens, *Vibrational Spectrosc.*, **2**, 81 (1991).
614. P. Mighels and Th. Zeegers-Huyskens, *J. Mol. Struct. (THEOCHEM)*, **247**, 173 (1991).
615. K. De Wael, J. Parmentier and Th. Zeegers-Huyskens, *J. Mol. Liq.*, **51**, 67 (1992).
616. M. Goethals, B. Czarnik-Matusiewicz and Th. Zeegers-Huyskens, *J. Heterocycl. Chem.*, **36**, 49 (1999).
617. D. Reyntjens-Van Damme and Th. Zeegers-Huyskens, *J. Phys. Chem.*, **84**, 282 (1980).
618. J. De Taeye and Th. Zeegers-Huyskens, *J. Pharm. Sci.*, **74**, 660 (1985).
619. O. Kasende and Th. Zeegers-Huyskens, *J. Phys. Chem.*, **88**, 2132 (1984).
620. J. Fritsch and G. Zundel, *Spectrosc. Lett.*, **17**, 41 (1984).
621. A. Filarowski and A. Koll, *Vib. Spectrosc.*, **17**, 123 (1998).
622. P. Imhof, W. Roth, C. Janzen, D. Spangenberg and K. Kleinermanns, *Chem. Phys.*, **242**, 141 (1999).
623. P. Imhof, W. Roth, C. Janzen, D. Spangenberg and K. Kleinermanns, *Chem. Phys.*, **242**, 153 (1999).
624. D. Hadži, A. Novak and J. E. Gordon, *J. Phys. Chem.*, **67**, 1118 (1963).
625. S. M. Melikova, A. Ju. Inzebekin, D. N. Shchepkin and A. Koll, *J. Mol. Struct. (THEOCHEM)*, **552**, 273 (2000).
626. S. F. Bureiko, G. S. Denisov and R. M. Martsinkovsky, *React. Kinet. Catal. Lett.*, **2**, 343 (1975).
627. S. F. Bureiko, N. S. Golubev and I. Ya. Lange, *React. Kinet. Catal. Lett.*, **16**, 32 (1981).
628. A. Rabold, B. Brzezinski, R. Langner and G. Zundel, *Acta Chim. Slov.*, **44**, 237 (1997).

629. T. Keil, B. Brzezinski and G. Zundel, *J. Phys. Chem.*, **96**, 4421 (1992).
630. B. Brzezinski, G. Schroeder, G. Zundel and T. Keil, *J. Chem. Soc., Perkin Trans. 2*, 819 (1992).
631. B. Brzezinski, H. Maciejewska and G. Zundel, *J. Phys. Chem.*, **94**, 6983 (1990).
632. B. Brzezinski, B. Brycki, G. Zundel and T. Keil, *J. Phys. Chem.*, **95**, 8598 (1991); see also R. J. Alvarez and E. S. Kryachko, *J. Mol. Struct. (THEOCHEM)*, **433**, 263 (1998).
633. B. Brycki, B. Brzezinski, G. Zundel and T. Keil, *Magn. Reson. Chem.*, **30**, 507 (1992).
634. H. Merz, U. Tangermann and G. Zundel, *J. Phys. Chem.*, **90**, 6535 (1986).
635. H. Merz and G. Zundel, *Chem. Phys. Lett.*, **95**, 529 (1983).
636. A. Weichert, C. Riehn and B. Brutschy, *J. Phys. Chem. A*, **105**, 5679 (2001).
637. G. Zundel and A. Nagyrei, *J. Phys. Chem.*, **82**, 685 (1978).
638. G. Buczak, Z. Dega-Szafran, A. Katrusiak and M. Szafran, *J. Mol. Struct. (THEOCHEM)*, **436**, 143 (1997).
639. A. Koll and I. Majerz, *Bull. Soc. Chim. Belg.*, **103**, 629 (1994).
640. I. Majerz and A. Koll, *Polish J. Chem.*, **68**, 2109 (1994).
641. S. F. Bureiko and N. S. Golubev, *Zh. Strukt. Khim. (USSR) (Engl. Transl.)*, **28**, 171 (1987).
642. B. Brzezinski and G. Zundel, *J. Mol. Struct. (THEOCHEM)*, **380**, 195 (1996).
643. S. F. Bureiko, N. S. Golubev, G. S. Denisov and I. Ya. Lange, *Izv. Akad. Sci. Latv. SSR (Engl. Transl.)*, **3**, 369 (1980).
644. S. F. Bureiko and V. P. Oktyabrskii, *React. Kinet. Catal. Lett.*, **31**, 245 (1986).
645. S. F. Bureiko, N. S. Golubev and I. Ya. Lange, *Kinetika i Katalyz (USSR) (Engl. Transl.)*, **1**, 209 (1982).
646. A. Rabold and G. Zundel, *J. Phys. Chem.*, **99**, 12158 (1995).
647. E. Haslinger and P. Wolschann, *Monatsh. Chem.*, **11**, 563 (1980).
648. V. M. Schreiber, A. Koll and L. Sobczyk, *Bull. Acad. Polon. Sci., Ser. Sci. Chim.*, **24**, 651 (1978).
649. K. Rutkowski, S. M. Melikova and A. Koll, *Vib. Spectrosc.*, **7**, 265 (1994).
650. A. Koll, M. Rospenk and L. Sobczyk, *J. Chem. Soc., Faraday Trans. 1*, **77**, 2309 (1981).
651. A. Fedorowicz, J. Mavri, P. Bala and A. Koll, *Chem. Phys. Lett.*, **289**, 457 (1998).
652. A. Koll, M. Rospenk, E. Jagodzinska and T. Dziembowska, *J. Mol. Struct. (THEOCHEM)*, **552**, 193 (2000).
653. M. Rospenk, L. Sobczyk, A. Rabold and G. Zundel, *Spectrochim. Acta, Part A*, **55**, 85 (1999).
654. A. Filarowski, T. Glowia and A. Koll, *J. Mol. Struct. (THEOCHEM)*, **484**, 75 (1999).
655. M. Przeslawska, A. Koll and M. Witanowski, *J. Phys. Org. Chem.*, **12**, 486 (1999).
656. A. Koll and P. Wolschann, *Monatsh. Chem.*, **127**, 475 (1996).
657. K. Rutkowski and A. Koll, *J. Mol. Struct. (THEOCHEM)*, **322**, 195 (1994).
658. A. Szemik-Hojniak and A. Koll, *J. Photochem. Photobiol. A: Chem.*, **72**, 123 (1993).
659. A. Filarowski, A. Koll and T. Glowia, *J. Chem. Cryst.*, **27**, 707 (1997).
660. A. Filarowski, A. Koll, T. Glowia, E. Majewski and T. Dziembowska, *Ber. Bunsenges. Phys. Chem.*, **102**, 393 (1998).
661. A. Mandal, A. Koll, A. Filarowski, D. Majumder and S. Mukherjee, *Spectrochim. Acta, Part A*, **55**, 2861 (1999).
662. L. Sobczyk, *Appl. Magn. Reson.*, **18**, 47 (2000).
663. L. Sobczyk, *J. Mol. Struct.*, **177**, 111 (1988).
664. H. Ptasiwicz-Bak, R. Tellgren, I. Olovsson and A. Koll, *Z. Kristallogr.*, **212**, 126 (1997).
665. A. Filarowski, A. Koll and T. Glowia, *Monatsh. Chem.*, **130**, 1097 (1999).
666. A. Mandal, A. Koll, A. Filarowski, D. Majumder and S. Mukherjee, *Spectrochim. Acta, Part A*, **55**, 2868 (1999).
667. A. Koll and P. Wolschann, *Monatsh. Chem.*, **130**, 983 (1999).
668. D. Guha, A. Mandal, A. Koll, A. Filarowski and S. Mukherjee, *Spectrochim. Acta, Part A*, **56**, 2669 (2000).
669. A. Fedorowicz and A. Koll, *J. Mol. Liq.*, **87**, 1 (2000).
670. M. Rospenk, A. Koll and L. Sobczyk, *Chem. Phys. Lett.*, **261**, 283 (1996).
671. B. Brzezinski, P. Radziejewski, A. Rabold and G. Zundel, *J. Mol. Struct. (THEOCHEM)*, **355**, 185 (1995).
672. B. Brzezinski, J. Olejnik, G. Zundel and R. Krämer, *J. Mol. Struct. (THEOCHEM)*, **212**, 247 (1989).
673. B. Brzezinski, J. Olejnik and G. Zundel, *J. Mol. Struct. (THEOCHEM)*, **238**, 89 (1990).

674. H. Schmideder, O. Kasende, H. Merz, P. P. Rastogi and G. Zundel, *J. Mol. Struct. (THEOCHEM)*, **161**, 87 (1987).
675. B. Brzezinski, H. Maciejewska and G. Zundel, *J. Phys. Chem.*, **96**, 6564 (1992).
676. B. Brzezinski, H. Urjasz, F. Bartl and G. Zundel, *J. Mol. Struct. (THEOCHEM)*, **435**, 59 (1997).
677. T. G. Wright, E. Gordes, O. Dopfer and K. Müller-Dethlefs, *J. Chem. Soc., Faraday Trans.*, **89**, 1601 (1993).
678. M. Schmitt, H. Müller, U. Henrichs, M. Gerhards, W. Perl, C. Deussen and K. Kleiner-mann, *J. Chem. Phys.*, **103**, 584 (1995).
679. J. Küpper, A. Westphal and M. Schmitt, *Chem. Phys.*, **263**, 41 (2001).
680. O. Tishchenko, E. S. Kryachko and V. I. Staninets, *Theor. Expt. Khim. (Engl. Transl.)*, **35**, 331 (1999).
681. E. J. Bieske, M. W. Rainbird, I. M. Atkinson and A. E. W. Knight, *J. Chem. Phys.*, **91**, 752 (1989).
682. M. Schmidt, M. Mons and J. Le Calve, *Z. Phys. D*, **17**, 153 (1990).
683. M. Mons, J. Le Calve, F. Piuze and I. Dimicoli, *J. Chem. Phys.*, **92**, 2155 (1990).
684. X. Zhang and J. L. Knee, *Faraday Discuss.*, **97**, 299 (1994).
685. C. E. H. Dessent, S. R. Haines and K. Müller-Dethlefs, *Chem. Phys. Lett.*, **315**, 103 (1999).
686. A. Fujii, M. Miyazaki, T. Ebata and N. Mikami, *J. Chem. Phys.*, **110**, 11125 (1999).
687. S. R. Haines, C. E. H. Dessent and K. Müller-Dethlefs, *J. Chem. Phys.*, **111**, 1947 (1999).
688. D. M. Chapman, K. Müller-Dethlefs and J. B. Peel, *J. Chem. Phys.*, **111**, 1955 (1999).
689. N. Solcá and O. Dopfer, *Chem. Phys. Lett.*, **325**, 354 (2000).
690. R. I. Cukier, *J. Phys. Chem. A*, **103**, 5989 (1999).
691. P. Hobza, R. Burel, V. Špirko, O. Dopfer, K. Müller-Dethlefs and E. W. Schlag, *J. Chem. Phys.*, **101**, 990 (1994).
692. A. Goto, M. Fujii, N. Mikami and M. Ito, *J. Phys. Chem.*, **90**, 2370 (1986).
693. R. J. Lipert and S. D. Colson, *J. Phys. Chem.*, **93**, 3894 (1389) (1989).
694. R. J. Lipert and S. D. Colson, *J. Phys. Chem.*, **94**, 2358 (1990).
695. M. Schmitt, H. Mueller and K. Kleiner-mann, *Chem. Phys. Lett.*, **218**, 246 (1994).
696. M. Gerhards and K. Kleiner-mann, *J. Chem. Phys.*, **103**, 7392 (1995).
697. Ch. Jacoby, W. Roth, M. Schmitt, Ch. Janzen, D. Spangenberg and K. Kleiner-mann, *J. Phys. Chem. A*, **102**, 4471 (1998).
698. G. Berden, W. L. Meerts, M. Schmitt and K. Kleiner-mann, *J. Chem. Phys.*, **104**, 972 (1996).
699. M. Gerhards, M. Schmitt, K. Kleiner-mann and K. Stahl, *J. Chem. Phys.*, **104**, 967 (1996).
700. K. Kleiner-mann, M. Gerhards and M. Schmitt, *Ber. Bunsenges. Phys. Chem.*, **101**, 1785 (1997).
701. M. Schmitt, Ch. Jacoby and K. Kleiner-mann, *J. Chem. Phys.*, **108**, 4486 (1998).
702. W. Roth, M. Schmitt, Ch. Jacoby, D. Spangenberg, Ch. Janzen and K. Kleiner-mann, *Chem. Phys.*, **239**, 1 (1998).
703. S. Tanabe, T. Ebata, M. Fujii and N. Mikami, *Chem. Phys. Lett.*, **215**, 347 (1993).
704. N. Mikami, *Bull. Chem. Soc. Jpn.*, **68**, 683 (1995).
705. T. Watanabe, T. Ebata, S. Tanabe and N. Mikami, *J. Chem. Phys.*, **105**, 408 (1996).
706. A. Fujii, T. Sawamura, S. Tanabe, T. Ebata and N. Mikami, *Chem. Phys. Lett.*, **225**, 104 (1994).
707. T. Ebata, A. Fujii and N. Mikami, *Int. Rev. Phys. Chem.*, **17**, 331 (1998).
708. R. J. Stanley and A. W. Castleman, Jr., *J. Chem. Phys.*, **98**, 796 (1993).
709. M. Schütz, T. Bürgi, S. Leutwyler and H. B. Bürgi, *J. Chem. Phys.*, **99**, 5228 (1993).
710. S. Leutwyler, T. Bürgi, M. Schütz and A. Taylor, *Faraday Disc. Chem. Soc.*, **96**, 456 (1994).
711. T. Bürgi, M. Schütz and S. Leutwyler, *J. Chem. Phys.*, **103**, 6350 (1995).
712. O. Dopfer and K. Müller-Dethlefs, *J. Chem. Phys.*, **101**, 8508 (1994).
713. R. M. Helm and H. J. Neusser, *Chem. Phys.*, **239**, 33 (1998).
714. H.-D. Barth, K. Buchhold, S. Djafari, B. Reimann, U. Lommatzsch and B. Brutschy, *Chem. Phys.*, **239**, 49 (1998).
715. R. M. Helm, H.-P. Vogel and N. J. Neusser, *J. Chem. Phys.*, **108**, 4496 (1998).
716. H. J. Neusser and K. Siglow, *Chem. Rev.*, **100**, 3921 (2000).
717. C. E. H. Dessent and K. Müller-Dethlefs, *Chem. Rev.*, **100**, 3999 (2000).

718. E. W. Schlag, in *Adv. Chem. Phys., Volume 101: Chemical Reactions and Their Control on the Femtosecond Time Scale, XXth Solvay Conference on Chemistry* (Eds. P. Gaspard, I. Burghardt, I. Prigogine and S. A. Rice), Wiley, New York, 1997, pp. 607–623.
719. J. A. Syage, *J. Phys. Chem.*, **99**, 5772 (1995).
720. K. Kim, K. D. Jordan and T. S. Zwier, *J. Am. Chem. Soc.*, **116**, 11568 (1994).
721. K. Liti, M. G. Brown, C. Carter, R. J. Saykally, J. K. Gregory and D. C. Clary, *Nature* **381**, 501 (1996).
722. E. S. Kryachko, *Int. J. Quantum Chem.*, **70**, 831 (1998).
723. E. S. Kryachko, *Chem. Phys. Lett.*, **314**, 353 (1999) and references therein.
724. D. M. Benoit, A. X. Chavagnac and D. C. Clary, *Chem. Phys. Lett.*, **283**, 269 (1998).
725. D. M. Benoit and D. C. Clary, *J. Phys. Chem. A*, **104**, 5590 (2000).
726. D. C. Clary, D. M. Benoit and T. Van Mourik, *Acc. Chem. Res.*, **33**, 441 (2000).
727. R. C. Guedes, B. J. Costa Cabral, J. A. Martinho Simões and H. P. Diogo, *J. Phys. Chem. A*, **104**, 6062 (2000).
728. W.-H. Fang and R.-Z. Liu, *J. Chem. Phys.*, **113**, 5253 (2000).
729. H. Watanabe and S. Iwata, *J. Chem. Phys.*, **105**, 420 (1996).
730. H. Watanabe and S. Iwata, *Int. J. Quantum Chem., Quantum Chem. Symp.*, **30**, 395 (1996).
731. E. S. Kryachko and H. Nakatsuji, *J. Phys. Chem. A*, **106**, 73 (2002).
732. E. S. Kryachko and M. T. Nguyen, *J. Chem. Phys.*, **115**, 833 (2001).
733. By analogy with the earlier studies (Reference 729), the PES search of the phenol-(water)_n complexes was initially performed by using a split-valence double-zeta 6-31G(d) basis set via a GAUSSIAN 98 suit of packages.
734. We distinguish five computational levels of theory/basis sets used for geometry optimizations although a 6-31G(d) basis set denoted throughout the present work as A plays a key role. The ground level corresponds to the common HF/A one, which is also employed for calculating harmonic frequencies, ZPVE, and thermodynamic properties. Empirical scaling factor of 0.8907 employed in Reference 729 was not used in the present work. Single-point (sp) energy calculations of the lower-energy PhOH(H₂O)_n complexes were then performed at the MP2(sp)/A level in order to investigate the effect of correlation on their energy differences. The most stable PhOH(H₂O)_{n=1-4} structures as the key structures in the present study were further refined at the MP2(fc)/A (fc is hereafter omitted) and, besides, the four lowest-energy PhOH(H₂O)₄ structures were also reoptimized at the MP2/6-31+G(d) (≡MP2/A⁺) and B3LYP/A levels. The latter one was also used to recalculate their harmonic frequencies.
735. Z. Bačič and R. E. Miller, *J. Phys. Chem.*, **100**, 12945 (1996).
736. K. S. Kim, J. L. Lee, H. S. Choi, J. Kim and J. H. Jang, *Chem. Phys. Lett.*, **265**, 497 (1997).
737. K. S. Kim, P. Tarakeshwar and J. Y. Lee, *Chem. Rev.*, **100**, 4145 (2000).
738. J. M. Flaud, C. Camy-Payret and J. P. Maillard, *Mol. Phys.*, **32**, 499 (1976).
739. J. A. Riddick, W. B. Bungh and T. K. Sakano, *Organic Solvents*, 4th edn., Wiley, New York, 1986.
740. T. Takamuku, M. Tabata, M. Yamaguchi, J. Nishimoto, M. Kumamoto, H. Wakita and T. Yamaguchi, *J. Phys. Chem. B*, **102**, 8880 (1998) and references therein.
741. D. J. Jamroz, J. Stangret and J. Lingdren, *J. Am. Chem. Soc.*, **115**, 6165 (1993).
742. S. C. White and H. W. Thompson, *Proc. Roy. Soc. London A*, **291**, 460 (1966).
743. M. S. Sousa Lopes and H. W. Thompson, *Spectrochim. Acta, Part A*, **24**, 1367 (1968).
744. S. S. Mitra, *J. Chem. Phys.*, **36**, 3286 (1962).
745. A. Allerhand and P. v. R. Schleyer, *J. Am. Chem. Soc.*, **85**, 371 (1963).
746. T. Gramstadt and J. Sandström, *Spectrochim. Acta, Part A*, **25**, 31 (1969).
747. J. M. Campbell, Y. S. Park and H. F. Shurvell, *Can. J. Spectrosc.*, **36**, 6 (1991).
748. J. C. F. Ng, Y. S. Park and H. F. Shurvell, *J. Raman Spectrosc.*, **23**, 229 (1992).
749. J. C. F. Ng, Y. S. Park and H. F. Shurvell, *Spectrochim. Acta, Part A*, **48**, 1137 (1992).
750. S. M. Quadri and H. F. Shurvell, *Spectrochim. Acta, Part A*, **51**, 1355 (1995).
751. D. A. Buckingham, *Proc. Roy. Soc. London A*, **248**, 169 (1958).
752. M. Horak, J. Polakova, M. Jakoubkova, J. Moravec and J. Pliva, *Collect. Czech. Chem. Commun.*, **31**, 622 (1966).
753. M. Horak and J. Moravec, *Collect. Czech. Chem. Commun.*, **36**, 2757 (1971).

754. J. Yarwood, in *Spectroscopy and Structure of Molecular Complexes* (Ed. J. Yarwood), Plenum, London, 1973, pp. 182ff.
755. B. Czarnik-Matusewicz and Th. Zeegers-Huyskens, *J. Phys. Org. Chem.*, **13**, 237 (2000).
756. H. Figeys, P. Geerlings, D. Berckmans and C. Van Alsenoy, *J. Chem. Soc., Faraday Trans. 2*, **77**, 721 (1981).
757. T. Gramstadt and K. Tjessem, *J. Mol. Struct.*, **41**, 231 (1977).
758. M.-I. Baraton, *J. Mol. Struct.*, **10**, 231 (1971).
759. H. Abramczyk, W. Reimschuessel, H. Barańska and A. Labudzińska, *Chem. Phys.*, **94**, 435 (1985).
760. It was not actually our intention to explore the PES using a large basis set and more sophisticated computational level, so we have confined our PES search to the use of a rather simple density functional hybrid B3LYP computational level in conjunction with a split-valence double-zeta 6-31+G(d,p) basis set with the help of a GAUSSIAN 98 suit of packages². The chosen computational level, which by no means could not be considered as rather inaccurate, was further employed for calculating harmonic frequencies and, therefore, for identifying the stationary points on the studied PES and also obtaining zero-point vibrational energy (ZPVE) in order to deduce the binding energy of the hydrogen-bonded complex AB as $E_{\text{HB}}(\text{AB}) = -([E(\text{AB}) - \text{ZPVE}(\text{AB})] - ([E(\text{A}) - \text{ZPVE}(\text{A})] + [E(\text{B}) - \text{ZPVE}(\text{B})]))$ expressed throughout the present work in kJ mol^{-1} . The effect of the basis set superposition error (BSSE) was only tested for the phenol- acetonitrile complexes using the standard counterpoise procedure.
761. E. S. Kryachko and M. T. Nguyen, *J. Phys. Chem. A*, **106**, 4267 (2002). For a recent study of the π -H bonding between phenol and HCN, HOCN, HF and HCl see E. S. Kryachko and M. T. Nguyen, *Polish J. Chem.*, **76**, 1233 (2002).
762. The B3LYP/6-31+G(d,p) optimized geometry of the acetonitrile molecule shown parenthetically in Figure 6 is fairly consistent with the microwave data [J. Demaison, A. Dubrelle, D. Boucher, J. Burie and V. Typke, *J. Mol. Spectrosc.*, **76**, 1 (1979) and C. C. Costain, *J. Chem. Phys.*, **29**, 864 (1958)]: $r(\text{C}-\text{N}) = 1.157 \text{ \AA}$, $r(\text{C}-\text{C}) = 1.462 (1.458) \text{ \AA}$, $r(\text{C}-\text{H}) = 1.095 (1.102) \text{ \AA}$, and $\angle \text{C}-\text{C}-\text{H} = 109.8^\circ (109.5^\circ)$ and appears to be more accurate than that obtained at the B3LYP/DZVP2 level [D. H. Barich, T. Xu, W. Song, Z. Wang, F. Deng and J. F. Haw, *J. Phys. Chem. B*, **102**, 7163 (1998)]. See also J. R. Reimers, J. Zeng and N. S. Hush, *J. Phys. Chem. A*, **100**, 1498 (1996) and compare with the values in Table 1 in Reference 763. It becomes evident there that the MP2/6-311++G(d,p) level (Reference 763) overestimates the C-N and C-C bond lengths by *ca* 0.005–0.017 \AA and underestimates the C-H one by 0.010 \AA .
763. E. M. Cabaleiro-Lago and M. Ríos, *J. Phys. Chem. A*, **101**, 8327 (1997) and references therein.
764. U. P. Agarwal, R. S. Green and J. Yarwood, *Chem. Phys.*, **74**, 35 (1983).
765. J. R. Reimers and L. E. Hall, *J. Am. Chem. Soc.*, **121**, 3730 (1999).
766. According to the MP2/cc-pVDZ calculations (Reference 765), the cyclic dimer has the binding energy of 18.7 kJ mol^{-1} whereas the 'head-to-tail' one is 8.7 kJ mol^{-1} . The HF/STO-3G computational level substantially underestimates the former value by a factor of 2.6 as quoted by A. Wakisaka, Y. Shimizu, N. Nishi, K. Tokumaru and H. Sakuragi, *J. Chem. Soc., Faraday Trans.*, **88**, 1129 (1992) based on the incorrect Reference 209.
767. J. Jawed, *Bull. Chem. Soc. Jpn.*, **49**, 659, 1155 (1976).
768. K. Tanabe, *Chem. Phys.*, **63**, 135 (1981).
769. H. Abramczyk and W. Reimschuessel, *Chem. Phys.*, **100**, 243 (1985).
770. T. Steiner, C. C. Wilson and I. Majerz, *Chem. Commun.*, 1231 (2000).
771. I. Dodgson, K. Griffen, G. Barberis, F. Pignatoro and G. Tauszik, *Chem. Ind.*, 830 (1989).
772. E. Y. Bezuglaya, A. B. Shchutskaya and I. V. Smirnova, *Atmos. Environ.*, **27**, 773 (1998).
773. S. K. Ong and A. R. Bowers, *J. Environ. Eng.*, **116**, 1013 (1990).
774. E.-J. Shin and M. A. Keane, *Ind. Eng. Chem. Res.*, **39**, 883 (2000).
775. M. Engstrom, F. Himo and H. Angren, *Chem. Phys. Lett.*, **319**, 191 (2000).
776. A. F. Hegarty and J. P. Keogh, *J. Chem. Soc. Perkin Trans. 2*, 758 (2001) and references therein.

777. B. J. C. Cabral, R. G. B. Fonseca and J. A. Martinho Simões, *Chem. Phys. Lett.*, **258**, 436 (1996).
778. J. Florian and A. Warshel, *J. Phys. Chem. B*, **101**, 5583 (1997).
779. W. Siebrand, M. Z. Zgierski and Z. K. Smedarchina, *Chem. Phys. Lett.*, **279**, 377 (1997).
780. C. Chipot, *J. Phys. Chem. B*, **105**, 5987 (2001).
781. A. Weichert, C. Riehn and B. Brutschy, *J. Phys. Chem. A*, **105**, 5679 (2001) and references therein.
782. Z. Bikadi, G. Keresztury, S. Holly, O. Egyed, I. Mater and M. Simonyi, *J. Phys. Chem. A*, **105**, 3471 (2001) and references therein.